UV-assisted isomerization studies of active compounds in *bush tea* (*Athrixia phylicoides)* leaf extracts and investigations of their potential to inhibit acid corrosion of mild steel and zinc

by

Ratshikombo Rinae

Student Number: 15015809

A thesis submitted in fulfillment of the requirements for the degree of

Doctor of Philosophy in Chemistry (MNPDPC)

Department of Chemistry

Faculty of Science, Engineering, and Agriculture

University of Venda

Supervisor: Prof. L.C MURULANA

Co-Supervisor: Prof. M.M KABANDA

Co-Supervisor: Prof. N.E MADALA

February 2025

© University of Venda

Declaration

I, Rinae Ratshikombo, declare that this thesis titled "UV-assisted isomerization studies of active compounds in bush tea (*Athrixia phylicoides)* leaf extracts and investigations of their potentials to inhibit acid corrosion of mild steel and zinc'' is the results of a study carried out originally by me under the guidance and supervision of Prof L.C Murulana and co-supervision of Prof N.E Madala and Prof M.M Kabanda. This work is being submitted in fulfillment of the Doctor of Philosophy in Chemistry at the University of Venda and has not been submitted to any university for any degree and examination. The information that I have collected from secondary sources has been properly acknowledged in the reference pages.

Signature: …… Date: …….

© University of Venda

University of Venda
Creating Future Leaders

Table of Contents

Declaration ii

Acknowledgments vi

Abstract vii

List of Abbreviations ix

List of Figures xi

List of Tables xiv

CHAPTER ONE 1

1. Introduction 2

1.1 Origin of the Research 3

1.2 Project Rationale 4

1.3 Problem Statement 6

1.4 Timeline of Significant Corrosion-Related Incidents 7

1.5 The Scope of Current Research 8

1.6 Aims and Objectives of the Study 11

1.7 Hypothesis 11

CHAPTER TWO 12

2. Background of the Research 13

2.1 Corrosion Definition 13

2.2 Classification of Corrosion 14

2.3 Thermodynamics and Kinetics of Corrosion 16

2.4 The Rate of Corrosion 17

2.5 Aspects Affecting Corrosion Rate 17

2.6 Impact of Corrosion 22

2.7 Understanding the Economic Impact of Corrosion and the Benefits of Preventive Measures 25

2.8 Strategies for Understanding and Mitigating Metal Corrosion in Various Environments 27

2.9 Corrosion Prevention Methods 30

2.10 Advantages of Using Corrosion Inhibitors in Industrial Applications 32

2.11 Exploring the Role of Corrosion Inhibitors in Metal Protection 34

2.12 The Potential of *athrixia phylicoides* as a Corrosion Inhibitor 37

2.12 Metal Corrosion on Acidic Medium of Interest 40

2.13 Corrosion Observation Procedure 44

2.14 Introduction to Computational Chemistry 51

© University of Venda

2.15 Literature Review on the Corrosion Inhibition of Mild Steel, and Zinc Using Plant Extracts in Aqueous Media 53
CHAPTER THREE 56
3. Experimental Procedures 57
3.1 Introduction 57
3.2 Inhibitor Solution Preparation 57
3.3 Electrochemical Measurements 61
3.4. Wettability Study 68
3.5 Scanning Electron Microscopy (SEM) 68
3.6 Fourier Transform Infrared Spectroscopy (FTIR) 69
3.7 Weight Loss Measurements (WLM) 70
3.8 Geometry of Molecules 73
3.9 Quantum Chemical Approaches 73
CHAPTER FOUR 97
4.1 Liquid Chromatography-Mass Spectrometry 98
4.2 Isolation of Compounds Causing Corrosion Inhibition 101
CHAPTER FIVE 111
5.1 Fourier Transform Infrared Spectroscopy (FTIR) 112
CHAPTER SIX 126
6.1 Gravimetric Analysis 127
6.2 Weight Loss Measurement Using Non-UV-Radiated *A. Phylicoides* Extract 130
6.3 Weight Loss Measurement Using UV-Radiated *A. Phylicoides* Extract 134
6.4 Time Stability of Non-UV radiated *A. phylicoides* Extract 137
6.5 Surface Coverage on Metal Exposed in Acidic Medium Over 24-Hour Timeframe 140
6.6 Inhibition Efficiency of Non-UV Radiated *A. Phylicoides* Extract 142
6.7 Time Stability of UV-Radiated *A.Phylicoides* Extract 144
6.8 Surface Coverage for UV-Radiated *A. Phylicoides* Extract 147
6.9 Inhibition Efficiency for UV Radiated *A. Phylicoides* Extract 149
6.10 Corrosion Rate of Metals Exposed in Acidic Medium 152
6.10.1 Corrosion Rate of Metal Exposed to Acidic Medium in the Presence of Non-UV Radiation *A. Phylicoides* Extract 152
6.10.2 Corrosion Rate of Metal Exposed to Acidic Medium in the Presence of UV Radiation *A. phylicoides* Extract 155
6.11 Surface Coverage of Metal Exposed to Acidic Medium in the Presence and Absence of UV Radiated *A. phylicoides* Extract 158

© University of Venda

University of Venda
Creating Future Leaders

6.11.1 Surface Coverage of Metals Exposed to Acidic Medium Using Non-UV Radiated *A. phylicoides* Extract 159

6.11.2 The Surface Coverage of Metal in the Presence of UV-Radiated *A. phylicoides* 162

6.12 Inhibition Efficiency of Metals Offered by Non-UV Radiated and UV-Radiated *A. phylicoides* 165

6.12.1 Inhibition Efficiency of Metals in the Presence of Non-UV Radiated *A. phylicoides* Extract 166

6.12.2 Inhibition Efficiency of Metal Exposed in Acidic Media Using UV Radiated *A. phylicoides* Extracts 169

6.13 Adsorption Isotherm for Non-UV Radiated and UV Radiated *A. phylicoides* Extracts 171

6.14 Temperature Effect for *A. phylicoides* Extracts 181

CHAPTER SEVEN 192

7.1 Open Circuit Voltage (OCV) 193

7. 2 Potentiodynamic Polarization (PDP) 199

7.3 Electrochemical Impedance Spectroscopy (EIS) 207

CHAPTER EIGHT 218

8.1. Contact angles (Wettability study) 219

CHAPTER NINE 224

9.1 Scanning Electron Microscopy (SEM) and Energy Dispersive Spectroscopy (EDS) 225

9.1.1 Scanning Electron Microscopy (SEM) images 225

CHAPTER TEN 237

10 Computational Studies Results 238

10.1 Introduction 238

10.2 Interaction of Zinc Metal Surface with the Inhibitor Molecules 238

10.3 Interaction of Mild Steel Surface with the Inhibitor Molecules 242

CHAPTER ELEVEN 244

11 Conclusions and Recommendations 245

11.2 Contribution and Recommendations 247

References 249

© University of Venda

Acknowledgments

Above all, I express my gratitude and deep respect to God, whose grace has been indispensable in enabling me to finalize this thesis.

I offer my heartfelt gratitude to my supervisor, Prof L.C. Murulana, for his invaluable guidance and inspiration throughout this project.

My **p**rofound thanks to Prof M.M Kabanda and Prof N.E Madala, **r**esearch **c**o-supervisors, Department of Chemistry and Biochemistry, for their scholarly guidance and valuable suggestions during my research.

I also express my gratitude to the broader University of Venda community and the Chemistry Department for providing me with the opportunity to pursue my studies at this institution. Without the support of the University of Venda, this endeavour would not have been achievable.

Lastly, I extend my heartfelt thanks to my family for their unwavering emotional support throughout this journey.

© University of Venda

Abstract

Corrosion of metals can be controlled by using corrosion inhibitors. Plant metabolites undergo geometrical isomerization under the influence of UV light radiation. The use of corrosion inhibitors is one of the useful methods to reduce or decrease corrosion on metals. While synthetic inhibitors are useful in preventing the corrosion of metals, they can sometimes be harmful and costly. There is an alternative solution in the form of green inhibitors, which can offer the same level of protection at an affordable price. Inhibitors of corrosion are applied to the environment and the metal they protect against deterioration. Considering this information, it is necessary to examine different metals exposed to an acidic environment in the presence and absence of inhibitors. The impact of UV light radiation on *bush tea* (*A. phylicoides*) plant extract was investigated for zinc, and mild steel corrosion exposed to 1.5 M hydrochloric and sulphuric acids at 303-333K. This study employs liquid chromatography-mass spectrometry (LC-MS) to investigate the geometric isomerization of compounds within plant extracts, aiming to identify and quantify different isomers and understand the conditions influencing their stability and transformation. Gravimetric analysis (GA), Electrochemical Impedance Spectroscopy (EIS), and Potentiodynamic Polarization (PDP) were used to study corrosion inhibition, Fourier Transform Infrared Spectroscopy (FTIR) was used to analyze functional groups in the presence and absence of corrosion inhibitors. Contact angle or wettability studies (CA / WS) have been conducted to assess the hydrophobicity or hydrophilicity of the surface. Scanning Electron Microscopy (SEM) and computational studies were employed to gain a deeper understanding of the surface morphology and interactions between the *A. phylicoides* plant extracts and the metal surface. LC-MS chromatograph shows that the extract undergoes geometric isomerization. The GA, EIS, and PDP tests showed that the extracts were able to reduce the amount of corrosion that occurred on the metal surface. FTIR tests confirmed that the extracts were able to form a protective layer on the metal surfaces, which inhibited the corrosion process. The SEM and computational studies provided additional evidence that the extracts were able to reduce the corrosion rate by forming a protective layer on the metal surfaces. The results of the study showed that the extracts had a strong adhesive capacity and were able to form a stable protective layer on the metal surfaces. This layer was able to resist the corrosive action of the environment and prevent further corrosion. The study also showed that the extracts had good stability and were able to remain intact on the metal surface for a long time.

© University of Venda

Keywords: *Athrixia Phylicoides,* Ultraviolet Light, Geometrical Isomerization, Corrosion Rate, Inhibition Efficiency, Zinc, and Mild Steel.

© University of Venda

List of Abbreviations

UV	Ultraviolet
EIS	Electrochemical Impedance Spectroscopy
PDP	Potentiodynamic Polarization
FTIR	Fourier Transform Infrared Spectroscopy
SEM	Scanning Electron Microscopy
LCMS	Liquid Chromatography Mass Spectrometry
WL	Weight loss
CA	Contact angle
MS	Mild steel
Zn	Zinc
HCl	Hydrochloric acid
H_2SO_4	Sulphuric acid
SE	Secondary electrons
EDS	Energy dispersive spectrometer
DFT	Density Functional Theory
HF	Hartree-Fock
MP2	Moller-Plesset Perturbation Theory
CC	Coupled Cluster Theory
AIMD	Ab Initio Molecular Dynamics
ONIOM	Our own N-layered Integrated molecular Orbital and Molecular Mechanics
MG	Mish Gush
PPUN	Pear Nopales Pulp
Ppm	Parts per million
G	Gram
E_{corr}	Corrosion potential
VSEPR	Valence Shell Electron Pair Repulsion
SCF	Self Consistent Field
LCAO	Linear Combination of Atomic Orbitals

© University of Venda

CO_2	Carbon dioxide
LUMO	Lowest Unoccupied Molecular Orbital
HOMO	Highest Occupied Molecular Orbital
BCC	Body-Centred Cubic
FCC	Face-Centered Cubic
HCP	Hexagonal Close-Packed
NaI	Sodium iodide
Qtof	Quadrupole time-of-flight
OCV	Open Circuit Voltage
CPE	Constant Phase Element

© University of Venda

List of Figures

Figure 1.1: Process of corrosion. 3
Figure 2.1: Distribution map for Athrixia phylicoides in South Africa. 37
Figure 2.2: Athrixia phylicoides plant 37
Figure 2.3: Athrixia phylicoides cutting trays 39
Figure 2.4: A model of electrochemical parallel circuit mostly used for measurements of EIS parameters in corrosion analysis systems. 46
Figure 3.1: Tafel extrapolation (corrosion of metal in acidic medium). 65
Figure 3.2: Planes with different Miller indices in cubic crystals 96
Figure 4.1: LCMS spectrum for non-UV-radiated and UV-radiated *Athrixia phylicoides* extract shaken for 24 hours. 100
Figure 4.2 : Sirius software showing all the possible compounds found in the *Athrixia phylicoides extract* before UV radiation. 102
Figure 4.3: Sirius software showing all the possible compounds found in the *Athrixia phylicoides extract* after UV radiation. 102
Figure 4.4: The Sirius software data displays the complete list of potential compounds identified in the *Athrixia phylicoides* plant extract corresponding to fraction number 6. 104
Figure 4.5: The Sirius software data displays the complete list of potential compounds identified in the *Athrixia phylicoides* plant extract corresponding to fraction number 7. 105
Figure 4.6: The Sirius software data displays the complete list of potential compounds identified in the *Athrixia phylicoides* plant extract corresponding to fraction number 8. 105
Figure 4.7: The Sirius software data displays the complete list of potential compounds identified in the *Athrixia phylicoides* plant extract corresponding to fraction number 4. 106
Figure 4.8: The Sirius software data displays the complete list of potential compounds identified in the *Athrixia phylicoides* plant extract corresponding to fraction number 5. 106
Figure 4.9: The Sirius software data displays the complete list of potential compounds identified in the *Athrixia phylicoides* plant extract corresponding to fraction number 9. 107
Figure 5.1: FT-IR spectra for the studied non-UV Radiated and UV Radiated *Athrixia phylicoides* extract 112
Figure 5.2.1: FT-IR spectra for the studied *Athrixia phylicoides* and adsorption films formed before and after exposed to UV on Zn in 1.5 M H_2SO_4 114
Figure 5.2.2: FT-IR spectra for the studied *Athrixia phylicoides* and adsorption films formed before and after exposed to UV on Zn in 1.5 M HCl 114
Figure 5.3.1: FT-IR spectra for the studied *Athrixia phylicoides* and adsorption films formed before and after exposed to UV on MS in 1.5 M H_2SO_4 119
Figure 5.3.2: FT-IR spectra for the studied *Athrixia phylicoides* and adsorption films formed before and after exposed to UV on MS in 1.5 M HCl 119
Figure 5.3.2.1: Zoomed version of FT-IR spectra for the studied adsorption films formed before and after being exposed to UV on MS in 1.5 M HCl 120
Figure 6.1: Langmuir adsorption isotherm for the adsorption of non-UV radiated and UV radiated *Athrixia phylicoides* extract on mild steel metal in 1.5 M HCl at 303 K, 313 K, 323 K, and 333 K. 173
Figure 6.2: Langmuir adsorption isotherm for the adsorption of non-UV radiated and UV radiated *Athrixia phylicoides* extract on mild steel metal in 1.5 M H_2SO_4 at 303 K, 313 K, 323 K, and 333 K. 173
Figure 6.3: Langmuir adsorption isotherm for the adsorption of non-UV radiated and UV radiated *Athrixia phylicoides* extract on zinc metal in 1.5 M HCl at 303 K, 313 K, 323 K, and 333 K. 174

© University of Venda

Figure 6.4: Langmuir adsorption isotherm for the adsorption of non-UV radiated and UV radiated *Athrixia phylicoides* extract on zinc metal in 1.5 M H_2SO_4 at 303 K, 313 K, 323 K, and 333 K. 174
Figure 6.5: Arrhenius plots for mild steel metal corrosion in 1.5 M H_2SO_4 solution using non-UV radiated and UV-radiated *Athrixia phylicoides plant extract* as the inhibitor..... 183
Figure 6.6: Arrhenius plots for mild steel metal corrosion in 1.5 M HCl solution non-UV radiated and UV-radiated *Athrixia phylicoides plant extract* as the inhibitor. 183
Figure 6.7: Arrhenius plots for zinc metal corrosion in 1.5 M H_2SO_4 solution non-UV radiated and UV-radiated *Athrixia phylicoides plant extract* as the inhibitor. 184
Figure 6.8: Arrhenius plots for zinc metal corrosion in 1.5 M HCl solution non-UV radiated and UV-radiated *Athrixia phylicoides plant extract* as the inhibitor. 184
Figure 6.9: Transition state plots for mild steel metal corrosion in 1.5 M HCl solution in the absence and presence of different concentrations of *Athrixia phylicoides plant extract* as the inhibitor..... 185
Figure 6.10: Transition state plots for mild steel metal corrosion in 1.5 M H_2SO_4 solution in the absence and presence of different concentrations of *Athrixia phylicoides plant extract* as the inhibitor. 186
Figure 6.11: Transition state plots for zinc metal corrosion in 1.5 M HCl solution in the absence and presence of different concentrations of *Athrixia phylicoides plant extract* as the inhibitor..... 186
Figure 6.12: Transition state plots for zinc metal corrosion in 1.5 M H_2SO_4 solution in the absence and presence of different concentrations of *Athrixia phylicoides plant extract* as the inhibitor..... 187
Figure 7.1: Open circuit voltage for mild steel 1.5 M H_2SO_4 solution and *UV radiated Athrixia phylicoides.* 194
Figure 7.2: Open circuit voltage for mild steel 1.5 M H_2SO_4 solution and non-UV *radiated Athrixia phylicoides.* 194
Figure 7.3: Open circuit voltage for mild steel 1.5 M HCl solution and non-UV *radiated Athrixia phylicoides.* 195
Figure 7.4: Open circuit voltage for mild steel 1.5 M HCl solution and *UV radiated Athrixia phylicoides.* 195
Figure 7.5: Open circuit voltage for zinc 1.5 M H_2SO_4 solution and non-UV *radiated Athrixia phylicoides.* 197
Figure 7.6: Open circuit voltage for zinc 1.5 M H_2SO_4 solution and *UV radiated Athrixia phylicoides.* 197
Figure 7.7: Open circuit voltage for zinc 1.5 M HCl solution and non-UV *radiated Athrixia phylicoides.* 198
Figure 7.8: Open circuit voltage for zinc 1.5 M HCl solution and *UV radiated Athrixia phylicoides.* 198
Figure 7.9: Tafel plots for MS in 1.5 M H_2SO_4 before and after UV exposure in the absence and presence of different concentrations of *Athrixia phylicoides*..... 200
Figure 7.10: Tafel plots for MS in 1.5 M HCl before and after UV exposure in the absence and presence of different concentrations of *Athrixia phylicoides*..... 200
Figure 7.11: Tafel plots for Zn in 1.5 M H_2SO_4 before and after UV exposure in the absence and presence of different concentrations of *Athrixia phylicoides*..... 200
Figure 7.12: Tafel plots for Zn in 1.5 M HCl before and after UV exposure in the absence and presence of different concentrations of *Athrixia phylicoides*..... 201
Figure 7.13: Nyquist plot for mild steel in sulphuric acid exposed in *Athrixia phylicoides* before & after UV exposure. 208
Figure 7.14: Bode plots of mild steel in 1.5 M H_2SO_4 in the absence and presence of different concentrations of non-UV radiated *Athrixia phylicoides* extract inhibitor. 208

© University of Venda

Figure 7.15: Bode plots of mild steel in 1.5 M H_2SO_4 in the absence and presence of different concentrations of UV radiated *Athrixia phylicoides* extract inhibitor.....208
Figure 7.16: Nyquist plot for mild steel in hydrochloric acid exposed in Athrixia phylicoides *before & after UV exposure.* 209
Figure 7.17: Bode plots of mild steel in 1.5 M HCl in the absence and presence of different concentrations of non-UV radiated Athrixia phylicoides extract inhibitor.....209
Figure 7.18: Bode plots of mild steel in 1.5 M HCl in the absence and presence of different concentrations of UV radiated *Athrixia phylicoides* extract inhibitor.....209
Figure 7.19: Nyquist plot for zinc in sulphuric acid exposed in *Athrixia phylicoides before & after UV exposure.* 210
Figure 7.20: Bode plots of zinc in 1.5 M H_2SO_4 in the absence and presence of different concentrations of non-UV radiated *Athrixia phylicoides* extract inhibitor. 210
Figure 7.21: Bode plots of zinc in 1.5 M H_2SO_4 in the absence and presence of different concentrations of UV radiated *Athrixia phylicoides* extract inhibitor.....210
Figure 7.22: Nyquist plot for zinc in hydrochloric acid exposed in Athrixia phylicoides before & after UV exposure. 209
Figure 7.23: Bode plots of zinc in 1.5 M HCl in the absence and presence of different concentrations of non-UV radiated *Athrixia phylicoides* extract inhibitor. 211
Figure 7.24: Bode plots of zinc in 1.5 M HCl in the absence and presence of different concentrations of UV radiated *Athrixia phylicoides* extract inhibitor.....211
Figure 7.25: Equivalent circuit used to fit the impedance spectra obtained for MS and Zn corrosion in 1.50 M HCl, H_2SO_4 in the absence and presence of *Athrixia phylicoides* extract. 212
Figure 8.1: Surface wettability behaviors of (a) polished untreated zinc metal substrate, (b) zinc metal substrate after 6 hours of immersion in 1.5 M HCl medium with no inhibitor, and (c) in the presence of 1300 ppm of non-radiated *Athrixia phylicoides*. 220
Figure 8.2: Surface wettability behaviors of (a) polished untreated zinc metal substrate, (b) zinc metal substrate after 6 hours of immersion in 1.5 M H_2SO_4 medium with no inhibitor, and (c) in the presence of 1300 ppm of non-radiated *Athrixia phylicoides*. 220
Figure 8.3: Surface wettability behaviors of (a) polished untreated zinc metal substrate, (b) zinc metal substrate after 6 hours of immersion in 1.5 M HCl medium with no inhibitor, and (c) in the presence of 1300 ppm of radiated *Athrixia phylicoides*.....220
Figure 8.4: Surface wettability behaviors of (a) polished untreated zinc metal substrate, (b) zinc metal substrate after 6 hours of immersion in 1.5 M H_2SO_4 medium with no inhibitor, and (c) in the presence of 1300 ppm of radiated *Athrixia phylicoides*.....221
Figure 8.5: Surface wettability behaviors of (a) polished untreated mild steel metal substrate, (b) mild steel metal substrate after 6 hours of immersion in 1.5 M HCl medium with no inhibitor, and (c) in the presence of 1300 ppm of non-radiated *Athrixia phylicoides*. 221
Figure 8.6: Surface wettability behaviors of (a) polished untreated mild steel metal substrate, (b) mild steel metal substrate after 6 hours of immersion in 1.5 M H_2SO_4 medium with no inhibitor, and (c) in the presence of 1300 ppm of non-radiated *Athrixia phylicoides*.....221
Figure 8.7: Surface wettability behaviors of (a) polished untreated mild steel metal substrate, (b) mild steel metal substrate after 6 hours of immersion in 1.5 M HCl medium with no inhibitor, and (c) in the presence of 1300 ppm of radiated *Athrixia phylicoides*.....222
Figure 8.8: Surface wettability behaviors of (a) polished untreated mild steel metal substrate, (b) mild steel metal substrate after 6 hours of immersion in 1.5 M H_2SO_4 medium with no inhibitor, and (c) in the presence of 1300 ppm of radiated *Athrixia phylicoides*.....222

© University of Venda

List of Tables

Table 2.1: Various countries Gross Domestic Product because of corrosion of materials 26
Table 2.1 List of green corrosion inhibitor investigated recently by other scientist. 54
Table 4.2: showing weight loss for metals and percentage inhibition efficiency for the 15 fractions in an acidic medium. 103
Table 4.3. Identified compounds from the *Athrixia phylicoides* plant extract. 109
Table 5.1: Functional groups from the FTIR spectra for zinc in sulphuric acid 116
Table 5.2: Functional groups from the FTIR spectra for zinc in hydrochloric acid 117
Table 5.3: Functional groups from the FTIR spectra for mild steel in sulphuric acid 122
Table 5.4: Functional groups from the FTIR spectra for mild steel in hydrochloric acid..... 123
Table 6.1: Weight loss measurements on mild steel exposed to various concentrations of sulphuric acid. 127
Table 6.2: Weight loss measurements on mild steel exposed to various concentrations of hydrochloric acid. 127
Table 6.3: Weight loss measurements on zinc exposed to various concentrations of sulphuric acid. 128
Table 6.4: Weight loss measurements on zinc exposed to various concentrations of hydrochloric acid. 128
Table 6.5: Weight loss measurements on mild steel exposed to sulphuric acid (1.5M) in the presence of non-UV radiated *Athrixia phylicoides* extract. 131
Table 6.6: Weight loss measurements on mild steel exposed to hydrochloric acid (1.5M) in the presence of non-UV radiated *Athrixia phylicoides* extract. 131
Table 6.7: Weight loss measurements on zinc exposed to sulphuric acid (1.5M) in the presence of non-UV radiated *Athrixia phylicoides* extract. 132
Table 6.8: Weight loss measurements on zinc exposed to hydrochloric acid (1.5M) in the presence of non-UV radiated *Athrixia phylicoides* extract. 132
Table 6.9: Weight loss measurements on mild steel exposed to sulphuric acid (1.5M) in the presence of UV-radiated *Athrixia phylicoides* extract. 135
Table 6.10: Weight loss measurements on mild steel exposed to hydrochloric acid (1.5M) in the presence of UV-radiated *Athrixia phylicoides* extract. 135
Table 6.11: Weight loss measurements on zinc exposed to sulphuric acid (1.5M) in the presence of UV-radiated *Athrixia phylicoides* extract. 135
Table 6.12: Weight loss measurements on zinc exposed to hydrochloric acid (1.5M) in the presence of UV-radiated *Athrixia phylicoides* extract. 136
Table 6.13: Weight loss measurements on mild steel exposed to sulphuric acid (1.5M) in the presence of non-UV radiated *Athrixia phylicoides* extract. 138
Table 6.14: Weight loss measurements on mild steel exposed hydrochloric acid (1.5M) in the presence of non-UV radiated *Athrixia phylicoides* extract. 138
Table 6.15: Weight loss measurements on zinc exposed to sulphuric acid (1.5M) in the presence of non-UV radiated *Athrixia phylicoides* extract. 138
Table 6.16: Weight loss measurements on zinc exposed in hydrochloric acid (1.5M) in the presence of non-UV radiated *Athrixia phylicoides* extract. 139
Table 6.17: Surface coverage measurements on mild steel exposed to sulphuric acid (1.5M) in the presence of non-UV radiated *Athrixia phylicoides* extract. 140
Table 6.18: surface coverage measurements on mild steel exposed hydrochloric acid (1.5M) in the presence of non-UV radiated *Athrixia phylicoides* extract. 140
Table 6.19: surface coverage measurements on zinc exposed to sulphuric acid (1.5M) in the presence of non-UV radiated *Athrixia phylicoides* extract. 141

© University of Venda

Table 6.20: surface coverage measurements on zinc exposed in hydrochloric acid (1.5M) in the presence of non-UV radiated *Athrixia phylicoides* extract. 141
Table 6.21: Inhibition efficiency measurements on mild steel exposed to sulphuric acid (1.5M) in the presence of non-UV radiated *Athrixia phylicoides* extract. 142
Table 6.22: Inhibition efficiency measurements on mild steel exposed hydrochloric acid (1.5M) in the presence of non-UV radiated *Athrixia phylicoides* extract. 143
Table 6.23: Inhibition efficiency measurements on zinc exposed to sulphuric acid (1.5M) in the presence of non-UV radiated *Athrixia phylicoides* extract. 143
Table 6.24: Inhibition efficiency measurements on zinc exposed in hydrochloric acid (1.5M) in the presence of non-UV radiated *Athrixia phylicoides* extract. 143
Table 6.25: Weight loss measurements on mild steel exposed to sulphuric acid (1.5M) in the presence of UV radiated *Athrixia phylicoides* extract. 145
Table 6.26: Weight loss measurements on mild steel exposed hydrochloric acid (1.5M) in the presence of UV radiated *Athrixia phylicoides* extract..... 145
Table 6.27: Weight loss measurements on zinc exposed to sulphuric acid (1.5M) in the presence of UV radiated *Athrixia phylicoides* extract..... 145
Table 6.28: Weight loss measurements on zinc exposed in hydrochloric acid (1.5M) in the presence of UV radiated *Athrixia phylicoides* extract..... 146
Table 6.29: surface coverage measurements on mild steel exposed to sulphuric acid (1.5M) in the presence of UV-radiated *Athrixia phylicoides* extract. 147
Table 6.30: surface coverage measurements on mild steel exposed hydrochloric acid (1.5M) in the presence of UV radiated *Athrixia phylicoides* extract..... 147
Table 6.31: surface coverage measurements on zinc exposed to sulphuric acid (1.5M) in the presence of UV radiated *Athrixia phylicoides* extract. 147
Table 6.32: surface coverage measurements on zinc exposed in hydrochloric acid (1.5M) in the presence of UV radiated *Athrixia phylicoides* extract..... 148
Table 6.33: Inhibition Efficiency measurements on mild steel exposed to sulphuric acid (1.5M) in the presence of UV radiated *Athrixia phylicoides* extract..... 149
Table 6.34: Inhibition Efficiency measurements on mild steel exposed hydrochloric acid (1.5M) in the presence of UV-radiated *Athrixia phylicoides* extract. 149
Table 6.35: surface coverage measurements on zinc exposed to sulphuric acid (1.5M) in the presence of UV-radiated *Athrixia phylicoides* extract. 150
Table 6.36: surface coverage measurements on zinc exposed in hydrochloric acid (1.5M) in the presence of UV radiated *Athrixia phylicoides* extract..... 150
Table 6.37: Corrosion rate on mild steel exposed to sulphuric acid (1.5M) in the presence of *Athrixia phylicoides* extract. 153
Table 6.38: Corrosion rate on mild steel exposed to hydrochloric acid (1.5M) in the presence of *Athrixia phylicoides* extract. 153
Table 6.39: Corrosion rate measurements on zinc exposed in sulphuric acid (1.5M) in the presence of *Athrixia phylicoides* extract. 154
Table 6.40: Corrosion rate measurements on zinc exposed in hydrochloric acid (1.5M) in the presence of *Athrixia phylicoides* extract. 154
Table 6.43: Corrosion rate measurements on zinc exposed in sulphuric acid (1.5M) in the presence of *Athrixia phylicoides* extract. 156
Table 6.44: Corrosion rate measurements on zinc exposed in hydrochloric acid (1.5M) in the presence of *Athrixia phylicoides* extract. 157
Table 6.45: surface coverage on mild steel exposed to sulphuric acid (1.5M) in the presence of *Athrixia phylicoides*. 159

© University of Venda

Table 6.46: Surface coverage on mild steel exposed in hydrochloric acid (1.5M) in the presence of *Athrixia phylicoides*. 160
Table 6.47: Surface coverage on zinc exposed in sulphuric acid (1.5M) in the presence of *Athrixia phylicoides*. 160
Table 6.48: Surface coverage on zinc exposed in hydrochloric acid (1.5M) in the presence of *Athrixia phylicoides*. 161
Table 6.49: surface coverage on mild steel exposed in sulphuric acid (1.5M) in the presence of *Athrixia phylicoides*. 162
Table 6.50: Surface coverage on mild steel exposed in hydrochloric acid (1.5M) in the presence of *Athrixia phylicoides*. 163
Table 6.51: Surface coverage on zinc exposed in sulphuric acid (1.5M) in the presence of *Athrixia phylicoides*. 163
Table 6.52: Surface coverage on zinc exposed in hydrochloric acid (1.5M) in the presence of *Athrixia phylicoides*. 164
Table 6.53: Inhibition Efficiency on mild steel exposed in sulphuric acid (1.5M) in the presence of *Athrixia phylicoides* extract. 166
Table 6.54: Inhibition Efficiency on mild steel exposed in hydrochloric acid (1.5M) in the presence of *Athrixia phylicoides* extract. 166
Table 6.55: Inhibition Efficiency on zinc exposed in sulphuric acid (1.5M) in the presence of *Athrixia phylicoides* extract. 167
Table 6.56: Inhibition Efficiency on zinc exposed in hydrochloric acid (1.5M) in the presence of *Athrixia phylicoides* extract. 167
Table 6.57: Inhibition Efficiency on mild steel exposed in sulphuric acid (1.5M) in the present of *Athrixia phylicoides*. 169
Table 6.58: Inhibition Efficiency on mild steel exposed in hydrochloric acid (1.5M) in the present of *Athrixia phylicoides*. 169
Table 6.59: Inhibition Efficiency on zinc exposed in sulphuric acid (1.5M) in the present of *Athrixia phylicoides*. 170
Table 6.60: Inhibition Efficiency on zinc exposed in hydrochloric acid (1.5M) in the present of *Athrixia phylicoides*. 170
Table 6.61: Adsorption parameters from Langmuir Adsorption Isotherm plots for non-UV radiated *Athrixia phylicoides* extract in 1.5 M H_2SO_4 and 1.5 M HCl 176
Table 6.62: Adsorption parameters from Langmuir Adsorption Isotherm plots for UV radiated *Athrixia phylicoides* extract in 1.5 M H_2SO_4 and 1.5 M HCl 178
Table 6.63: Arrhenius and transition parameters for the adsorption of different concentrations of non-UV radiated *Athrixia phylicoides* in 1.5 M HCl on mild steel and zinc metal. 187
Table 6.64: Arrhenius and transition parameters for the adsorption of different concentrations of UV radiated *Athrixia phylicoides* in 1.5 M HCl on mild steel and zinc metal. 189
Table 7.1 The potentiodynamic polarization parameters of non-UV radiated *Athrixia phylicoides* extracts and UV radiated *Athrixia phylicoides* extracts for mild steel metal in sulphuric acid 202
Table 7.2 The potentiodynamic polarization parameters of non-UV radiated *Athrixia phylicoides* extracts and UV radiated *Athrixia phylicoides* extracts for mild steel metal in hydrochloric acid. 205
Table 7.3: Electrochemical impedance spectroscopy (EIS) parameters such as the resistance of charge transfer (R_{ct}) and constant phase element (Q) using non-UV-radiated *Athrixia phylicoides* in 1.5 M H_2SO_4 in mild steel metal. 213
Table 7.4: Electrochemical impedance spectroscopy (EIS) parameters such as the resistance of charge transfer (R_{ct}) and constant phase element (Q) using UV-radiated *Athrixia phylicoides* in 1.5 M H_2SO_4 in mild steel metal. 213

© University of Venda

Table 7.5: Electrochemical impedance spectroscopy (EIS) parameters such as the resistance of charge transfer (R_{ct}) and constant phase element (Q) using non-UV-radiated *Athrixia phylicoides* in 1.5 M HCl in mild steel metal. 213
Table 7.6: Electrochemical impedance spectroscopy (EIS) parameters such as the resistance of charge transfer (R_{ct}) and constant phase element (Q) using UV-radiated *Athrixia phylicoides* in 1.5 M HCl in mild steel metal. 214
Table 7.7: Electrochemical impedance spectroscopy (EIS) parameters such as the resistance of charge transfer (R_{ct}) and constant phase element (Q) using non-UV-radiated *Athrixia phylicoides* in 1.5 M H_2SO_4 in zinc metal. 214
Table 7.8: Electrochemical impedance spectroscopy (EIS) parameters such as the resistance of charge transfer (R_{ct}) and constant phase element (Q) using UV-radiated *Athrixia phylicoides* in 1.5 M H_2SO_4 in zinc metal. 214
Table 7.9: Electrochemical impedance spectroscopy (EIS) parameters such as the resistance of charge transfer (R_{ct}) and constant phase element (Q) using non-UV-radiated *Athrixia phylicoides* in 1.5 M HCl in zinc metal. 215
Table 7.10: Electrochemical impedance spectroscopy (EIS) parameters such as the resistance of charge transfer (R_{ct}) and constant phase element (Q) using UV-radiated *Athrixia phylicoides* in 1.5 M HCl in zinc metal. 215

© University of Venda

CHAPTER ONE

INTRODUCTION

© University of Venda

1. Introduction

Corrosion of metals such as zinc and mild steel is a serious problem worldwide causing financial losses due to the need to replace and repair damaged metals [1,2,3]. To solve this problem, a corrosion inhibitor obtained from a plant named *bush tea,* also called *A. phylicoides,* was utilized to mitigate corrosion. The interesting part of the *A. phylicoides* plant was the leaves. The choice of selecting leaf extract instead of other parts of the plant such as roots or stems was because leaves can be easily harvested from plants without killing the plant itself whereas removal of roots and stems may lead to plant killing [4, 5]. Another interesting aspect was investigating the effect of geometrical isomerization of UV-radiated and non-UV-radiated *A. phylicoides* leaves extracts. It was therefore necessary to first prove if geometrical isomerization occurred or not. As indicated in the title, "UV-assisted isomerization studies of active compounds in *A. phylicoides* leaves extracts and investigations of their potential to inhibit acid corrosion of mild steel and zinc" the focus involves investigating if UV-radiated *A. phylicoides* leaves extract has the potential to mitigate acid corrosion of mild steel and zinc. Proving if geometrical isomerization occurred or not, will require employing Liquid Chromatography Mass Spectrometry (LC-MS), and Fourier Transform Infrared Spectroscopy (FTIR) to obtain the functional group's presence in the UV radiated *A. phylicoides* leaves extract, however, since proving will require comparing evidence obtained before exposing *A. phylicoides* extract to UV radiation and after exposing *A. phylicoides* extract to UV radiation this study take additional dimension to investigate if non UV radiated *A. phylicoides* leaves extract has potentials to inhibit corrosions too. Naturally, plant extracts are initially found in a trans configuration and undergo geometrical isomerization to assume a cis configuration [6]. Due to the structural disparity between the trans and cis configurations, it is plausible to hypothesize that the cis configuration might exhibit superior inhibition efficiency. This is because the cis configuration typically demonstrates a higher binding affinity than the trans configuration [7]. A significant portion of this study, particularly within the results section, will focus extensively on comparing the impact of non-UV-radiated *A. phylicoides* leaf extract and UV-radiated *A. phylicoides* leaf extracts. This comparison aims to provide deeper insights into which of the two variants offers better inhibition efficiency and under what specific conditions this can be achieved.

© University of Venda

1.1 Origin of the Research

Corrosion is a process that occurs in metals and alloys, that ultimately leads to the deterioration of the metals [8]. It is a challenge to keep materials in their original state as they often release energy when exposed to air and moisture [9]. Iron ores are usually in a low-energy state, but when products such as reinforcing steel are made from them, they become more unstable and release energy [10].

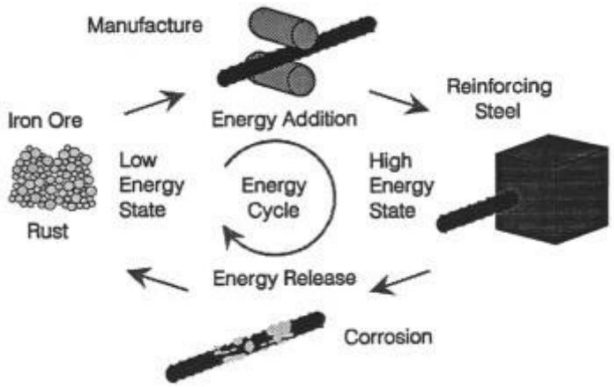


Figure 1.1: Process of corrosion

Corrosion of metals is an issue that poses a considerable danger and expenses globally [11]. If neglected, it can lead to the destruction of bridges, buildings, etc [12]. The corrosion process can rupture oil pipelines, leak chemical plants, and flood plumbing systems [13]. Corrosion can cause various problems, such as structural failure, contamination of water or liquid transported by metallic pipes, etc [14]. It can also result in costly repair and replacement of corroded metallic equipment [15]. Preventative maintenance and regular inspections are essential to minimize the impact of corrosion. Corrosion occurs due to the interaction of a metal surface with its environment, usually involving water, oxygen, and an electrolyte [16]. The corrosion process leads to the breakdown of the metal's protective layer, which can then cause the metal to become brittle and prone to cracking and breaking [17]. Regular inspection of equipment is necessary to ensure that corrosion has not set in, as it can cause significant damage if left unchecked. Corrosion occurs when metals are exposed to moisture and oxygen, which cause chemical reactions that break down the metal [18]. Corrosion can also cause the structure to weaken and potentially fail, leading to a collapse [18]. Corrosion products may be hazardous and could leach into the environment if the waste isn't properly contained. Corrosion of materials over an extended period has posed a major

© University of Venda

problem in various industries, including the marine industry, construction, mining machinery, and packaging [19]. For this reason, it is essential to use corrosion inhibitors to protect metals [20]. Additionally, monitoring and regular maintenance should be implemented to ensure the integrity of these metals.

Metals such as mild steel and zinc usually corrode when exposed to acidic solutions because when acid reacts with metals, it breaks down the metal atoms and causes rust [21, 22]. This is because the acid molecules can penetrate the metal's protective layer, making it vulnerable to further corrosion [23]. The presence of oxygen can expedite corrosion by initiating reactions with the metal, leading to additional corrosion [24]. Corrosion usually weakens the metal, reducing its structural integrity. Metal corrosion often leads to the formation of rust [25]. Corrosion can be a severe hazard to humans, apart from harming economies, it can also cause harm to people's health and safety [26].

1.2 Project Rationale

The study of corrosion is vital for numerous reasons. It helps ensure the longevity of materials by guiding the selection of appropriate substances for specific environments, which ultimately extends the lifespan of structures and components. Understanding corrosion is also crucial for safety, as it can lead to structural failures in critical infrastructure, such as bridges and pipelines, posing significant risks to public safety. Economically, corrosion can be incredibly costly due to the need for repairs and replacements, so effective management can save industries substantial amounts of money [27]. Additionally, corrosion can have environmental implications, as it may lead to leaks of harmful substances, impacting ecosystems; thus, studying it helps develop strategies to mitigate these risks. Furthermore, ongoing research into corrosion can result in innovative solutions, such as new protective coatings and materials that are more resistant to deterioration, benefiting various industries. Lastly, many sectors must adhere to regulatory standards regarding material durability and safety, making a solid understanding of corrosion essential for compliance. Corrosion study plays a crucial role in enhancing safety, economic efficiency, and environmental protection across many fields.

This study focuses on mitigating metal corrosion using *A. phylicoides* plant extract as a corrosion inhibitor. *A. phylicoides* plant contains polyphenols, which are antioxidants and anti-inflammatory compounds that can help protect the body from disease [28]. It is also

© University of Venda

known to have antibacterial and antiviral properties, making it beneficial for treating a variety of illnesses and conditions [29]. It is a natural remedy for headaches, stomach aches, and colds. It can be consumed as a tea or applied topically as a paste. There is currently no available data regarding the efficacy of *A. phylicoides* extract in inhibiting metal corrosion. This gap in research highlights the novelty and significance of this study. The *A. phylicoides* extracts were evaluated for their effectiveness in inhibiting metal corrosion in 1.5 M HCl and H_2SO_4. This study can help develop inhibitors that are better suited for different applications and environments by understanding the chemical and physical properties of corrosion inhibitors. This can lead to improved corrosion protection, which can help reduce costs for industries that rely heavily on metals. The success of this study could result in significant cost savings for companies and a reduction in environmental pollution. In this study, the *A. phylicoides* extracts are effective at inhibiting acid corrosion. Furthermore, due to the plant's natural origins, the extracts are environmentally friendly and non-toxic, making them suitable green alternatives to conventional corrosion inhibitors.

Plant-derived inhibitors offer an effective and safe solution to metal corrosion [30]. Research and development of these plant extracts as corrosion inhibitors should be encouraged to reduce the environmental and economic impacts of metal corrosion [31]. Corrosion is a natural process, so understanding how to mitigate corrosion is important to protect infrastructure, reduce the costs associated with maintenance, and repairs, and reduce the release of toxic metals into the environment [32]. Plant-derived inhibitors have proven to be an effective solution to corrosion. Research and development of these inhibitors can help address corrosion more effectively [33]. Alloys and metals are used for different purposes worldwide. Expensive metals are used in modern technology, and protecting these metals is important.

Corrosion prevention methods are crucial. They play a vital role in safeguarding metals' direct costs and indirect impacts [34]. To develop more efficient strategies for combating corrosion and gain a deeper comprehension of the specific mechanisms of corrosion, this kind of research is essential. The first step in developing and implementing a successful strategy to combat corrosion is to comprehend corrosion.

© University of Venda

1.3 Problem Statement

There are several mines and metal-producing companies across African countries [35]. They dominate the industry because of their vast resources, technology, and experience. These companies can extract and process large amounts of minerals, metals, and other resources from the ground efficiently and cost-effectively [36]. Most of these companies are responsible for providing the country with the resources and materials necessary for economic growth and success. These companies are responsible for the production of some of the world's most important commodities such as gold, diamonds, coal, iron ore, platinum, nickel, and zinc. In South Africa, these companies also provide employment opportunities for many South Africans and contribute to the economic growth of the country. The same companies are responsible for most mining and metals production in the region, and their operations are vital to the economic success of the country [37]. Metals are utilized in one way or another worldwide. There are numerous ways in which these metals improve human life. In modern society and international trade, metallic coins like gold and silver play a significant role. It is evident that the metallurgical industry plays a pivotal role in supplying various metals and alloys essential to produce goods [38]. These metals serve diverse purposes, from manufacturing tools and appliances to constructing furniture, electrical devices, vehicles, and more [39]. However, the inherent challenge lies in the fact that these metallic products exist in an unstable high-energy state and inevitably undergo corrosion to revert to a stable low-energy state [40]. Corrosion does not only affect the appearance of metal products but also diminishes their lifespan and performance, thereby compromising their quality. Moreover, when rust particles are washed away, the metal loses weight. Corrosion can incur substantial damage to metal objects, resulting in resource loss and increased expenses for repair or replacement. Furthermore, it poses safety hazards as the corroded metal becomes weak and prone to failure. Hence, it's imperative to prioritize corrosion prevention and control to uphold the integrity of metal objects and extend their lifespan [41].

The repercussions of corrosion are risky and costly, potentially leading to catastrophic events such as building collapses, pipeline ruptures, chemical leaks, and flooding incidents [42]. This electrochemical process occurs due to reactive environments, breaking down the material and causing it to corrode, weaken, and become brittle over time [43]. Corrosion is accelerated by the presence of oxygen, water, and ions, and is often initiated by imbalances in electrical potential between materials [44]. The corrosive process produces chemical

© University of Venda

reactions that weaken the material's molecular bonds, making it susceptible to further degradation [45]. This has wide-ranging consequences, including mechanical damage, environmental pollution, depletion of natural resources, decreased efficiency, increased industry costs, product failures, and safety hazards. Corrosion of metal poses significant global challenges, impacting various materials and industries [46]. Addressing corrosion issues requires proactive measures to prevent and mitigate its detrimental effects, safeguarding assets and the environment.

1.4 Timeline of Significant Corrosion-Related Incidents

A timeline of significant corrosion-related incidents serves as a powerful tool for understanding the past, preparing for the future, and advancing the science and practice of corrosion management. Through learning from history, one can strive towards more sustainable, resilient, and corrosion-resistant infrastructure and technologies, ensuring a safer and more prosperous world for future generations. Here's a timeline of significant corrosion-related incidents across different countries, and industries:

- Oil Industry Disaster - United States, Gulf of Mexico:

Date: April 20, 2010

Description: The Deepwater Horizon oil rig explosion occurred due to a blowout preventer failure caused by corrosion, leading to one of the largest oil spills in history [47].

- Bridge Collapse - Italy, Genoa:

Date: August 14, 2018

Description: The collapse of the Morandi Bridge was attributed to corrosion of the steel cables and structural elements, resulting in multiple fatalities [48].

- Chemical Plant Accident - India, Visakhapatnam:

Date: May 7, 2020

Description: The LG Polymers gas leak incident occurred due to corrosion in storage tanks, releasing toxic gas into the surrounding area, causing several deaths and injuries [49].

© University of Venda

- Pipeline Rupture - Nigeria, Niger Delta:

Date: Various incidents over the years

Description: Corrosion in oil pipelines has led to numerous spills in the Niger Delta region, causing environmental damage and impacting local communities' livelihoods [50].

- Building Collapse - Bangladesh, Dhaka:

Date: April 24, 2013

Description: The Rana Plaza building collapse occurred due to structural failure exacerbated by corrosion of support columns, resulting in significant loss of life in one of the deadliest industrial disasters in history [51]. These incidents highlight the widespread impact of corrosion across different sectors and regions, underscoring the importance of corrosion prevention and maintenance strategies.

1.5 The Scope of Current Research

The scope of the current study involves a comprehensive investigation into the corrosion inhibition effects of *A. phylicoides* leaves extract under various conditions, particularly focusing on its geometric isomerization and functional group dynamics. The research encompasses non-UV and UV radiation treatments of *A. phylicoides* extracts to observe the effects of geometric isomerization. To confirm whether UV radiation induces geometric isomerization or not, Liquid Chromatography-Mass Spectrometry (LC-MS) has been utilized. This technique provided precise confirmation of the isomeric changes occurring in the *A. phylicoides* extract. Additionally, Fourier Transform Infrared Spectroscopy (FTIR) has been employed to identify the functional groups present in the *A. phylicoides* extract and to monitor any changes when the inhibitor adsorbs onto the metal surface. The efficacy of *A. phylicoides* as a corrosion inhibitor has been assessed through several methods. Weight loss measurements have been used to quantify the amount of corrosion over a specified period. Potentiodynamic Polarization (PDP) and Electrochemical Impedance Spectroscopy (EIS) provided detailed insights into the metal's electrochemical behavior and resistance characteristics in the presence and absence of *A. phylicoides* extract. To visually examine the surface morphology of the metal, Scanning Electron Microscopy (SEM) was conducted. This revealed the extent of damage caused by the acidic environment and the smooth, protective

© University of Venda

layer formed by the *A. phylicoides*. Additionally, a wettability study, or contact angle study (WS/CAS), was performed to understand the surface interactions and hydrophobicity induced by the *A. phylicoides* extract layer. Furthermore, computational studies were carried out to explore the energy interactions between the *A. phylicoides* molecules and the metal surface. These studies provide a molecular-level understanding of the bonding and protective mechanisms. This study thoroughly combines experimental and computational techniques to evaluate the corrosion inhibition properties of *A. phylicoides* extract, providing valuable insights into its potential applications in protecting metals from corrosion.

Expectations from each technique to evaluate the potentials of the *A. phylicoides* inhibiting acid corrosion

To determine whether *A. phylicoides* effectively mitigate corrosion, this study expects specific outcomes from each technique employed in the study. Here's what to look for:

- Liquid Chromatography-Mass Spectrometry (LC-MS)

Objective: Confirm geometric isomerization of *A. phylicoides* due to UV radiation.

Expectation: A clear difference in the chromatograms and mass spectra between non-UV and UV-radiated samples, indicating the presence of isomerized compounds.

- Fourier Transform Infrared Spectroscopy (FTIR)

Objective: Identify functional groups present and any changes that occurred upon adsorption.

Expectation: For non-UV-radiated *A. phylicoides* extracts and UV-radiated *A. phylicoides* extracts, distinct peaks corresponding to functional groups like OH, C=O, and C-O are expected. When adsorbed on metal, changes in the intensity or position of these peaks, indicate interaction with the metal surface and formation of a protective layer.

- Weight Loss Measurements

Objective: Quantify the extent of corrosion over time.

Expectation: Lower weight loss in metal samples treated with the *A. phylicoides* compared to untreated samples. This indicates that the *A. phylicoides* effectively reduce the rate of corrosion.

© University of Venda

- Potentiodynamic Polarization (PDP)

Objective: Analyze the electrochemical behavior of the metal.

Expectation: A decrease in the corrosion current density (I_{corr}) in the presence of the *A. phylicoides* extracts. A shift in the corrosion potential (E_{corr}) towards more noble values, indicating a reduction in corrosion activity.

- Electrochemical Impedance Spectroscopy (EIS)

Objective: Measure the impedance and resistance of the metal surface.

Expectation: Higher charge transfer resistance (R_{ct}) values in the presence of the *A. phylicoides* indicate a more protective barrier against corrosion. Increased impedance, suggesting improved protection.

- Scanning Electron Microscopy (SEM)

Objective: Examine surface morphology and damage.

Expectation: For untreated metal: Visible signs of corrosion such as pitting, roughness, and surface degradation. For treated metal: Smoother surface with fewer corrosion features, indicating effective protection caused by *A. phylicoides* extracts.

- Wettability Study /Contact Angle Studies (WS/CAS)

Objective: Assess surface interactions and hydrophobicity.

Expectation: A higher contact angle in the presence of the *A. phylicoides* extract indicates a hydrophobic surface that helps repel corrosive agents. Improved wettability suggests effective surface coverage caused by *A. phylicoides* extract.

- Computational Studies (CS)

Objective: Understand energy interactions and bonding at the molecular level.

Expectation: Strong interaction energies between the inhibitor molecules and the metal surface. Favourable binding geometries indicate that the inhibitor forms a stable and protective layer.

© University of Venda

Observing these specific outcomes from each technique allows evaluation of the effectiveness of *A. phylicoides* as a corrosion inhibitor. Consistent indications of reduced corrosion activity, protective film formation, and favourable surface interactions will demonstrate whether *A. phylicoides* extract is working effectively to mitigate corrosion or not.

1.6 Aims and Objectives of the Study

The *A. phylicoides* plant extract contains antioxidants that help to reduce the rate of oxidation of certain metals, such as mild steel and zinc, which can be corroded by acid. The project aims to find out if the *A. phylicoides* plant extract can help to reduce the rate of acid corrosion of mild steel and zinc.

The objectives are to:

- investigate UV-induced isomerization of metabolites in the leaves extracts of *A. phylicoides* through LC-MS analysis.
- investigate the inhibition of acid corrosion of mild steel and zinc by different isomers of the metabolites found in the *A. phylicoides* leaves extracts using PDP, EIS, and WL.
- use FTIR spectroscopy to characterize the functional groups in the *A. phylicoides* extracts before and after adsorption onto the surface of the metal.
- investigate the surface morphology of the metals using SEM/EDS technique.
- determine relevant quantum chemical parameters that correlate anticorrosion properties to molecular and electronic descriptors.

1.7 Hypothesis

There is a possibility that *A. phylicoides* may be a novel green corrosion inhibitor of mild steel and zinc due to the many chemical constituents it produces. Studies have already shown that *A. phylicoides* demonstrate nontoxicity and are environmentally friendly and consumable by human beings [52]. The hypothesis of this study is "*A. phylicoides* undergo geometric isomerization when exposed to UV radiation and may possess corrosion inhibition properties for both mild steel and zinc in acidic solutions"

© University of Venda

CHAPTER TWO

BACKGROUND OF THE RESEARCH

© University of Venda

2. Background of the Research

Corrosion has long been a persistent challenge in various industries [53]. Despite its inevitability, efforts to mitigate and minimize its impact are crucial. Traditionally, organic inhibitors have been employed to curb metal corrosion, albeit at considerable expense. Recognizing the economic and practical advantages of utilizing natural resources, such as green plant extracts, for corrosion inhibition, researchers have turned their attention to these alternatives [54]. The incorporation of UV radiation into *A. phylicoides* extracts introduce a variable that could either enhance or diminish their effectiveness in corrosion inhibition. UV radiation is known to induce changes in the composition of metabolites present in *A. phylicoides* extracts, potentially altering their corrosion-inhibitive properties [55]. This study aims to explore the potential of UV-radiated *A. phylicoides* extract in mitigating metal corrosion. The findings of this research hold promise for the corrosion management industry, offering potentially cost-effective solutions to the challenges posed by metal degradation. This work provides insights into the efficacy of UV-radiated *A. phylicoides* extract as a corrosion inhibitor, supporting the development of strategies to reduce costly metal replacement and repair due to corrosion damage.

2.1 Corrosion Definition

Metal corrosion is an expensive and serious problem worldwide. The Latin word "Coronus," which means "gnawed away," is the origin of the word "corrosion" [56]. A corrosion phenomenon can be defined as the gradual deterioration of metals or their quantities because of a chemical or electrochemical reaction between exposure environments and materials, typically metals. Corrosion is the destructive outcome of a chemical reaction between metals and the environment [53]. Most studies indicated that metals are not permanently stable, and a process known as corrosion plays a role in their transition back into a more stable state [57]. Material corrosion has been defined by a few researchers as the persistent destruction of material beginning at its surface through electrochemical or unintentional engineered attack [58].

© University of Venda

2.2 Classification of Corrosion

Various types of corrosion exist, each with distinct characteristics visible to the naked eye. Uniform corrosion is the most common type of corrosion resulting from chemical reactions between a material and its environment, causing damage to the metal. Pitting corrosion manifests as localized holes or pits on the metal surface due to corrosion. Crevice corrosion occurs in confined spaces or cracks where corrosive agents accumulate. Galvanic corrosion arises when dissimilar metals encounter an electrolyte solution, accelerating the corrosion of one metal. Environmental cracking, or stress corrosion cracking, results from a combination of mechanical stress and corrosive elements in the environment, leading to material cracking. Fretting corrosion, caused by repeated surface rubbing or vibration, contributes to material wear and damage. Each type requires specific attention and mitigation strategies to preserve material integrity and prevent structural degradation [59]. A brief explanation of each corrosion type is as follows.

Uniform corrosion: This type occurs when a metal corrodes evenly across its surface due to chemical reactions with the environment, such as metal reacting with oxygen. It's common in materials like mild steel or zinc, degrading through electrochemical or chemical reactions that uniformly corrode the surface. This oxidation process is predictable and can be prevented, though the rate of corrosion depends on environmental factors and the metal type [60].

Pitting corrosion: Unlike uniform corrosion, pitting corrosion is localized and caused by uneven distribution of electrolytes, like saltwater, on the metal surface. This leads to faster corrosion in specific areas, weakening the metal structure. Pitting corrosion can cause significant damage if not addressed promptly, as the corroded areas act as sites for further deterioration [61].

Crevice corrosion: Another form of localized corrosion. Crevice corrosion occurs in tight spaces where access to the environment is restricted. It often happens at joints, couplings, or beneath deposits, leading to further damage if not addressed. Crevice corrosion poses challenges in detection and management due to its hidden nature and limited accessibility [62].

Galvanic Corrosion: When two metals with different electrical potentials come into contact in the presence of an electrolyte, the metal with the lower potential (the more reactive metal) acts as the anode and corrodes, while the other serves as the cathode. The electrolyte

© University of Venda

facilitates ionic conduction, allowing the corrosion process to occur as electrons flow from the anode to the cathode through the metal path. This leads to the breakdown of the more reactive metal, which undergoes oxidation. The presence of an electrolyte expedites corrosion, particularly when there's a substantial difference in electrochemical potentials between the metals [63].

Environmental Cracking: Often observed in carbon steel exposed to adverse conditions, environmental cracking occurs when a material's surface encounters a corrosive environment, such as salt water, combined with mechanical stress. This stress leads to microscopic crack initiation, allowing corrosive agents to penetrate and accelerate corrosion. Thin steel components under cyclic loading in corrosive conditions are particularly vulnerable, with cumulative cracking posing a significant risk of material failure. The corrosive environment weakens the steel structure, while cyclic loading exacerbates stress, promoting crack propagation and eventual material failure [64].

Flow-Aided and Intergranular Corrosion: Over time, wind or water movement disintegrates the protective oxide film on metal surfaces, rendering subsequent layers more susceptible to corrosion. Intergranular corrosion targets metal grain edges due to contamination, with grain boundaries serving as conduits for impurity diffusion and subsequent degradation. High temperatures further accelerate this corrosion by hastening impurity diffusion along grain boundaries [65].

Fretting Corrosion: Caused by cyclic loads and micro-movements between materials in contact, fretting corrosion produces a brittle oxide layer due to repeated frictional wear. This layer is prone to cracking, exposing fresh metal surfaces to further oxidation and accelerating corrosion. Environmental contaminants, such as moisture or salts, can act as catalysts, intensifying the corrosion process. As vibrations dislodge parts of the oxide layer, accumulated corrosion products contribute to material degradation and potential failure [66].

Corrosion at Elevated Temperatures: Corrosion at high temperatures may result from oxidation, sulphuration, carbonization, or vanadium-containing fuels. Sulphate can form sulphuric acid upon contact with water or other acids, damaging the protective oxide layer on carbon steel and inducing corrosion [67].

Soil Erosion: Dampness and oxygen in soil form electrolytic cells, accelerating corrosion of steel, particularly in moist, electrically conductive, acidic soils with dissolved salts. Water

© University of Venda

and oxygen react with carbon steel, expediting corrosion, particularly when other factors like acidity, salts, and electrical conductivity are present. Understanding and managing these factors can mitigate the costly consequences of carbon steel corrosion [68].

2.3 Thermodynamics and Kinetics of Corrosion

The study of corrosion encompasses thermodynamics and kinetics, which are fundamental aspects governing the process. In thermodynamics, the focus lies on understanding whether a corrosion process will occur spontaneously under specific conditions. This involves parameters such as Gibbs Free Energy (ΔG), Standard Electrode Potential (E°), and the use of Pourbaix diagrams to illustrate the stability of chemical species in aqueous environments relative to pH and electrode potential [69].

Thermodynamics and kinetics are crucial in understanding corrosion reactions [70]. Thermodynamics elucidates energy changes associated with corrosion reactions, while kinetics delves into the reaction mechanism and its rate of progression [70]. Through employing kinetics, one can gauge the speed of corrosion and predict its onset. This branch of study considers various factors such as the reaction's energy, free energy of activation, transport of reactants and products, reactant solubility, ion diffusion rates in solution, and more. Understanding these properties aids in estimating corrosion rates under diverse conditions. Corrosion kinetics analyses corrosion rate concerning material properties, environmental factors, and chemical constituents [71]. It also scrutinizes factors like reactant polarization and the impact of corrosion inhibitors or accelerants. This comprehensive understanding enables the prediction of corrosion likelihood and the identification of conditions conducive to its occurrence. Furthermore, the evaluation of coating system corrosion kinetics, including potential coating thicknesses over time, can be achieved through polarization resistance techniques like linear and potentiodynamic approaches. Comprehending thermodynamics and kinetics of corrosion is vital for developing effective corrosion control strategies [72]. This knowledge allows engineers and scientists to design materials and coatings that mitigate corrosion, thereby prolonging the lifespan of metal components across various applications.

© University of Venda

2.4 The Rate of Corrosion

The corrosion rate is typically gauged by measuring the weight loss of the metal. This rate is influenced by various factors including the surrounding environment, temperature, and the specific type of metal undergoing corrosion. Corrosion, fundamentally, is a chemical reaction wherein metal atoms are displaced by ions from the environment, resulting in a gradual breakdown over time. Its pace is contingent upon the environmental conditions, the metal's composition, and the duration of exposure. Corrosion rate serves as a crucial metric, quantifying the amount of molecular mass lost per unit time and providing insights into the metal's susceptibility to degradation.

Mild steel, often chosen for its ready availability, contrasts with zinc, which boasts superior corrosion resistance, particularly suitable for outdoor applications like roofing. Mild steel, containing iron, exhibits heightened susceptibility to corrosion due to iron's reactivity with the environment. In contrast, zinc's protective attributes make it an ideal choice for structures exposed to the elements. The absence of a robust passive film, which shields against corrosion, renders mild steel and zinc more vulnerable. Mild steel and zinc, lacking this protective mechanism to the same degree, experience a more rapid breakdown of any formed passive films when exposed to aggressive environments, hastening the onset of corrosion [74].

2.5 Aspects Affecting Corrosion Rate

Apart from diffusion, various factors contribute to the speed of metal corrosion, this includes temperature, substance type, acidity, and electrical potential [73]. Temperature plays a pivotal role as it influences molecular diffusion rates, thereby impacting corrosion kinetics. The type of substance and its acidity dictate the nature of the metal-environment interaction, influencing corrosion behavior. Electrical potential is also significant, as it can trigger electrochemical reactions that accelerate corrosion processes. To mitigate corrosion, protective measures such as applying coatings or corrosion inhibitors can be employed. Adjusting the pH of the environment can also curb corrosion rates. Utilizing specialized materials or techniques to counter rust or damage can effectively impede or prevent corrosion [74]. This study will explore the multifaceted elements influencing corrosion rates to gain comprehensive insights into corrosion phenomena.

© University of Venda

2.5.1 The Role of Diffusion in Metal Degradation and Corrosion Kinetics

Diffusion plays a significant role in determining the rate of metal degradation, primarily by influencing the movement of chemicals towards or away from the metal surface. In the initial stages, when steel surfaces are devoid of rust, they are more susceptible to corrosion compared to surfaces with existing rust layers [21]. The accessibility of oxygen to the steel surface, facilitated by water, is crucial in regulating the pace of rust formation. Corrosion tends to occur more rapidly in areas where oxygen diffusion is efficient. For instance, in locations where water flows swiftly, such as near the inlet of a pipe, corrosion can accelerate due to higher oxygen levels in the water. Interestingly, corrosion can paradoxically expedite rust formation on metal surfaces. Metals covered by a thin, moist layer capable of conducting electricity exhibit faster rusting rates than those fully submerged underwater. This underscores the complex interplay between environmental factors and corrosion kinetics in metal degradation processes [75].

2.5.2 Temperature's Influence on Corrosion Kinetics in Metal Interactions

Temperature plays a crucial role in the kinetics of corrosion, significantly affecting the rate at which metals corrode when exposed to various environments. As temperature increases, the rate of chemical reactions typically accelerates, including those that contribute to corrosion processes [76]. This is because higher temperatures provide more energy to the reacting molecules, increasing their kinetic energy and, consequently, the frequency and intensity of collisions between them. In metal interactions, elevated temperatures can enhance the dissolution rate of the metal, accelerate the oxidation process, and increase the solubility of corrosive agents such as oxygen and salts in the electrolyte. Furthermore, higher temperatures can also influence the formation and stability of protective films on metal surfaces [77]. For instance, passive films that form on metals like stainless steel may become less stable or even break down at elevated temperatures, leading to increased corrosion rates. Conversely, in some cases, increased temperature can enhance the formation of protective layers, depending on the specific metal and environment. Understanding the temperature dependence of corrosion kinetics is essential for predicting the lifespan of metal components and developing effective corrosion prevention strategies, particularly in industries where equipment operates under high-temperature conditions [78].

© University of Venda

Increase in temperature: Generally, higher temperatures often result in an acceleration of corrosion reactions [389]. This is due to the increased kinetic energy of the reacting particles, which can facilitate more frequent and energetic collisions between the metal surface and corrosive species [390]. The higher temperature can enhance the corrosion rate, leading to an increase in weight loss [391]. It is important to note that these trends may not hold universally for all metals and acid systems. The corrosion behavior can be influenced by various factors, including the specific metal, the type and concentration of acid, the presence of impurities, and the nature of the metal surface.

2.5.3 The Role of Conductivity in Accelerating Metal Corrosion: Implications for Environmental Factors

Conductivity plays a pivotal role in the acceleration of metal corrosion, acting as a critical factor in the electrochemical processes that drive corrosion reactions [79]. High conductivity in an environment indicates a greater ability to carry electric current, which facilitates the movement of ions necessary for the electrochemical reactions involved in corrosion. In aqueous environments, the presence of dissolved salts, acids, or bases increases the conductivity of the solution, enhancing the rate of corrosion. This is because the ionic species in the solution act as electrolytes, providing a conductive path for electron transfer and facilitating the anodic and cathodic reactions that lead to metal degradation [80].

Environmental factors such as salinity, humidity, and temperature can significantly influence the conductivity of the surrounding medium. For instance, coastal areas with high salinity levels have environments with higher conductivity, which can lead to more severe corrosion of metal structures. Similarly, industrial areas with high levels of pollutants can create acidic conditions that increase the conductivity of rainwater, accelerating corrosion rates. Temperature also plays a role; higher temperatures can increase the solubility of ionic species in water, thereby enhancing its conductivity and corrosion rate [81].

Understanding the role of conductivity in metal corrosion is essential for developing effective corrosion prevention and control strategies. It underscores the importance of environmental monitoring and the implementation of protective measures such as coatings, corrosion inhibitors, and cathodic protection. Mitigating factors that increase conductivity enables industries to extend the lifespan of metal structures and components, reduce maintenance costs, and prevent catastrophic failures [82].

© University of Venda

2.5.4 The Influence of Ionic Composition on Metal Corrosion in Maritime and Industrial Environments

The ionic composition of an environment profoundly impacts the rate and extent of metal corrosion, particularly in maritime and industrial settings. In maritime environments, seawater contains a high concentration of various ions such as sodium (Na^+), chloride (Cl^-), magnesium (Mg^{2+}), and sulphates (SO_4^{2-}). These ions act as electrolytes, facilitating electrochemical reactions that drive the corrosion process. Chloride ions are particularly aggressive, penetrating protective oxide layers on metal surfaces and leading to localized pitting corrosion. The presence of chloride accelerates the anodic dissolution of metals, making it one of the most significant contributors to corrosion in marine settings [83].

In industrial environments, the ionic composition can vary widely depending on the specific processes and pollutants presence. Industrial effluents often contain acids, bases, and salts that increase the ionic strength of water. For example, H_2SO_4 and HCl are common in industrial wastes and can significantly lower the pH of water, enhancing its corrosive potential. The high concentration of hydrogen ions (H^+) in acidic conditions accelerates the anodic dissolution of metals, while sulphate and nitrate ions can also contribute to the formation of corrosive compounds on metal surfaces [84].

The combined effect of various ions in these environments leads to complex corrosion mechanisms. In maritime settings, the presence of dissolved oxygen (O_2) further exacerbates corrosion by participating in the cathodic reduction process [84]. In industrial environments, pollutants such as ammonia (NH_3) and sulphides (S^{2-}) can form corrosive intermediates that attack metal surfaces. The synergistic interaction between different ions often results in a more aggressive corrosion environment, necessitating robust corrosion control measures.

Understanding the influence of ionic composition on metal corrosion is crucial for developing effective corrosion prevention strategies. In maritime environments, protective coatings, cathodic protection, and the use of corrosion-resistant alloys are commonly employed. In industrial settings, neutralizing acidic effluents, implementing proper waste treatment procedures, and using inhibitors can mitigate corrosion [85]. Industries can enhance the durability and lifespan of metal structures, reducing maintenance costs and preventing failures by controlling the ionic composition and understanding its effects [86].

© University of Venda

2.5.5 pH Dynamics: Implications for Corrosion Risk Assessment and Maintenance Strategies

The pH scale serves as a tool for discerning the acidity or alkalinity of a solution, ranging from 1 to 14. A pH of 7 indicates neutrality, with an equal balance of acidic and alkaline molecules present [87]. When oxygen dissolves in water, it can react with iron, causing it to dissolve as well. However, if oxygen reacts with other substances and generates hydroxyl ions instead, it prevents iron from dissolving. In acidic environments where the pH decreases, hydrogen ions outnumber hydroxyl ions. Steel may corrode more rapidly in acidic environments due to the ease with which hydrogen ions and gas can permeate through it. When transporting substances like pet coke, sulphur, or sour crude oils, surrounding metals can be affected. Steel remains protected from corrosion in basic environments with abundant hydroxyl ions and a high pH level of 14 [88]. In certain scenarios, such as within ballast tanks, blisters containing a liquid with high acidity can be found, particularly in the lower sections of tanks with double layers. Removing the blister caps may reveal a shiny steel surface underneath. If the liquid inside one or more blisters is alkaline, it's essential to inspect the remaining blisters in the group, as they could sustain damage upon opening [89]. Understanding pH dynamics is crucial for assessing corrosion risks and implementing appropriate maintenance measures to safeguard metal structures [89].

2.5.6 Electrochemical Potential: Understanding Corrosion Propensity and Protection Strategies

It is crucial to understand the concept of electrochemical potential and its role in determining the propensity of metals to corrode and the strategies available for corrosion protection. Electrochemical potential, often measured in a conductive fluid or electrolyte, is a fundamental property that defines how a metal interacts with its environment [90]. Each metal exhibits a unique electrochemical potential, which can be measured against a reference cathode—typically metals such as zinc, copper, or iron. To determine the corrosion propensity of a metal, its half-cell potential is measured in comparison to the reference cathode, which is immersed in a solution with known activity [91]. This comparison provides insight into the metal’s tendency to undergo oxidation and reduction reactions, which are integral to the corrosion process. The reference cathode serves as a standard benchmark, ensuring the accuracy and reliability of the potential measurements. Understanding the electrochemical potential is pivotal in predicting both the likelihood and rate of corrosion. Metals with higher

© University of Venda

tendencies to lose electrons (more negative potentials) are more prone to corrosion [73]. This knowledge allows for the implementation of effective corrosion protection strategies, such as galvanic corrosion control and cathodic protection. Galvanic corrosion occurs when two dissimilar metals are electrically connected in a conductive environment, leading to the accelerated corrosion of the more anodic metal (the one with a more negative electrochemical potential). Through carefully selecting compatible metal pairs and using insulating materials or coatings, galvanic corrosion can be mitigated.

Cathodic protection is another critical strategy, involving the application of an external electrical potential to shift the metal's potential in a more negative direction, thus reducing its tendency to corrode. This can be achieved through sacrificial anodes, which are more anodic metals that corrode preferentially or impressed current systems, where an external power source supplies the protective current. In both galvanic and cathodic protection methods, the alteration of the metal's potential is key to preventing or minimizing corrosion [41, 16]. These strategies not only extend the service life of metal structures but also ensure safety and reduce maintenance costs in various industries [86].

2.6 Impact of Corrosion

This section addresses three primary effects of corrosion: the financial burdens associated with repairing corrosion damage, the potential for life-threatening accidents, and the environmental damage inflicted on ecosystems. Corrosion significantly impacts the economies of industrialized nations, resulting in substantial expenses [92]. Annually, both direct and indirect costs are incurred due to corrosion. Machine or system failures, deviating from established specifications or norms, are among the consequences of corrosion. Extensive studies on failure patterns have identified six fundamental trends, informing maintenance strategies and operational protocols. The chapter provides examples illustrating failures attributed to corrosion. While many corrosion challenges are common across various sectors, some are unique to the nuclear industry. Environmental pollution resulting from corrosion contributes to adverse effects such as acid rain, the greenhouse effect, and depletion of the ozone layer. Corrosion exerts detrimental effects on our society's economy, health, safety, technology, and cultural heritage [93].

© University of Venda

2.6.1 Corrosion Effects on Health

Metal implants like hip joints, pacemakers, pins, and other prosthetic devices have become increasingly common in recent years. Despite advancements in implantation techniques and the development of new alloys, corrosion remains a significant concern. Examples of issues resulting from corrosion include inflammation in the tissue surrounding implants, failures due to faulty connections in pacemakers, and fractures in weight-bearing prosthetic devices [94]. Additionally, the use of metal hip joints illustrates how they address some of the challenges associated with arthritic hips [95]. Due to their improved durability, hip joints, previously reserved for individuals over 60, are now being used by younger patients thanks to recent enhancements. Addressing corrosion in medical devices, infrastructure, and environmental systems is essential for safeguarding public health and minimizing the associated risks and health impacts [96].

2.6.2 Corrosion's Impact on Safety: Risks Across Gas Pipelines, Vehicles, Aircrafts, and More

Corrosion presents a widespread safety concern across various sectors, including gas pipelines, automotive, aviation, and other metal structures [27]. Its potential to weaken or compromise structural integrity can result in catastrophic failures, endangering human lives and property [5]. Gas pipeline leaks from corrosion can lead to explosions or fires, threatening communities. In vehicles, corrosion in critical components like brake lines can cause accidents. Similarly, in airplanes, corrosion weakens structures, risking in-flight failures. Preventive measures such as regular inspections, corrosion-resistant materials, and advanced monitoring technologies are vital for ensuring safety amidst corrosion challenges [97].

2.6.3 Technological Corrosion: Impacts and Economic Ramifications

Corrosion presents significant challenges to technological advancement, affecting various industries by compromising the integrity and longevity of materials and systems [97]. The impact of corrosion is particularly pronounced in environments where materials are exposed to high temperatures and pressures. Such conditions heighten the risk of material degradation, posing severe safety hazards for personnel and equipment. Corrosion can lead to structural failures, necessitating extensive repairs or replacements, which incur substantial costs. Additionally, the downtime associated with these repairs can disrupt operations, leading to

© University of Venda

further economic losses [5].

The economic ramifications of corrosion are far-reaching industries like oil and gas, chemical processing, and power generation, which operate under extreme conditions, bear the brunt of these costs. Corrosion-related failures can halt production, causing not only direct financial losses due to halted operations but also potential secondary costs such as environmental cleanup, legal liabilities, and loss of reputation [98]. Preventative measures, while initially costly, are essential investments to mitigate these risks. Effective corrosion management strategies, including the use of resistant materials, protective coatings, and regular maintenance, can significantly reduce the incidence of corrosion and its associated economic burden [99].

Addressing corrosion is critical for ensuring the reliability and safety of technological systems. The economic implications of corrosion extend beyond immediate repair costs to include operational downtime and broader financial impacts [100]. Through investing in advanced materials and preventative strategies, industries can safeguard their infrastructure, protect their workforce, and minimize economic losses.

The progression of technology often faces obstacles due to corrosion issues, especially as materials are required to withstand elevated temperatures and pressures, thereby increasing safety risks for personnel. Systems functioning under such conditions necessitate materials that are resistant to corrosion induced by high temperatures and fluid pressures. Additionally, these materials must endure prolonged exposure to hot circulating heat transfer fluids without degrading. Failure to address these issues can lead to substantial damage to drilling infrastructure, necessitating expensive repairs and potentially causing operational shutdowns. Ensuring the safety of personnel and equipment demands the implementation of effective corrosion prevention strategies. If not properly managed, corrosion can cause structural weakening and failure, resulting in catastrophic events such as explosions, fires, pollution, and operational interruptions. The resulting costs encompass not only repairs and part replacements but also the financial impact of lost production [100].

2.6.4 The Impact of Corrosion on Cultural Heritage

Corrosion poses a significant threat to cultural heritage, affecting a wide array of historical artifacts, monuments, and structures. Cultural heritage, encompassing artifacts made from various metals and alloys, often suffers from corrosion when exposed to environmental factors such as humidity, pollution, and fluctuating temperatures. This degradation process not only

© University of Venda

diminishes the aesthetic and historical value of these objects but can also lead to their destruction if left unchecked [101]. Historic buildings, sculptures, and monuments crafted from materials like bronze, iron, and copper are particularly vulnerable. For example, iconic structures such as the Statue of Liberty and ancient bronze statues have experienced corrosion, requiring extensive and meticulous conservation efforts to prevent further damage. The patina that forms on these surfaces, while sometimes considered aesthetically pleasing, can mask deeper, more destructive corrosion processes that undermine the structural integrity of the artifacts.

Museums and cultural institutions face significant challenges in preserving metal artifacts. The delicate balance between displaying these items and protecting them from corrosive environments demands innovative conservation strategies. Controlled environments with regulated humidity and temperature, protective coatings, and regular maintenance are crucial in mitigating the effects of corrosion [102].

The economic implications of corrosion on cultural heritage are substantial. Restoration and conservation projects require significant financial investment, often sourced from public funds, private donations, and governmental grants. The cost of preserving cultural heritage can strain resources, particularly in regions where funding is limited. Moreover, the loss of cultural heritage due to corrosion has a profound impact on communities and societies, eroding a sense of identity and continuity with the past.

In short, corrosion significantly impacts cultural heritage, threatening the preservation of invaluable historical artifacts and structures [103]. Effective conservation efforts are essential to protect these treasures from the ravages of time and environmental exposure. Investing in advanced preservation technologies and raising awareness about the importance of cultural heritage conservation help societies safeguard their history for future generations.

2.7 Understanding the Economic Impact of Corrosion and the Benefits of Preventive Measures

The direct expenses linked with corrosion encompass annual expenditures on maintenance and repair, alongside various control techniques such as coatings, linings, chemical treatments, cathodic protection, corrosion-resistant alloys, and non-metallic materials [103]. Additionally, costs related to inspections and testing contribute to the overall corrosion expense. Corrosion presents a significant challenge for most industrialized nations. Its ramifications include

© University of Venda

compromised structural integrity, heightened maintenance outlays, potential hazardous leaks, production interruptions, and diminished system longevity when designing industrial equipment or infrastructure [104]. Thus, it is imperative to account for these factors during the design, construction, and maintenance phases. Despite substantial investments by oil companies worldwide to combat corrosion, it remains a formidable issue with potentially devastating consequences. Heightened awareness and proactive measures are essential to mitigate the risk of corrosion-related disasters. Corrosion-induced failures can impact a wide array of components, including boilers, pressure vessels, motor and turbine blades, chemical containers, aircraft components, and vehicle routing systems. Furthermore, corrosion's impact extends beyond metallic surfaces, encompassing increased energy consumption due to maintenance and repair needs and adverse effects on water quality from chemical releases. The associated costs entail not only structural repairs but also labour, materials, and other resources [105]. Notably, these expenses can vary significantly across countries, influenced by infrastructure levels, resource availability, and regulatory frameworks. Therefore, conducting thorough research on labour and material costs specific to a given country is crucial before initiating any repair projects to ensure adherence to budgetary constraints. Studies have estimated the global cost of corrosion at 4.2 trillion US dollars, with the World Bank highlighting potential cost reductions of up to 25% through preventive measures [106]. Consequently, investing in corrosion prevention emerges as a strategic approach to alleviate the economic burden of corrosion on a global scale [107].

Table 2.1: Various countries Gross Domestic Product because of corrosion of materials [15]

Economic Regions	**Sector**					
	Agriculture	**Industry**	**Services**	**Total**	**Total GDP**	**%GDP**
United states	2	303.2	146	451.3	16270	2.7
India	17.7	20.3	32.3	70.3	1670	4.2
European Region	3.5	401	297	701.5	18331	3.8
Arab world	13.3	34.2	92.6	140.1	2789	5
China	56.2	192.5	146.2	394.9	9330	4.2
Russia	5.4	37.2	41.9	84.5	2113	4
Japan	0.6	45.9	5.1	51.6	5002	1
Four Asian Tigers Plus Macau	1.5	29.9	27.3	58.6	2302	2.5
Rest of the world	52.4	382.5	117.6	552.5	16057	3.4
Global	152.7	1446.7	906	2505.4	74314	3.4

© University of Venda

2.8 Strategies for Understanding and Mitigating Metal Corrosion in Various Environments

To ensure long-term and reliable operation in various environments, it is crucial to understand corrosion and its effects on products and systems. Selecting the appropriate material for a specific application can significantly minimize corrosion-related deterioration and component failure. The factors influencing a liquid's ability to corrode metals include [18]:

- Oxygen, chloride, and sulphur dioxide content
- Temperature
- pH level

Key anti-corrosion strategies include [108]:

- Selecting suitable materials
- Designing the product appropriately
- Implementing preventative measures (such as coatings and anodes)
- Ensuring proper installation and maintenance
- Conducting testing, development, and research

2.8.1 Corrosion of Mild Steel: Applications and Importance

Mild steel, composed primarily of iron with a small amount of carbon, is widely used in various industries due to its affordability and mechanical properties. However, mild steel is highly susceptible to corrosion, which is a chemical or electrochemical reaction between the metal and its environment that leads to the degradation of its properties [109]. Corrosion can significantly impact the performance, safety, and lifespan of mild steel components. The corrosion process in mild steel is influenced by several factors, including oxygen content, chloride ions, sulphur dioxide, temperature, and pH level. The presence of oxygen in the environment accelerates the oxidation process, leading to the formation of rust [109]. Chlorides, commonly found in saltwater environments, promote pitting corrosion, creating small, deep pits on the steel surface. Sulphur dioxide in the atmosphere can react with water to form sulphurous acid, which corrodes steel. Higher temperatures generally increase the rate of corrosion, and acidic environments (low pH) significantly enhance the corrosion rate of mild steel [110].

To combat corrosion, several anti-corrosion techniques are employed. These include the

© University of Venda

selection of suitable materials, using alloys or materials more resistant to corrosion. Design considerations involve designing products to minimize exposure to corrosive elements. Preventative measures include applying protective coatings, such as paints or galvanization, and using sacrificial anodes. Proper installation and maintenance ensure correct installation and regular maintenance to prevent corrosion [111]. Additionally, testing and research involve conducting thorough testing and continuous research to develop better corrosion-resistant materials and coatings. Mild steel's versatility makes it a preferred material in numerous applications. It is widely used in the construction industry for structural components, beams, and reinforcements due to its high tensile strength and malleability. In the automotive industry, it is employed in the manufacture of car bodies, frames, and other components because of its weldability and durability. It is utilized in the production of various machinery parts and equipment, including gears, shafts, and frames. Mild steel is also used in the construction of pipelines and storage tanks for its strength and resistance to pressure [112]. Additionally, it is found in many household items, such as cookware, cutlery, and appliances, due to its ease of fabrication and cost-effectiveness.

Mild steel's importance stems from its combination of properties and economic benefits. It is cost-effective, making it accessible for large-scale use in various industries. It offers a good balance of strength, ductility, and toughness, making it suitable for structural applications. Mild steel can be easily welded, machined, and formed into different shapes and sizes, providing flexibility in manufacturing. It is readily available in various forms and grades, ensuring a consistent supply for industrial needs. Furthermore, mild steel is recyclable, contributing to sustainable practices and reducing environmental impact.

Despite its susceptibility to corrosion, mild steel's widespread applications and advantages underscore its critical role in modern industry [113]. Addressing the challenges of corrosion through protective measures and innovative materials ensures its continued relevance and reliability in diverse applications.

2.8.2 Corrosion of Zinc: Applications and Importance

Zinc is a metal widely known for its excellent corrosion resistance. Unlike many other metals, zinc forms a protective oxide layer on its surface when exposed to the atmosphere. This layer, primarily composed of zinc carbonate, acts as a barrier that slows down the corrosion process, thereby extending the metal's lifespan [114]. However, zinc is not completely immune to corrosion, especially in environments containing high levels of sulphur dioxide, chloride ions,

© University of Venda

or acids. When zinc is exposed to such corrosive agents, it can undergo galvanic corrosion, particularly if it is in contact with more noble metals. This is because zinc acts as a sacrificial anode in galvanic cells, corroding preferentially to protect the other metal. The rate of zinc corrosion is also influenced by environmental factors such as temperature and humidity [115].

Zinc's corrosion-resistant properties make it an ideal material for various applications. One of its primary uses is in the galvanization of steel and iron, a process where a protective zinc coating is applied to prevent rusting. This is common in the construction industry, where galvanized steel is used for roofing, gutters, and structural beams. In the automotive industry, zinc is used to coat parts such as body panels, which helps to prevent rust and extend the vehicle's lifespan. Zinc alloys, such as brass (an alloy of zinc and copper), are used in a wide range of applications including plumbing fittings, musical instruments, and hardware due to their durability and corrosion resistance [39]. Additionally, zinc is employed in the manufacture of batteries, particularly alkaline and zinc-carbon batteries, where it serves as an anode material. Zinc oxide, a compound derived from zinc, is widely used in the production of rubber, ceramics, and cosmetics due to its anti-corrosive and antimicrobial properties [116] [117].

Zinc plays a crucial role in numerous industries due to its unique properties [118]. Its ability to form a protective barrier makes it invaluable for preventing corrosion and prolonging the life of steel and iron structures, thereby reducing maintenance costs and enhancing safety. Zinc's versatility as an alloying element enables the creation of materials with improved mechanical properties and resistance to environmental degradation. In the automotive industry, the use of zinc-coated components helps to maintain vehicle integrity and performance over time. The widespread application of zinc in battery production supports the energy sector by providing reliable and efficient energy storage solutions [119]. Furthermore, zinc's presence in various consumer products, from cosmetics to healthcare items, underscores its significance in everyday life.

The environmental benefits of zinc should also be noted. Zinc is 100% recyclable, and recycling zinc products reduces energy consumption and greenhouse gas emissions compared to primary production [120]. This contributes to sustainable development practices and lessens the environmental footprint of zinc usage. Zinc's corrosion resistance, versatility, and recyclability make it an essential material in modern industry and an important factor in the development of sustainable practices [120].

© University of Venda

2.9 Corrosion Prevention Methods

Corrosion prevention is crucial to ensuring the longevity and reliability of metal structures and components. Effective corrosion prevention methods can significantly reduce maintenance costs, improve safety, and extend the service life of materials [121]. Here are several key methods used to prevent corrosion:

2.9.1 Material Selection

Selecting appropriate materials is the primary defense against corrosion. Metals with natural corrosion resistance, such as stainless steel, aluminum, and specific alloys, are commonly chosen for environments prone to corrosion [122]. It's essential to consider the specific environmental conditions, including humidity, temperature, and the presence of corrosive agents, when choosing materials. This approach emphasizes the importance of understanding the environmental conditions to which materials will be exposed [123]. It is important to combine material selection with other protective measures, such as coatings and inhibitors, for optimal corrosion prevention. Selecting the right materials is a crucial step in mitigating corrosion. Here's a breakdown of the points made:

Inherent Corrosion Resistance: Some metals, like stainless steel, aluminum, and specific alloys, have natural corrosion resistance. For instance, stainless steel contains chromium, which forms a protective oxide layer, and aluminum also forms an oxide layer that protects it from further oxidation [124].

Environmental Considerations: The specific environmental conditions (such as humidity, temperature, and presence of corrosive agents) play a significant role in material selection. Different environments pose different corrosion risks, and materials must be chosen based on their performance in these conditions [125].

Alloying: The process of alloying, which involves adding elements like chromium, nickel, and molybdenum, can enhance a material’s resistance to corrosion. This makes the base metal more durable in harsh environments [126].

Coatings and Surface Treatments: Applying protective coatings and surface treatments can provide an additional layer of defence against corrosion. These methods can significantly extend the life of the base material by preventing direct exposure to corrosive elements.

Balance of Factors: Material selection is a balance of corrosion resistance, cost, mechanical properties, and environmental impact. For example, while stainless steel is highly resistant to

© University of Venda

corrosion, it might not always be the most cost-effective option for every application. Hence, engineers must weigh the benefits and drawbacks of each material based on the specific application requirements [127]. The principles discussed about material selection for corrosion resistance are accurate and reflect standard practices in engineering and materials science. These strategies help ensure the longevity and reliability of components and structures in various industrial and environmental settings.

2.9.2 Protective Coatings

Applying protective coatings to metal surfaces is a common and effective method to prevent corrosion. These coatings act as barriers, preventing corrosive substances from coming into direct contact with the metal. Common types of coatings include:

- Paints and Varnishes: These are used to create a physical barrier that prevents moisture and air from reaching the metal surface.
- Galvanization: This involves coating steel or iron with a layer of zinc, which acts as a sacrificial anode and protects the underlying metal.
- Powder Coating: This method involves applying a dry powder that is cured under heat to form a hard, protective layer.
- Epoxy Coatings: These provide excellent resistance to chemicals and moisture, making them suitable for harsh environments [127].

2.9.3 Cathodic Protection

Cathodic protection is a technique used to control the corrosion of a metal surface by making it the cathode of an electrochemical cell. There are two main types of cathodic protection:

- Sacrificial Anode: This method involves attaching a more reactive metal (anode) to the metal structure. The anode corrodes instead of the protected metal, thus preserving it.
- Impressed Current: This system uses an external power source to provide a constant electrical current, which protects the metal structure from corrosion [128].

2.9.4 Corrosion Inhibitors

Corrosion inhibitors are chemicals that, when added to a corrosive environment, decrease the rate of metal corrosion. They can be used in various industries, including oil and gas, water treatment, and cooling systems. These inhibitors work by forming a protective film on the

© University of Venda

metal surface or by neutralizing corrosive agents [129].

2.9.5 Environmental Control

Controlling the environmental factors that contribute to corrosion can also be an effective prevention strategy. This includes:

- Reducing Humidity: Using dehumidifiers and maintaining proper ventilation can reduce moisture levels, thereby minimizing corrosion.
- Temperature Control: Maintaining stable temperatures and avoiding extreme fluctuations can prevent thermal stress and condensation.
- pH Control: Adjusting the pH of the environment to neutral or slightly alkaline levels can reduce the corrosiveness of acidic or basic conditions [130].

2.9.6 Design Considerations

Proper design can minimize the risk of corrosion by avoiding features that trap moisture or corrosive agents. Design considerations include :

- Drainage: Ensuring that water and other liquids can drain away from the structure.
- Accessibility: Designing structures for easy maintenance and inspection.
- Avoiding Dissimilar Metals: Using metals that are compatible to prevent galvanic corrosion [41].

2.9.7 Regular Maintenance

Regular maintenance and inspection are essential for early detection and mitigation of corrosion. This includes cleaning surfaces, repairing damaged coatings, and monitoring for signs of corrosion. Industries can protect their assets, reduce downtime, and ensure the safety and reliability of their operations by implementing these corrosion prevention methods [131].

2.10 Advantages of Using Corrosion Inhibitors in Industrial Applications

This study focuses on mitigating corrosion by using corrosion inhibitors. The reason for choosing corrosion inhibitors instead of other methods is due to several reasons, as these substances offer a practical and efficient way to combat the damaging effects of corrosion on

© University of Venda

metals. Corrosion inhibitors can be a cost-effective solution compared to other methods such as material replacement or extensive use of protective coatings [132]. They reduce the need for frequent maintenance and replacement of corroded parts, thereby saving costs in the long run. Corrosion inhibitors can be used in a wide range of environments and applications, including industrial processes, water treatment systems, oil and gas pipelines, and cooling systems [133]. This versatility makes them suitable for diverse industrial sectors. Applying corrosion inhibitors is generally straightforward. They can be added directly to fluids, applied as surface treatments, or incorporated into coatings. This ease of application simplifies the process of protecting metal surfaces from corrosion.

Corrosion inhibitors provide enhanced protection by forming a protective layer on the metal surface. This layer prevents corrosive agents such as oxygen, water, and salts from coming into direct contact with the metal, thus reducing the rate of corrosion. By preventing or significantly reducing corrosion, inhibitors help extend the service life of equipment and structures [134]. This prolongation translates into better utilization of assets and improved return on investment. Many modern corrosion inhibitors are designed to be environmentally friendly. Researchers continually develop inhibitors that are less toxic and more biodegradable, reducing the environmental impact of corrosion prevention methods. Corrosion can compromise the structural integrity of equipment and infrastructure, leading to potential safety hazards. Through using corrosion inhibitors, the risk of catastrophic failures and accidents can be minimized, ensuring safer operational conditions [135]. Corrosion inhibitors are often compatible with other corrosion prevention methods. They can be used in conjunction with coatings, cathodic protection, and material selection strategies to provide comprehensive corrosion protection. Inhibitors can be tailored to target specific types of corrosion and specific environments [136]. This targeted approach allows for more effective corrosion control, addressing the unique challenges posed by different industrial processes and conditions.

The field of corrosion inhibitors is continuously evolving, with ongoing research and development efforts leading to more effective and efficient solutions [136]. Advances in chemistry and materials science contribute to the development of new inhibitors with enhanced performance characteristics. This study prefers corrosion inhibitors because of their cost-effectiveness, versatility, ease of application, and ability to provide enhanced protection. Industries can achieve improved durability, safety, and environmental compliance by integrating corrosion inhibitors into their corrosion prevention strategies.

© University of Venda

2.11 Exploring the Role of Corrosion Inhibitors in Metal Protection

Corrosion inhibitors play a crucial role in various industries, including automotive, construction, and manufacturing [137]. They are versatile and can be applied to any metal surface in various forms such as liquids, aerosols, and coatings. Corrosion inhibitors effectively slow down the corrosion process by creating a protective barrier on the metal surface. The primary function of corrosion inhibitors is to prevent the metal from encountering corrosive substances like water, oxygen, and other environmental pollutants. This barrier reduces the likelihood of oxidation, which is the main driver of corrosion [138]. Through minimizing the exposure of the metal to these corrosive agents, corrosion inhibitors help to extend the lifespan of metal components and structures. Moreover, corrosion inhibitors can also modify the chemical environment of the metal surface, making it less conducive to corrosion. This alteration in chemistry disrupts the corrosion process and makes it more difficult for corrosion to occur. As a result, the metal remains protected and experiences slower rates of degradation over time. Corrosion inhibitors are a valuable tool in combating corrosion and preserving the integrity of metal surfaces. Through creating a protective barrier and altering the chemical environment, these inhibitors effectively reduce the rate of corrosion, thereby enhancing the longevity and durability of metal components in various industrial applications [102].

2.11.1 Brief Description of Corrosion Inhibitors

Corrosion inhibitors are typically categorized into two main types: chemical and physical [139]. Chemical inhibitors function by establishing a protective film atop the material's surface, while physical inhibitors alter the environmental conditions. Chemical inhibitors operate by creating a shield of molecules on the material's surface, impeding the corrosive elements from coming into contact with the metal and thus decelerating the reaction [140]. On the other hand, physical inhibitors modify the surrounding environment, rendering it less conducive to corrosion reactions. Physical inhibitors hinder corrosion by lowering the reaction's overall energy, making it more difficult for corrosion to occur.

These inhibitors function by modifying the chemical surroundings near the metal surface, thereby altering the concentration of reactants and products within the solution. This alteration raises the energy threshold required for corrosion to proceed, hindering its occurrence. Additionally, corrosion inhibitors provide a physical barricade against corrosive agents,

© University of Venda

shielding the material. Metals can be safeguarded against rust and anodic corrosion through the use of corrosion inhibitors [41]. This can often be achieved by enveloping the metal surface with a chromate layer. Oxygen scavengers may also be employed as corrosion inhibitors to react with dissolved oxygen in the environment and assist in preventing cathodic corrosion [20] [141].

2.11.2 Unravelling the Mechanism of Corrosion Inhibition: Insights into Plant Extracts as Effective Protectors in Acidic Environments

Extensive research has been conducted to introduce alternative organic corrosion inhibitors suitable for various corrosive environments. The primary function of inhibitors is to form a protective layer that shields the metal from acid attacks [142]. This protective process is facilitated by the surface of the adsorbent, which can be customized to attract specific molecules. It's important to note that the adsorption process is reversible, allowing the adsorbed substance to be released from the adsorbent under different environmental conditions, such as changes in temperature and pressure [143].

Plant extracts have emerged as effective corrosion inhibitors, particularly in acidic conditions [144]. These inhibitors work by either slowing down or completely halting the reaction between the metal and the corrosive medium. They achieve this by modifying the anodic and/or cathodic reactions. The corrosion inhibitor essentially acts as a barrier between the metal surface and the corrosive environment. It can also create a protective film on the metal surface, blocking the access of corrosive components [17]. Furthermore, corrosion inhibitors deactivate substances in the media that induce corrosion through several mechanisms:

- Formation of a monolayer of adsorbate on the metal surface.
- Modifying the rates of the anodic and/or cathodic reactions.
- Reducing the diffusion rate for reactants to reach the metal surface.
- Lowering the electrical resistance of the metal surface, which in turn reduces the energy required to initiate the corrosion reaction. The lower the electrical resistance, the more effective the inhibitor is in preventing corrosion [141].

© University of Venda

2.11.3 Exploring Adsorption and its Role in Corrosion Inhibition

Adsorption, a fundamental process in surface chemistry, entails the binding of molecules, atoms, or ions to a material's surface. This phenomenon occurs due to electrostatic interactions, where charged species are attracted to oppositely charged surfaces. The strength of this binding is influenced by various factors, including charge, size, and shape [145]. In the context of corrosion inhibition, adsorption inhibitors function by forming a thin layer on the metal surface, reducing its effective surface area and consequently slowing down the corrosion rate. Notably, adsorption-type inhibitors, such as *A. phylicoides* extracts, attach to either the cathodic or anodic sites and interfere with the corrosion process. The utilization of plant extracts as corrosion inhibitors offers a cost-effective and environmentally friendly alternative, with their effectiveness influenced by factors such as electron density, charge transfer, and interaction energy [30].

2.11.4 Inhibition Mechanisms of Cathodic and Anodic Corrosion Inhibitors

Cathodic inhibitors slow down the cathodic reactions responsible for forming corrosion products, while anodic inhibitors impede the anodic reactions that involve the oxidation of the metal [146]. Mixed inhibitors provide balanced protection by delaying both cathodic and anodic reactions, thereby reducing the overall rate of corrosion and prolonging the lifespan of the metal [147]. The effectiveness of inhibitors is enhanced when used alongside other corrosion prevention methods, as metals in the coating can function as either a cathode or an anode depending on the type of metal. When exposed to an electrolyte, electrons flow from the more active metal to the less active one, affecting the rate of corrosion. Inhibition is achieved through chemical compounds that adsorb onto the metal surface and form a protective film, which acts as a barrier to the corrosive environment and reduces corrosion [3] [129]. Cathodic inhibitors reduce the corrosion rate by suppressing the cathodic reaction, while anodic inhibitors slow down the oxidation of the metal surface, preventing the corrosive environment from penetrating the protective film [141]. The combined use of these inhibitors provides an effective barrier against corrosion. The type of protective film generated depends on the composition of the corrosion inhibitor, the properties of the metal, and the solution environment. A passivating film acts as a barrier to further oxidation, a precipitation film forms through the precipitation of metallic compounds, and an adsorption film results from the adsorption of corrosion inhibitor molecules [148].

© University of Venda

2.12 The Potential of *athrixia phylicoides* as a Corrosion Inhibitor

A. phylicoides is abundant throughout South Africa, thriving in various habitats such as grasslands, woodlands, bushveld, and even in challenging, sloping terrain. It's particularly favoured by gardeners interested in indigenous plant species, as it tends to spread in flowerbeds or form dense clusters of purple flowers when in bloom. Figure 2.1 indicates regions in South Africa where *A. phylicoides* is plentiful [149].

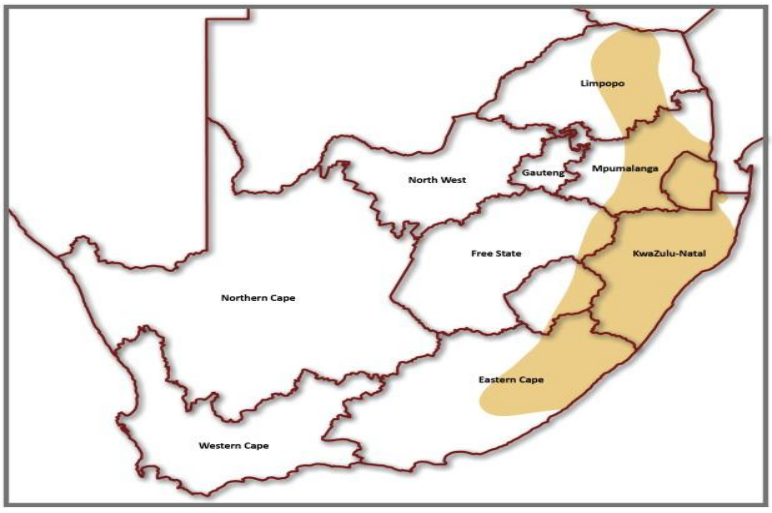


Figure 2.1: Distribution map for *A. phylicoides* in South Africa



Figure 2.2: *A. phylicoides* plant

This plant is a compact upright shrub with square-shaped foliage and small, pale pink or purplish-pink blooms. Its slender stems are covered in white, fuzzy hairs, and its foliage consists of small, pointed, dark green leaves. The *A. phylicoides* plant typically reaches a

© University of Venda

maximum height of around 1 meter [150]. The coloration of its flowers can vary depending on the soil composition and geographic region, resulting in hues ranging from light pink to deep mauve, and even dark purple *bush tea*, commonly known as *A. phylicoides*, holds significant cultural and medicinal importance among Indigenous peoples in South Africa. For generations, this perennial leafy shrub has been utilized for its diverse therapeutic properties. Among its medicinal uses, *A. phylicoides* is known for its effectiveness in curing boils and decontaminating infected wounds and cuts, promoting faster healing [151]. Additionally, it is believed to possess blood-cleansing properties, contributing to overall health. In traditional medicine, it is also employed in treating acne, potentially due to its anti-inflammatory or antimicrobial effects, and for addressing respiratory ailments such as colds, coughs, and headaches, possibly due to its soothing properties on the respiratory system. Beyond its medicinal applications, *A. phylicoides* holds cultural significance among various indigenous communities. It is used in the preparation of popular South African beverages, thereby enriching the cultural heritage and culinary traditions of the region. Moreover, the knowledge surrounding the use of *A. phylicoides* reflects the deep connection between people and plants in traditional healing methods. Among specific cultural practices, the Vhavenda people regard *A. phylicoides* as an aphrodisiac and utilize roots and leaves for deworming and digestive health [152]. Similarly, the Zulu people extract essence from the roots through boiling, using it as a remedy for wheezing and as a laxative [153].

The utilization of *A. Phylicoides* in indigenous communities not only highlights its medicinal properties but also underscores the importance of preserving traditional knowledge and practices. This plant serves as a reminder of the intricate relationship between nature and human well-being, as well as the cultural significance of indigenous healing methods. Through its multifaceted roles in traditional medicine and cultural practices, *A phylicoides* continues to play a vital role in promoting health and preserving cultural heritage among South African indigenous peoples.

Harvesting and extracting *A. phylicoides* leaves for use as a corrosion inhibitor is a sustainable choice. By focusing on leaves rather than roots or stems, the plant can continue to grow and thrive, ensuring its availability in the environment. This approach allows for the continual harvesting of leaves without harming the plant, thereby promoting its growth and sustainability. *A. phylicoides* plants are naturally abundant in various regions of Africa, including South Africa, where they grow in grasslands, woodlands, and bushveld areas [154]. While they primarily grow in the wild, their popularity and usefulness have led to intentional

© University of Venda

cultivation by gardeners and landscapers interested in native plant species. Cultivating *A. phylicoides* not only supports its availability but also increases accessibility to this valuable resource. Harvesting leaves for extraction while leaving the plant intact ensures a renewable and environmentally friendly source of *A. phylicoides* [155].



Figure 2.3: *A. phylicoides* cutting trays

The characteristics of a good corrosion inhibitor align closely with some of the properties of *A. phylicoides*, which makes it a promising candidate for investigating its potential as a corrosion inhibitor. For instance, *A. phylicoides* leaves could potentially form a protective barrier on metal surfaces, offering long-lasting protection and resisting degradation under various environmental conditions. Its natural compatibility with metals and coatings, along with its versatility against different types of corrosion, make it an intriguing option for further study.

Furthermore, the non-toxic or low toxicity levels of *A. phylicoides* add to its appeal, as it aligns with the desire for environmentally friendly corrosion inhibitors. Additionally, if *A. phylicoides* proves to be effective as a corrosion inhibitor, its ease of application and potential cost-effectiveness would further enhance its attractiveness for industrial or commercial use. The characteristics that make *A. phylicoides* a valuable resource in its natural habitat suggest that it may possess the qualities necessary to serve as an effective corrosion inhibitor, making it a compelling subject for research and exploration in this field [156].

© University of Venda

2.12 Metal Corrosion on Acidic Medium of Interest

Using *A. phylicoides* extract to mitigate acid corrosion, particularly against hydrochloric acid and sulphuric acid, is a fascinating area of study. Given the acidic nature of these compounds, effective corrosion inhibition is crucial to protect metal surfaces from degradation. *A. phylicoides* extract, with its potential as a corrosion inhibitor, offers a natural and sustainable solution to this challenge. The study assesses the ability of *A. phylicoides* extract to form a protective barrier on metal surfaces, thereby preventing the corrosive action of hydrochloric acid and sulphuric acid. Researchers may explore the mechanisms by which *A. phylicoides* extract interacts with metal surfaces and inhibits corrosion, as well as its effectiveness under different concentrations of acids and environmental conditions. By focusing on these specific acids of interest, the study can provide valuable insights into the potential applications of *A. phylicoides* extract in industries where these acids are commonly encountered, such as chemical processing, manufacturing, and infrastructure maintenance. If successful, this research could lead to the development of eco-friendly corrosion inhibitors derived from natural sources like *A. phylicoides*, offering sustainable alternatives to traditional chemical inhibitors [157].

2.12.1 Significance of Hydrochloric Acid

Hydrochloric acid is a potent and corrosive mineral acid capable of dissolving various metals and causing severe skin burns. In addition to its industrial applications, such as in the production of polyvinyl chloride (PVC) and cleaning metal surfaces, it plays a crucial role in the digestive system as a component of gastric acid, aiding in food digestion and pathogen elimination. With a molar mass of 36.458 g/mol, it is manufactured by reacting hydrogen and chlorine gases to form hydrogen chloride gas, a process commonly employed due to its efficiency and cost-effectiveness. Laboratory handling of hydrochloric acid requires caution due to its corrosive nature. It should be stored safely, away from heat and combustible materials, and handled with protective clothing and goggles. Mixing it with other substances can produce toxic fumes. Despite its hazards, hydrochloric acid finds various uses in adjusting solution pH, dissolving metals, and reacting with other chemicals [158]. However, proper safety precautions must be observed to prevent skin and eye irritation and material corrosion. Beyond laboratory settings, hydrochloric acid is utilized in leather processing, household cleaning, and construction. In oil extraction, injecting it into rock formations can enhance oil

© University of Venda

output by dissolving rock and forming pore structures. Industrially, it is indispensable in food processing, pharmaceuticals, and PVC production, as well as in pickling steel, leather processing, and water treatment. Its roles in adjusting water pH, removing metals and sulphur compounds, and softening water highlight its importance in ensuring water safety and industrial efficiency [159].

2.12.2 Significance of Sulphuric Acid

When dissolved in water, sulphuric acid molecules dissociate into hydrogen and sulphate ions [160]. The hydrogen ions further react with water molecules, forming hydronium ions, which then combine with the sulphate ions to regenerate sulphuric acid molecules. This process results in the formation of a highly corrosive sulphuric acid solution capable of causing severe burns. Pure sulfuric acid does not occur naturally on Earth due to its strong affinity for water vapor. As it absorbs water vapor from the environment, the acid becomes more concentrated and consequently more corrosive, posing a threat to rocks and metals by breaking down their molecular structure and inducing corrosion. Sulphuric acid finds diverse applications across various industries. It is utilized in petroleum refining to eliminate impurities from crude oil and in metal refining to separate metals from ore [161]. In the steel industry, it is employed in pickling processes to remove rust and scale from steel surfaces. Furthermore, it plays a crucial role in paper production and the extraction of metals such as copper, nickel, cobalt, and uranium. Additionally, sulphuric acid is a key ingredient in the manufacturing of cleaning products like detergents and bleaches, owing to its strong acidic properties [162]. It is commonly found in household cleaning solutions such as oven and toilet bowl cleaners. Moreover, its excellent solvent properties make it valuable in the production of dyestuffs for clothes [162].

2.12.3 Corrosion Reaction Occurring Between Metals (zinc and mild steel) and Acids (HCl AND H_2SO_4)

- **Zinc metal exposed to hydrochloric acid.**

When hydrochloric acid reacts with zinc metal (Zn), a chemical reaction occurs that results in the formation of zinc chloride ($ZnCl_2$) and hydrogen gas (H_2). The balanced chemical equation for this reaction is [163]:

© University of Venda

$$Zn\ (s) + 2HCl\ (aq) \rightarrow ZnCl_2\ (aq) + H_2\ (g) \qquad (2.1)$$

In this reaction, zinc (Zn) metal serves as the reactant, Hydrochloric acid is the acidic solution, and zinc chloride ($ZnCl_2$) is the product formed, which is a soluble salt, Hydrogen gas (H_2) is also produced as a product, and it evolves as bubbles.

This reaction is an example of a single replacement or displacement reaction, where the more reactive metal (zinc) displaces the less reactive hydrogen from the acid. The reaction between hydrochloric acid and zinc is exothermic, meaning it releases heat energy [164]. While corrosion is often associated with gradual degradation over time, the reaction between zinc and hydrochloric acid demonstrates a rapid form of corrosion. The acid dissolves the zinc metal, leading to the formation of soluble zinc chloride and the release of hydrogen gas bubbles. This reaction is an example of chemical corrosion, where the metal reacts with a corrosive substance to form new compounds. In practical terms, corrosion is typically undesirable because it can weaken structures, reduce the functionality of materials, and lead to safety hazards. However, in some contexts, such as in the production of hydrogen gas or in certain chemical processes, controlled corrosion reactions like the one between zinc and hydrochloric acid can be intentionally utilized for specific purposes [165].

- **Zinc metal exposed to sulphuric acid.**

When zinc metal reacts with sulphuric acid, a chemical reaction occurs resulting in the formation of zinc sulphate ($ZnSO_4$), hydrogen gas (H_2). The balanced chemical equation for this reaction is [166]:

$$Zn(s) + H_2SO_4(aq) \rightarrow ZnSO_4(aq) + H_2(g) \qquad (2.2)$$

In this reaction, zinc metal is the reactant, and sulphuric acid is the acidic solution. Zinc sulphate ($ZnSO_4$) is the product formed, which is a soluble salt. Hydrogen gas (H_2) is produced as a product and evolves as bubbles. Like the reaction with hydrochloric acid, this reaction is an example of a single replacement or displacement reaction. Zinc metal displaces hydrogen from sulphuric acid, resulting in the formation of zinc sulphate and hydrogen gas. As with the reaction between zinc and hydrochloric acid, this reaction can be considered a form of corrosion. The acidic solution (sulphuric acid) facilitates the dissolution of the zinc metal,

© University of Venda

leading to the formation of soluble zinc sulphate and the release of hydrogen gas [167]. This reaction demonstrates chemical corrosion, where the metal undergoes a chemical reaction with a corrosive substance resulting in the formation of new compounds.

- **Mild steel metal exposed to hydrochloric acid**

When mild steel, which primarily consists of iron with a small percentage of carbon and other trace elements, reacts with hydrochloric acid, a chemical reaction occurs. This reaction involves the dissolution of the iron in the mild steel, forming soluble iron chloride compounds and releasing hydrogen gas. The reaction can be represented by the following equation:

$$Fe(s) + 2HCl(aq) \rightarrow FeCl_2(aq) + H_2(g) \quad (2.3)$$

In this reaction, Fe(s) represents mild steel, which contains primarily iron. HCl(aq) denotes hydrochloric acid, which is the acidic solution. $FeCl_2(aq)$ is iron chloride, a soluble salt formed as a product of the reaction. $H_2(g)$ represents hydrogen gas, which evolves as bubbles [168].

This reaction demonstrates a form of corrosion known as acid corrosion or acid attack. The acidic solution (HCl) reacts with the iron in the mild steel, causing it to dissolve and form soluble iron chloride compounds. The release of hydrogen gas is a characteristic feature of this reaction. Acid corrosion can lead to the deterioration of mild steel over time, particularly in environments where exposure to acidic substances is prevalent. To mitigate acid corrosion, protective measures such as surface coatings or corrosion-resistant materials may be employed [102].

- **Mild steel metal exposed to sulphuric acid**

When mild steel, which primarily consists of iron with a small percentage of carbon and other trace elements, reacts with sulphuric acid, a chemical reaction occurs. This reaction involves the dissolution of the iron in the mild steel, forming soluble iron sulphate compounds and releasing hydrogen gas. The reaction can be represented by the following equation:

$$Fe(s) + H_2SO_4(aq) \rightarrow FeSO_4(aq) + H_2(g) \quad (2.4)$$

© University of Venda

In this reaction, Fe(s) represents mild steel, which contains primarily iron. H_2SO_4(aq) denotes sulfuric acid, which is the acidic solution. $FeSO_4$(aq) is iron sulphate, a soluble salt formed as a product of the reaction. H_2(g) represents hydrogen gas, which evolves as bubbles.

This reaction demonstrates a form of corrosion known as acid corrosion or acid attack. The acidic solution (H_2SO_4) reacts with the iron in the mild steel, causing it to dissolve and form soluble iron sulphate compounds. The release of hydrogen gas is a characteristic feature of this reaction. Acid corrosion can lead to the deterioration of mild steel over time, particularly in environments where exposure to acidic substances is prevalent [169]. To mitigate acid corrosion, protective measures such as surface coatings or corrosion-resistant materials may be employed.

2.13 Corrosion Observation Procedure

Corrosion monitoring procedures include using a Corrator (corrosion meter) or a combination of methods and equipment to provide off-line or online information on wear rates [170]. Improve maintenance and take or improve preventive measures to combat and prevent corrosion. Corrosion measurements use variety of quantitative methods to judge and approximate the efficacy of corrosion control and prevention and to provide information on appropriate prevention and control strategies that can be improved. Various techniques can be extended and enhanced using the evaluation results. As will be discussed in the following subsections, corrosion control methods can be broken down into electrochemical and non-electrochemical categories [171].

2.13.1 Electrochemical Methods

Electrochemistry is the study of the relationship between electricity and chemical reactions [172]. It is used to understand how electricity can be used to drive chemical reactions, and how chemical reactions can be used to generate electricity. Electrochemical impedance spectroscopy measures the resistance of a metal when exposed to different electrolytes [184]. Electrochemical impedance spectroscopy measures the impedance of a material in response to an externally applied signal [185]. Linear polarization resistance measures the current when a direct current is applied to a metal. Electrochemistry has many applications in industry, ranging from batteries to fuel cells. It can also be used to create new materials with unique properties [173]. By understanding how electrical energy can affect chemical reactions,

© University of Venda

engineers and researchers can design materials with specific properties for use in a variety of applications. For example, they can design materials that are more efficient in storing energy, or materials that are better able to resist corrosion. It involves the transfer of electrons from one species to another to produce a desired result. It can be used to study the mechanisms of chemical reactions, understand how batteries work, and develop more efficient ways to store energy. Redox reactions are important for many applications, such as energy storage, corrosion protection, and the production of batteries. They can also be used to create new materials, such as nanomaterials and catalysts. The reaction takes place in an electrochemical cell, composed of two electrodes and an electrolyte solution. The electrodes are connected to a power source, such as a battery. When electrons move from one electrode to the other, they generate electricity. Redox reactions can be manipulated to produce desirable outcomes, such as generating energy, protecting against corrosion, and creating advanced materials and catalysts. To achieve these results, an electrochemical cell is necessary, which requires two electrodes, an electrolyte solution, and an electrical current. The electrolyte solution acts as a medium for the electrons to travel between the electrodes, allowing a current to be generated. The current then produces the desired result, whether it be energy production, corrosion protection, or advanced materials and catalysts. Electrochemical techniques and their tools enable the study of corrosion phenomena [174]. Corrosion itself is an electrochemical process. Several electrochemical corrosion measurements accumulated over time support this research. These kinds of strategies are popular for corrosion rate studies because of their sensitivity, flexible, quick, accurate, and useful for studying many corrosion-related phenomena. Additionally, electrochemical measurements can be used to ascertain the susceptibility and cyclical corrosion rates of metals to localized corrosion (pitting or cracking) and study the effects of adverse effects and susceptibility. The method is based on fundamental scientific principles which are applicable to both field and laboratory settings. It is also flexible enough to adapt to different conditions which allows it to be effective in both settings. It is easy to use and cost-effective. It produces reliable results and is suitable for various applications. The method is based on principles of electrochemistry which states that by applying an electrical current to a metal surface, the corrosion rate can be controlled and monitored [175]. This means that it is possible to measure the effects of different treatments on the metal and determine the best approach for preventing corrosion. These techniques measure the current, potential, and impedance of a metal exposed to different treatments. This data helps to determine which treatments are most effective at preventing corrosion and how they compare to one another. It

© University of Venda

also helps to detect any corrosion that has already occurred, which can then be prevented in the future. A detailed description of the electrochemical impedance spectrometer and biasing techniques used in this study follows.

Through measuring the impedance of a system as a function of frequency, EIS can provide detailed information about the nature of the chemical species present within solution interface, as well as kinetics of interfacial processes [176]. This technique is especially useful for studying the interactions between proteins and metal surfaces. EIS also allows for the study of corrosion processes and the monitoring of electrochemical reactions in real time. It is a powerful tool for understanding the electrochemical properties of a system and can be used to optimize conditions to maximize desired outcomes. EIS is a technique for characterizing the electrical resistance characteristics of various materials at various frequencies [177]. Estimates made by EIS for corrosion studies are not distractive, typically using signals less than 30 mV peak-to-peak and bias magnitudes appropriate for the type of material being characterized [170]. AC-based EIS methods can be used to better understand corrosion mechanisms and determine the effectiveness of specific corrosion protection methods such as corrosion inhibitors and coatings. Resistance is used to determine the amount of current in an AC circuit at a given voltage and is a voltage and current scaling factor [178]. A straightforward model of the interface between solution and metal includes the following three main aspects :

- polarization resistance (Rp)
- Double layer capacitance (Cdl)
- Solution resistance (Rs).

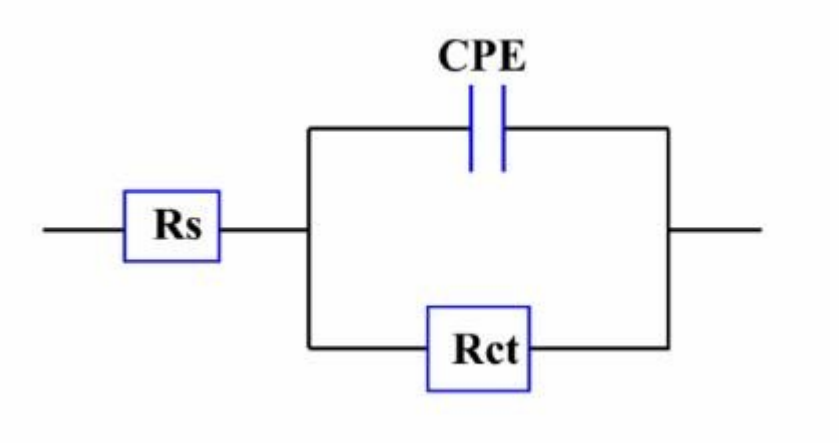


Figure 2.4: A model of electrochemical parallel circuit mostly used for measurements of EIS parameters in corrosion analysis systems [179]

© University of Venda

Within electrolyte and a metal surface, the exist Cdl which is an electrical phenomenon. This electrical double film is created through a charged connection point resulting from the connection of polar water particles on the metal surface and acts like a corroded and charged capacitor [180]. R_p is a measurement of reaction kinetics and resistance to diffusion and resistance away from reactive corrosion surfaces. The polarization resistor is a measure of the corrosion rate of an electrode in a corrosion cell. When the electrolyte permeability increases, the ionic current can flow more easily between the electrodes [181]. This decrease in resistance is due to the increased number of ions that can pass through the electrolyte, resulting in a decrease in the resistance to current flow. If you measure the DC at zero frequency, the capacitor's impedance will be infinite. When circuits are connected in parallel, preference is given to the circuit with the lowest resistance, the resulting data may be used to measure Rs and Rp values. EIS offers reasonable benefits over other methods of metal corrosion evaluation, including.

a) This allows researchers to gain a better understanding of how cells interact with each other and how they respond to different stimuli. It also helps to identify which components of a cell are most important for its functioning. By simulating these components in equivalent electronic circuits, researchers can gain insights into the inner workings of cells that may not be visible through traditional experimental methods.

b) This type of simulation allows researchers to manipulate parameters in a controlled environment, which can help them identify which components are essential for the cell to function and which can be removed or modified without disrupting its normal operation. Additionally, researchers can use this data to gain insights into how cells respond to different environmental conditions and how they adapt to changing conditions over time.

c) The protective properties of a coating are linked to its capacitance and resistance. As the capacitance and resistance change, the protective properties of the coating also change and can eventually be lost. This can be caused by several factors such as exposure to temperature changes or UV radiation.

Polarization occurs when the potential of a metal electrode is displaced from its equilibrium value due to the generation of an electric field around the electrode [182]. This results in a decrease in the current density at the electrode, which can lead to a decrease in the performance of the device. When two metal surfaces touch, energy flows from positive to negative, corroding the two metals. This decreases the efficiency of the device and increases

© University of Venda

the rate of corrosion of the electrode materials. This decrease in charge stored on the electrodes reduces the electric field strength, which in turn reduces the magnitude of the open-circuit potential difference between the anode and cathode regions. This further reduces the flow of current, and the corrosion rate continues to increase until it reaches an equilibrium. This further reduces the open-circuit potential difference, and thus the current magnitude. The reduction of current magnitude is proportional to the reduction in open-circuit potential difference and depends on electrode polarization properties. This is because the increased concentration of corrosive species causes the cathode to become less efficient at releasing electrons, thus reducing the amount of current that can flow through the circuit. These species accumulate at the anode as corrosion proceeds near each electrode. The increased resistance caused by these species causes an increase in voltage, known as electrode polarization. With the increase in voltage, the current flowing through the circuit is reduced. This results in a decrease in the magnitude of the current. This is because the corrosion process produces a build-up of corrosion products on the anode and cathode, which impedes the flow of current. As the corrosion process continues, the amount of corrosion products increases, further reducing the amount of current that can flow through the circuit. Eventually, the OCP difference between the anode and cathode is great enough to halt the corrosion process. The technique allows for the measurement of corrosion current density and corrosion potential in a single step. It is also capable of giving data on the corrosion rate, corrosion resistance, and the corrosion mechanism of the material in the test environment. The technique can be used to study the effects of different environmental conditions on corrosion.

2.13.2 Non-electrochemical Methods

These techniques allow researchers to measure the amount of corrosion and identify the various factors that can affect it, such as the composition of the metal, the presence of corrosive agents, and environmental conditions. Anodic polarization measures the corrosion rate by measuring the current that is produced when a metal is exposed to an electrolyte [183]. All these techniques provide an accurate measure of the corrosion rate of a metal. These techniques allow for a more detailed analysis of corrosion processes and can provide insight into microstructural changes that occur over time. Anodic polarization allows for the study of corrosion rate by measuring the current as a function of applied potential. Linear polarization resistance measures the corrosion rate by measuring the potential difference between the material and a reference electrode. Surface and gravimetric analyses can be used to measure

© University of Venda

the damage done to metal and the corrosion rate by determining the amount of material lost due to corrosion [186].

Gravimetric analysis: In gravimetric analysis, a sample of metal is weighed before and after corrosion. The difference in weight is an indication of the extent of corrosion. Inhibitors are compounds that interfere with the chemical reaction that causes corrosion [187]. They can slow down or stop the reaction, thus helping to reduce the rate of corrosion. The effectiveness of the inhibitor can be determined by measuring the difference in weight before and after the addition of the inhibitor. This method is useful for comparing different inhibitors and determining the most effective one. Through measuring the difference in weight before and after the addition of the inhibitor, it is possible to determine how much of the corrosion was prevented by the inhibitor. This allows scientists to compare different inhibitors and determine which one is the most effective in protecting the metal sample from corrosion. Once the corrosion rate is determined, it can be used to predict the service life of the material [188]. This test is a quick and effective way to determine the corrosion rate of a material and is widely used in industries. Corrosion testing is essential in ensuring the safety and reliability of components used in various industries, as well as in predicting the service life of materials [189]. It is an important part of quality control and assurance. Although corrosion testing is a quick and effective way to determine the corrosion rate of a material, there are some limitations to this method. For example, the test does not consider the type of corrosion that will occur. The test is also limited in that it only measures the rate of corrosion and not the type of corrosion that will occur. Additionally, it does not consider any environmental factors that could affect the rate of corrosion, such as humidity.

Weight loss studies measure the amount of material lost due to corrosion over time [190]. This is done by measuring the sample's weight before and after exposure to a corrosive environment. The difference in weight indicates the amount of corrosion that has occurred. This method is favoured because:

a) it is relatively easy to perform and provides a good indication of the corrosion rate of a material.

b) It is adaptable: It may be used in all corrosive situations and provides details on all the different types of corrosion.

c) It is clear: Without making any approximations or theoretical assumptions, direct

© University of Venda

measurements are achieved.

Surface analysis methods are extremely effective in highlighting almost every element of the corrosion phenomenon [191]. To better understand inhibition mechanism, surface analyses of metals are carried out in both the presence and absence of an inhibitor. Adsorption processes can be used for different applications such as catalytic reactions, hydrogen storage, and energy conversion. The morphology of the metal surface is important for understanding the mechanism of the adsorption process. It can also help in the design of new materials with better properties. By studying the morphology of the metal surface, it is possible to understand how the different molecules interact with it and how the adsorbates are organized [192]. This can provide insights into how the materials behave when used for different applications and which properties can be improved. FTIR spectroscopy is a technique that measures the vibrational and rotational energy levels of the molecules on the surface of the specimen [193]. This data is then used to determine the composition of the material. FTIR, and SEM/EDS are two of the methods used in this investigation. In this research, these techniques were used in the post-analysis of the examined samples (Zn and MS).

When the infrared radiation is absorbed, the vibrational energy of the molecules increases, causing the bonds to stretch, bend, or twist. This creates a change in the molecular structure of the material, which can be seen by the infrared spectrometer. This change alters the absorption spectrum of the material, allowing for the identification of the molecular structure. Through this process, it is possible to identify the components of a material and understand its physical and chemical properties. The infrared spectrometer works by passing infrared light through the material [194]. The molecules in the material absorb some of the light, causing a decrease in intensity. Through analysing the absorption spectrum of the material, the molecular structure of the material can be determined. This allows for the identification of different components, as well as their physical and chemical properties. Chemical functional groups exhibit alterations in the wavenumber range because of this interaction [195]. Vibration mode can be identified by looking at the IR radiation's absorption. The use of FT-IR has several advantages over traditional IR spectroscopy, including speed and a higher signal-to-noise ratio . A plot of transmittance vs wavenumber represents the FT-IR spectrum. As a result, a transmittance spectrum is obtained [196].

The absorbance spectra can be calculated by taking the negative logarithm of the transmittance spectra, thus yielding the equation A = -log(%T) [197]. This equation is useful because it allows us to measure the intensity of light absorbed by a sample and compare it to the intensity

© University of Venda

of light absorbed by the background. This can give us an indication of how much of the light is being absorbed by the sample, which can be useful for studying the properties of the sample. SEM is a powerful tool for determining the surface structure and composition of a wide range of materials [198]. The beam of electrons that is used in SEM interacts with the sample uniquely, allowing researchers to observe features on the sample's surface not visible in other types of microscopies [199]. This interaction also allows researchers to measure the chemical composition of the sample, as the electrons will react differently depending on the material they interact with. One of the most effective tools for studying microstructure morphology and chemical composition is scanning electron microscopy. The acquisition of interacting signals—either elastic or inelastic—between the coupons understudied and beam electron is what results in the image [200]. Backscattered electrons, also known as wide-angle backscattered electrons, are typical of elastic interactions, which cause a tiny amount of energy to be lost during the impact. when the sample is irradiated with electrons, the electrons interact with the sample's atoms which causes them to lose energy and change direction. This is known as elastic scattering and the electrons that are reflected are called backscattered electrons. Secondary electrons (SE) are produced by inelastic scattering, which happens when incident electrons connect with atoms that are close to or at the sample's surface (in this case, a metal sample), transferring a significant amount of energy from the primary beam electron on the atom. The binding energy of each electron-atom pair is determined by the difference in energies between the electron and the atom, and the number of electrons in the system affects how much energy is lost when an electron is excited [201]. When electrons within the system increase, the amount of energy lost increases, making it important to understand the relationship between electron-atom binding energy and the number of electrons in the system. Every time an incident electron disintegrates by ejecting a core-shell electron, an energetic X-ray is released, which can be used to locate the excited atom. An energy dispersive spectrometer (EDS) can analyze the X-rays to identify and ascertain the elemental composition of the sample surface [202].

2.14 Introduction to Computational Chemistry

Computational chemistry has experienced a surge in popularity over recent years, attracting an influx of part-time theoreticians who engage in computational work alongside their primary focus in other areas of chemistry [203]. The increased adoption of computational methods can be attributed to user-friendly computer software, enabling individuals with limited knowledge

© University of Venda

of the underlying principles to perform calculations effortlessly. This study is divided into two parts. The first part of the study focuses on experimental studies to identify and characterize potential corrosion inhibitors. In the second part, this study delves into the theoretical aspects, providing an overview of quantum mechanics. Through bridging the gap between experimental and theoretical approaches, this study seeks to enhance our understanding of corrosion inhibition mechanisms and accelerate the discovery of efficient inhibitors.

Corrosion occurs naturally as a phenomenon that happens when metal encounters oxygen and water [204]. The corrosion process can be slowed by using inhibitors such as plant extracts. Computational chemistry is useful to understand the molecular structure of the plant extract, which is useful to determine how it interacts with the metal and slows down the corrosion process. This knowledge will then be useful in developing better corrosion inhibitors for industrial applications. Corrosion inhibitors can help extend the life of metallic structures, reduce maintenance costs, and improve safety [205]. These corrosion inhibitors are often made from natural plant extracts, which are more cost-effective and environmentally friendly than traditional inhibitors. With the help of computational chemistry, these plant extracts can be studied in greater detail and optimized for industrial use.

Corrosion inhibitors play a crucial role in safeguarding materials and structures against degradation caused by corrosion [143]. Traditional methods for designing corrosion inhibitors rely heavily on experimental trial and error, which can be time-consuming and costly. In recent years, theoretical computer-assisted approaches have emerged as powerful tools for accelerating the discovery of novel corrosion inhibitors [206]. This session aims to introduce the fundamental aspects and terminology associated with theoretical computer-assisted corrosion inhibitor design. By leveraging computational techniques, scientists can now contribute significantly to the development of efficient and environmentally friendly corrosion inhibitors.

To explain experimental data in-depth, theoretical approaches are mainly used. The molecular properties of inhibitor molecules can be correlated with their inhibition efficiencies through quantum chemical calculations [207]. Furthermore, designing and investigating new corrosion inhibitors requires an understanding of the interaction between inhibitor molecules, and metal surfaces, molecular dynamics simulation has proven to be an efficient method. Common quantum chemical approaches used for studying the reaction between metal and corrosion inhibitors include Density Functional Theory (DFT), Hartree-Fock (HF) Method, Moller-

© University of Venda

Plesset Perturbation Theory (MP2), Coupled Cluster Theory (CC), Semi-Empirical Methods, Ab Initio Molecular Dynamics (AIMD), Time-Dependent DFT (TD-DFT), ONIOM (Our own N-layered Integrated molecular Orbital and molecular Mechanics)

2.15 Literature Review on the Corrosion Inhibition of Mild Steel, and Zinc Using Plant Extracts in Aqueous Media

Many researchers have utilized plant extracts as corrosion inhibitors and effectively reduced corrosion. These kinds of studies demonstrate the potential of natural products to mitigate corrosion and offer eco-friendly alternatives to traditional inhibitors [140]. Each research paper contributes valuable insights into the effectiveness and mechanisms of corrosion inhibition using plant extracts. Here's a brief overview of each study:

- Shahini *et al*. (2021): Investigated the inhibition action of Mish Gush (MG) leaves extract on mild steel corrosion in HCl solution, employing theoretical and electrochemical studies [208].
- Haque *et al*. (2021): Examined the corrosion inhibition of mild steel in 1M HCl using Thevetia peruviana flower extracts, focusing on environmentally benign options [209].
- Sedik *et al*. (2020): Studied the eco-friendly corrosion inhibition properties of Dardagan fruit extract for mild steel in 1 M HCl, employing electrochemical and surface morphological analyses [210].
- Ezeugo *et al*. (2017): Optimized the corrosion inhibition of zinc in 1.0 M HCl using Picralima nitida leaves extract as a green corrosion inhibitor, contributing to the development of sustainable corrosion protection strategies [211].
- Fouda *et al*. (2021): Investigated Ferula hermonis plant extract as a safe corrosion inhibitor for zinc in hydrochloric acid solution, highlighting its potential as a bio-based alternative for corrosion prevention [212].
- Madaci *et al*. (2023): Conducted experimental and theoretical studies on polysaccharides extracted from prickly pear nopales pulp (PPUN) of Opuntia ficus-indica as corrosion inhibitors, providing insights into the corrosion inhibition mechanism of natural polysaccharides [213].

These studies collectively demonstrate the growing interest in utilizing plant extracts as corrosion inhibitors and contribute to the development of sustainable and environmentally friendly corrosion protection methods. Further research in this area could lead to the discovery

© University of Venda

of new plant-based inhibitors and enhance our understanding of their corrosion inhibition mechanisms. The inhibition efficiency obtained from other study, was tabulated in Table 2.2.

Table 2.2 List of green corrosion inhibitors investigated recently by other scientists

Inhibitor	Metal Medium	η (%)	Concentration
Mish Gush	Mild steel 1.0 M HCl	95.0	1600 ppm
Thevetia peruviana	Mild steel 1.0 M HCl	91.69	250 ppm
Dardagan Fruit	Mild steel 1.0 M HCl	93.0	3000 ppm
Picralima nitida	zinc in 1.0 M HCl	86.78	1.2 gl^{-1}
Ferula hermonis	zinc in 1.0 M HCl	90.6	300 ppm

Table 2.2 provides a list of green corrosion inhibitors investigated recently by other scientists, along with their corresponding efficacy (η) percentages and concentrations in the specified metal medium.

- The inhibitor "Mish Gush" was tested on mild steel in 1.0 M HCl solution, demonstrating a high inhibition efficiency of 95.0% at a concentration of 1600 ppm [208].
- "Thevetia peruviana" extract, also tested on mild steel in 1.0 M HCl, exhibited an inhibition efficiency of 91.69% at a lower concentration of 250 ppm [214].
- "Dardagan Fruit" extract, when applied to mild steel in 1.0 M HCl, showed an inhibition efficiency of 93.0% at a higher concentration of 3000 ppm [210].
- For zinc in 1.0 M HCl, "Picralima nitida" extract demonstrated an inhibition efficiency of 86.78% at a concentration of 1.2 g/L [211].
- Similarly, "Ferula hermonis" extract, when used as a corrosion inhibitor for zinc in 1.0 M HCl, showed a high inhibition efficiency of 90.6% at a concentration of 300 ppm [212].
- The inhibition efficiency of "Opuntia ficus indica" was tested in 5% HCl, yielding an inhibition efficiency of 80.0% [215].

Table 2.2 provides valuable insights into the effectiveness of various green corrosion inhibitors

© University of Venda

across different metal mediums and concentrations, highlighting their potential for mitigating corrosion in acidic environments. Exploring the potential of *A. phylicoides* leaves extract as a corrosion inhibitor for zinc and mild steel in hydrochloric and sulphuric acid environments is commendable. Given the effectiveness of plant extracts demonstrated in previous studies, it's indeed an exciting and promising avenue for research.

Conducting a study to investigate the corrosion inhibition properties of *A. phylicoides* leaf extract could contribute valuable insights to the field of corrosion science. Not only would it add to the growing body of knowledge on green corrosion inhibitors, but it could also have practical implications for industries where corrosion prevention is a critical concern.

© University of Venda

University of Venda
Creating Future Leaders

CHAPTER THREE

EXPERIMENTAL PROCEDURES

© University of Venda

3. Experimental Procedures

3.1 Introduction

Materials needed to conduct a corrosion inhibition study under controlled conditions, with appropriate measures in place to protect the metal substrates and accurately assess the effectiveness of the *A. phylicoides* leaves extract as a corrosion inhibitor are listed below. Each component plays a crucial role in the experimental setup and contributes to the reliability and validity of research findings.

- Mild steel and zinc metals:

Purchased mild steel and zinc metals had specified weights estimation of 3.250 g and 2.600 g, respectively. These metals have been prepared with a small hole in the middle for ease handle and a surface area of 6 cm^2 each. These metals served as the substrates for corrosion experiments.

- Hydrochloric and sulphuric acid:

Hydrochloric acid and sulphuric acid were utilized to prepare the corrosive solutions for corrosion experiments. These acids created the acidic environment necessary to induce corrosion on the metal substrates.

- Methanol:

Methanol purchased from Sigma-Aldrich had been used as a solvent for extracting the active compounds from the *A. phylicoides* leaves. Methanol is commonly used in extraction processes due to its ability to dissolve a wide range of organic compounds.

- Epoxy resin and catalyst:

Epoxy resin and catalyst, purchased from Build It hardware, in South Africa, Thohoyandou branch, were used to prepare the samples for electrochemical studies. Epoxy resin is often used as a protective coating to encapsulate metal samples and prevent direct contact with the corrosive solution during electrochemical measurements [216].

3.2 Inhibitor Solution Preparation

The importance of corrosion inhibitor preparation lies in its potential to protect metal surfaces from degradation caused by corrosion. Corrosion can lead to structural damage, decreased efficiency, and ultimately, failure of equipment or infrastructure [135]. Corrosion inhibitors are substances designed to mitigate or prevent corrosion by forming a protective layer on the metal

© University of Venda

surface, thus reducing the rate of corrosion [217].

A. phylicoides leaves, often derived from plants like rooibos or other herbal varieties, contain various organic compounds that may exhibit corrosion-inhibiting properties. These compounds could potentially interact with the metal surface to form a protective layer, hindering the corrosion process. However, before utilizing *A. phylicoides* leaves extract as a corrosion inhibitor, thorough testing and evaluation are necessary to determine its effectiveness, compatibility with different metals and environments, and long-term stability. Additionally, the extraction process and formulation of the inhibitor solution would need careful consideration to ensure consistent performance and ease of application. Research into natural corrosion inhibitors, including those derived from plant extracts, is ongoing and holds promise for environmentally friendly and sustainable corrosion protection solutions [218]. Nonetheless, it's essential to approach such alternatives with scientific rigor to validate their efficacy and practicality in real-world applications.

Extraction procedures and the preparation of various concentrations are integral steps in utilizing *A. phylicoides* leaves extract or any natural substance as a corrosion inhibitor. These processes impact the efficiency, purity, consistency, effectiveness, and practicality of the inhibitor, ultimately determining its suitability for corrosion protection applications. Thorough optimization and testing are necessary to develop effective and economically viable corrosion inhibition solutions.

3.2.1 Extraction of *A. Phylicoides* Leaves

The *A. phylicoides* leaves were harvested from the Thohoyandou area of the Vhembe district in South Africa's Limpopo province. To preserve their integrity, they were air-dried at room temperature for a week, avoiding direct sunlight to prevent potential damage from solar radiation to the plant's components. Once dried, the leaves were ground into a fine powder. A portion of this powder, weighing 2 grams, was then added to a centrifuge tube containing 20 ml of 80% analytical-grade methanol solution (a 4:1 ratio of methanol to water). The mixture was agitated for 24 hours using a dragon shaker. After this period, the remaining extract was filtered using filter paper and subjected to a rotary evaporator to remove the methanol and water, resulting in a jelly-like residue. This residue was then dried and weighed. Subsequently, it was dissolved in a 1.5 M solution of H_2SO_4 and HCl in a 1000 mL volumetric flask to create the stock solution. From this stock solution, corrosion inhibitor test solutions were prepared at concentrations of 100 ppm, 400 ppm, 700 ppm, 1000 ppm, and 1300 ppm. This was achieved

© University of Venda

by diluting appropriate volumes of the stock solution with 1.5 M H_2SO_4 and HCl in 1000 mL volumetric flasks. The 1.5 M HCl and H_2SO_4 solutions were prepared by diluting precise amounts of 37% analytical-grade HCl and 99% analytical-grade H_2SO_4, respectively, in 1000 ml volumetric flasks. This process was done repeatedly to obtain a reasonable amount (mass) of *A. phylicoides* extract in solid form before the actual experiment was conducted.

3.2.2 Stock Solution Preparation

Once the extract is obtained, a stock solution is prepared by diluting a known volume of the concentrated extract with a suitable solvent to achieve the desired initial concentration. The concentration of the stock solution depends on the intended application and the expected corrosion inhibition performance.

After preparing the stock solution, it can be utilized to prepare a series of small concentrations for testing purposes. Dilution calculations are straight forward as shown below:

- Dilution Calculation: Determine the desired concentrations for the series of small solutions based on the range you want to test. Calculate the volume of stock solution needed to achieve each concentration using the formula:

$$C_1V_1 = C_2V_2 \tag{3.1}$$

where:

  - C_1 = Concentration of stock solution
  - V_1 = Volume of stock solution needed
  - C_2 = Desired concentration of the diluted solution
  - V_2 = Final volume of the diluted solution

- Dilution Procedure: Using the calculated volumes, prepare the series of small concentrations by diluting the stock solution with the appropriate amount of solvent (e.g., distilled water). Mix the solutions thoroughly to ensure uniformity.
- Labelling and Storage: Label each solution with its respective concentration to avoid confusion during testing. Store the solutions in suitable containers, properly sealed to prevent evaporation or contamination.

© University of Venda

- Testing: Utilize the prepared solutions to conduct corrosion inhibition tests using suitable experimental techniques, such as electrochemical measurements or immersion tests. Evaluate the performance of each concentration to determine the optimal inhibitor concentration for effective corrosion protection.

3.2.3 *A. Phylicoides* Leaves Extract Exposed to Ultraviolet light (UV)

Ultraviolet light (UV) refers to electromagnetic radiation with wavelengths shorter than those of visible light, but longer than X-rays. It is categorized into three main types based on wavelength:

- UVA (320-400 nm): Also known as long-wave or black light, UVA is the least harmful type of UV radiation. It is primarily responsible for tanning and skin aging effects [219].
- UVB (280-320 nm): UVB radiation is partially absorbed by the Earth's ozone layer. It is more energetic than UVA and causes sunburn and can contribute to skin cancer [220].
- UVC (100-280 nm): UVC radiation is the most energetic and potentially harmful type of UV radiation. However, it is almost entirely absorbed by the Earth's atmosphere and does not reach the surface [221].

UV-induced geometric isomerization is a fascinating phenomenon with diverse implications in fields such as photochemistry, materials science, and pharmacology. Understanding the underlying mechanisms of this process can provide valuable insights into the behaviour of molecules under light exposure and facilitate the design of novel materials or compounds with tailored properties. In this research, a portion of the liquid extract obtained from the filtered solid extract was subjected to UV radiation treatment. Specifically, this liquid extract was transferred into a quartz tube and exposed to UV lamp radiation for 24 hours. Following this exposure period, the extract underwent a rotary evaporation process to remove residual methanol and water until a concentrated, dark black, jelly-like liquid extract was obtained. Subsequently, this extract was dried until it solidified. It's important to note that two types of extracts were utilized for the corrosion inhibition test: the UV-radiated *A. phylicoides* extract and the non-UV-radiated *A. phylicoides* extract. This experimental setup allows for a comparative analysis of the corrosion inhibition properties between the UV-treated extract and the untreated (control) extract. Evaluating both extracts can help researchers gain access to

© University of Venda

the potential impact of UV radiation on the corrosion-inhibiting effectiveness of the *A. phylicoides* extract.

3.3 Electrochemical Measurements

Typically, the initial step in electrochemical investigations involves measuring OCV before proceeding with Potentiodynamic Polarization (PDP) and Electrochemical Impedance Spectroscopy (EIS) in corrosion analyses. This initial OCV measurement aims to establish a foundational corrosion potential, verify system stability, and offer insights into the initial electrochemical characteristics of the material [222]. This systematic approach empowers researchers to execute electrochemical experiments with greater significance and clarity, thereby ensuring the dependability and uniformity of their findings [222].

PDP measures the current-potential relationship of the corrosion process, while EIS enables the determination of corrosion parameters, such as corrosion rate and corrosion current density [223]. PDP measures the amount of current that flows between the corroding material and the reference electrode, while EIS measures the impedance of the corroding material [224]. These two methods provide more detailed information about corrosion. PDP and EIS allow researchers to measure the current and impedance of a corroding material over time [224]. This provides a much more comprehensive picture of the corrosion process than other methods, which only measure corrosion at one point in time. Additionally, PDP and EIS measurements are much more reliable and accurate. Meanwhile, EIS measures the impedance of a metal surface, which indicates the degree of corrosion protection. These techniques are necessary to gain an accurate understanding of the corrosion process. PDP and EIS have proven to be effective in evaluating corrosion protection systems and providing valuable insights into the corrosion process. They are essential tools for corrosion engineers and researchers.

3.3.1 Open Circuit Voltage (OCV)

In corrosion studies, the Open Circuit Voltage (OCV) serves as a pivotal parameter for understanding the electrochemical activity transpiring at the interface of metal surfaces and their surrounding environments. Essentially, OCV denotes the voltage disparity between a corroding metal's surface and a reference electrode in the absence of an external current ("open circuit") [225]. This voltage differential mirrors the thermodynamic driving force governing spontaneous corrosion reactions. Over time, monitoring changes in OCV enables researchers

© University of Venda

to discern shifts in corrosion potential, signalling the initiation or progression of corrosion mechanisms. A rise in OCV may suggest the development of protective oxide layers, while a decline could indicate active corrosion or the breakdown of protective coatings [226].

The selection of a 30-minute interval within the corrosion study timeline likely corresponds to a strategic period for observing short-term corrosion trends. During this timeframe, metal samples are typically subjected to various environmental conditions or inhibitors, with OCV measurements taken at regular intervals to evaluate corrosion behavior and inhibitor efficacy. This approach allows for the timely assessment of corrosion dynamics and the effectiveness of corrosion protection measures. In the specific context of this study, researchers are investigating the corrosion inhibition properties of *A. phylicoides* extracts treated with UV radiation (UV-radiated) compared to untreated extracts (non-UV-radiated). Conducting OCV measurements at 30-minute intervals will help elucidate any disparities in corrosion behaviour between samples treated with UV-radiated and non-UV-radiated extracts. These measurements serve to assess the impact of UV radiation on enhancing the corrosion inhibition capabilities of the *A. phylicoides* extract. Ultimately, the observed changes in corrosion potential and kinetics between the two sample sets provide valuable insights into the underlying mechanisms of corrosion inhibition and the role of UV radiation in modifying the extract's inhibitory properties.

3.3.2 Potentiodynamic Polarization (PDP)

One of the most extensively used methods for assessing specimen corrosion is the potentiodynamic polarization test. This potential difference is used to measure the potential of the working electrode with respect to the reference electrode [227]. The potential difference can be used to determine the concentration of a substance in a solution [228]. The two electrodes are subjected to a cell to measure the potential difference and the current generated [229]. The Auto lab Potentiostat / Galvanostat is designed to measure the potential difference between a reference electrode and a working electrode, and the three-electrode cell allows for precise measurements of current and potential [230]. The Ag/AgCl reference electrode provides a stable and accurate E_{corr} value, and the mild steel or zinc working electrodes allow for different electrochemical reactions to be studied [231]. The Auto lab Potentiostat/Galvanostat was used to measure the desired E_{corr} value by creating an electric circuit between the three electrodes, allowing the current to flow between them. This enabled the Auto lab to measure the desired E_{corr} value by monitoring the current flow through the

© University of Venda

circuit. For all electrochemical tests, the stabilization time was 30 minutes. With the use of the collected information, inhibition efficiency was calculated and compared to that of other methods. Tafel slopes are the slopes of the linear portions of the polarization curve near the corrosion potential. They provide information about the kinetics of the anodic and cathodic reactions involved in the corrosion process. The Tafel slopes can be used to calculate parameters such as the exchange current density and the corrosion rate [232]. Polarization resistance is the resistance to electron transfer at the metal-electrolyte interface [233]. It is inversely proportional to the corrosion rate and can be calculated from the slope of the polarization curve near the corrosion potential. Analysing these polarization dynamic parameters help researchers gain insights into the mechanisms and kinetics of corrosion processes, evaluate the effectiveness of corrosion inhibitors or protective coatings, and predict the long-term performance of metallic materials in specific environments. PDP analysis is an essential tool in corrosion science and engineering for designing corrosion-resistant materials, optimizing corrosion protection strategies, and mitigating the economic and safety implications of corrosion-related failures [234].

Various polarization techniques are utilized in corrosion studies, including Tafel extrapolation, potentiodynamic measurements, cyclic polarization, and linear polarization resistance. However, the focus is solely on Tafel extrapolation due to its significant relevance in corrosion investigations. Tafel extrapolation is a widely employed polarization method for swiftly measuring corrosion rates, offering a faster experimental approach compared to traditional weight-loss estimations [235]. Although corrosion rates determined through Tafel extrapolation of polarization curves often differ from those obtained via weight loss, the versatility of the Tafel equation enables the description of numerous reactions involved in corrosion. This facilitates the representation of mixed potential theory, enabling the prediction of corrosion rates and potentials based on the kinetics and thermodynamics of all reactions occurring on an electrode surface. Tafel kinetics typically provide an accurate depiction of corrosion kinetics under conditions where mass transport limitations are negligible, as corrosion conditions generally deviate from reversible potentials for all reactions [70].

When a metallic electrode is immersed in a corrosive aqueous environment, anodic and cathodic reactions spontaneously occur on its surface, initiating electrode corrosion [236]. The rate of charge transfer at the electrode-electrolyte interface is hindered, indicating that the concentration at the electrode surface is equivalent to that of the bulk when mass transport outpaces charge transfer rate. The relationship between the reaction rate, expressed by current

© University of Venda

density (i), and the driving force or potential (E) is governed by the Butler-Volmer equation for reactions limited by activation overvoltage [237].

$$i = i_0 \exp\left[\frac{\alpha nF\left(E - E_{rev}\right)}{RT}\right] - i_0 \exp\left[\frac{-\left(1-\alpha\right)nF\left(E - E_{rev}\right)}{RT}\right] i = i_0 \exp\left[\frac{\alpha nF\eta}{RT}\right] - i_0 \exp\left[\frac{-\left(1-\alpha\right)nF\eta}{RT}\right] \quad (3.2)$$

In these equations, η represents the overpotential calculated as the difference between the applied potential ($E_{applied}$) and the corrosion potential (E_{corr}), the variables i_0, F, n, T, R, and α denote the exchange current density, Faraday constant, number of electrons, absolute temperature, gas constant, and charge transfer coefficient, respectively. When dealing with distinct anodic and cathodic reactions, if an anodic polarization significantly exceeds the reversible potential by more than 50 mV (overpotential $\eta_a > 50$ mV), the resulting net current density can be determined as follows:

$$i_{net} = i_0 \exp\left[\frac{\alpha nF\eta_a}{RT}\right] \quad (3.3)$$

Upon rearrangement, the Tafel equation becomes:

$$\eta_a = \frac{\beta_a \log i_a}{i_0} \quad (3.4)$$

And

$$\eta_c = -\frac{\beta_c \log i_c}{i_0} \quad (3.5)$$

where β_a and β_c, known as Tafel slopes, are given by:

$$\beta_a = 2.303\frac{RT}{\alpha nF} \quad (3.6)$$

© University of Venda

And

$$\beta_c = 2.303\frac{RT}{(1-\alpha)nF}. \quad (3.7)$$

Utilizing the linear segment of the curve extended to E_{corr} allows for the determination of corrosion current density, as illustrated in Figure 3.1. Assuming uniform corrosion, Faraday's law can be applied to convert corrosion density into the rate of penetration or weight loss. Employing this method enables the measurement of significantly low corrosion rates and facilitates continuous monitoring of the system under examination.

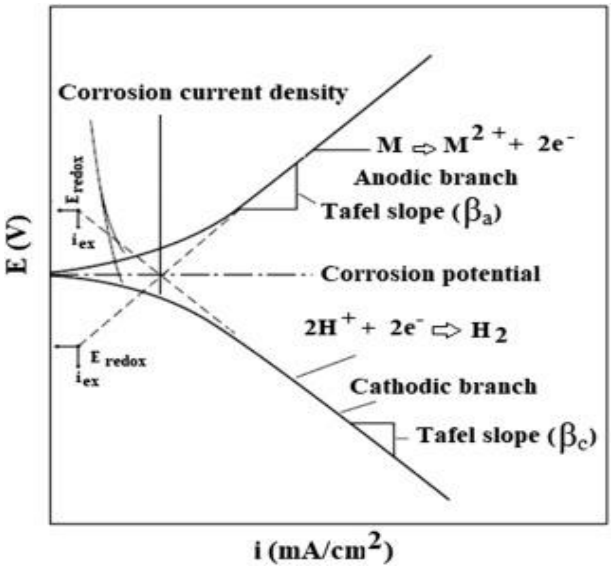


Figure 3.1: Tafel extrapolation (corrosion of metal in acidic medium)

In corrosion studies, the Stern-Geary equation allows for the extraction of quantitative data regarding corrosion potentials and corrosion currents from the slope of the curves, as follows [238]:

$$i_{corr} = \frac{1}{\left(2.303R_p\right)\left(\frac{\beta_a \times \beta_c}{\beta_a + \beta_c}\right)} \quad (3.8)$$

© University of Venda

In this context, i_{corr}, R_p, β_a, and β_c represent the corrosion current density measured in amperes per square centimeter, the corrosion resistance expressed in ohms square centimeter, the anodic Tafel slope given in volts or millivolts pe/r decade of current density, and the cathodic Tafel slope stated in volts or millivolts per decade of current density, respectively. The extent of corrosion inhibition effectiveness was assessed using the subsequent formula:

$$\eta(\%) = 100\left(\frac{i^*_{corr} - i_{corr}}{i^*_{corr}}\right) \quad (3.9)$$

In this equation, i_{corr} and i^*_{corr} represent the corrosion current density for inhibited and uninhibited scenarios, respectively, determined by extrapolating Tafel lines at the corrosion potential.

3.3.3 Electrochemical Impedance Spectroscopy (EIS)

Utilizing EIS measurements in corrosion studies can be performed without damaging the material, allowing for more accurate and up-to-date analysis [239]. The low signal potential applied to the materials being studied is not enough to cause any physical damage but is enough to measure the corrosion rate and other relevant data. Furthermore, the data can be collected quickly and easily, which allows for continuous monitoring and more accurate predictions performance of the material. This makes EIS an invaluable tool for the study of corrosion, as the data can be collected quickly and accurately, with minimal risk of damage to the material being studied via a model made up of solution resistance, polarization resistance, and capacitance of double-layer, impedance is beneficial in analysing how metal and inhibitor solution interact (Rp) [240]. These parameters can provide insight into the interactions between the inhibitor and the surface, helping to optimize the inhibitor's efficacy. Measuring these variables, researchers can use mathematical equations to calculate the efficiency of the inhibitor. Understanding the interactions, scientists can adjust the inhibitor's chemical structure so that it binds more strongly to the surface, making it more effective at preventing corrosion. Ultimately, this helps to create more effective inhibitors for a variety of surfaces, leading to improved efficiency and performance. The corrosion inhibition efficiency was calculated using equation (3.10).

© University of Venda

$$\%IE_{IES} = \left(1 - \frac{R_{ct}^{0}}{R_{ct}}\right) \text{x}100 \quad (3.10)$$

where R_{ct} and $R°_{ct}$ are the charge transfer resistance in the presence and absence of the extract inhibitor.

The resistance transfer charge is the amount of charge that is transferred between two electrodes when current is applied. In the absence of an inhibitor, the charge transfer resistance is relatively low since the current is easily able to flow [241]. However, the inhibitor prevents ions from moving through the gap between the electrodes, increasing the resistance and reducing the current flow [242]. This causes the charge transfer resistance to rise, as the current is blocked. This is because the inhibitor blocks the active sites on the molecules, preventing them from accepting or releasing charges [243]. The more active sites that are blocked, the higher the charge transfer resistance, and the harder it is for molecules to move. The alternating current-based EIS method can be used to better understand the corrosion mechanism and assess the efficacy of various corrosion-prevention strategies, such as inhibitors or coatings. At infinite frequency, the impedance of the capacitor is zero. In between, impedance is determined by the capacitance and the frequency of the alternating current [244]. This is because the capacitor's ability to store energy is proportional to the frequency of the alternating current [180]. As the frequency increases, the capacitor's ability to store energy decreases, which leads to a decrease in impedance [245]. In parallel electrical circuits, the smallest impedance circuits predominate, and the information gathered can be used to calculate the sum of Rs and Rp [80]. EIS has several benefits over other methods for assessing metal corrosion, including the following:

a) This data helps researchers understand how cells respond to changes in the environment and how to best manipulate them for various purposes.

b) Examining the data, researchers can look for patterns in cellular behaviour and use those insights to inform their research. For example, they can use the data to create models to simulate the effects of different environmental conditions on cells.

c) The detailed data allows researchers to identify the rate of corrosion, and the chemical processes involved in the corrosion. This can help them understand the corrosion process mechanics.

d) The detailed data can help researchers determine the rate at which metals corrode, and what

© University of Venda

factors can accelerate or slow down the process. It also allows researchers to track the chemical processes involved in the corrosion, which can help them identify which parts of the metal are most susceptible to corrosion and create preventive measures. Additionally, the data can provide details on the capacitance and resistance of metal coatings, which can help researchers develop coatings that are more resistant to corrosion.

3.4. Wettability Study

Exploring corrosion behavior and assessing wettability, particularly through contact angle measurements, is vital for various reasons such:

- Preventive Measures: comprehending how materials corrode in different environments help engineers and scientists to develop preventive measures to prolong the lifespan of structures, equipment, and devices [246].
- Safety: Corrosion can compromise the structural integrity of metals, leading to catastrophic failures in critical systems. Investigating corrosion behaviour helps identify potential risks and implement safety protocols [247].
- Cost Reduction: Corrosion-related damage incurs substantial costs for maintenance, repairs, and replacements [248]. Studying corrosion behaviour enables the optimization of materials and coatings, minimizing expenses in the long term.

The wettability of mild steel and zinc was examined through contact angle surface measurements. High-resolution images were captured using a smartphone camera set to macro mode. The angles of the drops were analysed using ImageJ software in conjunction with drop analysis-LB-ADSA. The drops were deposited onto the metal surface using a pipette.

3.5 Scanning Electron Microscopy (SEM)

The electrons interact with the sample, creating a signal that is used to generate an image [249]. The image is then used to study the sample's topography, chemistry, and other properties. The electrons interact with the sample's atoms and molecules, which causes them to emit their own secondary electrons [249]. These secondary electrons are then collected and used to create a three-dimensional image of the sample's surface. This image gives scientists insight into the sample's topography, chemistry, and other properties. Adjusting the voltage of

© University of Venda

the electron beam help scientists gain refined view of the sample's properties. This is because different voltages cause the electrons to interact differently with the sample's atoms and molecules [250]. Additionally, increasing the voltage increases the energy of the electrons, which can penetrate deeper into the sample, allowing scientists to study deeper layers of the sample. This allows scientists to magnify the sample and study it in detail. The electrons interact with the sample's atoms and molecules in very specific ways, allowing scientists to determine the composition and structure of the sample [199].

3.6 Fourier Transform Infrared Spectroscopy (FTIR)

FTIR is accomplished by using a beam of infrared light that passes through a sample and is then divided into its component wavelengths [251]. The sample then absorbs certain wavelengths of light, which are then measured by the FTIR spectrometer [252]. This data is then used to create an infrared absorption spectrum, which can be used to identify the composition and properties of the sample. Measuring the amount of infrared light absorbed by each bond help the FTIR spectrometer to then determine the types of bonds present in the molecule and the strength of those bonds. This information is then used to identify the composition of the sample and its properties. The specific position of the absorption bands in the spectrum can be used to identify the functional groups present in the molecule [253]. The intensity of the absorption bands can indicate the ratio of the bond types, such as C-H, C-C, C-O, and C-N bonds, in the sample. This information can be used to identify the molecular structure and determine its physical and chemical properties. The results of the FTIR spectroscopic analysis provided clues as to how the corrosion inhibitor interacted with the corroded zinc and mild steel and how effective it was in protecting the metals from corrosion. The analysis showed that the inhibitor could form a protective barrier on the surface of the metals, thus preventing further corrosion. The results also showed that the inhibitor is highly effective in mitigating corrosion damage on the metals. The results indicated that the inhibitor was able to bind to the metal surface and form a protective layer that repelled water, thus preventing corrosion. The inhibitor should also reduce the rate at which corrosion occurs, which allowed it to remain effective for longer periods of time [22]. The analogue signal is read by a detector, which then transforms it into a spectrum. The signals are analyzed by a computer, which also locates the peaks. Using a partially silvered mirror, an IR beam is split into two equal-intensity beams [254].

© University of Venda

3.7 Weight Loss Measurements (WLM)

Weight loss measurements are one of the best methods to use in corrosion study because it considers the mass loss of the metal due to the corrosive attack. It is also easy to conduct, as it can be done in a laboratory setting, and the results are usually accurate and reliable [255]. Additionally, it is a cost-effective method, as it does not require expensive equipment or a large workforce. Furthermore, it can be used to measure the corrosion rate and the corrosion products of a metal. It is also suitable for measuring different types of metals, including stainless steel and aluminum, and can be used to test different environmental conditions.

This method helps determine the protective properties of a coating or other surface treatment, as well as for predicting the lifetime of a metal product in each environment [256]. It also provides an accurate measure of corrosion rate that can be used to make more informed decisions about product design, materials selection, and preventive maintenance requirements. Using glass rods and hooks, MS and Zn having a surface area of 12 cm^2 were fully immersed in the corrosive medium for 6 hours. This experiment was conducted to determine the corrosion rate of those metals in the corrosive medium. The results of the experiment can be used to help understand how different metals respond to different corrosive environments, and how they can be protected against corrosion.

For the blank test, 0.2 M, 0.4M, 0.6M, 1.0M, and 1.5M concentrations of sulphuric and hydrochloric acids were used without the corrosion inhibitor as corrosive media. Various concentrations of inhibitor molecules, 100ppm, 400ppm, 700ppm, 1000ppm, and 1300ppm, were prepared in 1.5 M HCl and H_2SO_4. The purpose of the test was to evaluate the corrosion inhibition of the inhibitor molecules in different concentrations of sulphuric and hydrochloric acids. The corrosion inhibitor and acids were added to the beakers and metal was immersed to determine the effectiveness of the inhibitor at different concentrations. Weight loss was recorded and analysed in all experiments with and without the inhibitor.

The gravimetric analysis measures a change in mass to estimate the mass or concentration of a substance [372]. The term "analyte" refers to the substance about to be measured [373]. In this study, gravimetric analysis has been utilized to measure mass loss during the corrosion of zinc and mild steel. The mass loss was measured in the absence and presence of a corrosion inhibitor. It was necessary to perform a blank corrosion experiment before adding a corrosion inhibitor for several reasons such as:

- Baseline Measurement: A blank corrosion experiment provides a baseline measurement

© University of Venda

of the corrosion rate without the presence of a corrosion inhibitor. This baseline serves as a reference point for comparison when the inhibitor is introduced [374].

- Assessment of Inhibitor Effectiveness: Through comparing the corrosion rate in the absence of an inhibitor (blank experiment) with the corrosion rate in the presence of an inhibitor, researchers can assess the effectiveness of the inhibitor. The difference between the two measurements helps determine the extent to which the inhibitor reduces the corrosion rate [375].
- Control for External Factors: Blank experiments help control for external factors that may influence the corrosion process. Any changes observed in the presence of an inhibitor can be more confidently attributed to the inhibitor's effects when compared to a baseline without the inhibitor [376].
- Establishing Corrosion Environment Stability**:** Performing a blank experiment allows researchers to ensure that the experimental conditions, such as temperature, humidity, and exposure time, are stable and consistent. This is important for drawing reliable conclusions about the corrosion inhibitor's impact [377].
- Accounting for Background Effects: Blank experiments help account for any background effects, including impurities in the testing environment or experimental setup, that might contribute to changes in mass [378]. This ensures that the observed changes are specific to the corrosion process and inhibitor interaction.
- Data Interpretation and Validity: Having a baseline measurement helps in the interpretation of results. It ensures that any observed changes are significant and not simply variations that could occur naturally during the experiment [379].

Performing a blank corrosion experiment before introducing a corrosion inhibitor is a standard practice to establish a baseline, control for external factors, and ensure that observed changes can be attributed to the inhibitor's effects. This systematic approach enhances the reliability and validity of the experimental results. This methodological principle is widely recognized in corrosion studies, as highlighted in the work of Laurent, Bennett, and Harrington (2017) on the development of test methods and factors for the evaluation of oilfield corrosion inhibitors at high temperatures, presented at NACE CORROSION [380].

© University of Venda

Effect of Temperature

After conducting a blank corrosion experiment and observing the corrosion behavior of a metal in a specific environment without any inhibitors, introducing inhibitor experiments becomes crucial for several reasons:

- Assessment of corrosion inhibition efficiency: The primary purpose of adding inhibitors is to evaluate their effectiveness in reducing or preventing corrosion. During the comparison of the corrosion rate and extent of metal loss in the presence and absence of inhibitors, one can assess the inhibiting efficiency of the *A. phylicoides* extract.
- Identification of effective inhibitors: Various inhibitors may exhibit different degrees of effectiveness against corrosion. Conducting inhibitor experiments helps in identifying which inhibitors are most successful in mitigating the corrosion process. This information is vital for selecting the most suitable corrosion inhibitor for a given application. In this study, *A. phylicoides* leaves extract has thousands of compounds, it is then important to identify which compounds are responsible for inhibition.
- Optimization of inhibitor concentration: Inhibitors are typically used in different concentrations. Through a series of experiments with varying inhibitor concentrations, one can determine the optimal amount needed to achieve the desired level of corrosion protection. Too much or too little inhibitor may not provide the best results.
- Understanding inhibition mechanisms: Inhibitors work through various mechanisms, such as forming a protective film on the metal surface, altering the electrochemical processes, or scavenging corrosive species [392]. conducting inhibitor experiments, help gain insights into the specific mechanisms by which the inhibitors function.
- Compatibility and stability testing: It's important to ensure that the chosen inhibitors are compatible with the system and do not introduce unwanted side effects. Additionally, the stability of inhibitors under the experimental conditions needs to be assessed to determine their long-term effectiveness.
- Economic considerations: Inhibitors may have associated costs. Assessing their performance in corrosion experiments helps in evaluating the cost-effectiveness of using inhibitors in a particular application.

The addition of inhibitor experiments is crucial for understanding the protective capabilities of corrosion inhibitors, optimizing their use, and selecting the most effective and economically

© University of Venda

viable solution for corrosion mitigation in a specific system [137].

3.8 Geometry of Molecules

The shape of a molecule is determined by the electron-pair geometry, which is based on the arrangement of the electron pairs around the central atom [257]. This arrangement is determined by the repulsion of the electron pairs, which causes them to move away from each other and take up a three-dimensional shape. It depends on the surrounding atoms and electron pairs as well as the core atom. The Valence Shell Electron Pair Repulsion (VSEPR) approach can be used to forecast the shape of most molecules [258].

3.8.1 The Geometry Parameters

The second set of design variables is made up of geometric parameters, and using the kinematic refinement technique, a connection with a better kinematic performance criterion is established.

3.8.2 Molecular Conformations

Any spatial configuration of a molecule's atoms that can be changed by rotations around formally single bonds is known as a molecular conformation. Polynucleotides, polypeptides, and polysaccharides are examples of biopolymers that can alter shape in response to environmental changes [259].

3.8.3 Molecular Geometry and Potential Energy Surface

A potential energy surface is a frequent idea in theoretical and computational chemistry. The relationship between a molecular geometry, or the positions of its constituent atoms in relation to one another, and energy is described by the molecular of the surface of potential energy.

3.9 Quantum Chemical Approaches

Quantum chemical approaches involve using principles of quantum mechanics to understand and predict the behavior of molecules and materials at the atomic and electronic levels. In chemistry, these approaches help calculate properties such as molecular structure, reactivity,

© University of Venda

and interactions with other molecules. Here are some core quantum chemical methods used in research:

3.9.1. Schrödinger Equation

This session will provide a detailed explanation of quantum chemical approaches to study the corrosion inhibition potential of *A. phylicoides* plant extract. Quantum chemical approaches are widely useful to study the interaction between metals and corrosion inhibitors [260]. In this study, quantum chemical approaches are used to examine the interaction between mild steel, zinc, and *A. phylicoides* plant extract as corrosion inhibitors. These quantum chemical approaches involve applying quantum mechanics principles to calculate electronic structures, energies, and properties of molecules involved in the corrosion inhibition process. Quantum chemical calculations were used because of their ability to give evidence to experimental results obtained from other approaches like electrochemical techniques, and gravimetric analysis. The quantum mechanical approach differs from the molecular mechanics approach because it focuses on the interactions between electrons within molecules to explain the chemistry of molecules [261]. An electron and a nucleus are the components of a molecule. The Schrödinger Equation defines knowledge about the system. The Schrödinger equation was proposed by Erwin Schrödinger, the Austrian physicist in 1926 [262]. This equation is the basis for finding the wavefunction of any system. Equation 2.10 shows the time-independent Schrödinger equation. This equation is suitable for a particle of mass m that is moving in one dimension with energy E in a system that is time independent. The Schrödinger equation for a particle of mass m moving in one dimension with energy E in a time-independent system can be written as [263]:

$$-\frac{\hbar^2}{2m}\frac{d^2\psi}{dx^2} + V_{(x)}\psi = E\psi \tag{3.11}$$

where:

- ħ is the reduced Planck's constant (h-bar),
- ψ(x) is the wavefunction of the particle as a function of position x,
- V(x) is the potential energy function of the system, which depends on the position x,

© University of Venda

- E is the total energy of the particle.

In this equation, the left-hand side represents the kinetic energy operator, which is related to the second derivative of the wavefunction with respect to position. The right-hand side represents the potential energy of the system multiplied by the wavefunction. The equation states that the sum of the kinetic energy and the potential energy of the particle is equal to its total energy. To solve equation 2.10, boundary conditions or additional constraints are typically applied to obtain specific solutions for the wavefunction ψ(x) and corresponding energy levels E. The solutions provide information about the probability distribution of finding the particle at different positions in the system.

Note that this is the time-independent Schrödinger equation, applicable when the system does not vary with time. For time-dependent systems, the time-dependent Schrödinger equation is used, which incorporates the time evolution of the wavefunction [264].

For three-dimensional systems, the equation above can be expressed as.

$$-\frac{\hbar^2}{2m}\nabla^2\psi + V_{(x)}\psi = E\psi \tag{3.12}$$

In this equation, V depends on the position, and the right-side part of the first term in the equation can be expressed as below [264].

$$\nabla^2 = \left(\frac{\partial}{\partial x^2} + \frac{\partial}{\partial y^2} + \frac{\partial}{\partial z^2}\right) \tag{3.13}$$

According to the Schrödinger equation, the Hamiltonian operator and wave function of a system or molecule are determined entirely by the coordinates of its particles. As a result, all electrons and nuclei coordinate for a molecule or system play a crucial role. In addition to providing an expression for the wavefunction, solving the Schrödinger equation also produces the corresponding energy values of the system. The solutions obtained with this equation are known as atomic orbitals for chemical systems like atoms, and molecular orbitals for chemical systems like molecules [261].

© University of Venda

3.9.2. The Born Oppenheimer Approximation Approach

There is a simplification at the outset of all theories of molecular structure. Unlike the Schrödinger equation for hydrogen atoms, where an exact solution can be found, the Schrödinger equation for molecules cannot be solved exactly because the simplest molecules contain three particles (two nuclei, one electron) [265]. Due to the vast mass difference between a nucleus and an electron, the Born–Oppenheimer approximation is employed, whose assumption is that nuclei move relatively slowly and are treated as stationary while electrons move. Thus, we can solve the Schrödinger equation for the wave function of electrons alone by considering the nuclei to be fixed at arbitrary locations [266]. The Born-Oppenheimer Approximation is the assumption that the electronic motion and the nuclear motion in molecules can be separated [267]. It leads to a molecular wave function in terms of electron positions and nuclear positions.

This involves the following assumptions:

- The electronic wavefunction depends upon the nuclear positions but not upon their velocities, i.e., the nuclear motion is so much slower than electron motion that it can be fixed [268].
- The nuclear motion (e.g., rotation, vibration) sees a smeared-out potential from the speedy electrons.

The total wavefunction is often expressed as the product of the electronic wavefunction and the nuclear wavefunction [268]. This concept is fundamental to the Born-Oppenheimer. Consider the equation (3.14):

$$\Psi_{total}(x, y) = \psi_{electrons}(x)\,\psi_{nuclei}(y), \tag{3.14}$$

where x is the coordinates of the electrons and y represents the coordinates of the nuclei. The total energy of the system is the summation of the potential and kinetic energies of the electrons, as well as the repulsion potential energies of the nuclei, expressed as:

$$E_{total} = E_{electrons} + E_{nuclei}. \tag{3.15}$$

© University of Venda

Electronic computations are executed for various fixed nuclei frameworks, each of which corresponds to distinct energy values [269]. The frameworks that correspond to the minimum energy values are deemed the equilibrium geometries of the molecule.

3.9.3. The Hartree-Fock Approximation Approach

In molecular systems, there are multiple electrons, so this is another method of approximating the Schrödinger equation. Assuming electrons are independent in a multi-electron system is the simplest way of writing the wavefunction in the HF approximation [270]. A single electron's motion is not affected by the motions of the others. A molecule can only take two electrons at a time using Pauli's Exclusion Principle [271]. Additionally, electrons have intrinsic spin, so each electron has both the space coordinates (molecular orbital) and the spin coordinates (spin-orbital). Molecular spin orbitals are denoted by (ψ) and represent the overall molecular orbital. The total wavefunction can then be expressed as the product of functions (ψ), each determined by the coordinates of a single electron [272].

$$\Psi = \psi_1 (1)\, \psi_2 (2) \ldots \psi_N (N), \tag{3.16}$$

where electron 1 occupies molecular spin-orbital ψ_1 and electron 2 occupies molecular spin-orbital ψ_2. The molecular spin-orbital must follow the anti-symmetric condition, i.e., for any system with N-electrons, the sign of the wavefunction must change when the electrons are exchanged.

As an example, if a wavefunction contains the coordinates of two or more electrons, the signs must alter upon switching their positions. Consequently, the molecule is deemed unsymmetrical as per equation (3.17). Conversely, if the signs remain unaltered, the molecule is regarded as symmetric as per equation (3.18).

$$\psi (1, 2) = - \psi (2, 1) \tag{3.17}$$

$$\psi (1, 2) = \psi (2, 1) \tag{3.18}$$

© University of Venda

Upon consideration of all possible permutations of particles, a superior anti-symmetric wavefunction as described by equation (3.19) is achieved through the utilization of a linear combination of said permutations within the total wavefunction [273].

$$\psi_{total}(1,2,\ldots.n) = \frac{1}{\sqrt{n!}}\Sigma(-1)^{p}\psi_1(k_1)\psi_2(k_2)\ldots.\psi_n(k_n) \quad (3.19)$$

The letter "p" represents the number of transpositions performed on the starting $\psi_1(1)$ $\psi_2(2)$ … $\psi_n(N)$ to obtain the given term in the linear combination; k_1, k_2..., k_n are the coordinates resulting after the permutations and $\frac{1}{\sqrt{n!}}$ is the normalization factor. The factor $(-1)^p$ ensures that the wavefunction does not change sign for an even number of transpositions, but only changes sign for an odd number of transpositions.

An additional approximation that is associated with the Hartree-Fock approximation entails substituting the many-electron Hamiltonian operator with an effective one-electron Hamiltonian, known as the Fock operator [274]. The Fock operator encompasses all the one-electron terms of the Hamiltonian operator, including kinetic energy and nuclei-electron attraction potential terms. It also accounts for an effective potential that is perceived by one electron due to the presence of Z-1 electrons surrounding it. However, a challenge arises when attempting to determine an average value of the potential, as it necessitates knowledge of the electron distribution to accurately evaluate the potential energy. Unfortunately, the electron distribution can only be determined after solving the Schrödinger equation, which requires an iterative procedure known as the Self Consistent Field (SCF) procedure [275].

The Self Consistent Field (SCF) procedure is a method that is applied to both the study of atoms and molecules [276]. This approach is particularly well-suited for use in computational analysis due to its algorithmic nature. Initially, an estimated average potential is incorporated into the Hamiltonian operator, and the resulting Schrödinger equation may be solved [277]. The solutions obtained are then utilized to evaluate the average potential energy. If this value differs significantly from the initial estimate, the new value is used to rewrite the Schrödinger equation. This process is repeated until the difference between the value obtained at the end of a cycle and the value utilized at the beginning of that cycle is less than a predetermined cut-off value. This iterative procedure is commonly referred to as the Self Consistent Field (SCF) procedure [277].

© University of Venda

3.9.4 Linear Combination of Atomic Orbitals and Basis Sets

To conduct a calculation using molecular-orbital theory, it is necessary to ascertain each of the molecular orbitals, denoted as ψi in equation 2.18, and to determine the energy associated with the total wavefunction. The conventional approach for determining the molecular orbitals and their corresponding energies involves expressing the molecular orbitals as a linear combination of atomic orbitals (LCAO) and subsequently determining the coefficients in the LCAO through a self-consistent field method [276]. The LCAO approximation is founded on the premise that molecular orbitals can be constructed by combining simpler functions, such as the atomic wave function from which the molecule is composed. For example, if an electron is in an atomic orbital belonging to atom X and in an atomic orbital belonging to atom Y, the overall wavefunction is a superposition of the two atomic orbitals [278].

$$\psi\pm = N\,(X \pm Y) \tag{3.20}$$

The normalization factor is denoted by N in the above equation. The term commonly used to express superposition in this equation is the linear combination of atomic orbitals. Basis functions, such as atomic wavefunctions, are combined to form a molecular function. A collection of basis functions utilized to construct a molecular function is referred to as a basis set. The LCAO-MO, an estimated molecular orbital derived from a linear combination of atom orbitals, is obtained [279]. When generating a molecular orbital using more than two basis functions, it is more appropriate to employ the equation [279].

$$\psi\pm = \sum_i c_i \chi_i \tag{3.21}$$

The basic functions, denoted by χ (typically centered on atoms), and the expansion coefficients, represented by c_i, are utilized in the formation of basis sets. Typically, atomic orbitals are employed in the creation of these sets. For example, in the instance of the H_2 molecule, the molecular orbital can be established as a linear combination of the sigma (S) atomic orbital on one H atom (H_A) and the sigma atomic orbital on the other H atom (H_B). Consequently, the molecular orbital (ψ) for the hydrogen molecule can be expressed as:

$$\psi \approx 1S_{H_A} + 1S_{H_B} \tag{3.22}$$

© University of Venda

The precision of the approximations to the molecular orbitals increases proportionally with the magnitude of the basic functions chosen for their formation. It is imperative to acknowledge, nonetheless, that the identification of an appropriate basis set is contingent upon the magnitude of the molecule under investigation.

Minimal basis set: Basis sets of this type describe only the most basic aspects of atomic orbitals, one basis function for each angular momentum component of an orbital [280]. It has the minimum number of basis functions (c) that is needed to describe the ground states of the component atoms in a molecule. Ammonia molecules (NH_3) need eight basis functions instead of the eight atomic functions available in an ammonia molecule. The hydrogen atoms would have three 1s orbitals, whereas the nitrogen atoms would have 1s, 2s, $2p_x$, $2p_y$, and $2p_z$ atomic orbitals [281]. In a similar manner, the carbon dioxide (CO_2) molecule would require 15 basis functions in place of the 15 atomic functions present in the molecule. A Slater-type orbital may also be approximated by a combination of two or more Gaussian-type orbitals leading to such basis functions as STO-2G, STO-3G, etc [282].

It should be noted that all minimal basis sets possess certain limitations. One such limitation is that all basis functions are either spherical or form sets that collectively describe a sphere. As a result, minimal basis sets are well-suited for describing molecular systems with a spherical molecular environment but are not appropriate for characterizing atoms with an aspherical molecular environment. Another limitation of minimal basis sets is that the basis functions are centered on the atom, rather than between atoms. This deficiency implies that minimal basis sets are unable to accurately describe the electron distribution between nuclei, which is a crucial factor in chemical systems [283].

Double zeta basis sets: The basis sets utilized in this study are constructed in a manner whereby each atomic orbital within a molecule is expressed as a linear combination of two Slater-type orbitals [284]. For example, in the case of water, which comprises seven atomic orbitals, the double zeta basis set is designed to contain 14 basis functions, with two basis functions assigned to each atomic orbital in the water molecule. The inclusion of two Slater-type functions to describe the molecular orbital is intended to enhance the flexibility of the molecular orbital, thereby enabling the accurate description of the electron distribution within the molecule [285]. This approach allows for the use of contracted orbitals to describe atoms with a positive charge, while diffuse orbitals can be employed to describe atoms with a negative charge. To achieve a more precise description of the various molecular

© University of Venda

environments, the two Slater-type functions utilized in the basis set (to represent each atomic orbital) need not be of equal size, as they are constructed from different ζ orbital exponents [286]. For instance, a 2s function can be constructed through a linear combination of two STO functions, with orbital exponents ζ_1 and ζ_2.

$$\chi_{2s}(r) = \chi_{2s}^{STO}(r, \zeta_1) + d\chi_{2s}^{STO}(r, \zeta_2) \tag{3.23}$$

The constant d is utilized to factor in the contribution of the second Slater-type orbital (STO) in the basis function that has been constructed. Given that the two atomic orbitals may possess varying sizes, the double zeta basis set exhibits a certain degree of reduced spherical character, which can be characterized as having anisotropic properties concerning minimal basis sets.

Split valence basis set: the representation of inner-shell atomic orbitals is accomplished through a single basis function, while valence orbitals are represented by two or more basis functions [287]. For example, the 3-21G basis set employs a contracted Gaussian function to describe the inner core orbital (1s), which is formed through a linear combination of three primitive Gaussian functions. The valence atomic orbitals are further categorized into inner (2s) and outer (2p) valence atomic orbitals. The inner valence atomic orbital is described by a contracted Gaussian function, which is a linear combination of two primitive Gaussians, while the outer valence atomic orbital is described by a single primitive Gaussian function [288]. For instance, in the case of the oxygen atom, the inner core orbital is a 1s and is described by a linear combination of three primitive Gaussian functions. The inner valence atomic orbital is the 2s and is described by a linear combination of two primitive Gaussian functions, while the outer valence orbitals are the $2p_x$, $2p_y$, and $2p_z$, each of which is described by a single primitive Gaussian function. Consequently, the overall basis set for the oxygen atom comprises eight primitive Gaussian functions. The 6-31G basis set, on the other hand, specifies that each inner-core orbital is represented by a contracted Gaussian function, which is a linear combination of six primitive Gaussian functions. Each valence orbital, on the other hand, is represented by two basis functions, namely, a contracted Gaussian function that is a linear combination of three primitive Gaussians describing the inner valence electrons and a primitive Gaussian function describing the outer valence electrons [289].

© University of Venda

Polarization functions: The utilization of polarization functions is imperative in achieving an accurate description of chemical bonds within molecular systems [290]. It has been observed that both minimal basis sets and split-valence basis set functions, which are atom-centered, are inadequate in providing a comprehensive depiction of the region between atoms. The inclusion of additional basis functions is therefore necessary to improve the quality of the basis set. Polarized basis functions are commonly employed to account for the region between atoms. Polarization refers to the distortion of a system's electron cloud because of the presence of neighboring species. To address this, contracted Gaussian functions that consider the distortion of the electron cloud of chemical species must be selected and incorporated into the basis set. These functions are referred to as polarization functions and are constructed by adjusting the angular momentum parameters (equations 2.30 and 2.31) [290]. The polarization functions are constructed by adjusting the angular momentum parameters polarized basis functions are denoted by an asterisk (*) at the end of the notation of the basis set. For example, the 6-31G* (also known as 6-31(d)) represents the addition of polarization functions of the d type for each of the heavy atoms. When polarization functions are also added to the H atoms, the basis set is denoted as 6-31G** (also known as 6-31G(d, p)), where the second asterisk represents the p functions added to the H atom. These types of functions are crucial in describing various phenomena, such as hydrogen bonding, where the orbitals on the H atom are distorted due to the electron cloud of the neighboring O atom and are not necessarily spherical.

Diffuse functions: Diffuse functions are formulated to account for instances where the electron distribution may be situated further away from the nucleus, such as in anionic systems [291]. To incorporate these features, the inclusion of diffuse functions is necessary. These functions are generated by the addition of minute zeta exponents to a basis set, which is represented using + signs. The addition of one + sign indicates the inclusion of diffuse functions on heavy atom orbitals, while the use of ++ signifies the inclusion of diffuse functions on both s orbitals of the hydrogen atom and heavy atom orbitals. For example, the 6-31G(d) basis set is denoted as 6-31+G(d) when diffuse functions are added to the s and p atomic functions to describe the character of heavy atoms, and as 6-31++G(d) when diffuse functions are also added to the s orbital on the hydrogen atom [280].

Effective core potentials (ECP) basis set: The basis sets that have been described above are appropriate for the characterization of molecules that contain main group elements, provided that the number of core electrons is not excessively large [292]. However, when the number

© University of Venda

of core electrons is substantial, as is the case with transition metal atoms (such as Fe, Co, Cu, etc.), the utilization of such basis sets becomes computationally prohibitive. To address this limitation, basis sets that employ an effective potential to describe the nucleus and core electrons/orbitals, as well as pseudo-potentials to describe the valence electrons, are frequently employed for the characterization of transition metal atoms/ions. The rationale for the use of such basis sets is based on the observation that core (inner) orbitals are typically not significantly affected by changes in chemical bonding. These basis sets, while simulating the presence of the core electrons using an effective potential, explicitly treat only the valence electrons or the two outermost electron shells of the atom. The utilization of pseudo-orbitals, which are characterized by their smooth and node-free nature, serves as a replacement for valence orbitals [293]. These pseudo-orbitals possess the ability to accurately replicate the behavior exhibited in the valence region. The omission of explicit computation of core electrons accounts for the observed decrease in computational time required for the evaluation of systems containing transition metal atoms [294].

One advantageous attribute of ECP basis sets is their incorporation of relativistic effects, which are crucial for the accurate characterization of heavy atoms, particularly transition metal atoms. As such, these effects cannot be disregarded in precise investigations. Unlike conventional basis sets, ECP basis sets are not regarded as orbitals, but rather as modifications to the effective Hamiltonian. However, a limitation associated with ECP basis sets is their inability to eliminate electron density in the core region, despite their capacity to eliminate density originating from core orbitals. Instead, the core-region density of the true core orbitals is replaced by the core-region density of the pseudo valence orbitals, which are valence orbitals without nodes that are determined in the presence of an ECP and the absence of explicit core orbitals [295].

3.9.4.1. Linear Combination of Atomic Orbitals

The LCAO method is a mathematical approach used to construct molecular orbitals for a molecule by combining atomic orbitals from the constituent atoms. The basic idea is to express the molecular wavefunction as a linear combination of atomic wavefunctions (atomic orbitals), which are known solutions to the Schrödinger equation for individual atoms.

© University of Venda

Mathematically, the LCAO method involves adding up the contributions of atomic orbitals with appropriate coefficients to form molecular orbitals. The coefficients are typically determined through variational methods to minimize the energy of the system [296].

The LCAO method is widely used in quantum chemistry because it provides a relatively simple and practical way to approximate the electronic structure of molecules. It can be used with various levels of complexity, from simple diatomic molecules to larger and more complex systems [297].

Using the LCAO method help predict molecular properties and study chemical reactions, making it an essential tool in computational quantum chemistry.

The molecular orbital resulting from the linear combination of atomic orbitals is called Linear Combination of Atomic Orbitals-Molecular Orbital (LCAO-MO). The wavefunction is dependent to the type of the orbitals, such as bonding and antibonding orbitals. In cases of bonding orbitals, the probability density is expressed as [298].

$$\psi_+^2 = N^2(A^2 + B^2 + 2AB) \tag{3.24}$$

In this case both atomic orbitals have similar amplitudes. From equation (3.24), A^2 is the probability density of electrons when confined to atomic orbital A, B^2 is the probability density if electrons were confined to atomic orbital B and 2AB is the contribution to the density from atomic orbitals A and B. This contribution is also known as the overlap density, and it assist in finding the electron in the internuclear region. In cases of antibonding orbitals, the probability density is expressed as in equation (3.25) [299].

$$\psi_-^2 = N^2(A^2 + B^2 - 2AB) \tag{3.25}$$

The symbols in the equation (3.25) are the same as the symbols in the equation (3.24). According to their bonding nature, linear combinations of atomic orbitals correspond to different energies. An antibonding orbital's wavefunction corresponds to a higher energy than a bonding orbital. During destructive interference, two atomic orbitals overlap each other and cause antibonding orbitals. From equation (3.25), it can be seen that -2AB reduces the probability density [300].

© University of Venda

Molecular orbitals and the LCAO method are essential concepts in understanding the electronic structure of molecules. The LCAO method allows us to construct molecular orbitals by combining atomic orbitals from constituent atoms, and the resulting molecular orbitals provide valuable information about the behaviour and properties of molecules.

3.9.4.2. Basis Sets

In theoretical and computational chemistry, a basis set is a set of functions (called basis functions) that is used to represent the electronic wave function in the Hartree–Fock method or density-functional theory to turn the partial differential equations of the model into algebraic equations suitable for efficient implementation on a computer [301].

The basis set can either be composed of atomic orbitals (yielding the linear combination of atomic orbitals approach), which is the usual choice within the quantum chemistry community; plane waves which are typically used within the solid-state community, or real-space approaches. Several types of atomic orbitals can be used: Gaussian-type orbitals, Slater-type orbitals, or numerical atomic orbitals. Out of the three, Gaussian-type orbitals are by far the most often used, as they allow efficient implementations of post-Hartree–Fock methods [302].

3.9.5. Ab Initio Methods

Ab initio methods enable the determination of the fundamental properties of materials through the application of quantum mechanics principles. The term "ab initio" originates from Latin and denotes "from the beginning". This phrase is utilized to describe methods that rely on the direct solution of the Schrödinger equation, without the incorporation of experimental data. As a result, ab initio methods are highly rigorous but also tend to be relatively costly compared to techniques that incorporate experimental values. Various ab initio methods are distinguished based on the approach employed to solve the Schrödinger equation. Semi-empirical methods are derived from the Hartree-Fock method and do not directly solve the Schrödinger equation [303]. Instead, they neglect or substitute certain integrals in the Schrödinger equation with empirical or experimental parameters. Examples of the neglected integral terms include the differential overlap integrals, as described in Roothaan-Hall equations. As indicated in the three bullet below, the remaining integrals can be:

© University of Venda

- Used to determine the functional form of atomic orbitals.
- Converted into parameters and given values based on few experimental data;
- Made into parameters and given values based on the fitting to many experimental values.

3.9.5.1 Roothaan-Hall Equation and the Hartree-Fock Method

The development of the Roothaan-Hall equations is predicated upon the observation that, to accurately describe the spherical nature of atoms, the Hartree-Fock (HF) approximation must be numerically solved for the spin orbitals. However, such numerical solutions are not feasible within a reasonable computational timeframe for the purpose of characterizing molecular properties. The Roothaan-Hall equations represent modifications of the HF approximation and were developed through the application of the Hartree-Fock and Linear Combination of Atomic Orbitals (LCAO) approximations to the electronic Schrödinger equation [304]. The Hartree-Fock equations, upon which this procedure is based, can be obtained by considering the Hamiltonian operator in the following form [305]:

$$\hat{H} = \sum_{i} h + \frac{1}{2} \sum_{ii} \frac{e^2}{4\pi\varepsilon_0 r_{ii}} \tag{3.26}$$

The hydrogenic Hamiltonian, denoted as h and referred to as the core Hamiltonian, describes the behavior of electron i in the presence of a bare nucleus with a charge of Ze. The inclusion of a factor of $\frac{1}{2}$ in the double sum serves to avoid the duplication of interactions. The prime notation on the summation signifies the exclusion of terms where i = i′, as it is commonly accepted that electrons do not interact with one another. Subsequently, the Hartree-Fock equation can be derived for a spatial orbital (ψ_a) that is occupied by a single electron [306].

$$\left\{h_1 + \sum_{u} (2J_u - k_u)\right\}\Psi_a(1) = \varepsilon_a \psi_a(1) \tag{3.27}$$

© University of Venda

where the sum is over all occupied spatial wavefunctions, J_u is the Coulomb operator, K_u is the exchange operator and ε_a is the one-electron orbital energy. The coulomb operator (J_u) representing the Coulomb interaction of electron 1 with electron 2 in the orbital ψ_u and is defined as

$$J_u\psi_a(1) = \left\{\int \Psi_u^*(2)\left(\frac{e^2}{4\pi\varepsilon_0 r_{12}}\right)\psi_u(2)\,d\tau_2\right\}\psi_u(1) \tag{3.28}$$

Let us for a moment consider equation (3.27) for the spatial function and write it such that;

$$f_1\psi_a(1) = \varepsilon_a\Psi_a(1) \tag{3.29}$$

3.9.5.2. Density Functional Theory (DFT) Method

Density functional theory (DFT) has gained considerable traction in recent years as one of the most used methods for calculating molecular structures [307]. The advantages of this method include its ease of computational implementation, its reduced computer time, and its ability to produce a better agreement with experimental results than Hartree–Fock methods do (particularly for d-metal complexes) [308].

In DFT, the electron density is the primary focus, rather than the wavefunction (ψ). The 'functional' part of the name comes from the fact that the energy of the molecule is a function of the electron density, written E[ρ], and the electron density is itself a function of position, ρ(r), and in mathematics, a function of a function is called a functional. The exact ground-state energy of an n-electron molecule is [309].

$$E[\rho] = E_k + E_{p;e,N} + E_{p;e,e} + E_{XC}[\rho] \tag{3.30}$$

where E_K is the total electron kinetic energy, $E_{P;\,e,N}$ the electron–nucleus potential energy, $E_{P;e,e}$ the electron–electron potential energy, and $E_{XC}[\rho]$ the exchange–correlation energy, which takes into account all the effects due to spin. The orbitals used to construct the electron density from [310].

© University of Venda

$$\rho_{(r)} = \sum_{i=1}^{N} |\psi_i(r)|^2$$

(3.31)

are calculated from the Kohn–Sham equations, which are found by applying the variation principle to the electron energy, and are like the Hartree–Fock equations except for a term V_{XC}, which is called the exchange-correlation potential [311]:

$$\left\{ -\frac{\hbar^2}{2m_e}\nabla_1^2 - \sum_{j=1}^{N} \frac{Z_j e^2}{4\pi\varepsilon_0 r_{j1}} + \int \frac{\rho(r_2)e^2}{4\pi\varepsilon_0 r_{12}} dr_2 + v_{xc}(r_1) \right\} \psi_i(r_1) = \varepsilon_i \psi_i(r_1)$$

(3.32)

The first part of equation above denoted by $\left\{ -\frac{\hbar^2}{2m_e}\nabla_1^2 \right\}$ is meant for kinetic energy.

The second part denoted by $\left\{ \sum_{j=1}^{N} \frac{Z_j e^2}{4\pi\varepsilon_0 r_{j1}} \right\}$ is electron-nucleolus attraction.

The third part denoted by $\left\{ \int \frac{\rho(r_2)e^2}{4\pi\varepsilon_0 r_{12}} dr_2 \right\}$ is electron-electron repulsion.

The exchange–correlation potential is the 'functional derivative' of the exchange– correlation energy:

$$v_{xc}[\rho] = \frac{\delta E_{xc}[\rho]}{\delta \rho}$$

(3.33)

The Kohn–Sham equations are solved iteratively and self-consistently [312]. First, we guess the electron density. For this step it is common to use a superposition of atomic electron densities.

Then the exchange–correlation potential is calculated by assuming an approximate form of the dependence of the exchange–correlation energy on the electron density and evaluating the

© University of Venda

functional derivative in equation 3. For this step, the simplest approximation is the local-density approximation and to write;

$$E_{x_C}[\rho] = \int \rho(r)\varepsilon_{xC}[\rho_{(r)}]dr \tag{3.34}$$

where ε_{xC} is the exchange–correlation energy per electron in a homogeneous gas of constant density [313].

3.9.6. Molecular Reactivity Parameters

Molecular reactivity parameters tell us how likely a given system is to interact with another. In this case is the interaction between the inhibitor and the metal surface. This parameter would be able to tell us which inhibitor molecule is most likely to interact with a metal surface based on the reactivity parameters of a series of inhibitor molecules [314]. An example of a molecular reactivity parameter is the Highest Occupied Molecule Orbital (HOMO), the Lowest Unoccupied Molecule Orbital (LUMO), the energy gap, electronegativity, global hardness (h), global electrophilicity index (w), global softness (s), electron affinity (A), and ionization potential (I). A brief description of each of these molecular reactivity parameters can be found below. They are used to determine the regions of molecules that are likely to interact with metal surfaces [315].

Highest Occupied Molecular Orbital (HOMO) and Lowest Unoccupied Molecular Orbital (LUMO). A molecular orbital is a mathematical function used to explain electron wave-like behaviour within a molecule. Molecular orbitals can be defined as wavefunctions of electrons in a molecule [316]. There are two vital molecular orbitals named Highest Occupied Molecular Orbital (HOMO) and Lowest Unoccupied Molecular Orbital (LUMO). These orbitals are useful for predicting molecule's reactivity. Molecular electron acceptivity is determined by the energy of the Lowest Unoccupied Molecular Orbital (E_{LUMO}). The lower the (E_{LUMO}) value of the molecules, the more its able to accept electrons during the reaction. In a similar manner, the energy of the Highest Occupied Molecular Orbital (E_{HOMO}) highlights the information on the electron donating ability of the molecule. The lower the E_{HOMO}, the easier it would be for that molecule to donate electrons during the reaction [317].

© University of Venda

The Energy Gap ($\Delta E_{HOMO\ -\ LUMO}$)

The energy gap, also known as the band gap, refers to the difference in energy between two electronic energy levels in a material [318]. The equation $\Delta E = E_{LUMO} - E_{HOMO}$ represents the energy difference between the Lowest Unoccupied Molecular Orbital (LUMO) and the Highest Occupied Molecular Orbital (HOMO) in a molecular system .

In molecular orbital theory, orbitals are used to describe the distribution of electrons in a molecule. The HOMO is the highest energy orbital that is occupied by electrons, while the LUMO is the lowest energy orbital that is unoccupied [319].

The energy difference ΔE between the LUMO and HOMO is an important quantity in understanding the electronic properties and reactivity of molecules. It can provide insights into various phenomena such as the stability of molecules, their ability to undergo chemical reactions, and their electronic transitions.

A large energy gap (ΔE) indicates a more stable molecule with limited reactivity, as it requires a significant amount of energy to promote an electron from the HOMO to the LUMO [320]. Conversely, a smaller energy gap suggests a more reactive molecule, as electron transitions between the HOMO and LUMO can occur more readily [319].

Electronegativity (χ).

Equation below relates the frontier molecular orbitals (HOMO and LUMO) to the electronegativity of molecules.

$$\chi \cong -\tfrac{1}{2}\,(E_{HOMO} + E_{LUMO}) \qquad (3.35)$$

This molecular reactivity parameter is important because it measures the ability of an electron or group of atoms to attract electrons [321]. This is an essential factor in the formation of chemical bonds and reactions. It helps scientists understand how atoms interact with one another and facilitates the prediction of the outcomes of chemical reactions.

© University of Venda

Global Hardness (η).

Another important parameter of molecular reactivity is the global hardness of the molecule, which is related to the HOMO and LUMO orbitals [322]. As shown in the equation below, the global hardness of a molecule is determined by the resistance of an atom to a charge transfer.

$$\eta \cong -\frac{1}{2}(E_{HOMO} - E_{LUMO}) \quad (3.36)$$

Global Electrophilicity Index (ω).

A molecule's electrophilicity is its ability to act as an electrophile. This parameter provides information regarding the molecule's electrophilicity. In general, molecules with large or higher values of the global electrophilicity index are good electrophiles, whereas molecules with smaller or lower values are good nucleophiles [323]. The equation below describes the relationship between the global electrophilicity index, electronegativity, and global hardness. Electronegativity indicates how willing an atom is to accept electrons, and global hardness measures the amount of energy necessary to add an electron to the molecule [324]. understanding the relationship between these three parameters help to determine the molecule's electrophilicity.

$$\omega = \frac{x^2}{2\eta} \quad (3.37)$$

Global Softness (σ).

It is worth noting that softness is a relative measure and can provide insights into the reactivity of different species in comparison to each other. Soft species tend to be more reactive and have a higher tendency to accept electrons, while hard species are less reactive and have a higher tendency to donate electrons [325].

In the equation, σ represents the global softness, and η is the global hardness. The global softness is the reciprocal of the global hardness, so $\sigma = 1/\eta$.

The global hardness (η) is defined as the energy difference between the highest occupied molecular orbital (HOMO) and the lowest unoccupied molecular orbital (LUMO):

© University of Venda

$$\eta = E_{HOMO} - E_{LUMO} \quad (3.38)$$

The HOMO represents the highest energy level occupied by electrons in a molecule, while the LUMO represents the lowest energy level unoccupied by electrons [326].

The equation, $\sigma \approx -2/(E_{HOMO} - E_{LUMO})$, gives an approximate relationship between the global softness and the energy difference between the HOMO and LUMO. It suggests that the smaller the energy gap between the HOMO and LUMO, the larger the global softness. A smaller energy gap indicates a more reactive system with a higher capacity to accept electrons [327]. This equation provides a simplified expression for estimating the global softness based on the frontier orbitals.

Electron Affinity (A);

The electron affinity (A) is closely related to the concept of the lowest unoccupied molecular orbital (LUMO) in the context of molecular electronic structure [328].

The LUMO represents the lowest energy level in a molecule that is unoccupied by electrons. It is an orbital that can accept electrons during chemical reactions or when an external electron is added to the molecule. The LUMO is often associated with electron accepting behaviours.

In this context, the electron affinity (A) is defined as the energy change when an atom or molecule gains an electron to form a negative ion (anion). This electron capture process corresponds to the filling of the LUMO with an electron [328].

Therefore, one can make a connection between electron affinity (A) and the energy of the LUMO (E_{LUMO}) as follows:

$$A \approx -E_{LUMO} \quad (3.39)$$

The negative sign indicates that the energy change is a favourable release of energy when an electron is added to the system (lowering the energy of the molecule) [329]. The magnitude of the LUMO energy can provide insights into the electron accepting ability of a molecule or

© University of Venda

species. A smaller, more negative value for the LUMO energy suggests a higher electron affinity and a greater tendency to accept electrons [330].

Ionization Potential (I);

Ionization potential (I), also known as ionization energy or ionization potential energy, is the energy required to remove an electron from a neutral gaseous atom or molecule, resulting in the formation of a positively charged ion. It is a measure of the binding strength between the electron and the atom or molecule [331].

The highest occupied molecular orbital (HOMO) is the highest energy level in a molecule that contains electrons. It represents the orbital from which an electron is most easily removed during ionization. The energy of the HOMO (E_{HOMO}) is therefore related to the ionization potential [331].

Specifically, the ionization potential (I) is equal to the negative of the energy of the HOMO:

$$I \cong - E_{HOMO} \tag{3.10}$$

The negative sign indicates that the ionization process involves the removal of an electron, resulting in a positive energy change or an energy cost [332]. Ionization potential is typically expressed in units of energy, such as electron volts (eV) or kilojoules per mole (kJ/mol).

The energy of the HOMO can provide insights into the stability and reactivity of a molecule, as well as its ability to donate electrons during chemical reactions. A lower energy of the HOMO corresponds to a higher ionization potential, indicating that it is more difficult to remove an electron from the molecule [333].

3.9.7 Metallic Crystal Structures

Metallic crystal structures are arrangements of metal atoms in a repeating pattern that gives rise to the characteristic properties of metals. These structures play a crucial role in determining metals' mechanical, electrical, and thermal properties. There are several common

© University of Venda

metallic crystal structures, each with its unique arrangement of atoms. The three most important ones are [334]:

- Body-Centred Cubic (BCC) Structure: In the body-centered cubic structure, each metal atom is located at the corners of a cube and one additional atom is placed at the centre of the cube. This central atom is shared by eight adjacent unit cells. The coordination number (number of nearest neighbouring atoms) in a BCC structure is 8. Examples of metals that crystallize in the BCC structure include iron (alpha-iron at room temperature) and chromium [335].

- Face-Centered Cubic (FCC) Structure: The face-centered cubic structure has metal atoms positioned at the corners and on the centres of each face of the cube. Each atom is shared by four adjacent unit cells. The coordination number in an FCC structure is 12. Many common metals, including aluminium, copper, and gold, crystallize in the FCC structure [336].

- Hexagonal Close-Packed (HCP) Structure: In the hexagonal close-packed structure, the metal atoms form a hexagonal lattice with additional layers stacked on top of each other in an ABAB pattern. Each atom is surrounded by six nearest neighbours in a hexagonal arrangement. The coordination number in an HCP structure is 12. Metals such as magnesium and titanium commonly adopt the HCP structure [337].

It's worth noting that some metals can exist in multiple crystal structures, depending on temperature and pressure. For example, iron can undergo a phase transition from BCC to FCC at high temperatures.

The metallic bonding in these crystal structures arises from the delocalization of valence electrons over many atoms, leading to the characteristic properties of metals, such as electrical conductivity, malleability, and high thermal conductivity. The specific crystal structure of a metal can influence its mechanical strength, ductility, and response to external forces or temperature changes, making it a critical aspect of materials science and engineering [338].

© University of Venda

3.9.7.2 Miller Indices

Miller indices are a notation system used to describe the orientation of crystal planes and crystallographic directions within a crystal lattice. They are commonly used in materials science and crystallography to represent the arrangement of atoms in a crystal structure [339].

For cubic crystals, the Miller indices are denoted by three integers (h, k, ℓ), written within parentheses or brackets as (hkl). These indices are used to define both crystallographic planes and directions. The process of determining Miller indices involves the following steps [340]:

- Identifying the Plane or Direction: To determine the Miller indices for a specific plane or direction, one must first identify the set of parallel atomic planes or the direction of interest within the crystal lattice.
- Finding the Intercept Values: Next, the plane or direction is intersected by the crystallographic axes (usually x, y, and z axes). The intercepts of the plane or direction with these axes are then determined and expressed as fractional parts of the unit cell parameters (a, b, and c) or their reciprocals (1/a, 1/b, and 1/c).
- Taking Reciprocals: The fractional intercepts are then inverted to obtain integer values by taking the reciprocals. If the intercept along an axis is at infinity (parallel to the axis), it is denoted by a zero in the corresponding Miller index.
- Reducing to Smallest Integers: Finally, the resulting integers (h, k, ℓ) are simplified to their smallest possible values while maintaining the same ratio. This means that if the indices have common factors, they are divided by those factors to obtain the simplest representation.

The Miller indices for crystallographic planes are represented within parentheses, e.g., (hkl), whereas the Miller indices for crystallographic directions are represented within square brackets, e.g., [hkl].

© University of Venda

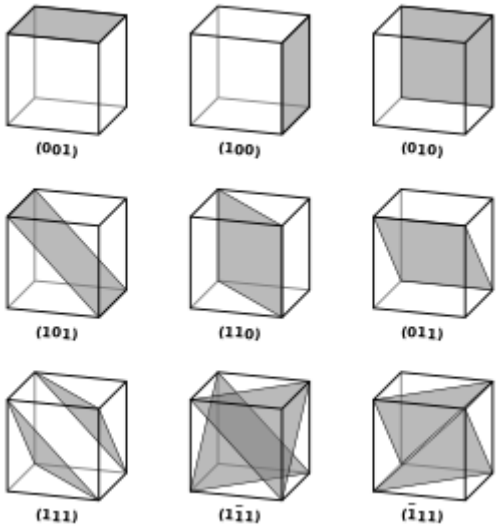


Figure 3.2: Planes with different Miller indices in cubic crystals

By using Miller indices, crystallographers can precisely describe the arrangement of atoms in crystal structures and analyse crystallographic features, such as crystal faces, lattice planes, and preferred crystallographic orientations in materials [341].

© University of Venda

University of Venda
Creating Future Leaders

CHAPTER FOUR

RESULTS AND DISCUSSION

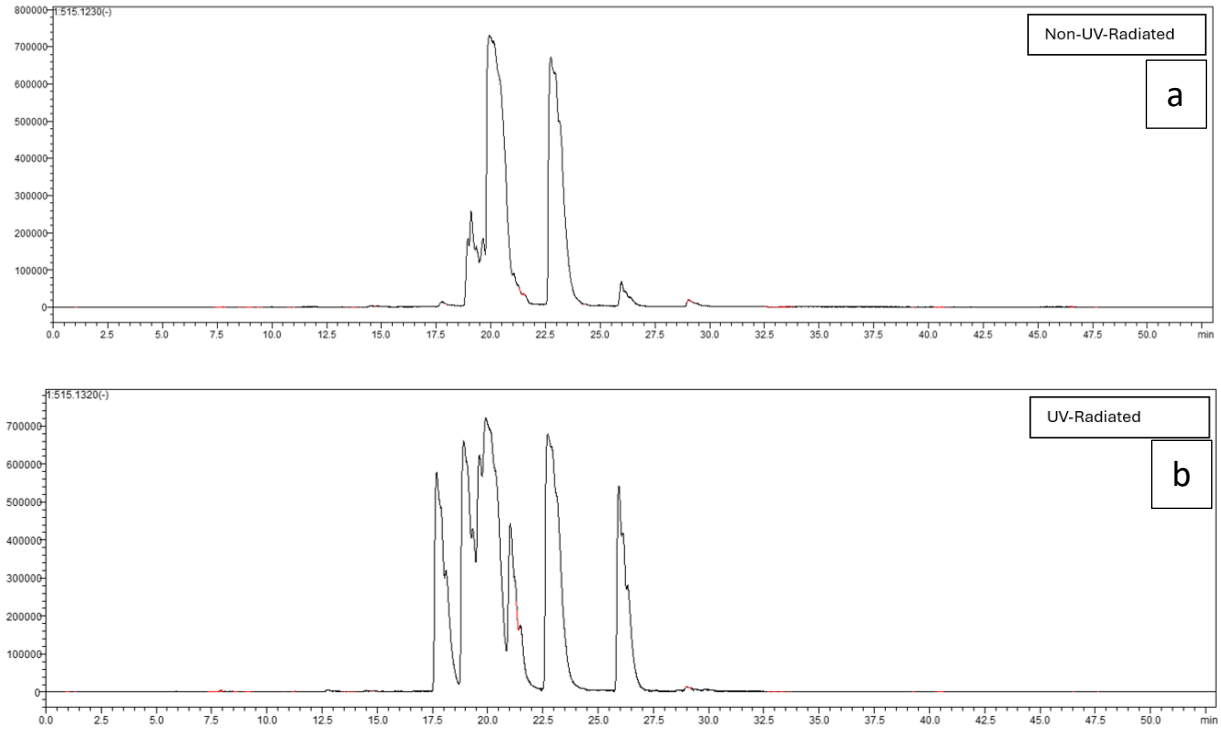
Liquid chromatography-mass spectrometry

(LC-MS)

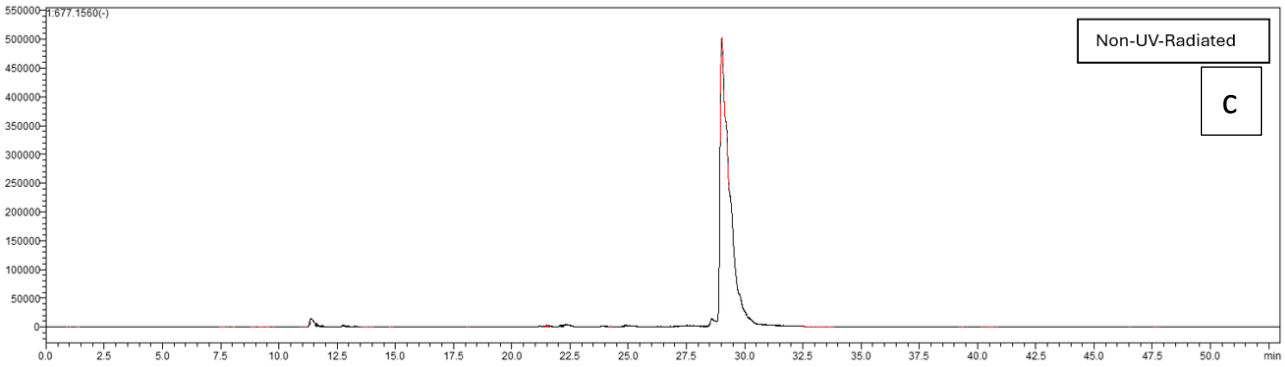
© University of Venda

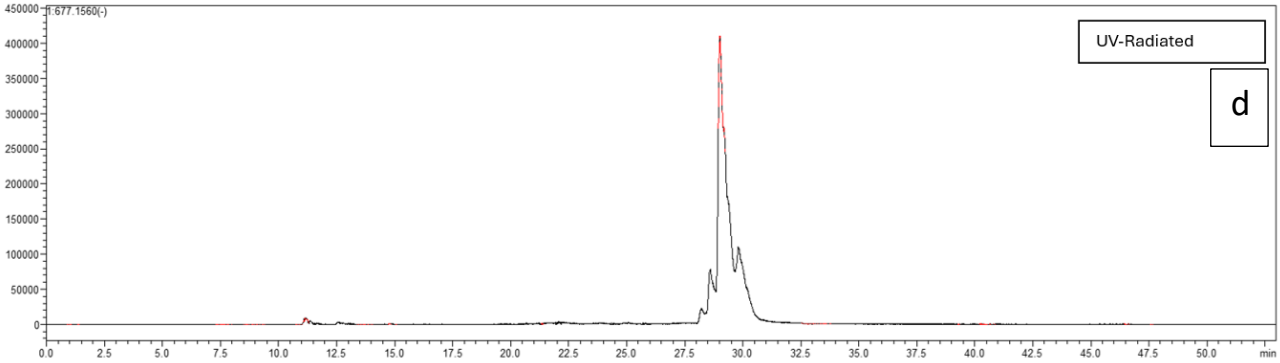
4.1 Liquid Chromatography-Mass Spectrometry

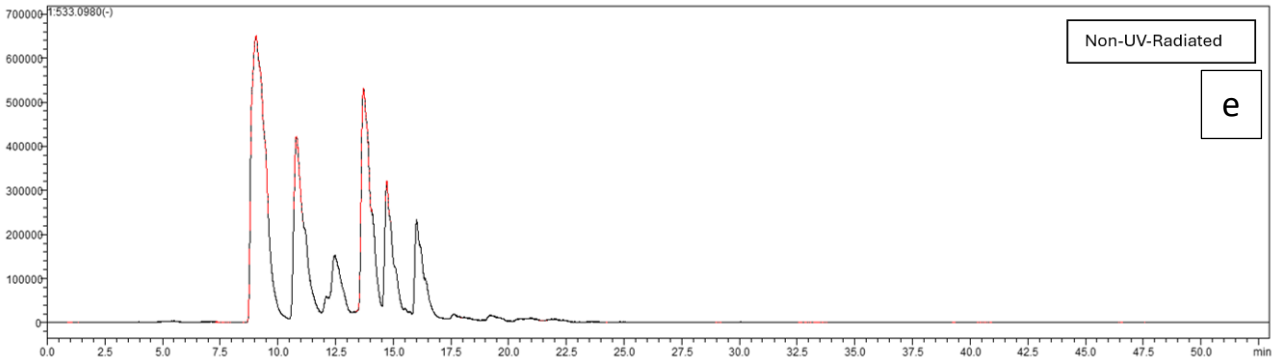
LC-MS analysis was conducted to identify and compare the geometric isomerization composition of *A. phylicoides* extract before and after UV exposure. Key compounds detected in the non-irradiated extract showed prominent peaks at m/z values indicative of flavonoid-like structures. Following UV treatment, significant changes were observed in the chromatogram profile, including a reduction in peak intensity and the appearance of new peaks, suggesting transformation of active constituents from trans to cis isomers. The number of peaks observed in non UV radiation are less than number of peaks when *A. phylicoides* is exposed to UV radiations. These results indicate that UV exposure alters the chemical composition of the extract, potentially affecting its corrosion inhibition properties. The spectra are presented in Figure 4.1.

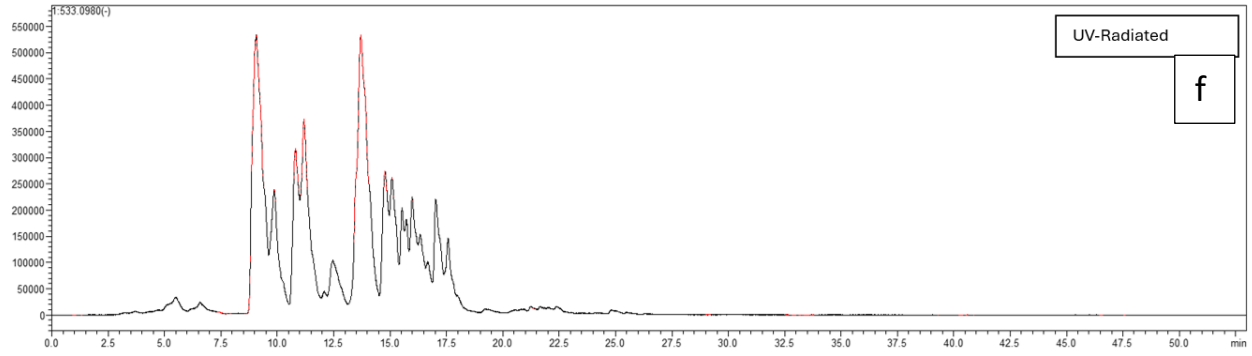


© University of Venda









© University of Venda

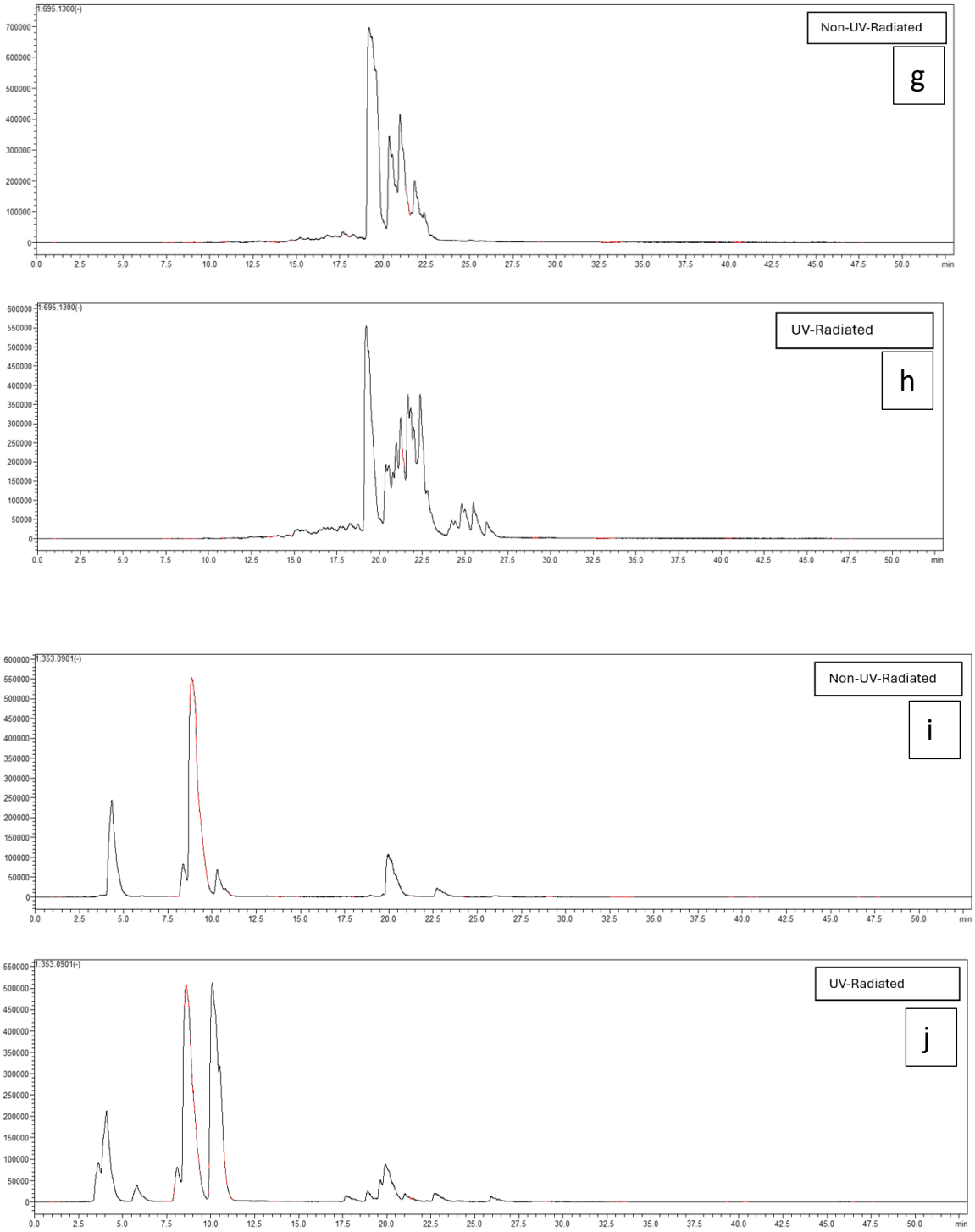


Figure 4.1: LC-MS chromatogram for non-UV-radiated and UV-radiated *A. phylicoides* extract shaken for 24 hours

The LC-MS chromatograms of *A. phylicoides* extract before and after UV exposure are presented in Figure 4.1. The non-UV-radiated sample displays fewer peaks, while the UV-radiated sample shows a greater number of peaks, indicating geometrical isomerisation changes. In Figure 4.1(i), a single peaks appears between 7.5 and 12.5 minutes. However, in the UV-radiated counterpart (Figure 4.1(j)), this region displays two distinct peaks,

© University of Venda

suggesting a possible trans-to-cis isomerisation. Additionally, at retention time of 25 minutes, no peak is visible in the non-UV chromatogram (Figure 4.1(g)), but a peak emerges after UV exposure (Figure 4.1(h)), further supporting compound transformation. At 18 minutes, Figure 4.1(a) shows a poorly developed peak with low intensity (~20,000), whereas after UV exposure (Figure 4.1(b)), a prominent peak with ~600,000 intensity appears at the same retention time. These observations imply that the plant's active compounds naturally exist in the trans form and undergo geometric isomerisation to cis upon UV exposure. Similar findings were reported by Ramphinwa *et al*. (2022), who observed UV-induced isomerisation of hydroxyl-cinnamic acid derivatives in *A. phylicoides* using UHPLC-QTOF-MS.

From a polarity perspective, the first peak in the UV-radiated chromatogram (Figure 4.1(j)) appears between 3.5 and 4.5 minutes, whereas in the non-UV chromatogram (Figure 4.1(i)), a peak appears slightly later, between 4 and 5 minutes. This suggests that the compounds formed after UV exposure are more polar, as polar compounds typically elute earlier on a non-polar stationary phase due to weaker interactions. Cis isomers generally exhibit greater polarity than their trans counterparts due to changes in molecular geometry. These polarity-driven elution shifts support the conclusion that UV radiation not only alters isomeric forms but also enhances both the polarity of the *A. phylicoides* metabolome. These findings align with observations by Makola *et al*. (2016), who also reported UV-induced isomerization effects in this species [342].

4.2 Isolation of Compounds Causing Corrosion Inhibition

The software used to identify the total number of compounds in the extract is Sirius 5.5.7. Some of the data obtained from Sirius 5.5.7 software include molar mass, molecular formula, and structural formulas of compounds possibly found on the radiated and non-radiated *A. phylicoides* extract. Figures 4.2 and 4.3 show that 2053 compounds are present in the non-radiated *A. phylicoides* extract and 1978 compounds are present in the radiated *A. phylicoides* extract respectively.

© University of Venda

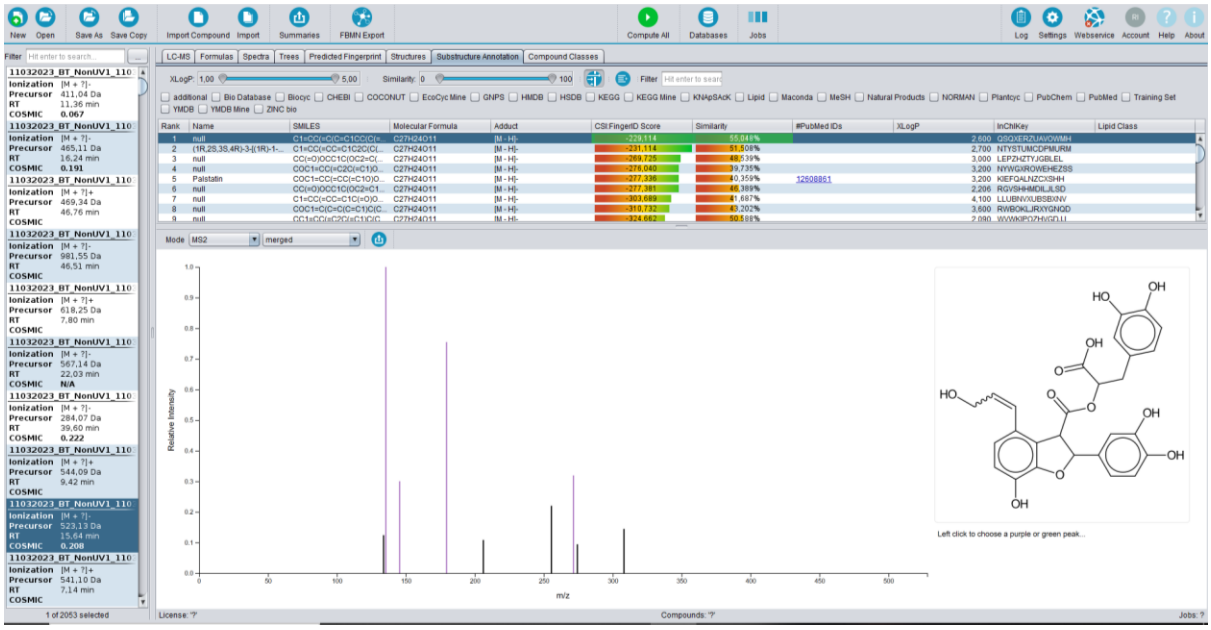


Figure 4.2: Sirius software showing all the possible compounds found in the *A. phylicoides* extract before UV radiation.

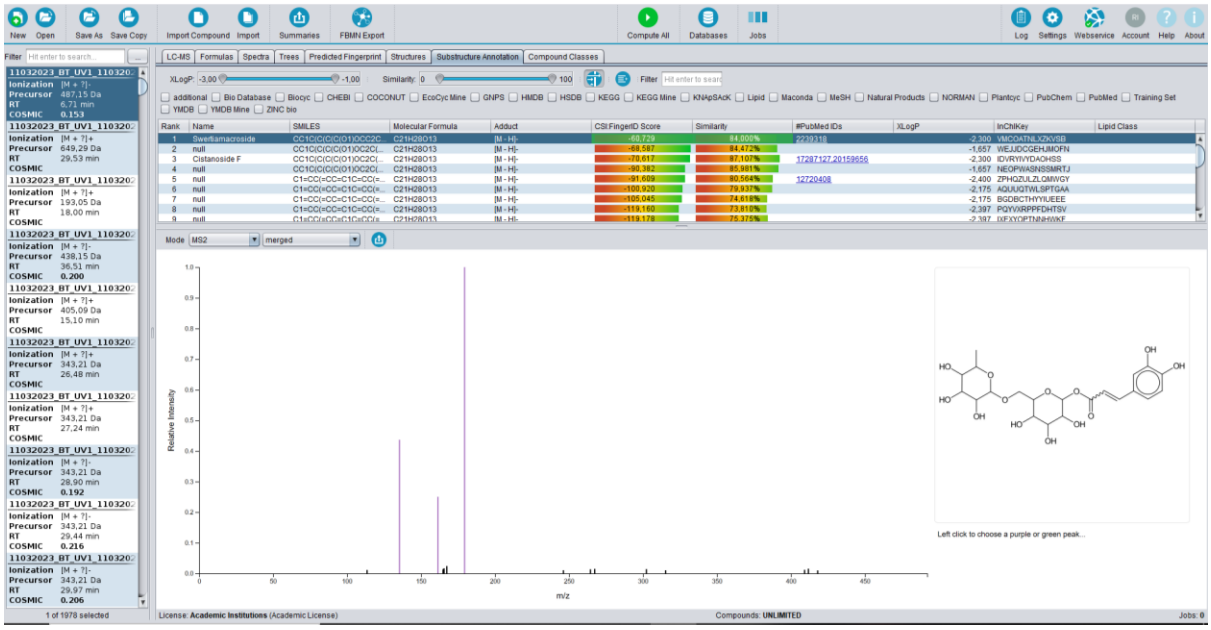


Figure 4.3: Sirius software showing all the possible compounds found in the *A. phylicoides* extract after UV radiation.

© University of Venda

Table 4.2: Weight loss for metals and percentage inhibition efficiency for the 15 fractions in an acidic medium.

FN	MS in H_2SO_4		MS in HCl		Zn in H_2SO_4		Zn in HCl	
	WL (g)	IE%	WL (g)	IE%	WL (g)	IE%	WL (g)	IE%
0	0.2383	-	0.2391	-	0.2789	-	0.2699	-
1	0.1528	35.88	0.1130	52.74	0.1120	59.84	0.2421	10.300
2	0.2938	-25.18	0.2409	-0.753	0.2315	16.99	0.2510	7.0026
3	0.2199	7.72	0.1106	53. 74	0.1021	63.39	0.0711	73.657
4	0.2118	11.12	0.3210	-34.25	0.1002	64.07	0.2122	21.378
5	0.3179	-33.40	0.1320	44.79	0.2134	23.49	0.2600	3.668
6	0.0703	70.50	0.0107	95.52	0.0839	69.92	0.0129	95.22
7	0.3156	-32.44	0.2300	3.806	0.2021	27.54	0.0100	96.29
8	0.3040	-27.57	0.0210	91.22	0.0100	96.41	0.0919	65.95
9	0.2734	-14.73	0.1108	53.66	0.3312	-18.75	0.1202	55.46
10	0.2534	-6.34	0.3209	-34.21	0.2799	-0.358	0.0889	67.062
11	0.1528	35.88	0.1100	53.99	0.2013	27.82	0.1299	51.87
12	0.1632	31.51	0.1021	57.29	0.1919	31.19	0.2111	21.786
13	0.0936	61.98	0.2340	2.133	0.2289	17.93	0.2502	7.299
14	0.1674	29.75	0.0190	92.05	0.1055	62.17	0.2554	5.372
15	0.1770	25.72	0.1907	20.24	0.2090	25.06	0.2133	20.97

Key: FN = Fraction Number, WL = Weight loss, IE = Inhibition Efficiency

The Sirius 5.5.7 software was utilized to determine the number of compounds, their molar masses, and molecular formulas possibly present in the *A. phylicoides* extracts. Through an elimination process, compounds causing corrosion inhibition were distinguished from those enhancing metal corrosion by analyzing the m/z data obtained from LC-MS in the SIRIUS software. Table 4.2 revealed that fraction number 6 exhibited the highest inhibition efficiency for mild steel in sulphuric and hydrochloric acid at 70.50% and 95.52% respectively. For

© University of Venda

zinc, fraction number 6 showed inhibition efficiencies of 69.92% and 95.22% in sulphuric and hydrochloric acid respectively, with the highest inhibition values achieved at 96.41% for zinc in sulphuric acid and 96.29% in hydrochloric acid for fraction numbers 8 and 7 respectively. The lowest inhibition efficiencies were recorded at -33.40% and -34.25% for mild steel in fractions number 5 and 4 respectively in sulphuric and hydrochloric acid. For zinc, the lowest inhibition efficiencies were -18.75% and 3.668% in fractions number 9 and 5 respectively. Fraction 6, which exhibited the highest inhibition against mild steel in both sulphuric and hydrochloric acid, was discovered to encompass a total of 533 compounds. Conversely, fractions 8 and 7, displaying greater inhibition efficiency for zinc in sulphuric and hydrochloric acid, contained 556 and 195 compounds, respectively. Most compounds identified in fractions 6, 7, and 8 were similar. Fractions 4, 5, and 9 demonstrated the lowest inhibition efficiency, suggesting the presence of compounds that promote corrosion. The number of compounds detected in fractions 4, 5, and 9 were 433, 572, and 603, respectively. Compounds present in fractions 4, 5, and 9 were eradicated in fractions 6, 7, and 8, with only a few remaining, considered among those contributing to corrosion inhibition. These findings are consistent with the work of Sithuba *et al*. (2024), who investigated UV-induced geometrical isomer-enriched *Helichrysum kraussii* extract as a corrosion inhibitor for the Al (111) surface in 1.0 M hydrochloric acid, combining both experimental and theoretical approaches (Results in Surfaces and Interfaces, 16, 100268) [351].

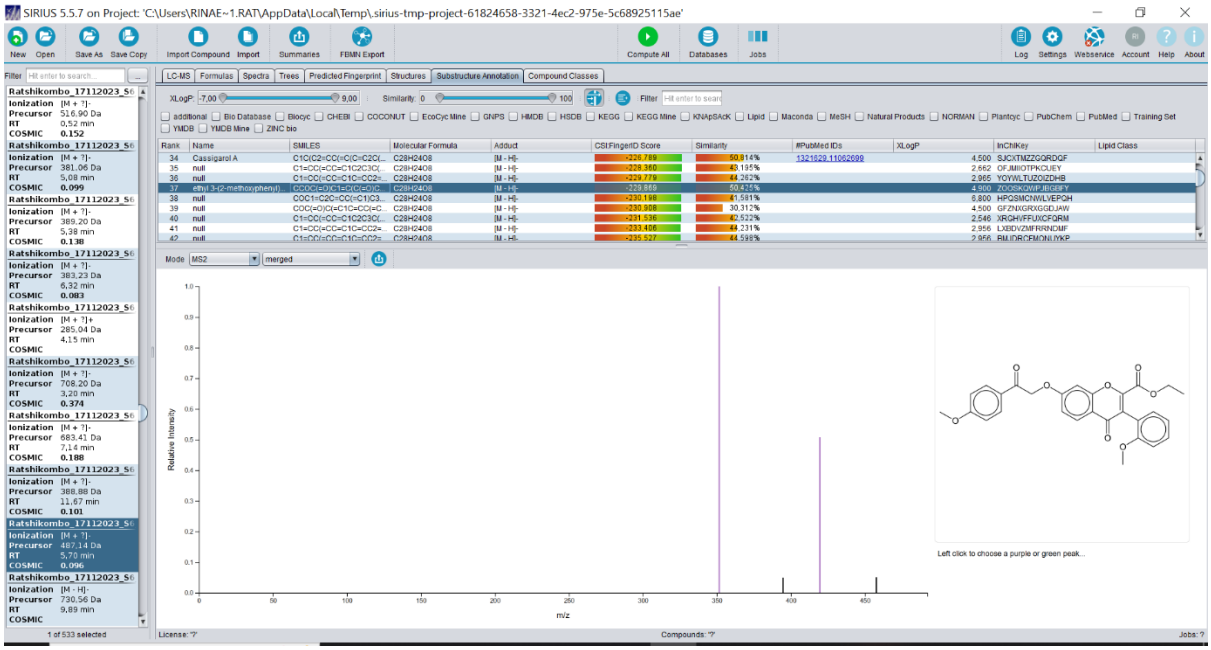


Figure 4.4: The Sirius software data displays the complete list of potential compounds identified in the *A. phylicoides* plant extract corresponding to fraction number 6.

© University of Venda

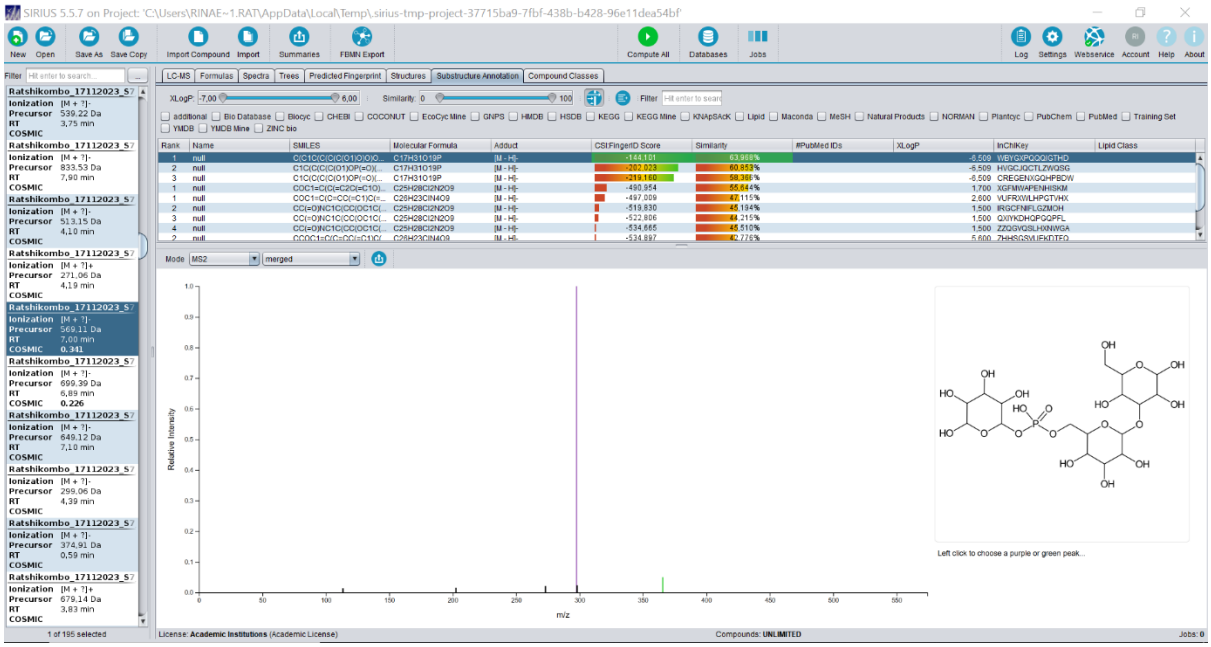


Figure 4.5: The Sirius software data displays the list of potential compounds identified in the *A. phylicoides* plant extract corresponding to fraction number 7.

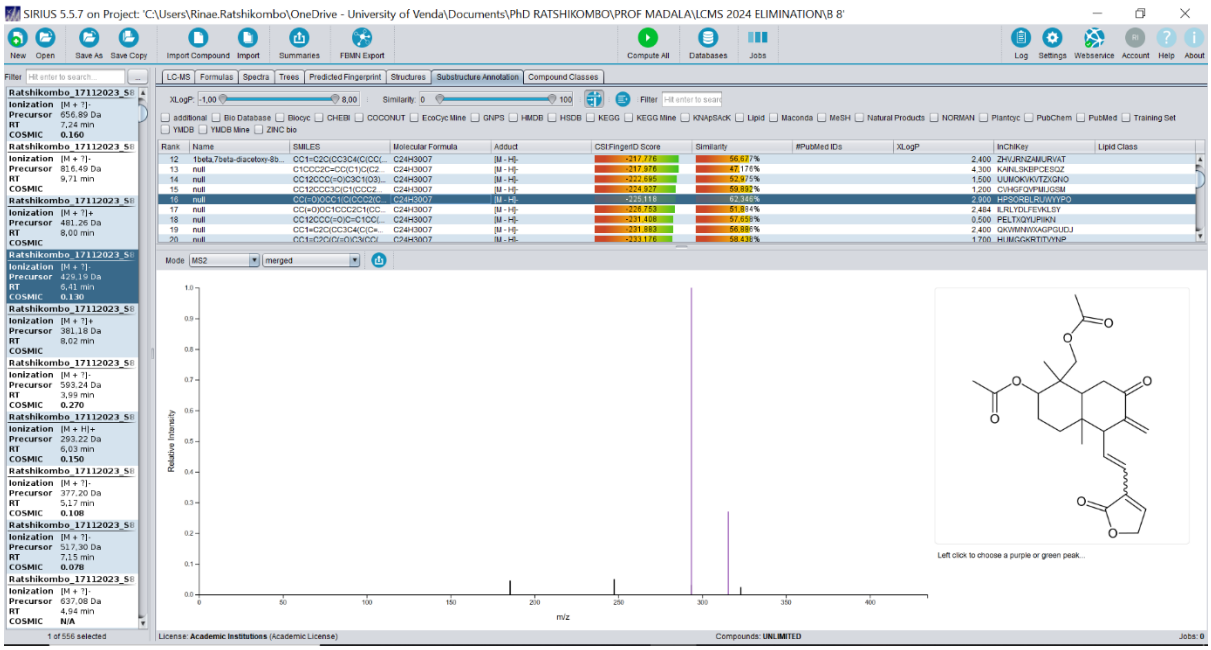


Figure 4.6: The Sirius software data displays the complete list of potential compounds identified in the *A. phylicoides* plant extract corresponding to fraction number 8.

© University of Venda

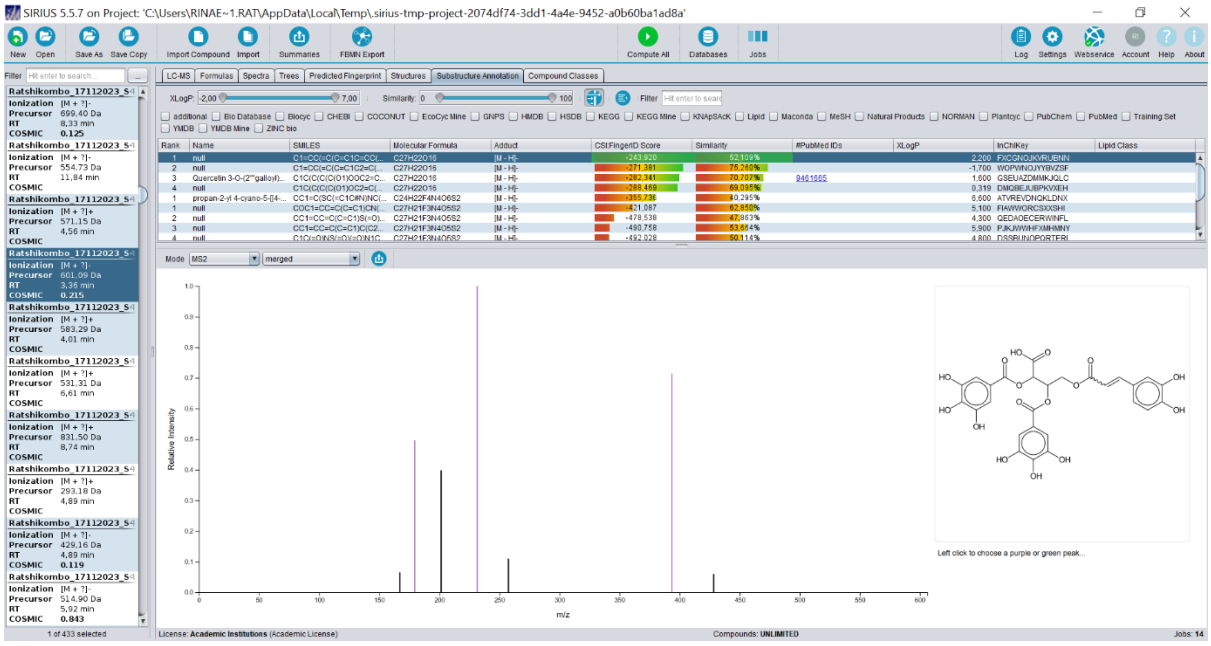


Figure 4.7: The Sirius software data displays the list of potential compounds identified in the *A. phylicoides* plant extract corresponding to fraction number 4.

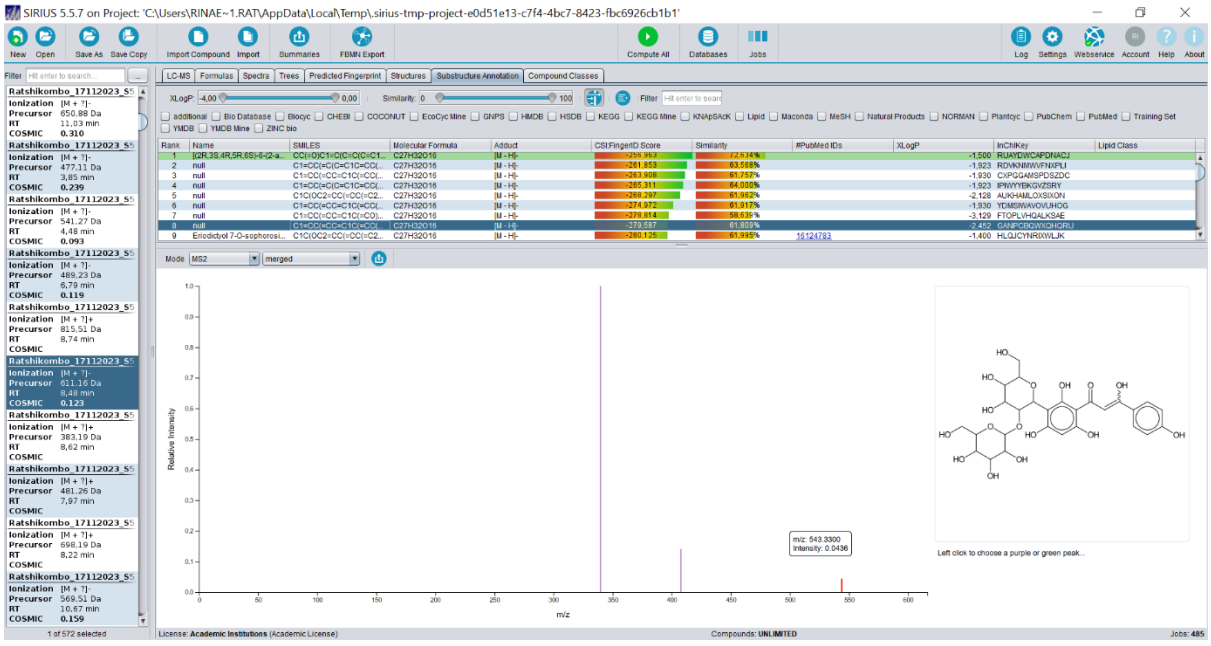


Figure 4.8: The Sirius software data displays the potential compounds identified in the *A. phylicoides* plant extract corresponding to fraction number 5.

© University of Venda

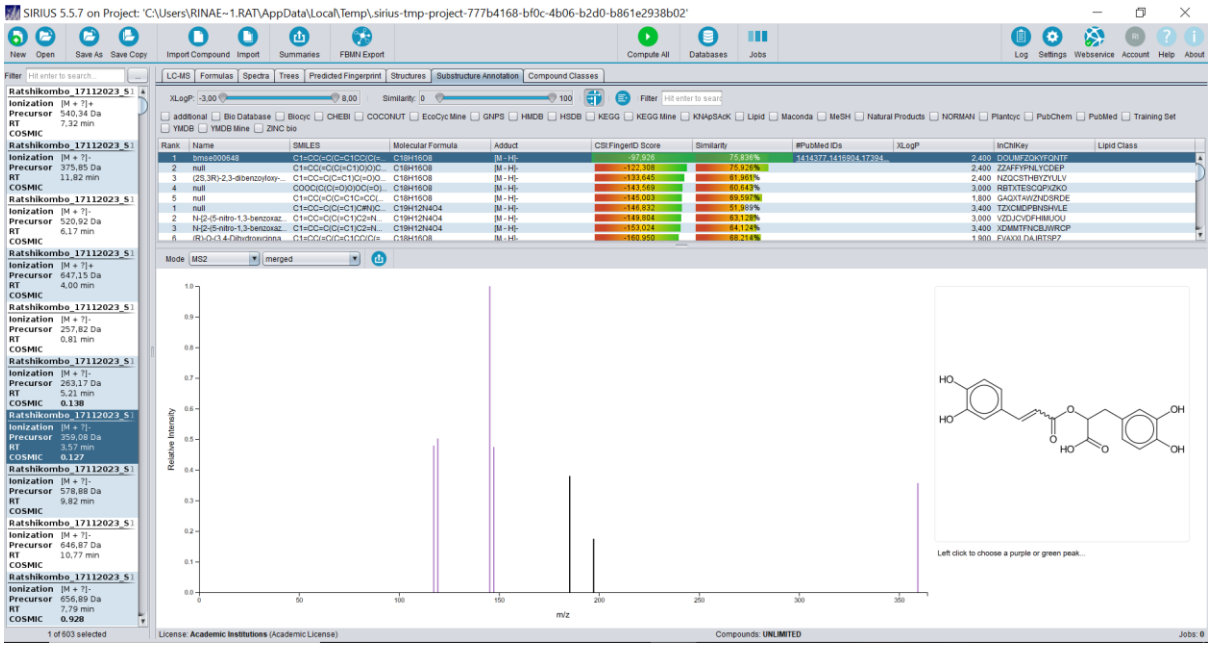


Figure 4.9: The Sirius software data displays the list of potential compounds identified in the *A. phylicoides* plant extract corresponding to fraction number 9.

Figure 4.1-4.3 shows a list of 533 + 195 + 556 compounds which sum to 1284 compounds identified to give higher inhibition efficiency, whereas Figure 4.4-4.6 shows a list of 433 + 572 + 603 compounds which sum to 1608 compounds failing to inhibit corrosion. Any compound that appeared in Figure 4.4-4.6 has been eliminated from Figure 4.1-4.3 because it appears on the fraction that fails to inhibit corrosion and as such is regarded as a corrosion enhancer. There are situations where the finger ID recycles appear empty. This indicates that for all the molecular formulas initially computed, there are no suitable candidates in the structure database to be displayed. This could happen if you selected a small structure database when using Sirius [351].

The Sirius software calculates the posterior probability, which is a measure of the likelihood that a given compound identified by the software is present in the sample [352]. This probability is based on numerous factors such as the mass spectral data, fragmentation patterns, and isotopic distributions of the compounds. Higher posterior probabilities indicate greater confidence in the identification of a compound, while lower probabilities suggest a higher degree of uncertainty [353]. This approach is crucial for reliable compound annotation in metabolomics studies, as it helps researchers assess the validity of identified compounds and prioritize further investigation of those with higher probabilities. This methodology aligns with recent advancements in compound annotation techniques, such as those described

© University of Venda

by Ludwig *et al*. (2019), which utilize database-independent molecular formula annotation using Gibbs sampling to reveal unknown small molecules [354]. These innovative approaches enhance the accuracy and depth of compound identification in metabolomics research, facilitating a more comprehensive understanding of complex biological systems.

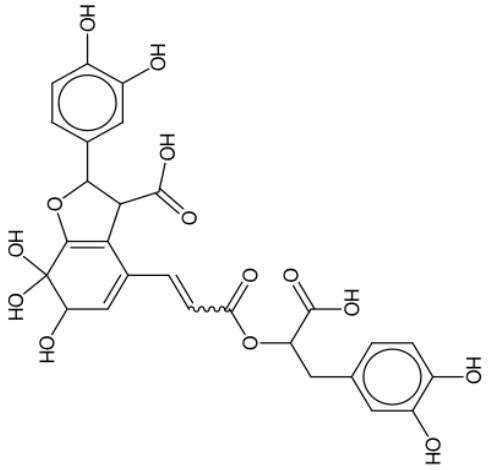
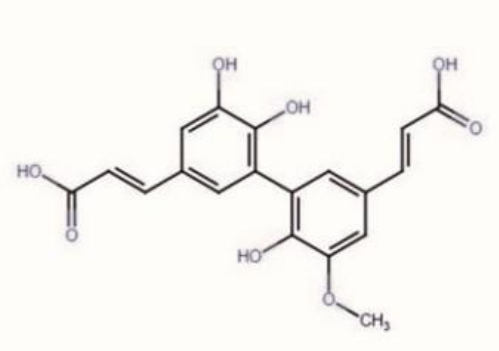
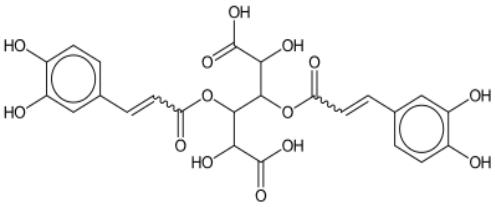
The predictor quality in Sirius software refers to the reliability and accuracy of the predictions made by the software regarding the identity and properties of chemical compounds [355]. This includes factors such as the consistency of the predicted molecular formulas, the match between experimental and predicted mass spectra, and the reliability of predicted compound classes or functional groups. Higher predictor quality indicates more reliable and accurate predictions, while lower predictor quality suggests a higher degree of uncertainty in the results [356]. This aspect of compound annotation and structure elucidation aligns with computational methods and data analysis techniques discussed in the work by Ludwig *et al*. (2020). Their research focuses on de novo molecular formula annotation and structure elucidation using Sirius 4, highlighting the importance of robust computational approaches in metabolomics for ensuring accurate compound identification and characterization [355].

After the elimination process, Knapsack was employed to verify whether the obtained compounds belonged to the family of the *A. phylicoides* plant. The *A. phylicoides* plant belongs to the Asteraceae family. Any compounds that were identified not to belong to the Asteraceae family were subsequently removed. This approach ensures that only relevant compounds associated with the Asteraceae family are retained for further analysis, aligning with similar methodologies described in research by Mombeshora *et al*. (2021) [357].

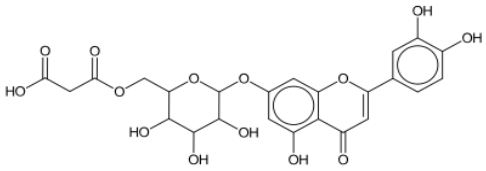
Four compounds, namely (E)-4-(3-(1-carboxy-2-(3,4-dihydroxyphenyl)ethoxy)-3-oxoprop-1-en-1-yl)-2-(3,4-dihydroxyphenyl)-6,7,7-trihydroxy-2,3,6,7-tetrahydrobenzofuran-3-carboxylic acid (ECDO), (2E)-3-{5'-[(1E)-2-carboxyeth-1-en-1-yl]-2',3',6-trihydroxy-5-methoxy-[1,1'-biphenyl]-3-yl)prop-2-enoic acid (2ECTM), 3,4-bis(((E)-3-(3,4-dihydroxyphenyl)acryloyl)oxy)-2,5-dihydroxyhexanedioic acid (3BDA), 3-((6-((2-(3,4-dihydroxyphenyl)-5-hydroxy-4-oxo-4H-chromen-7-yl)oxy)-3,4,5-trihydroxytetrahydro-2H-pyran-2-yl)methoxy)-3-oxopropanoic acid (3DCT) were isolated and identified as the ones responsible for inhibiting corrosion. These compounds have the capability to undergo geometrical isomerization. These compounds were identified as synergistically contributing to the corrosion inhibition of metals. The compounds are detailed in Table 4.3

© University of Venda

Table 4.3. Identified compounds from the *A. phylicoides* plant extract.

No.	Name of compounds	Structure of compound	Molecular formula
1	(ECDO)		$C_{24}H_{24}O_{14}$
2	(2ECTM)		$C_{19}H_{16}O_8$
3	(3BDA)		$C_{24}H_{22}O_{14}$

© University of Venda

4	(3DCT)		$C_{24}H_{22}O_{14}$

© University of Venda

University of Venda
Creating Future Leaders

CHAPTER FIVE

RESULTS AND DISCUSSION

Fourier Transform Infrared Spectroscopy

(FTIR)

© University of Venda

5.1 Fourier Transform Infrared Spectroscopy (FTIR)

This analysis was done to check the functional groups on corroded zinc and mild steel in the absence and presence of *A. phylicoides* plant extract at 303K before and after UV exposure. The difference between the FTIR spectra of UV-radiated *A. phylicoides* extract and non-UV-radiated *A. phylicoides* extract lies in the presence or absence of certain peaks or bands, indicating changes in chemical composition or structure due to UV radiation exposure. In the UV-radiated *A. phylicoides* extract, there are additional or intensified peaks in certain spectrum regions compared to the non-UV-radiated extract. These changes suggest alterations in molecular bonds or functional groups induced by UV radiation. Conversely, certain peaks present in the non-UV-radiated *A. phylicoides* extract are absent and/or reduced in intensity in the UV-radiated *A. phylicoides* extract. This indicates that some molecular components or structures may have been affected or degraded by UV radiation exposure. Comparing the FTIR spectra of UV radiated, and non-UV-radiated *A. phylicoides* extracts can provide insights into the specific chemical changes induced by UV radiation and its potential effects on the properties or functionality of the extract. A. phylicoides plants naturally produce a variety of cinnamic acid derivatives, typically in a trans configuration. However, some compounds convert to a cis form when exposed to intense UV light. Figure 5.1 presents the FT-IR spectra of *A. phylicoides* plant extract, illustrating both (a) the trans isomer and (b) the cis isomer. Notably, differences between these isomers are visible within the 1000–1800 cm^{-1} range. Additionally, a peak around 3400 cm^{-1}, indicating the presence of an -OH group, is present in both the trans and cis forms.

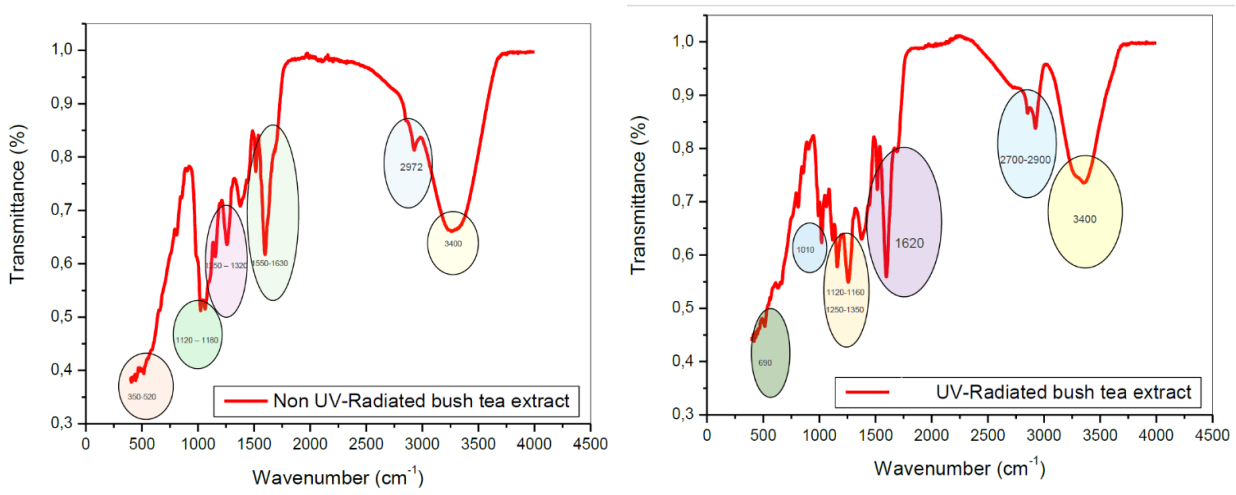


Figure 5.1: FT-IR spectra for the studied non-UV radiated and UV radiated *A. phylicoides* extract

© University of Venda

Figure 5.1 displays the FTIR spectrum of *A. phylicoides* extract before and after exposure to UV radiation. A notable distinction is evident that geometric isomerization occurs between the UV-radiated and non-UV-radiated extracts. This differentiation is expected since *A. phylicoides* naturally exists in the trans configuration and undergoes geometrical isomerization to the cis configuration upon UV radiation exposure. The spectrum in Figure 5.1 clearly illustrates the occurrence of isomerization through differences in peaks. Effective corrosion inhibitors typically feature functional groups like aromatic rings, multiple bonds, amides, oxygen, sulphur, etc. To determine which of the UV-radiated and non-UV-radiated extracts might serve as a better corrosion inhibitor, it was necessary to assess the presence or absence of functional groups in the extracts, as shown in Figure 5.1. This analysis is in line with similar spectroscopic investigations conducted by Prabakaran *et al*. (2016) in their study on the highly efficient Ligularia fischeri green extract for the protection against corrosion of mild steel in acidic medium [358]. Their research underscores the importance of spectroscopic techniques in understanding the chemical composition and properties of natural extracts for potential applications in corrosion inhibition.

In both extracts, the broad band centered at 3400 cm^{-1} corresponds to the OH functional groups of alcohols and phenols. For the non-UV-radiated extract, the singlet bands at 2972 cm^{-1} are attributed to the C-H (CH_3) group or methyl group. In contrast, the doublet band at 2700-2900 cm^{-1} in the UV-radiated extract implies the presence of the O-C-H group. The band at 1550-1630 cm^{-1} is attributed to carboxylate ions (RCO_2^-) in the non-UV-radiated extract, while the bands around 1620 cm^{-1} indicate aromatic ring vibrational modes in the UV-radiated extract. The common peak around 1250-1350 cm^{-1} indicates the presence of the -CH=CH_2 group in both extracts. Additionally, in the UV-radiated extract, the presence of the C_6H_6Y group or benzene ring is indicated by the peak at 690 cm^{-1}. Similar spectroscopic studies have been conducted by Veilleux (2008) [359].

The functional groups present in both the UV-radiated and non-UV-radiated *A. phylicoides* extracts exhibit characteristics of effective corrosion inhibitors. However, the question remains as to which extract, among the UV-radiated and non-UV-radiated ones, demonstrates higher inhibition efficiency. This question is addressed by other methods employed in this study, such as gravimetric analysis. The rust obtained from the metal after conducting gravimetric analysis was further analyzed by FTIR, as indicated in Figure 5.2.

© University of Venda

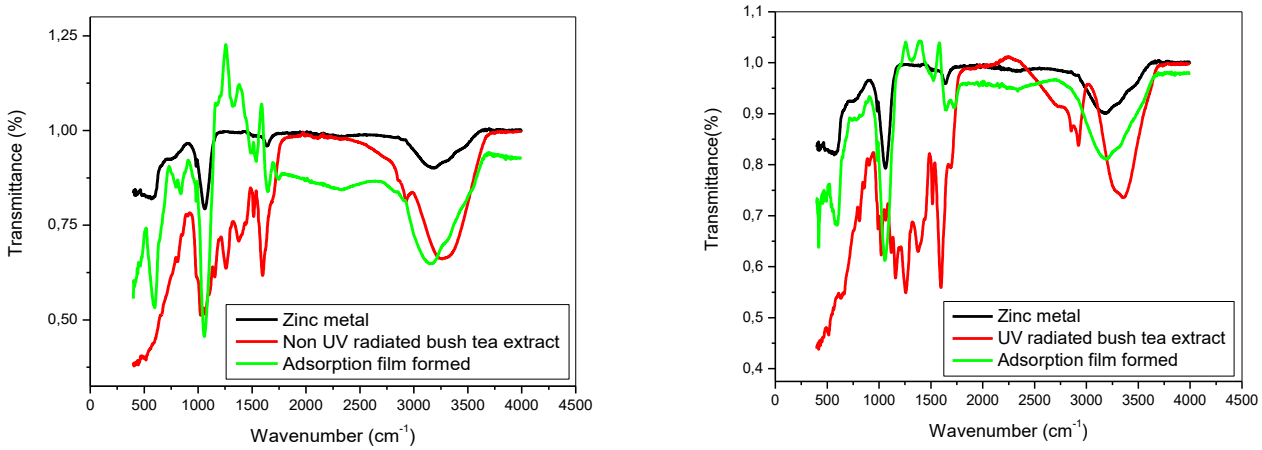


Figure 5.2: FT-IR spectra for the studied *A. phylicoides* and adsorption films formed before and after exposed to UV on Zn in 1.5 M H_2SO_4

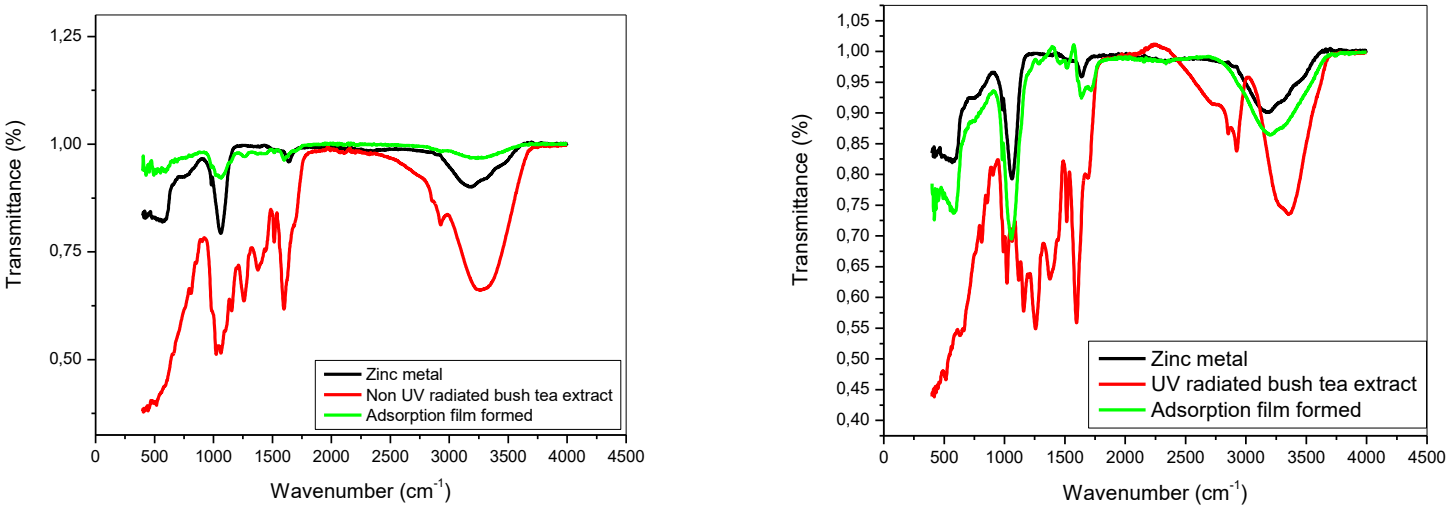


Figure 5.3: FT-IR spectra for the studied *A. phylicoides* and adsorption films formed before and after being exposed to UV on Zn in 1.5 M HCl

In FTIR spectroscopy, the intensity of peaks in the transmittance spectrum provides information about the absorbance or attenuation of infrared radiation by the sample at specific wavelengths. Figures 5.2 -5.3 clearly show that adsorption of *A. phylicoides* extract onto zinc metal occurs because in all plots (red line), the common peak in UV radiated and non-UV radiated extract found in Figure 5.1 which is found around 3300-3500 cm^{-1} representing the presence of OH group is also available on the adsorption film formed represented by the green line, however, it is presence in low intensity and from the literature if the transmittance peak is shorter but maintains the same shape, it means that the sample absorbs less infrared radiation at that specific wavelength [360]. Similar phenomena have

© University of Venda

been studied in other contexts, such as fog attenuation prediction for optical and infrared waves, as Al Naboulsi *et al*. (2004) described in their work in Optical Engineering [361]. This could indicate weaker functional groups or chemical bonds in the sample, or a lower concentration of the absorbing species, in this case, a low transmittance peak with a similar shape is due to a low amount of *A. phylicoides* on the rust because in the rust there exist not only *A. phylicoides* extract but acidic solution and zinc metal. However, the shape of the peak remains the same, suggesting that the same types of chemical bonds or functional groups are present but in lower abundance or with lower absorption strength. The transmittance peak for UV-radiated and non-UV-radiated *A. phylicoides* extracts are long and have a high intensity when compared to transmittance peaks of the adsorption film formed (rust). As indicated in Figure 5.2 the transmittance of UV-radiated and non-UV-radiated *A. phylicoides* extract decreases gradually from 100% down to 25% at a wavelength of 500 cm^{-1}, this suggests that the sample absorbs a significant amount of infrared radiation at that wavelength. This could indicate the presence of strong functional groups or chemical bonds in the sample that absorb infrared light strongly. The transmittance peaks of the adsorption film formed range between 100% to 70% except for Figure 5.2.

The peaks 2972 cm^{-1} in non-UV radiated *A. phylicoides* extract and 2700-2900cm^{-1} in UV radiated *A. phylicoides* extract disappeared on the adsorption film formed. This behaviour is normal and was expected, and it is attributed to the adsorption of *A. phylicoides* extract on the zinc surface resulting in the formation of a protective layer, which could mask or attenuate the infrared absorption peaks associated with the original *A. phylicoides* extract. This protective layer could act as a barrier, preventing further corrosion of the zinc. The components of the *A. phylicoides* extract chemically react with the zinc surface, forming new chemical species or complexes that do not exhibit the same infrared absorption characteristics as the original *A. phylicoides* extract. This chemical interaction leads to the disappearance or alteration of certain FTIR peaks. The disappearance of peaks in the FTIR spectrum of adsorption film formed when *A. phylicoides* extract adsorbs on zinc in this study suggests that the interaction between the extract and the zinc surface has altered the surface composition or properties, thereby affecting the infrared absorption characteristics of the rust. The functional groups were explicitly tabulated in Table 5.1. This observation aligns with similar studies investigating corrosion inhibition mechanisms, such as the work conducted by Vengatesh and Sundaravadivelu (2019) on non-toxic bisacodyl as an effective corrosion inhibitor for mild steel in acidic medium, as published in the Journal of Molecular Liquids [362].

© University of Venda

Table 5.1: Functional groups from the FTIR spectra for zinc in sulphuric acid

	Functional Groups			
Bands position (cm^{-1})	**Non–UV Radiated *A. phylicoides***	**UV-radiated *A. phylicoides***	**Adsorption film Non-UV-Radiated *A. phylicoides***	**Adsorption film UV-Radiated *A. phylicoides***
3300 – 3500	O–H alcohol	O–H alcohol	O–H alcohol	O–H alcohol
3100 –3550			N–H amines	N–H amines
2700 – 2900		O–C–H C–H (CH_3)		
2972 –2980	–C–H (CH_3)			
1550 –1630	$-RCO_2^-$ Carboxylates ions			
1600 – 1720	C=O ketone C=O aldehyde	C=O ketone C=O aldehyde		C=O ketone C=O aldehyde
1600 – 1650	C=C alkene	C=C alkene	C=C alkene	
1500 – 1570	C=C aromatic	C=C aromatic		
1250 – 1320	–CH=CH– (trans)	–CH=CH– (trans) Nitrates $RONO_2$		
1180 – 1360	$–RSO_2NH_2–$ Sulphonamides	$–RSO_2NH_2–$ Sulphonamides		
1000 – 1200		Sulfonates RSO_3M	Sulfonates RSO_3M	Sp^3 C-O
600 – 750			C-H aromatic	C-H aromatic
600 – 900		C-C alkane C-H aromatic	C-C alkane C-H aromatic	
350-520	Zn–O bond Zinc–Oxygen bond			Zn–O bond Zinc–Oxygen

© University of Venda

Table 5.2: Functional groups from the FTIR spectra for zinc in hydrochloric acid

	Functional Groups			
Bands position (cm^{-1})	**Non UV-Radiated *A. phylicoides***	**UV-radiated *A. phylicoides***	**Adsorption film Non-UV-Radiated *A. phylicoides***	**Adsorption film UV-Radiated *A. phylicoides***
3300 – 3500	O–H alcohol	O–H alcohol	O–H alcohol	O–H alcohol
3100 –3550			N–H amines	N–H amines
2700 – 2900		O–C–H C–H (CH_3)		
2972 –2980	–C–H (CH_3)			
1550 –1630	$-RCO_2^-$ Carboxylates ions			C=C alkene
1600 – 1720	C=O ketone C=O aldehyde	C=O ketone C=O aldehyde		C=O ketone C=O aldehyde
1600 – 1650	C=C alkene	C=C alkene	C=C alkene	
1500 – 1570	C=C aromatic	C=C aromatic		
1250 – 1320	–CH=CH– (trans)	–CH=CH– (trans) $RONO_2$ Nitrates		Sp^3 C-O
1180 – 1360	$–RSO_2NH_2–$ Sulphonamides	$–RSO_2NH_2–$ Sulphonamides	C-H aromatic	C-H aromatic
1000 – 1200		Sulfonates RSO_3M	Sulfonates RSO_3M	Sulfonates RSO_3M
600 – 750				C-C alkane C-H aromatic
600 – 900		C-C alkane C-H aromatic		
350-520	Zn–O bond Zinc–Oxygen bond		Zn–O bond Zinc–Oxygen bond	

From Figure 5.2, it is evident that the absorption peaks exhibit some variability. These three spectra were analyzed to identify the functional groups present and compare them to ascertain the functional groups found on the plant extract, which were also detected on the zinc metal surface following gravimetric analysis. The corrosion adsorption is not solely attributed to the remaining functional groups but also to any new functional groups that may arise during the corrosion reaction involving the plant extract and zinc metal. These new functional groups, if found adsorbed on the metal surface, can contribute to the corrosion inhibition efficiency. Tables 5.1 and 5.2 present all the potential functional groups identified from the two spectra. To determine which functional groups caused the corrosion inhibition, the first and third

© University of Venda

columns were compared since they correspond, as well as the second and fourth columns. The functional groups present in the second and fourth columns are responsible for impeding the corrosion process of zinc. These functional groups include O-H alcohol, N-H amines, N-H amide, C=C alkene, and C-H aromatic. The peak observed at the band position of 350-400 cm^{-1} in the adsorption film, whether in the presence or absence of UV radiation from the *A. phylicoides* extract, signifies the Zn-O bond, indicating a connection between the zinc metal and oxygen.

Scientifically, assumptions lacking empirical support are deemed invalid. Hence, one cannot confidently claim that the functional groups observed in the *A. phylicoides* extract interacting with zinc will necessarily be identical if a different metal is utilized. Nevertheless, this study was prompted by the notion that the functional groups noted in the interaction with zinc might also manifest when the extract interacts with other metals. To scrutinize this premise, the study conducted experiments using mild steel instead of zinc. Through examining how the *A. phylicoides* extract interacts with mild steel, the researchers sought to ascertain whether comparable functional groups would be detected. This method allowed investigation on how different metals might influence the chemical composition and behavior of the *A. phylicoides* extract. Essentially, while the assumption served as a starting point for exploration, the study sought to confirm or challenge it through empirical testing with mild steel. This empirical approach is vital in scientific inquiry to gather dependable data and draw meaningful conclusions regarding material behavior under specific circumstances. Figure 5.3 shows FTIR spectra of mild steel in acidic medium

© University of Venda

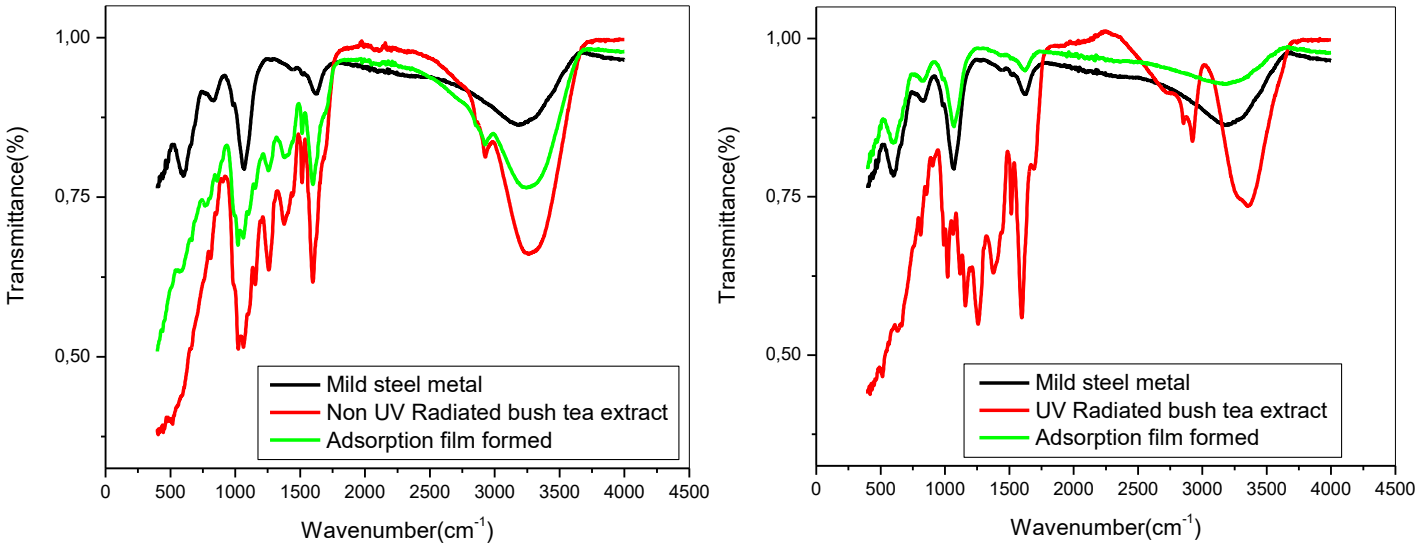


Figure 5.4: FT-IR spectra for the studied *A. phylicoides* and adsorption films formed before and after exposed to UV on MS in 1.5 M H_2SO_4

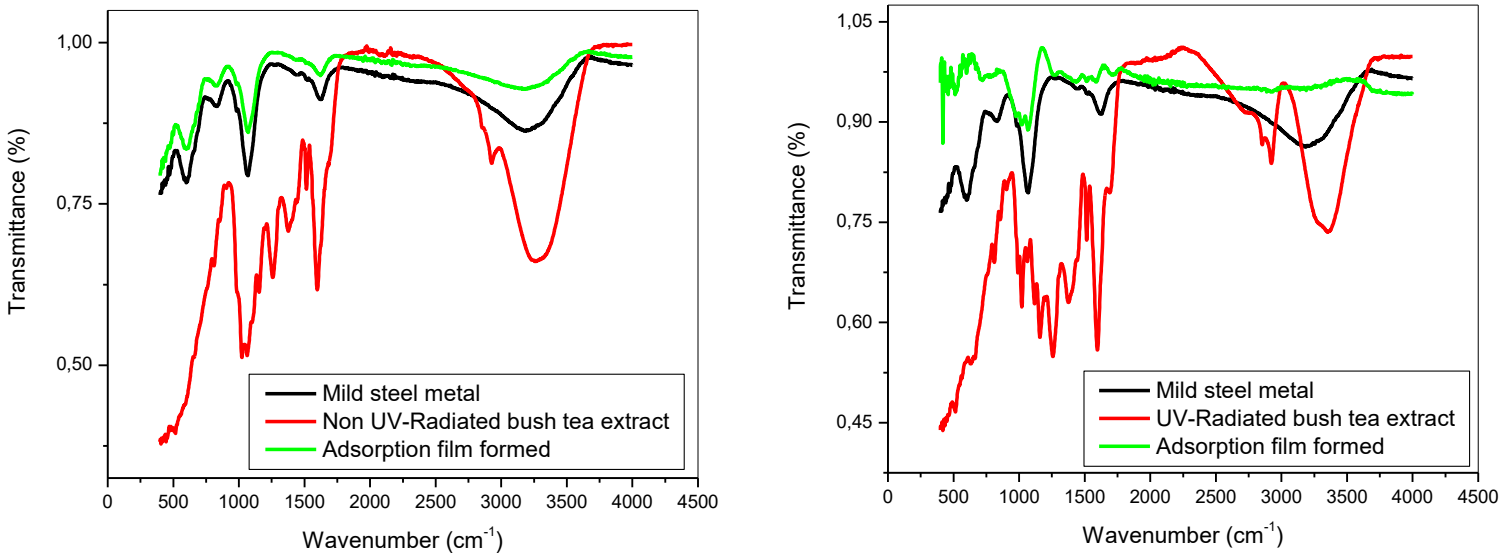


Figure 5.5: FT-IR spectra for the studied *A. phylicoides* and adsorption films formed before and after exposed to UV on MS in 1.5 M HCl

The transmittance peaks of the adsorption film, as highlighted by the green line, seem shorter when contrasted with those of the *A. phylicoides* extract. Despite some peaks potentially being less distinct, they still exist. This underscores the need for a zoomed-in depiction of the adsorption film formed, as shown in Figure 5.4. The zoomed versions of the adsorption film formed on non-UV-radiated and UV-radiated *A. phylicoides* extract are presented in Figure 5.5, positioned on the left and right sides respectively.

© University of Venda

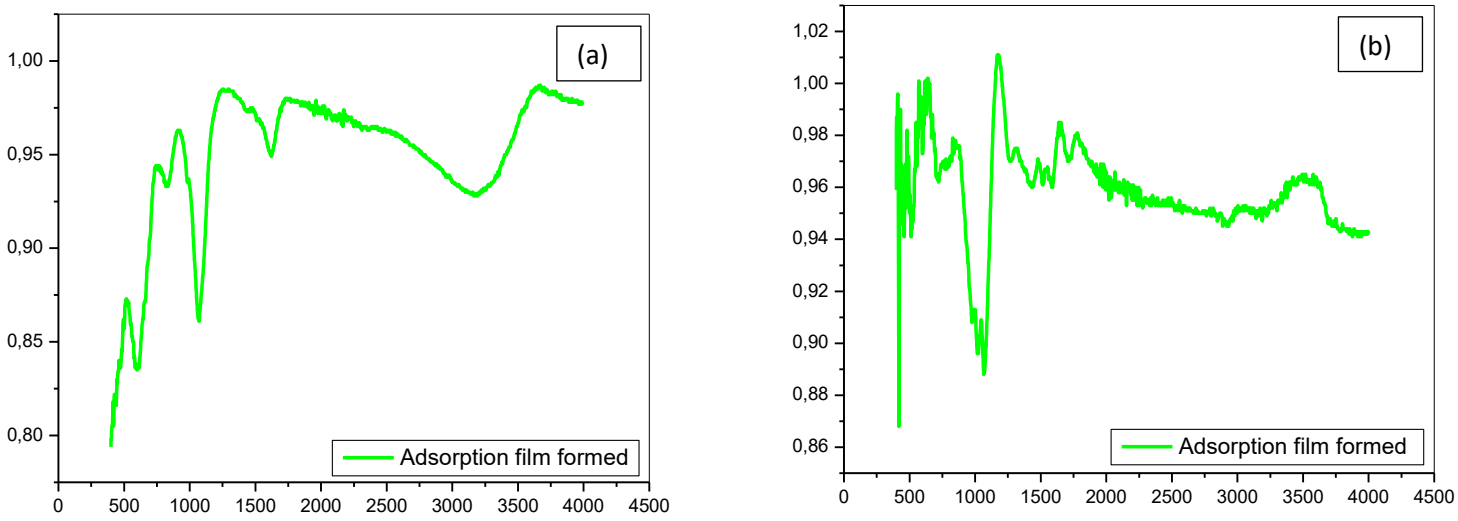


Figure 5.6: Zoomed version of FT-IR spectra for the studied (a) adsorption films formed before UV exposure and (b) after being exposed to UV on MS in 1.5 M HCl

Figure 5.6 shows that the transmittance spectra of rust or adsorption films formed on metal surfaces before UV exposure exhibit the same shape as the *A. phylicoides* extract itself but with reduced intensity. This phenomenon can be attributed to the inhibitor molecules chemically interacting with the metal surface, resulting in the formation of a protective film or layer (adsorption film). This film may have a similar chemical structure to the *A. phylicoides* itself, leading to a similar FTIR spectrum shape. The *A. phylicoides* extract molecules may not fully cover the metal surface, resulting in the formation of rust or corrosion products in areas where the inhibitor is not present. These corrosion products may have a similar chemical composition to the metal oxide/hydroxide compounds typically found in rust, which can lead to similar FTIR spectrum shapes.

UV radiation has been identified as a significant factor in altering the chemical composition and functional groups, particularly highlighted in Figure 5.6. In this figure, there is a notable presence of the –C–H (CH_3) bond at 2972-2980 cm^{-1} for *A. phylicoides* not exposed to UV radiation, whereas this peak disappears in the adsorption film formed on UV-exposed *A. phylicoides*. This observation sparks considerable interest among researchers to determine which type of *A. phylicoides*, UV-exposed or non-exposed, provides superior inhibition efficiency. While FTIR analysis does not directly indicate inhibition efficiency, alternative methods such as gravimetric analysis and electrochemical studies will be employed to

© University of Venda

evaluate the inhibition performance between UV-exposed and non-exposed *A. phylicoides* samples.

Figure 5.6 likely depicts an infrared (IR) spectrum showing the characteristic peaks of different functional groups presence in the *A. phylicoides* extract. The peak at wavenumbers 2972-2980 cm^{-1} corresponds to the stretching vibration of the C-H bonds in methyl groups (-CH_3). In both UV-radiated and non-UV-radiated *A. phylicoides* extracts, this peak exists, indicating the presence of -C-H (CH_3) bonds in the molecules. This observation aligns with similar spectroscopic investigations conducted by Arokiasamy *et al*. (2017) [363]. The similarity in the position and intensity of this peak suggests that UV radiation does not significantly alter the chemical structure of the molecules responsible for this absorption. However, when an adsorption film is formed, this peak disappears. This disappearance could be attributed to the interaction of the molecules in the *A. phylicoides* extract with the surface of the adsorption film. When molecules are adsorbed onto a surface, their vibrational modes may be altered due to the interactions with the surface molecules or due to confinement effects [364]. As a result, the characteristic peak corresponding to the C-H (CH_3) bonds may either shift to a different wavenumber or become broadened, making it difficult to observe in the spectrum. Therefore, the disappearance of the peak at 2972-2980 cm^{-1} in the adsorption film spectrum indicates that the molecules in the *A. phylicoides* extract are interacting with the surface of the film, leading to changes in their vibrational modes. This phenomenon aligns with similar studies investigating surface interactions and adsorption processes, such as the work conducted by Gao *et al*. (2021) [365]. This information can be valuable for understanding the behavior of the *A. phylicoides* extract when it interacts with different surfaces, which can have implications for various applications such as surface coatings or drug delivery systems.

© University of Venda

Table 5.3: Functional groups from the FTIR spectra for mild steel in sulphuric acid

	Functional Groups			
Bands position (cm^{-1})	**Non–UV Radiated *A. phylicoides***	**UV-radiated *A. phylicoides***	**Adsorption film Non-UV-Radiated *A. phylicoides***	**Adsorption film UV-Radiated *A. phylicoides***
3300 – 3500	O–H alcohol	O–H alcohol	O–H alcohol	O–H alcohol
3100 –3550				N–H amines
2700 – 2900		O–C–H C–H (CH_3)		
2972 –2980	–C–H (CH_3)		–C–H (CH_3)	
1550 –1630	$-RCO_2^-$ Carboxylates ions		$-RCO_2^-$ Carboxylates ions	
1600 – 1720	C=O ketone C=O aldehyde	C=O ketone C=O aldehyde	C=O ketone C=O aldehyde	C=O ketone C=O aldehyde
1600 – 1650	C=C alkene	C=C alkene	C=C alkene	
1500 – 1570	C=C aromatic	C=C aromatic	C=C aromatic	
1250 – 1320	–CH=CH– (trans)	–CH=CH– (trans) Nitrates $RONO_2$	–CH=CH– (trans)	
1180 – 1360	$–RSO_2NH_2–$ Sulphonamides	$–RSO_2NH_2–$ Sulphonamides	$–RSO_2NH_2–$ Sulphonamides	
1000 – 1200		Sulfonates RSO_3M		Sulfonates RSO_3M
600 – 750				C-H aromatic
600 – 900		C-C alkane C-H aromatic		
350-520	MS–O bond Mild steel–Oxygen bond		MS–O bond Mild steel–Oxygen bond	MS–O bond Mild steel–Oxygen

© University of Venda

Table 5.4: Functional groups from the FTIR spectra for mild steel in hydrochloric acid

	Functional Groups			
Bands position (cm^{-1})	**Non UV-Radiated *A. phylicoides***	**UV-radiated *A. phylicoides***	**Adsorption film Non-UV-Radiated *A. phylicoides***	**Adsorption film UV-Radiated *A. phylicoides***
3300 – 3500	O–H alcohol	O–H alcohol	O–H alcohol	O–H alcohol
3100 –3550			N–H amines	N–H amines
2700 – 2900		O–C–H C–H (CH_3)		
2972 –2980	–C–H (CH_3)			
1550 –1630	$-RCO_2^-$ Carboxylates ions			C=C alkene
1600 – 1720	C=O ketone C=O aldehyde	C=O ketone C=O aldehyde		C=O ketone C=O aldehyde
1600 – 1650	C=C alkene	C=C alkene	C=C alkene	
1500 – 1570	C=C aromatic	C=C aromatic		
1250 – 1320	–CH=CH– (trans)	–CH=CH– (trans) $RONO_2$ Nitrates		–CH=CH– (trans) $RONO_2$ Nitrates
1180 – 1360	$–RSO_2NH_2–$ Sulphonamides	$–RSO_2NH_2–$ Sulphonamides	C-H aromatic	C-H aromatic
1000 – 1200		Sulfonates RSO_3M	Sulfonates RSO_3M	Sulfonates RSO_3M
600 – 750				C-C alkane C-H aromatic
600 – 900		C-C alkane C-H aromatic		
350-520	MS–O bond Mild steel–Oxygen bond		MS–O bond Mild steel–Oxygen bond	

The effectiveness of *A. phylicoides* extracts in inhibiting corrosion hinges on the unique organic molecules they contain, characterized by heteroatoms, aromatic rings, and conjugated double or triple bonds [366]. To elucidate the composition of these extracts, FTIR spectroscopy was employed. The notable peak observed between 3300 and 3500 cm^{-1} corresponds to the stretching vibration of O-H bonds, indicating the presence of numerous hydroxyl groups within the molecules of the *A. phylicoides* extract. This observation is consistent with similar spectroscopic investigations conducted by Sahoo *et al*. (2012) in their study on FTIR and Raman spectroscopic investigations of a norfloxacin/carbopol934 polymeric suspension, as published in the Journal of Young Pharmacists [367]. Furthermore,

© University of Venda

an absorption peak at 1600-1650 cm^{-1} suggests the presence of C=C alkene bonds. This observation aligns with studies on the vibrations of C=N and N=N links conducted by Bellamy (1980) [368]. The peak at 1000-1200 cm^{-1} is indicative of Sulfonates (RSO_3M) bonds. M" typically represents a cation or a metal ion, and "R" represents an organic substituent or a hydrocarbon chain. This observation is consistent with studies on the structure and properties of phenol-2,4-disulfonic acid dihydrate conducted by Pisareva *et al.* (2008) in their research published in the Russian Journal of Physical Chemistry A, focusing on chemistry [369].

FTIR spectrum of UV radiated *A. phylicoides* exhibits a distinct absorption peak in the range of 400-500 cm^{-1}, attributed to the stretching vibration of Metal-O bonds. Specifically, in FTIR spectra, a peak around 500 cm^{-1} typically corresponds to the bending vibrations of metal-oxygen (M-O) bonds, where M represents a metal atom, as in the case of MS-O bonds. This spectral region often signifies the presence of metal oxides or compounds containing metal-oxygen bonds. This observation aligns with surface science and electrochemical studies conducted by Zellner and Chen (2005) in their research on WC and W2C PVD films as potential electrocatalysts, published in Catalysis Today [370].

This study, as indicated by its title, centred on inhibiting corrosion using extracts from *A. phylicoides* leaves that had undergone geometric isomerization due to exposure to ultraviolet (UV) light. This necessitates the use of FTIR to first prove if geometric isomerization occurs and differentiate functional groups' presence in non-UV radiated and UV radiated *A. phylicoides* extract. The FTIR successfully proves the occurrence of geometric isomerization. *A. phylicoides* typically exists in a trans configuration but undergoes geometric isomerization when exposed to UV light for 24 hours, converting to the cis configuration. Geometric isomerization involves a rearrangement of atoms in a molecule, resulting in the formation of isomers with the same molecular formula but differing in the spatial arrangement of atoms. This phenomenon occurs in *A. phylicoides* extract and it is also common in other natural products due to factors such as environmental conditions, temperature variations, light exposure, or enzymatic reactions. In this study, UV light exposure was the cause of geometric isomerization, as indicated in the study's title. When a compound transitions from the trans to the cis configuration, it means that the substituents or functional groups attached to the double bond have shifted positions relative to each other. This change in geometry can significantly affect the properties of the molecule, including its biological activity, stability, and reactivity. For instance, if a compound in *A. phylicoides* extract undergoes geometric

© University of Venda

isomerization from trans to cis configuration, it could potentially alter its flavor, aroma, or bioactivity [371].

Understanding the occurrence and effects of geometric isomerization in natural products like *A. phylicoides* extract is crucial for various applications, including food science, pharmacology, and herbal medicine, as it can impact the quality, efficacy, and safety of the product. The successful application of FTIR confirmed that isomerization indeed occurs, as the functional groups in non-UV radiation *A. phylicoides* extract differed from those in UV radiation *A. phylicoides*. If isomerization had not occurred, the FTIR spectra would have been identical. Moreover, *A. phylicoides* extracts exhibit different behaviours when applied to different metals, as zinc behaves differently from mild steel. This difference was also demonstrated by the FTIR spectra, as shown in Figures 5.2 and 5.3 (indicated by black lines). The formation of an adsorption film led to spectra showing various functional groups, raising questions about which among UV-radiated and non-UV-radiated *A. phylicoides* extracts would have a higher potential to inhibit acid corrosion, as stated in the title of this study. This requires the utilization of gravimetric analysis to address the pressing question: Will *A. phylicoides* UV-radiated extract, possessing functional groups such as aromaticity, oxygen atom, nitrogen, etc., exhibit higher inhibition efficiency? The next session will address this issue.

© University of Venda

University of Venda
Creating Future Leaders

CHAPTER SIX

RESULTS AND DISCUSSION

Gravimetric analysis/weight loss measurement

(WL)

© University of Venda

6.1 Gravimetric Analysis

This study aimed to explore the capacity of UV-radiated *A. phylicoides* extract to inhibit acid corrosion, as stated in the thesis title. The confirmation of geometric isomerization through LC-MS data, FTIR analysis, and observing distinct functional groups between UV-radiated and non-UV-radiated *A. phylicoides* extracts prompted this investigation. The current study sought to initially assess the corrosion inhibition potential of non-radiated *A. phylicoides* extract and then compare it with the inhibition efficiency obtained from UV-radiated *A. phylicoides* extract. The *A. phylicoides* extract may behave differently when employed on different metals since mild steel is different from zinc metal, this necessitates the need to thoroughly investigate the potential to inhibit acid corrosion on both metals. Tables 6.1-6.4 show blank experiments for MS and Zn in HCl and H_2SO_4.

Table 6.1: Weight loss measurements on mild steel exposed to various concentrations of sulphuric acid

Concentration of HCl (M)	**Weight loss (g)**			
	303K	**313K**	**323K**	**333K**
0.500	0.1319	0.2079	0.2811	0.4112
0.800	0.2021	0.2121	0.3008	0.4997
1.000	0.2306	0.2730	0.3012	0.6091
1.200	0.2390	0.3222	0.3379	0.6612
1.500	0.2533	0.3353	0.4947	0.6957

Table 6.2: Weight loss measurements on mild steel exposed to various concentrations of hydrochloric acid

Concentration of HCl (M)	**Weight loss (g)**			
	303K	**313K**	**323K**	**333K**
0.500	0.3888	0.7169	0.9910	1.2112
0.800	0.4990	0.9901	1.2990	1.3069
1.000	0.5001	1.0919	1.3012	1.4001
1.200	0.5019	1.1121	1.3180	1.4435
1.500	0.5644	1.1826	1.3181	1.5058

© University of Venda

Table 6.3: Weight loss measurements on zinc exposed to various concentrations of sulphuric acid

Concentration of HCl (M)	Weight loss (g)			
	303K	313K	323K	333K
0.500	0.1800	0.2032	0.3870	0.5155
0.800	0.2027	0.2291	0.4001	0.6005
1.000	0.2317	0.2311	0.4097	0.6689
1.200	0.2481	0.2507	0.4669	0.7001
1.500	0.2521	0.2648	0.4778	0.7063

Table 6.4: Weight loss measurements on zinc exposed to various concentrations of hydrochloric acid

Concentration of HCl (M)	Weight loss (g)			
	303K	313K	323K	333K
0.500	0.2122	0.3189	0.4400	1.1166
0.800	0.2222	0.3221	0.4921	1.1899
1.000	0.2638	0.4002	0.5011	1.2000
1.200	0.2813	0.4333	0.5049	1.2001
1.500	0.2953	0.4533	0.5346	1.2417

Table 6.1 gives a minimum weight loss of 0.1319g at 303K and a maximum weight loss of 0.6957g at 333K for mild steel in hydrochloric acid was achieved. It is clear that when temperature increases weight loss increases as noted in Table 6.1 at 0.500M of HCl and 303K, the weight loss series started with 0.1319, 0.2079, 0.2811, then 0.4112g. Table 6.2 also shows a similar trend observed in Table 6.1, however, it can be observed in Table 6.2 that the minimum and maximum weight losses are 0.3888g and 1.5058 g respectively. This observation is consistent with weight loss, and thermodynamics studies conducted by Aziz *et al*. (2022) on N-2-methylbenzylidene-4-antipyrineamine as an inhibitor for mild steel corrosion in hydrochloric acid, published in Lubricants [381]. Tables 6.1-6.2 show that between two acids namely, HCl and H_2SO_4, it was found that HCl tends to corrode metals faster and lead to higher weight loss [382]. An explicit explanation for this phenomenon is that due to its higher acidity, faster reaction kinetics, formation of more soluble reaction products, and lack of oxidizing properties, HCl tends to corrode metals faster and lead to higher weight loss compared to H_2SO_4. Tables 6.3-6.4 show a similar trend as observed in Tables 6.1-6.2 in a sense that when temperature increases weight loss also increases [383]. Table 6.1 shows weight loss as temperature and concentration of HCl increases, this

© University of Venda

observation simply means that when mild steel is immersed in sulphuric acid, it undergoes a process called corrosion. Corrosion is the deterioration of a material, usually a metal, due to a chemical reaction with its environment [384].

In the case of mild steel and HCl, the following reactions occur:

1. Formation of Iron(II) Chloride ($FeCl_2$):

$$Fe(s) + 2HCl(aq) \rightarrow FeCl_2(aq) + H_2(g) \quad (6.1)$$

2. Formation of Hydrogen Gas (H_2):

$$2HCl(aq) \rightarrow H_2(g) + Cl_2(g) \quad (6.2)$$

The formation of iron (II) chloride and the release of hydrogen gas are responsible for the corrosion of mild steel. Iron(II) chloride is a soluble compound, and as it forms on the surface of the steel, it exposes fresh metal to further reaction with the acid [57]. This continuous reaction leads to the loss of metal from the surface, resulting in the observed loss of mass as indicated in Table 6.1. Additionally, the formation of hydrogen gas bubbles can accelerate the removal of the corroded metal from the surface [385]. The reaction between mild steel and hydrochloric acid results in the dissolution of the metal and the formation of soluble iron chloride compounds, leading to the corrosion and loss of mass of the mild steel. Sulphuric acid was also utilized to explore if different observations would be found. Table 6.2 records a minimum weight loss of 0.3888g at 303K and maximum weight loss of 1.5058g at 333K implying that more weight loss was achieved in hydrochloric acid than in sulphuric acid. Table 6.3 records a maximum weight loss of 0.7063 g at 333K and a minimum weight loss of 0.1800 g at 303K, this weight loss is higher than that experienced by mild steel. The difference in mass loss between mild steel and zinc when exposed to similar conditions of 0.50 to 1.5 M H_2SO_4 can be attributed to their respective chemical properties and reactivity with the acid. Zinc is more reactive than iron (the main component of mild steel) in terms of its position in the reactivity series of metals [386]. Zinc readily reacts with hydrochloric acid to form zinc chloride and hydrogen gas according to the following equation:

© University of Venda

$$Zn(s) + 2HCl(aq) \rightarrow ZnCl_2(aq) + H_2(g) \quad (6.3)$$

This reaction tends to be more vigorous compared to the reaction of iron with hydrochloric acid. As a result, zinc undergoes faster corrosion and loss of mass when exposed to HCl compared to mild steel.

The common behaviour observed in Table 6.1-6.4 confirm that the concentration of the acid and the temperature can influence weight loss by metal, then the rate of corrosion. The general observation regarding concentration and temperature effects as indicated in Table 6.1-6.4 are as follows:

Effect of acid concentration

Increase in concentration: In an acidic environment, the concentration of protons (H+) and other corrosive species typically increases with the acid concentration [387]. This elevated concentration of corrosive agents can accelerate the corrosion process. More aggressive ions in the acidic medium can attack the metal surface, leading to increased weight loss [388]. When the concentration of acid increases from 0.500 M to 1.500 M the mass lost by metal increases. This trend has been observed in Tables 6.1-6.4.

Effect of Temperature:

In this study, as indicated in Tables 6.1-6.4, when temperature increases, weight loss also increases. This trend implies that raising temperature from 303K to 333K increased the kinetic energy of reacting particles causing more energetic collisions between mild steel and zinc metal specimens and corrosive species.

6.2 Weight Loss Measurement Using Non-UV-Radiated *A. Phylicoides* Extract

To ascertain which *A. phylicoides* extract offers the highest inhibition efficiency, this study initially conducted a gravimetric analysis of non-UV radiated *A. phylicoides* extract. This section presents the findings from the gravimetric analysis performed with *A. phylicoides* leaves extracts that have not been exposed to UV radiation. Various concentrations of the extracts were prepared in 1.5M solutions of H_2SO_4 and HCl and then utilized with zinc and

© University of Venda

mild steel. The choice of acidic concentration at 1.5M was based on its representation as the most challenging and aggressive condition, as indicated in Tables 6.1-6.4. The selection of the highest acid concentration is driven by its representation of the most severe conditions regarding corrosivity. Assessing the inhibitor under these rigorous conditions helps researchers ascertain its efficacy in the most demanding environment. Concentrating on the highest acid concentration when evaluating the efficacy of *A. phylicoides* extract allows researchers to effectively evaluate its performance under the most formidable conditions, offering crucial insights for corrosion mitigation strategies. Tables 6.5-6.8 illustrate the weight loss of the metals for blank and with various concentrations of non-UV radiated *A. phylicoides* leaves extract as corrosion inhibition.

Table 6.5: Weight loss measurements on mild steel exposed to sulphuric acid (1.5M) in the presence of non-UV radiated *A. phylicoides* extract

Concentration of *A. phylicoides* extract (ppm)	**Weight loss (g)**			
	303K	**313K**	**323K**	**333K**
0.000	0.2533	0.3353	0.4947	0.6957
100	0.0399	0.0689	0.1464	0.1911
400	0.0391	0.0621	0.1380	0.1840
700	0.0306	0.0480	0.1356	0.1762
1000	0.0210	0.0292	0.1267	0.1756
1300	0.0151	0.0209	0.1218	0.1687

Table 6.6: Weight loss measurements on mild steel exposed to hydrochloric acid (1.5M) in the presence of non-UV radiated *A. phylicoides* extract

Concentration of *A. phylicoides* extract (ppm)	**Weight loss (g)**			
	303K	**313K**	**323K**	**333K**
0.000	0.5644	1.1826	1.3181	1.5058
100	0.1381	0.3290	0.3910	0.3590
400	0.1229	0.3281	0.3435	0.3293
700	0.0590	0.2270	0.3026	0.3284
1000	0.0584	0.2244	0.2670	0.3180
1300	0.0429	0.1233	0.2240	0.3090

© University of Venda

Table 6.7: Weight loss measurements on zinc exposed to sulphuric acid (1.5M) in the presence of non-UV radiated *A. phylicoides* extract

Concentration of *A. phylicoides* extract (ppm)	**Weight loss (g)**			
	303K	**313K**	**323K**	**333K**
0.000	0.2521	0.2648	0.4778	0.7063
100	0.0799	0.0981	0.1484	0.3048
400	0.0650	0.0710	0.1365	0.2991
700	0.0452	0.0688	0.1264	0.2853
1000	0.0401	0.0606	0.1109	0.2838
1300	0.0332	0.0594	0.1089	0.1959

Table 6.8: Weight loss measurements on zinc exposed to hydrochloric acid (1.5M) in the presence of non-UV radiated *A. phylicoides* extract

Concentration of *A. phylicoides* extract (ppm)	**Weight loss (g)**			
	303K	**313K**	**323K**	**333K**
0.00	0.2953	0.4533	0.5346	1.2417
100	0.1101	0.1581	0.2390	0.5957
400	0.1080	0.1497	0.1861	0.4441
700	0.1071	0.1340	0.1697	0.4192
1000	0.0632	0.1069	0.1394	0.3584
1300	0.0511	0.1053	0.1246	0.3308

Tables 6.5-6.8 demonstrate a consistent trend in the relationship between weight loss and the concentration of non-UV radiated *A. phylicoides* extract across temperatures ranging from 303 to 333 Kelvin (K). The lowest weight loss occurred at the highest concentration of 1300 ppm of the extract. This reduction in weight loss at higher concentrations can be attributed to the increased availability of *A. phylicoides* molecules, leading to greater adsorption of the extract on the metal surface. This finding aligns with studies on corrosion inhibitors conducted by Abd El-Lateef *et al*. (2013) in their research on the effect of novel surfactants as corrosion inhibitors for carbon steel, published in the Journal of Surfaces and Interfaces of Materials [393]. Additionally, as temperature increased from 303K to 333K, weight loss also increased, indicating a decrease in the adsorption of *A. phylicoides* molecules on the metal surface. Specifically, in Table 6.5, at 100 ppm and 303K, the weight loss was 0.0399 g, which

© University of Venda

increased to 0.1911 g when the temperature rose to 333K. Similarly, at 100 ppm and 333K, weight loss was 0.1911 g, but with an increase in *A. phylicoides* extract concentration to 1300 ppm, weight loss decreased significantly to 0.1687 g. The minimum weight loss observed was 0.0151 g at 1300 ppm and 303K, while the maximum weight loss was 0.1911 g at 100 ppm and 333K. Furthermore, Table 6.6 indicates a minimum and maximum weight loss of 0.0429 g and 0.3590 g, respectively. This suggests that although both hydrochloric acid and sulphuric acid are strong acids, hydrochloric acid appears to be more aggressive than sulphuric acid. In Table 6.7, the results of corrosion experiments are documented, showing a minimum weight loss of 0.0332 g and a maximum weight loss of 0.7063 g. The lowest weight loss was observed at 1300 ppm and 303K, while the highest weight loss occurred at 100 ppm and 333K. These findings suggest that the effectiveness of the corrosion inhibitor is influenced by both its concentration and the temperature of the environment. Higher inhibitor concentrations at lower temperatures result in lower weight loss, indicating enhanced corrosion protection. Conversely, lower inhibitor concentrations at higher temperatures lead to higher weight loss, indicating reduced effectiveness in inhibiting corrosion. These insights provide valuable guidance for optimizing corrosion mitigation strategies in practical applications by understanding the interplay between inhibitor concentration, temperature, and corrosion inhibition. This observation is consistent with studies on the corrosion and scale inhibition of ordinary steel conducted by Touir *et al*. (2008) [394].

Table 6.8 presents data regarding the weight loss of zinc under various conditions, specifically focusing on the effect of different concentrations of non-UV radiated *A. phylicoides* extract. At a temperature of 323 K and a concentration of 100 ppm of the extract, the weight loss of zinc was measured to be 0.2390 g. When the concentration of the *A. phylicoides* extract was increased to 1300 ppm under the same temperature conditions, the weight loss of zinc decreased to 0.1246 g. This observation suggests that the non-UV radiated *A. phylicoides* extract effectively reduced the weight loss of zinc as its concentration increased. Comparing these results with those from Tables 6.7 and 6.8, which detail the weight loss of zinc using hydrochloric acid and sulphuric acid, respectively, further insights can be gained. Particularly, at a concentration of 1300 ppm and a temperature of 333 K, it is evident that hydrochloric acid causes more weight loss than sulphuric acid. The implications of these findings are twofold:

- Effectiveness of *A. phylicoides* Extract: The non-UV radiated *A. phylicoides* extract demonstrates corrosion inhibition properties, as evidenced by the reduction in zinc

© University of Venda

weight loss with increasing concentrations. This suggests that the extract has the potential to mitigate corrosion effectively.

- Differential corrosivity of acids: The comparison between hydrochloric acid and sulfuric acid highlights the differing corrosive effects of these acids on zinc. Hydrochloric acid induces greater weight loss compared to sulphuric acid, indicating its higher corrosivity towards zinc under the specified conditions.

These findings underscore the importance of corrosion inhibition strategies and the nuanced effects of different inhibitors and corrosive agents on metal corrosion. Such insights are valuable for developing tailored corrosion mitigation approaches in various industrial applications.

6.3 Weight Loss Measurement Using UV-Radiated *A. Phylicoides* Extract

The experiment results suggest that non-UV radiated *A. phylicoides* extract shows promise in inhibiting acid corrosion, as evidenced by the measured weight loss of mild steel and zinc. However, the primary focus of the study, as indicated by its title, is to investigate the potential of UV-assisted *A. phylicoides* extract in inhibiting acid corrosion. To address this objective, it is necessary to conduct a gravimetric analysis of mild steel and zinc in an acid medium using UV-radiated *A. phylicoides* extract. This step is crucial because it will provide insights into the comparative effectiveness of UV-radiated and non-UV-radiated *A. phylicoides* extract in inhibiting acid corrosion. Comparing the weight loss data obtained from both sets of experiments assists in determining which type of *A. phylicoides* extract demonstrates higher inhibition efficiency. This comparative analysis is essential for understanding the impact of UV radiation on the corrosion inhibition properties of *A. phylicoides* extract. It will help researchers evaluate whether UV radiation enhances or diminishes the extract's ability to protect metals from acid corrosion. Ultimately, the findings from this study will contribute valuable insights to the field of corrosion science and inform future research directions in corrosion inhibition strategies. Tables 6.9-6.12 show weight loss of metal exposed to UV-radiated *A. phylicoides* extract.

© University of Venda

Table 6.9: Weight loss measurements on mild steel exposed to sulphuric acid (1.5M) in the presence of UV-radiated *A. phylicoides* extract

Concentration of *A. phylicoides* (ppm)	**Weight loss (g)**			
	303 K	**313 K**	**323 K**	**333 K**
0.000	0.2533	0.3353	0.4947	0.6957
100	0.0990	0.1409	0.2269	0.3510
400	0.0781	0.1201	0.2121	0.3182
700	0.0648	0.1187	0.2019	0.2982
1000	0.0500	0.1001	0.1513	0.2191
1300	0.0160	0.0201	0.1018	0.1821

Table 6.10: Weight loss measurements on mild steel exposed to hydrochloric acid (1.5M) in the presence of UV-radiated *A. phylicoides* extract

Concentration of *A. phylicoides* (ppm)	**Weight loss (g)**			
	303 K	**313 K**	**323 K**	**333 K**
0.000	0.5644	1.1826	1.3181	1.5058
100	0.2189	0.4981	0.5821	0.6919
400	0.1918	0.4210	0.5019	0.6109
700	0.1509	0.3512	0.4213	0.5120
1000	0.1103	0.2821	0.3587	0.4518
1300	0.0512	0.1515	0.2189	0.3131

Table 6.11: Weight loss measurements on zinc exposed to sulphuric acid (1.5M) in the presence of UV-radiated *A. phylicoides* extract

Concentration of *A. phylicoides* (ppm)	**Weight loss (g)**			
	303 K	**313 K**	**323 K**	**333 K**
0.000	0.2521	0.2648	0.4778	0.7063
100	0.0923	0.0999	0.1832	0.3014
400	0.0615	0.0719	0.1715	0.2812
700	0.0504	0.0619	0.1419	0.2328
1000	0.0219	0.0317	0.0751	0.1298
1300	0.0103	0.0205	0.0399	0.0944

© University of Venda

Table 6.12: Weight loss measurements on zinc exposed to hydrochloric acid (1.5M) in the presence of UV-radiated *A. phylicoides* extract

Concentration of *A. phylicoides* (ppm)	**Weight loss (g)**			
	303 K	**313 K**	**323 K**	**333 K**
0.00	0.2953	0.4533	0.5346	1.2417
100	0.1296	0.2018	0.2591	0.6080
400	0.0941	0.1541	0.1908	0.5088
700	0.0812	0.1298	0.1601	0.4120
1000	0.0503	0.0918	0.1415	0.3702
1300	0.0218	0.0710	0.1017	0.2841

Table 6.9 displays a notable increase in weight loss with rising temperature. For example, at a concentration of 700 ppm, the weight loss was 0.0648 grams at 303 K, escalating to 0.2982 grams at 333K. This trend suggests that the effectiveness of UV-radiated *A. phylicoides* extract in protecting metal diminishes as the temperature rises. Particularly noteworthy is the observation at 333K with no inhibitor (0 ppm), where the weight loss was 0.6957 g. However, upon the introduction of UV-radiated *A. phylicoides* extract at the same temperature and a concentration of 1300 ppm, the weight loss decreased significantly to 0.1821 grams. This indicates that the introduction of UV-radiated *A. phylicoides* extract successfully mitigates corrosion, with higher concentrations providing better protection to the metal. Table 6.10 exhibits a similar trend to Table 6.9. A notable difference between the two tables is observed at 323 K and a concentration of 1000 ppm, where the weight loss was 0.1513 g for sulphuric acid and 0.3587 g for hydrochloric acid. This observation suggests that hydrochloric acid is more aggressive in inducing corrosion compared to sulphuric acid. The data from Tables 6.9 and 6.10 underscore the influence of temperature and inhibitor concentration on corrosion inhibition. The findings highlight the effectiveness of UV-radiated *A. phylicoides* extract in mitigating corrosion, with higher concentrations providing enhanced protection. Additionally, the comparative analysis between hydrochloric acid and sulphuric acid reveals differences in their corrosive aggressiveness, with hydrochloric acid exhibiting higher corrosion rates.

Table 6.11 provides further evidence supporting the effectiveness of UV-radiated *A. phylicoides* as a corrosion inhibitor. At a temperature of 313 K and with no inhibitor present (0 ppm), the weight loss was measured at 0.2648 g. However, when UV-radiated *A. phylicoides* extract was introduced, for example, at a concentration of 400 ppm, the weight

© University of Venda

loss decreased significantly to 0.0615 g. This observation suggests that UV-radiated *A. phylicoides* extract effectively protects metal from corrosion. Additionally, Table 6.12 highlights the influence of temperature on the protection of metal from corrosion. The data indicates that better protection of the metal can be achieved at lower temperatures. This is evidenced by the lower weight loss values obtained at 303 K compared to those obtained at 333 K. An intriguing aspect to explore further would be to compare the effectiveness of UV-radiated *A. phylicoides* extract with that of non-UV radiated *A. phylicoides* extract. This comparison could shed light on any potential differences in corrosion inhibition properties between the two types of extracts. The outcomes of this comparison will be addressed in the conclusion section of the study, providing valuable insights into the optimal use of *A. phylicoides* extracts as corrosion inhibitors under different conditions.

6.4 Time Stability of Non-UV radiated *A. phylicoides* Extract

The gravimetric analysis experiments involved varying concentrations of *A. phylicoides* extract and temperatures ranging from 303 K to 333 K for 6 hours. To further understand the effectiveness of *A. phylicoides* extract over time, it is essential to conduct stability research while keeping the temperature constant at 303 K. This choice of the temperature of 303K allows for longer experimental durations, such as 24 hours, which provides valuable insights into the temporal stability of the corrosion inhibition properties of the extract. Selecting 303 K ensures the feasibility of conducting experiments over extended periods, as this temperature allows for practical experimentation without risking the complete depletion of the metal specimens. Unlike higher temperatures such as 333 K, where the aggressive nature of the environment may lead to rapid corrosion and potential depletion of the metal specimens within 24 hours, 303 K offers a more controlled and stable environment for prolonged testing. Varying the duration of the experiments from 6 hours to 24 hours can help observe how the effectiveness of the *A. phylicoides* extract evolves, providing valuable data for understanding its long-term corrosion inhibition properties. This approach allows for a comprehensive assessment of the extract's performance under realistic conditions and contributes to informed decision-making in corrosion prevention strategies.

© University of Venda

Table 6.13: Weight loss measurements on mild steel exposed to sulphuric acid (1.5M) in the presence of non-UV radiated *A. phylicoides* extract

Concentration of *A. phylicoides* (ppm)	**Weight loss (g)**			
	6 hours	**12 hours**	**18 hours**	**24 hours**
0.00	0.2533	0.6123	0.9780	1.4910
100	0.0399	0.3408	0.5129	0.8191
400	0.0391	0.3109	0.5009	0.7791
700	0.0306	0.2910	0.4908	0.7711
1000	0.0210	0.1293	0.3889	0.5198
1300	0.0151	0.0910	0.3002	0.2008

Table 6.14: Weight loss measurements on mild steel exposed hydrochloric acid (1.5M) in the presence of non-UV radiated *A. phylicoides* extract

Concentration of *A. phylicoides* (ppm)	**Weight loss (g)**			
	6 hours	**12 hours**	**18 hours**	**24 hours**
0.00	0.5644	1.0140	1.3199	1.9021
100	0.1381	0.2980	0.4791	0.6187
400	0.1229	0.2517	0.4105	0.6091
700	0.0590	0.1131	0.1513	0.2409
1000	0.0584	0.1091	0.1193	0.2100
1300	0.0429	0.0914	0.1000	0.1937

Table 6.15: Weight loss measurements on zinc exposed to sulphuric acid (1.5M) in the presence of non-UV radiated *A. phylicoides* extract

Concentration of *A. phylicoides* (ppm)	**Weight loss (g)**			
	6 hours	**12 hours**	**18 hours**	**24 hours**
0.00	0.2521	0.6800	0.7698	1.1986
100	0.0799	0.1599	0.2136	0.4088
400	0.0650	0.1477	0.1700	0.2666
700	0.0452	0.0933	0.1442	0.1999
1000	0.0401	0.0713	0.1095	0.1465
1300	0.0332	0.0564	0.0903	0.1098

© University of Venda

Table 6.16: Weight loss measurements on zinc exposed in hydrochloric acid (1.5M) in the presence of non-UV radiated *A. phylicoides* extract

Concentration of *A. phylicoides* (ppm)	**Weight loss (g)**			
	6 hours	**12 hours**	**18 hours**	**24 hours**
0.00	0.2953	0.6027	0.9993	1.3761
100	0.1101	0.2077	0.4931	0.5008
400	0.1080	0.2113	0.3134	0.4766
700	0.1071	0.1988	0.2576	0.4139
1000	0.0632	0.1386	0.2154	0.3614
1300	0.0511	0.1110	0.1983	0.3329

Tables 6.13 to 6.16 present crucial data illustrating the dynamic relationship between metal weight loss and immersion time under varying inhibitor concentrations. The primary objective of these experiments is to discern how the effectiveness of inhibitors evolves. One notable finding emerges from observations at 0 ppm concentration: a clear escalation in weight loss as immersion time increases. For instance, at 6 hours, the weight loss was measured to be 0.2533g, nearly doubling to 0.6123g at 12 hours. This trend underscores the anticipated outcome that prolonged exposure to acidic environments exacerbates corrosion, resulting in greater metal degradation. Moreover, the data reveal that the degree of protection against corrosion correlates with inhibitor concentration. Notably, the highest level of protection, evidenced by the lowest weight loss, is attained at 1300 ppm concentration. Table 6.13 further accentuates the progressive increment in weight loss with extended immersion time. For instance, at 400 ppm concentration, weight loss registers 0.0391g initially, but escalates to 0.7791g after 24 hours, highlighting the exacerbation of corrosion over time. Table 6.14 validates the effectiveness of non-UV radiated *A. phylicoides* as a corrosion inhibitor. Here, the introduction of the *A. phylicoides* extract leads to a rapid reduction in weight loss compared to the weight loss without the inhibitor. This substantial decrease from 1.9021g to 0.1937g after 24 hours unequivocally demonstrates the inhibitor's capability to minimize corrosion. Similar trends are observed in Tables 6.15 and 6.16, wherein corrosion mitigation is evident, albeit accompanied by increased weight loss with prolonged immersion time. These collective observations incite scientific curiosity regarding the superior inhibition efficiency offered by non-radiation *A. phylicoides* extract. Consequently, this study is motivated to delve deeper into investigating the extent of surface coverage and inhibition efficiency afforded by this promising inhibitor.

© University of Venda

6.5 Surface Coverage on Metal Exposed in Acidic Medium Over 24-Hour Timeframe

Investigating the surface coverage of corrosion inhibitors over varying timeframes is essential for understanding their effectiveness, optimizing their application, and ensuring long-term protection against corrosion. This section discusses the outcomes of investigations done regarding surface coverage.

Table 6.17: Surface coverage measurements on mild steel exposed to sulphuric acid (1.5M) in the presence of non-UV radiated *A. phylicoides* extract

Concentration of *A. phylicoides* (ppm)	**Surface Coverage**			
	6 hours	**12 hours**	**18 hours**	**24 hours**
0.00				
100	0.8425	0.4434	0.4756	0.4506
400	0.8456	0.4922	0.4878	0.4775
700	0.8792	0.5247	0.4908	0.4828
1000	0.9171	0.7888	0.6024	0.6514
1300	0.9404	0.8514	0.6930	0.8653

Table 6.18: surface coverage measurements on mild steel exposed hydrochloric acid (1.5M) in the presence of non-UV radiated *A. phylicoides* extract

Concentration of *A. phylicoides* (ppm)	**Surface Coverage**			
	6 hours	**12 hours**	**18 hours**	**24 hours**
0.00				
100	0.7553	0.7061	0.6370	0.6747
400	0.7822	0.7518	0.6890	0.6798
700	0.8955	0.8885	0.8854	0.8734
1000	0.8965	0.8924	0.9096	0.8896
1300	0.9240	0.9099	0.9242	0.8982

© University of Venda

Table 6.19: surface coverage measurements on zinc exposed to sulphuric acid (1.5M) in the presence of non-UV radiated *A. phylicoides* extract

Concentration of *A. phylicoides* (ppm)	**Surface Coverage**			
	6 hours	**12 hours**	**18 hours**	**24 hours**
0.00				
100	0.6831	0.7649	0.7225	0.6589
400	0.7422	0.7828	0.7792	0.7776
700	0.8207	0.8628	0.8127	0.8332
1000	0.8409	0.8951	0.8578	0.8778
1300	0.8683	0.9171	0.8827	0.9084

Table 6.20: surface coverage measurements on zinc exposed in hydrochloric acid (1.5M) in the presence of non-UV radiated *A. phylicoides* extract

Concentration of *A. phylicoides* (ppm)	**Surface Coverage**			
	6 hours	**12 hours**	**18 hours**	**24 hours**
0.00				
100	0.6272	0.6554	0.5066	0.6361
400	0.6343	0.6494	0.6864	0.6537
700	0.6373	0.6702	0.7422	0.6992
1000	0.7860	0.7700	0.7844	0.7374
1300	0.8270	0.8158	0.8016	0.7581

Surface coverage refers to the extent to which a corrosion inhibitor covers the surface of the metal substrate [141]. A value of 1 would indicate complete coverage, meaning that the inhibitor has effectively formed a protective layer over the entire metal surface, thereby minimizing exposure to corrosive agents [392]. Therefore, higher surface coverage values signify greater protection against corrosion. The surface coverage values obtained were less than 1, indicating that the corrosion inhibitor did not completely cover the metal surface. However, at 1300ppm concentration, the values were very close to 1, suggesting that the non-UV radiated *A. phylicoides* extract almost provided maximum protection against corrosion since the surface coverage values approached 1.

Table 6.17 illustrates fluctuations in surface coverage values for non-UV radiated *A. phylicoides* at different concentrations and exposure times. At 100 ppm, the surface coverage

© University of Venda

decreases from 0.8425 to 0.4506 within 24 hours, indicating instability. Conversely, Table 6.18 demonstrates consistent and stable surface protection at 700 ppm and 1300 ppm, with surface coverage values around 0.9, implying reliable corrosion inhibition. However, Table 6.19 displays some fluctuations at 1300 ppm, though the overall trend suggests effective protection with surface coverage close to 0.9. Similarly, Table 6.20 shows stable surface coverage across various timeframes and concentrations. Notably, Table 6.17 reveals unstable surface coverage, particularly at lower concentrations. Based on these findings, non-UV radiated *A. phylicoides* extract shows promise as a corrosion inhibitor, especially at higher concentrations, to mitigate acid corrosion.

6.6 Inhibition Efficiency of Non-UV Radiated *A. Phylicoides* Extract

Corrosion inhibition efficiency is a measure of how effectively a corrosion inhibitor prevents or reduces corrosion on a metal surface [395]. It is typically expressed as a percentage and is calculated by comparing the corrosion rate of the inhibited system to that of the uninhibited system. A corrosion inhibition efficiency value of 100% would mean that the corrosion inhibitor completely prevents corrosion, resulting in no metal loss compared to the uninhibited system. In theory, corrosion inhibition efficiency can exceed 100% if the inhibitor not only prevents corrosion but also reduces the corrosion rate below what it was in the uninhibited system. However, this situation is rare and typically occurs only under specific conditions or with highly effective inhibitors. Tables 6.21-6.24 show the inhibition efficiency of non-UV radiated *A. phylicoides* extract.

Table 6.21: Inhibition efficiency measurements on mild steel exposed to sulphuric acid (1.5M) in the presence of non-UV radiated *A. phylicoides* extract

Concentration of *A. phylicoides* (ppm)	**Inhibition efficiency**			
	6 hours	**12 hours**	**18 hours**	**24 hours**
0.00	-	-	-	-
100	84.25	44.34	47.56	45.06
400	84.56	49.22	48.78	47.75
700	87.92	52.47	49.08	48.28
1000	91.71	78.88	60.24	65.14
1300	94.04	85.14	69.30	86.53

© University of Venda

Table 6.22: Inhibition efficiency measurements on mild steel exposed hydrochloric acid (1.5M) in the presence of non-UV radiated *A. phylicoides* extract

Concentration of *A. phylicoides* (ppm)	**Inhibition efficiency**			
	6 hours	**12 hours**	**18 hours**	**24 hours**
0.00	-	-	-	-
100	75.53	70.61	63.70	67.47
400	78.22	75.18	68.90	67.98
700	89.55	88.85	88.54	87.34
1000	89.65	89.24	90.96	88.96
1300	92.40	90.99	92.42	89.82

Table 6.23: Inhibition efficiency measurements on zinc exposed to sulphuric acid (1.5M) in the presence of non-UV radiated *A. phylicoides* extract

Concentration of *A. phylicoides* (ppm)	**Inhibition efficiency**			
	6 hours	**12 hours**	**18 hours**	**24 hours**
0.00	-	-	-	-
100	68.31	76.49	72.25	65.89
400	74.22	78.28	77.92	77.76
700	82.07	86.28	81.27	83.32
1000	84.09	89.51	85.78	87.78
1300	86.83	91.71	88.27	90.84

Table 6.24: Inhibition efficiency measurements on zinc exposed in hydrochloric acid (1.5M) in the presence of non-UV radiated *A. phylicoides* extract

Concentration of *A. phylicoides* (ppm)	**Inhibition efficiency**			
	6 hours	**12 hours**	**18 hours**	**24 hours**
0.00	-	-	-	-
100	62.72	65.54	50.66	63.61
400	63.43	64.94	68.64	65.37
700	63.73	67.02	74.22	69.92
1000	78.60	77.00	78.44	73.74
1300	82.70	81.58	80.16	75.81

The trend observed in Tables 6.21-24 is the same as the observation from Tables 6.17-20 because corrosion inhibition efficiency and surface coverage are related concepts, but they measure different aspects of corrosion inhibition. surface coverage and corrosion inhibition

© University of Venda

efficiency are complementary measures that together provide a comprehensive understanding of the performance of a corrosion inhibitor. While surface coverage quantifies the extent of physical protection, corrosion inhibition efficiency assesses the inhibitor's ability to mitigate corrosion effectively [396].

Table 6.21 illustrates fluctuations in surface coverage values for non-UV radiated *A. phylicoides* at different concentrations and exposure times. At 100 ppm, the inhibition efficiency decreases from 84.25% to 45.06% within 24 hours, indicating instability. Conversely, Table 6.22 demonstrates consistent and stable surface protection at 700 ppm and 1300 ppm, with inhibition efficiency values around 90%, implying reliable corrosion inhibition. However, Table 6.23 displays some fluctuations at 1300 ppm, though the overall trend suggests effective protection with inhibition efficiency close to 90%. Similarly, Table 6.24 shows stable inhibition efficiency across various timeframes and concentrations. Notably, Table 6.21 reveals unstable inhibition efficiency, particularly at lower concentrations. Based on these findings, non-UV radiated *A. phylicoides* extract shows promise as a corrosion inhibitor, especially at higher concentrations, to mitigate acid corrosion.

6.7 Time Stability of UV-Radiated *A.Phylicoides* Extract

The primary objective of this study is to explore the efficacy of UV-assisted *A. phylicoides* extract in mitigating acid corrosion. To achieve this goal, it is imperative to delve deeper into the time stability of UV-radiated *A. phylicoides* extract, extending beyond the initial 6-hour timeframe. This extended investigation will provide invaluable insights into the extract's effectiveness over longer durations, thereby enhancing the robustness of the research and augmenting the overall value of the study. Important experimental data is recorded in Tables 6.25-6.28.

© University of Venda

Table 6.25: Weight loss measurements on mild steel exposed to sulphuric acid (1.5M) in the presence of UV-radiated *A. phylicoides* extract

Concentration of *A. phylicoides* (ppm)	**Weight loss (g)**			
	6 hours	**12 hours**	**18 hours**	**24 hours**
0.00	0.2533	0.5130	0.7058	1.3077
100	0.0990	0.2813	0.6093	0.9667
400	0.0781	0.1655	0.2455	0.4162
700	0.0648	0.1410	0.2005	0.2500
1000	0.0500	0.1108	0.1631	0.1904
1300	0.0160	0.0199	0.1006	0.1404

Table 6.26: Weight loss measurements on mild steel exposed hydrochloric acid (1.5M) in the presence of UV-radiated *A. phylicoides* extract

Concentration of *A. phylicoides* (ppm)	**Weight loss (g)**			
	6 hours	**12 hours**	**18 hours**	**24 hours**
0.00	0.5644	1.2944	1.7130	2.1099
100	0.2189	0.4161	0.7001	0.9133
400	0.1918	0.4443	0.4990	0.9100
700	0.1509	0.3347	0.4001	0.6099
1000	0.1103	0.2809	0.3900	0.5000
1300	0.0512	0.1000	0.2002	0.2138

Table 6.27: Weight loss measurements on zinc exposed to sulphuric acid (1.5M) in the presence of UV-radiated *A. phylicoides* extract

Concentration of *A. phylicoides* (ppm)	**Weight loss (g)**			
	6 hours	**12 hours**	**18 hours**	**24 hours**
0.00	0.2521	0.7100	0.9999	1.0800
100	0.0923	0.2089	0.2119	0.3009
400	0.0615	0.1306	0.2076	0.2464
700	0.0504	0.1000	0.1799	0.2089
1000	0.0219	0.0500	0.0861	0.1098
1300	0.0103	0.0306	0.0421	0.0708

© University of Venda

Table 6.28: Weight loss measurements on zinc exposed in hydrochloric acid (1.5M) in the presence of UV-radiated *A. phylicoides* extract

Concentration of *A. phylicoides* (ppm)	**Weight loss (g)**			
	6 hours	**12 hours**	**18 hours**	**24 hours**
0.00	0.2953	0.3144	0.5550	0.9733
100	0.1296	0.2476	0.2900	0.4982
400	0.0941	0.2133	0.3009	0.3891
700	0.0812	0.1700	0.2766	0.3609
1000	0.0503	0.1008	0.1608	0.2000
1300	0.0218	0.0677	0.1502	0.1080

Analysing the weight loss of metal over time due to corrosion can provide valuable insights into the stability and effectiveness of corrosion inhibitors. In Table 6.25, it was observed that the weight loss of the metal at 12 hours without any inhibitor (0 ppm) was 0.5130 g. However, when UV-radiated *A. phylicoides* was introduced at a concentration of 100 ppm, the weight loss decreased to 0.2813g. This reduction in weight loss suggests that the metal has been protected to some extent by the inhibitor. Similarly, Table 6.26 demonstrates that as the immersion time increases, the weight loss also increases. For example, at 400 ppm, the weight loss is 0.1918g, but it rises to 0.9100g when the immersion time increases to 24 hours. This trend indicates that prolonged exposure leads to greater corrosion and thus higher weight loss. Table 6.27 reveals the minimum weight loss of 0.0708g at 1300 ppm after 24 hours of immersion. This suggests that at higher concentrations of the corrosion inhibitor, the metal experiences less corrosion and therefore less weight loss. In Table 6.28, it was observed that while weight loss generally increases over time, it decreases as the concentration of the corrosion inhibitor increases. This indicates that higher concentrations of the inhibitor are more effective at reducing corrosion and thus minimizing weight loss. Monitoring weight loss due to corrosion over time provides important data on the performance of corrosion inhibitors. Reduced weight loss with the introduction of inhibitors suggests their effectiveness in protecting the metal from corrosion. Additionally, the relationship between weight loss, immersion time, and inhibitor concentration helps to understand the stability and efficacy of corrosion inhibitors under various conditions.

© University of Venda

6.8 Surface Coverage for UV-Radiated *A. Phylicoides* Extract

Tables 6.29-6.32 show the surface coverage of metal by UV-radiated *A. phylicoides* extract in an acidic medium.

Table 6.29: surface coverage measurements on mild steel exposed to sulphuric acid (1.5M) in the presence of UV-radiated *A. phylicoides* extract

Concentration of *A. phylicoides* (ppm)	**Surface Coverage**			
	6 hours	**12 hours**	**18 hours**	**24 hours**
0.00	0.2533	0.5130	0.7058	1.3077
100	0.6092	0.4517	0.1367	0.2608
400	0.6917	0.6774	0.6522	0.6817
700	0.7442	0.7251	0.7159	0.8088
1000	0.8026	0.7840	0.7689	0.8544
1300	0.9368	0.9612	0.8575	0.8926

Table 6.30: surface coverage measurements on mild steel exposed hydrochloric acid (1.5M) in the presence of UV-radiated *A. phylicoides* extract

Concentration of *A. phylicoides* (ppm)	**Surface Coverage**			
	6 hours	**12 hours**	**18 hours**	**24 hours**
0.00	0.5644	1.2944	1.7130	2.1099
100	0.6122	0.6785	0. 5913	0.5671
400	0.6602	0.6568	0.7087	0.5687
700	0.7326	0.7414	0.7664	0.7109
1000	0.8046	0.7830	0.7723	0.7630
1300	0.9093	0.9227	0.8831	0. 8987

Table 6.31: Surface coverage measurements on zinc exposed to sulphuric acid (1.5M) in the presence of UV-radiated *A. phylicoides* extract

Concentration of *A. phylicoides* (ppm)	**Surface Coverage**			
	6 hours	**12 hours**	**18 hours**	**24 hours**
0.00	0.2521	0.7100	0.9999	1.0800
100	0.6339	0.7058	0.7881	0.7214
400	0.7560	0.8161	0.7924	0.7719
700	0.8001	0.8592	0.8201	0.8066
1000	0.9131	0.9296	0.9139	0.8983
1300	0.9591	0.9569	0.9579	0.9344

© University of Venda

Table 6.32: surface coverage measurements on zinc exposed in hydrochloric acid (1.5M) in the presence of UV-radiated *A. phylicoides* extract

Concentration of *A. phylicoides* (ppm)	**Surface Coverage**			
	6 hours	**12 hours**	**18 hours**	**24 hours**
0.00	0.2953	0.3144	0.5550	0.9733
100	0.5611	0.2125	0.4775	0.4881
400	0.6813	0.3216	0.4578	0.6002
700	0.7250	0.4593	0.5016	0.6292
1000	0.8297	0.6794	0.7103	0.7945
1300	0.9262	0.7845	0.7294	0.8890

Tables 6.29-6.32 provide surface coverage measurements from corrosion studies conducted on different metal substrates (mild steel and zinc) exposed to acidic solutions (sulphuric acid and hydrochloric acid) in the presence of UV-radiated *A. phylicoides* extract at various concentrations and exposure times. Table 6.29, which focuses on mild steel exposed to sulphuric acid, shows that surface coverage generally increases with both higher concentrations of *A. phylicoides* extract and longer exposure times. For instance, at 0 ppm concentration, the surface coverage increases from 0.2533 at 6 hours to 1.3077 at 24 hours, indicating a gradual protective effect over time. Table 6.30, which also examines mild steel but in hydrochloric acid, shows similar trends. Surface coverage values increase as the concentration of *A. phylicoides* extract increases and as the exposure time extends. However, compared to sulphuric acid, the surface coverage values in hydrochloric acid are generally lower, suggesting a potentially different corrosion inhibition mechanism. Table 6.31, which looks at zinc in sulphuric acid, shows a pattern like that seen in mild steel. Higher concentrations of *A. phylicoides* extract correspond to higher surface coverage values, indicating effective corrosion inhibition. Additionally, the surface coverage values generally increase with longer exposure times, although the rate of increase varies. Lastly, Table 6.32 examines zinc in hydrochloric acid. Higher concentrations of *A. phylicoides* extract result in higher surface coverage values, suggesting effective corrosion inhibition. However, some fluctuations in surface coverage are observed, indicating potential variations in the inhibitor's performance under different conditions. Tables 6.29-6.32 collectively demonstrate the influence of *A. phylicoides* extract concentration and exposure time on the surface coverage of mild steel and zinc in acidic environments. Higher concentrations of the inhibitor and

© University of Venda

longer exposure times generally lead to greater surface coverage, indicative of improved corrosion protection.

6.9 Inhibition Efficiency for UV Radiated *A. Phylicoides* Extract

Tables 6.33-6.36 show the inhibition efficiency of UV-radiated *A. phylicoides* extracts exposed to acidic media at various times.

Table 6.33: Inhibition Efficiency measurements on mild steel exposed to sulphuric acid (1.5M) in the presence of UV-radiated *A. phylicoides* extract

Concentration of *A. phylicoides* (ppm)	**Inhibition Efficiency**			
	6 hours	**12 hours**	**18 hours**	**24 hours**
0.00				
100	60.92	0.45.17	0.13.67	26.08
400	69.17	0.67.74	0.65.22	68.17
700	74.42	0.72.51	0.71.59	80.88
1000	80.26	0.78.40	0.76.89	85.44
1300	93.68	0.96.12	0.85.75	89.26

Table 6.34: Inhibition Efficiency measurements on mild steel exposed hydrochloric acid (1.5M) in the presence of UV-radiated *A. phylicoides* extract

Concentration of *A. phylicoides* (ppm)	**Inhibition Efficiency**			
	6 hours	**12 hours**	**18 hours**	**24 hours**
0.00				
100	61.22	67.85	59.13	56.71
400	66.02	65.68	70.87	56.87
700	73.26	74.14	76.64	71.09
1000	80.46	78.30	77.23	76.30
1300	90.93	92.27	88.31	89.87

© University of Venda

Table 6.35: surface coverage measurements on zinc exposed to sulphuric acid (1.5M) in the presence of UV-radiated *A. phylicoides* extract

Concentration of *A. phylicoides* (ppm)	**Surface Coverage**			
	6 hours	**12 hours**	**18 hours**	**24 hours**
0.00				
100	63.39	70.58	78.81	72.14
400	75.60	81.61	79.24	77.19
700	80.01	85.92	82.01	80.66
1000	91.31	92.96	91.39	89.83
1300	95.91	95.69	95.79	93.44

Table 6.36: surface coverage measurements on zinc exposed in hydrochloric acid (1.5M) in the presence of UV radiated *A. phylicoides* extract

Concentration of *A. phylicoides* (ppm)	**Surface Coverage**			
	6 hours	**12 hours**	**18 hours**	**24 hours**
0.00				
100	56.11	21.25	47.75	48.81
400	68.13	32.16	45.78	60.02
700	72.50	45.93	50.16	62.92
1000	82.97	67.94	71.03	79.45
1300	92.62	78.45	72.94	88.90

Tables 6.33-6.36 present the inhibition efficiency measurements for mild steel and zinc exposed to sulphuric acid and hydrochloric acid solutions in the presence of UV-radiated *A. phylicoides* extract at various concentrations and exposure times. Table 6.33, which focuses on mild steel in sulphuric acid, shows that the inhibition efficiency generally increases with both higher concentrations of *A. phylicoides* extract and longer exposure times. For instance, at 0 ppm concentration, inhibition efficiency is not applicable (NA) since there is no inhibitor present. However, as the concentration increases, inhibition efficiency values rise, reaching a maximum of 93.68% at 1300 ppm concentration after 6 hours. Table 6.34, which examines mild steel in hydrochloric acid shows similar trends. Inhibition efficiency tends to increase with higher concentrations of *A. phylicoides* extract and longer exposure times. The highest inhibition efficiency values are observed at 1300 ppm concentration, reaching 90.93% after 6 hours. Table 6.35 focuses on zinc in sulphuric acid. Inhibition efficiency generally increases

© University of Venda

with higher concentrations of *A. phylicoides* extract and longer exposure times. The highest inhibition efficiency values are observed at 1300 ppm concentration, reaching 95.91% after 6 hours. Finally, Table 6.36 examines zinc in hydrochloric acid. Inhibition efficiency also tends to increase with higher concentrations of *A. phylicoides* extract and longer exposure times. The highest inhibition efficiency values are observed at 1300 ppm concentration, reaching 92.62% after 6 hours. Tables 6.33 – 6.36 demonstrate the effectiveness of UV radiated *A. phylicoides* extract as a corrosion inhibitor for both mild steel and zinc in sulphuric acid and hydrochloric acid environments. Higher concentrations of the inhibitor and longer exposure times generally lead to greater inhibition efficiency, indicating improved corrosion protection.

Based on the data presented in Tables 6.33 – 6.36, one can draw conclusions regarding the reliability and stability of UV radiated *A. phylicoides* extract as a corrosion inhibitor for protecting metal surfaces over time:

Reliability: The inhibition efficiency and surface coverage measurements consistently show that higher concentrations of UV radiated *A. phylicoides* extract generally result in better corrosion protection for both mild steel and zinc exposed to sulphuric acid and hydrochloric acid solutions. This suggests that the inhibitor reliably provides protection against corrosion under various conditions.

Stability: The inhibition efficiency and surface coverage measurements also indicate that the effectiveness of UV-radiated *A. phylicoides* extract as a corrosion inhibitor remains stable over time. Despite fluctuations in values at certain concentrations and exposure times, the overall trend shows that inhibition efficiency tends to increase or remain relatively constant as exposure time extends, particularly at higher concentrations of the inhibitor. This suggests that the corrosion protection offered by the inhibitor is stable and consistent over extended periods. Therefore, based on the data analysis, one can conclude that UV-radiated *A. phylicoides* extract demonstrates both reliability and stability as a corrosion inhibitor for protecting metal surfaces against sulphuric acid and hydrochloric acid corrosion as time proceeds. Higher concentrations of the inhibitor lead to better corrosion protection, and this protection remains stable over prolonged exposure times, making UV-radiated *A. phylicoides* a promising option for corrosion control in various industrial applications.

© University of Venda

6.10 Corrosion Rate of Metals Exposed in Acidic Medium

Understanding the rate of corrosion, which is how fast metal deteriorates in a particular environment, is crucial in corrosion science and engineering for a multitude of reasons. Firstly, it aids in selecting the most suitable materials for environments where corrosion resistance is critical. Additionally, knowing the corrosion rate allows engineers to estimate the expected service life of materials, which is essential for designing durable structures and systems. Moreover, it helps in predicting maintenance, repair, and replacement costs over the lifetime of a structure or equipment affected by corrosion [93]. Furthermore, industries dealing with critical infrastructure, such as oil and gas, transportation, and aerospace, rely on knowledge of the corrosion rate to assess the risk of corrosion-induced failures and to manage and mitigate these risks effectively [397]. Corrosion monitoring over time provides valuable data for evaluating the effectiveness of corrosion prevention measures and identifying areas where adjustments may be needed [398]. Studying corrosion rates helps researchers and engineers to optimize corrosion protection strategies, such as the use of inhibitors, coatings, or cathodic protection, to reduce the corrosion rate. The corrosion rate also affects the release of metals into the environment, which can have ecological implications, making it crucial for environmental impact assessments [74]. Additionally, understanding the corrosion rate is essential for ensuring the structural integrity of critical components and avoiding safety hazards posed by corrosion-induced failures [135]. Furthermore, researchers use corrosion rate data to develop new materials with improved corrosion resistance, contributing to the advancement of materials science and engineering. Finally, various industries must comply with regulations related to environmental protection, safety, and quality, making it essential to understand and manage corrosion rates to meet these regulatory requirements. Studying the corrosion rate plays a pivotal role in informed materials selection, service life prediction, cost estimation, risk assessment, corrosion monitoring, protection optimization, environmental assessment, safety considerations, and research and development in the field of corrosion science and engineering [135].

6.10.1 Corrosion Rate of Metal Exposed to Acidic Medium in the Presence of Non-UV Radiation *A. Phylicoides* Extract

This section reports the effect of UV-radiated *A. phylicoides* leaf extracts against non-UV-radiated extracts. Tables 6.37-6.40 show the corrosion rate of metals exposed to an acidic

© University of Venda

medium in the absence of radiated *A. phylicoides* leaf extracts. Studying the corrosion rate of metal exposed to an acidic medium in the presence of non-UV radiation *A. phylicoides* extract provides valuable insights into the effectiveness of the extract as a corrosion inhibitor, helps in optimizing corrosion inhibition strategies, informs materials selection and application decisions, assesses environmental impact, and aids in cost estimation and risk assessment [399]. Tables 6.37-6.40 provide corrosion rate measurements for mild steel and zinc exposed to sulphuric acid and hydrochloric acid solutions in the presence of *A. phylicoides* extract at various concentrations and temperatures.

Table 6.37: Corrosion rate on mild steel exposed to sulphuric acid (1.5M) in the presence of *A. phylicoides* extract

Concentration of *A. phylicoides* extract (ppm)	**Corrosion rate (C_r) (g cm^{-2} h^{-1})**			
	303K	**313K**	**323K**	**333K**
0.00	0.007036	0.009314	0.013741	0.019325
100	0.001108	0.001914	0.004067	0.005308
400	0.001086	0.001725	0.003833	0.005111
700	0.000850	0.001333	0.003766	0.004894
1000	0.000583	0.000811	0.003519	0.004878
1300	0.000419	0.000581	0.003383	0.004686

Table 6.38: Corrosion rate on mild steel exposed to hydrochloric acid (1.5M) in the presence of *A. phylicoides* extract

Concentration of *A. phylicoides* extract (ppm)	**Corrosion rate (C_r) (g cm^{-2} h^{-1})**			
	303K	**313K**	**323K**	**333K**
0.00	0.015678	0.032850	0.036613	0.041828
100	0.003836	0.009138	0.010861	0.009972
400	0.003414	0.009114	0.009542	0.009147
700	0.001639	0.006306	0.008406	0.009122
1000	0.001622	0.006233	0.007417	0.008833
1300	0.001192	0.003425	0.006222	0.008583

© University of Venda

Table 6.39: Corrosion rate measurements on zinc exposed in sulphuric acid (1.5M) in the presence of *A. phylicoides* extract

Concentration of *A. phylicoides* extract (ppm)	**Corrosion rate (C_r) (g cm^{-2} h^{-1})**			
	303K	**313K**	**323K**	**333K**
0.00	0.007356	0.007356	0.013272	0.019619
100	0.002219	0.002725	0.004122	0.008467
400	0.001806	0.001972	0.003792	0.008308
700	0.001256	0.001911	0.003511	0.007925
1000	0.001114	0.001683	0.003081	0.007883
1300	0.000922	0.001650	0.003025	0.005442

Table 6.40: Corrosion rate measurements on zinc exposed in hydrochloric acid (1.5M) in the presence of *A. phylicoides* extract

Concentration of *A. phylicoides* extract (ppm)	**Corrosion rate (C_r) (g cm^{-2} h^{-1})**			
	303K	**313K**	**323K**	**333K**
0.00	0.008203	0.012592	0.014850	0.034492
100	0.003058	0.004392	0.006639	0.016547
400	0.003000	0.004158	0.005169	0.012336
700	0.002975	0.003722	0.004714	0.011644
1000	0.001756	0.002969	0.003872	0.009956
1300	0.001419	0.002925	0.003461	0.009189

In Table 6.37, for mild steel exposed to sulphuric acid, we observe that the corrosion rate generally decreases with increasing concentration of *A. phylicoides* extract and decreasing temperature. For instance, at 1300 ppm concentration, the corrosion rate decreases from 0.000419 g cm^{-2} h^{-1} at 303K to 0.004686 g cm^{-2} h^{-1} at 333K, indicating improved corrosion inhibition at higher concentrations and lower temperatures. Similarly, in Table 6.38, for mild steel exposed to hydrochloric acid, the corrosion rate decreases with increasing concentration of *A. phylicoides* extract and decreasing temperature. For example, at 1300 ppm concentration, the corrosion rate decreases from 0.001192 g cm^{-2} h^{-1} at 303K to 0.008583 g cm^{-2} h^{-1} at 333K, suggesting enhanced corrosion protection at higher concentrations and lower temperatures. In Tables 6.39 and 6.40, for zinc exposed to sulphuric acid and hydrochloric acid respectively, similar trends are observed. The corrosion rate generally decreases with increasing concentration of *A. phylicoides* extract and decreasing temperature. The results indicate that the presence of *A. phylicoides* extract leads to reduced corrosion

© University of Venda

rates for both mild steel and zinc in sulphuric acid and hydrochloric acid solutions. Higher concentrations of the extract and lower temperatures contribute to more effective corrosion inhibition, highlighting the potential of *A. phylicoides* extract as a corrosion inhibitor in acidic environments.

6.10.2 Corrosion Rate of Metal Exposed to Acidic Medium in the Presence of UV Radiation *A. phylicoides* Extract

Comparing the corrosion rate of non-UV-radiated *A. phylicoides* leaf extract with UV-radiated *A. phylicoides* leaf extract serves various purposes in corrosion research. Firstly, it aids in evaluating the effectiveness of each extract in inhibiting corrosion, allowing researchers to determine which type provides better protection against metal degradation. This comparison also helps in optimizing corrosion inhibition strategies by identifying whether UV radiation enhances or diminishes the inhibitory properties of the *A. phylicoides* extract. Additionally, it allows researchers to understand the underlying factors contributing to corrosion inhibition, such as alterations in chemical composition or concentration of active compounds due to UV radiation. Understanding these factors can inform decisions regarding the extraction process and application of *A. phylicoides* extracts in corrosion protection. Furthermore, comparing the corrosion rates helps in assessing the suitability of each type of extract for specific environments or materials, guiding their practical application. This comparison provides valuable insights into the effectiveness, applicability, and potential for optimization of non-UV-radiated and UV-radiated *A. phylicoides* extracts in corrosion inhibition strategies. Tables 6.41-6.44 .

Table 6.41: Corrosion rate on mild steel exposed to sulphuric acid (1.5M) in the presence of *A. phylicoides* extract

Concentration of *A. phylicoides* (ppm)	**Corrosion rate (C_R) (g cm^{-2} h^{-1})**			
	303K	**313K**	**323K**	**333K**
0.000	0.007036	0.009314	0.013742	0.019325
100	0.002750	0.003914	0.006303	0.009750
400	0.002169	0.003336	0.005892	0.008839
700	0.001800	0.003297	0.005608	0.008283
1000	0.001389	0.002781	0.004203	0.006086

© University of Venda

1300	0.000444	0.000558	0.002828	0.005058

Table 6.42: Corrosion rate on mild steel exposed to hydrochloric acid (1.5M) in the presence of *A. phylicoides* extract

Concentration of *A. phylicoides* (ppm)	**Corrosion rate (C_R) (g cm^{-2} h^{-1})**			
	303K	**313K**	**323K**	**333K**
0.000	0.008203	0.012592	0.014850	0.034492
100	0.003600	0.005606	0.007197	0.016889
400	0.002614	0.004281	0.005300	0.014133
700	0.002256	0.003606	0.004447	0.011444
1000	0.001397	0.002550	0.003931	0.010283
1300	0.000606	0.001972	0.002825	0.007892

Table 6.43: Corrosion rate measurements on zinc exposed in sulphuric acid (1.5M) in the presence of *A. phylicoides* extract

Concentration of *A. phylicoides* (ppm)	**Corrosion rate (C_R) (g cm^{-2} h^{-1})**			
	303K	**313K**	**323K**	**333K**
0.000	0.015678	0.032850	0.036614	0.041828
100	0.006081	0.013836	0.016169	0.019219
400	0.005328	0.011694	0.013942	0.016969
700	0.004192	0.009756	0.011703	0.014222
1000	0.003064	0.007836	0.009964	0.012550
1300	0.001422	0.004208	0.006081	0.008697

© University of Venda

Table 6.44: Corrosion rate measurements on zinc exposed in hydrochloric acid (1.5M) in the presence of *A. phylicoides* extract

Concentration of *A. phylicoides* (ppm)	**Corrosion rate (C_R)(g cm^{-2} h^{-1})**			
	303K	**313K**	**323K**	**333K**
0.000	0.007003	0.007356	0.013272	0.019619
100	0.002564	0.002775	0.005089	0.008372
400	0.001708	0.001997	0.004764	0.007811
700	0.001400	0.001719	0.003942	0.006467
1000	0.000608	0.000881	0.002086	0.003606
1300	0.000286	0.000569	0.001108	0.002622

Tables 6.41- 6.44 detail the corrosion rates of both mild steel and zinc when exposed to acidic mediums in the presence of UV-radiated *A. phylicoides* leaf extract. In Table 6.41, which examines mild steel in sulphuric acid, it can be observed that higher concentrations of *A. phylicoides* extract generally lead to decreased corrosion rates across all temperatures. For instance, at 1300 ppm concentration and 333K temperature, the corrosion rate drops significantly to 0.005058 g.cm^{-2} h^{-1} compared to 0.019325 g.cm^{-2} h^{-1} at 0 ppm concentration. Similarly, in Table 6.42, assessing mild steel in hydrochloric acid, higher concentrations of *A. phylicoides* extract correlate with lower corrosion rates, consistent with the trend observed in Table 6.41. At 1300 ppm concentration and 333K temperature, the corrosion rate reduces to 0.007892 g cm^{-2} h^{-1} compared to 0.034492 g cm^{-2} h^{-1} at 0 ppm concentration. Table 6.43 examines zinc in sulphuric acid, showcasing a similar pattern where increased concentrations of *A. phylicoides* extract result in decreased corrosion rates across different temperatures. Notably, at 1300 ppm concentration and 333K temperature, the corrosion rate drops to 0.008697 g cm^{-2} h^{-1} compared to 0.041828 g cm^{-2} h^{-1} at 0 ppm concentration. In Table 6.44, analysing zinc in hydrochloric acid, the trend continues with higher concentrations of *A. phylicoides* extract leading to reduced corrosion rates. For instance, at 1300 ppm concentration and 333K temperature, the corrosion rate decreases to 0.002622 g cm^{-2} h^{-1} compared to 0.019619 g cm^{-2} h^{-1} at 0 ppm concentration. These results demonstrate the potential of UV-radiated *A. phylicoides* extract in mitigating corrosion of

© University of Venda

both mild steel and zinc in acidic environments, with higher concentrations generally providing more effective corrosion protection.

6.11 Surface Coverage of Metal Exposed to Acidic Medium in the Presence and Absence of UV Radiated *A. phylicoides* Extract

Surface coverage refers to the degree to which a corrosion inhibitor effectively covers and protects a metal surface from corrosion [217]. It is essentially a measure of how much of the metal surface is shielded by the inhibitor. Corrosion inhibitors are chemicals that, when introduced into a corrosive environment, work to mitigate, or entirely prevent the corrosion of metals [129]. Their primary mechanism involves adsorption onto the metal surface. Corrosion inhibitors adsorb onto the metal surface, forming a protective layer [3]. This layer acts as a barrier, impeding the corrosive attack on the metal. The protective layer can interfere with the electrochemical reactions that drive corrosion. The effectiveness of a corrosion inhibitor is often evaluated by its ability to achieve significant or complete surface coverage. In other words, an effective inhibitor should form a robust and uniform protective layer over the metal surface, minimizing exposure to corrosive agents. Achieving high surface coverage is crucial for ensuring the longevity and integrity of the metal in a corrosive environment. Inhibitors that provide effective coverage help in reducing corrosion rates and extending the service life of materials. The ability of a corrosion inhibitor to achieve adequate surface coverage can be influenced by factors such as concentration, temperature, and the nature of the corrosive environment [400]. Optimizing these conditions is essential for maximizing the inhibitive performance.

Surface coverage is a critical parameter when evaluating the effectiveness of corrosion inhibitors. The goal is to have inhibitors that can form a protective layer with high coverage, providing effective corrosion protection to the metal surfaces in diverse industrial applications.

The study of surface coverage in metal corrosion is crucial for corrosion science and engineering. It provides quantitative measures of corrosion progression and rates, elucidates corrosion mechanisms, predicts corrosion product formation, and aids in designing corrosion-resistant materials. Surface coverage analysis also assists in evaluating the effectiveness of corrosion inhibitors, assessing environmental impacts, and ensuring regulatory compliance

© University of Venda

[401]. This information is essential for effective corrosion management practices in various industries.

6.11.1 Surface Coverage of Metals Exposed to Acidic Medium Using Non-UV Radiated *A. phylicoides* Extract

The surface coverage of non-UV radiated *A. phylicoides* extract provides insights into its ability to inhibit corrosion. Higher surface coverage values suggest better corrosion inhibition properties, indicating enhanced protection for metal surfaces. Typically, surface coverage values above 90% indicate excellent corrosion inhibition, while values between 70-90% indicate good inhibition. Lower values may signify limited corrosion protection. Understanding these values helps in assessing the effectiveness of *A. phylicoides* extract as a corrosion inhibitor and in optimizing its application in corrosion prevention strategies. Tables 6.45 – 6.48 show the surface coverage of metal exposed to acidic medium in the presence of non-UV radiated *A. phylicoides* leaves extract.

Table 6.45: surface coverage on mild steel exposed to sulphuric acid (1.5M) in the presence of *A. phylicoides*.

Concentration of *A. phylicoides* (ppm)	**Surface Coverage (θ)**			
	303K	**313K**	**323K**	**333K**
0.00	-	-	-	-
100	0.8425	0.7945	0.7041	0.7253
400	0.8456	0.8148	0.7210	0.7355
700	0.8792	0.8568	0.7259	0.7467
1000	0.9171	0.9129	0.7439	0.7476
1300	0.9404	0.9377	0.7538	0.7575

© University of Venda

Table 6.46: Surface coverage on mild steel exposed in hydrochloric acid (1.5M) in the presence of *A. phylicoides*.

Concentration of *A. phylicoides* (ppm)	**Surface Coverage (θ)**			
	303K	**313K**	**323K**	**333K**
0.00	-	-	-	-
100	0.7553	0.7218	0.7034	0.7616
400	0.7822	0.7226	0.7394	0.7813
700	0.8955	0.8081	0.7704	0.7819
1000	0.8965	0.8102	0.7974	0.7889
1300	0.9234	0.8957	0.8300	0.7948

Table 6.47: Surface coverage on zinc exposed in sulphuric acid (1.5M) in the presence of *A. phylicoides*

Concentration of *A. phylicoides* (ppm)	**Surface coverage (θ)**			
	303K	**313K**	**323K**	**333K**
0.00	-	-	-	-
100	0.6831	0.6295	0.6894	0.5685
400	0.7422	0.7319	0.7143	0.5765
700	0.8207	0.7402	0.7355	0.5961
1000	0.8409	0.7711	0.7679	0.5982
1300	0.8683	0.7757	0.7721	0.7226

© University of Venda

Table 6.48: Surface coverage on zinc exposed in hydrochloric acid (1.5M) in the presence of *A. phylicoides*

Concentration of *A. phylicoides* (ppm)	**Surface coverage (θ)**			
	303K	**313K**	**323K**	**333K**
0.00	-	-	-	-
100	0.6272	0.6512	0.5529	0.5203
400	0.6343	0.6698	0.6519	0.6423
700	0.6373	0.7044	0.6826	0.6624
1000	0.7860	0.7642	0.7392	0.7114
1300	0.8270	0.7677	0.7669	0.7336

Tables 6.45 – 6.48 display the surface coverage of mild steel and zinc when exposed to sulphuric acid and hydrochloric acid alongside various concentrations of non-UV radiated *A. phylicoides* extract at different temperatures. For mild steel in sulphuric acid, at 303K, surface coverage ranges from approximately 0.8425 (at 100 ppm) to 0.9404 (at 1300 ppm). As temperature increases to 333K, surface coverage varies from about 0.7253 (at 100 ppm) to 0.7575 (at 1300 ppm). In hydrochloric acid, at 303K, surface coverage ranges from around 0.7553 (at 100 ppm) to 0.9234 (at 1300 ppm), while at 333K, values range from approximately 0.7616 (at 100 ppm) to 0.7948 (at 1300 ppm). For zinc in sulphuric acid, at 303K, surface coverage varies from about 0.6831 (at 100 ppm) to 0.8683 (at 1300 ppm), and at 333K, it ranges from approximately 0.5685 (at 100 ppm) to 0.7226 (at 1300 ppm). In hydrochloric acid, at 303K, surface coverage ranges from around 0.6272 (at 100 ppm) to 0.8270 (at 1300 ppm), and at 333K, values vary from approximately 0.5203 (at 100 ppm) to 0.7336 (at 1300 ppm). Across all scenarios, an increase in *A. phylicoides* extract concentration generally leads to higher surface coverage, indicating better corrosion inhibition. However, the effect of temperature on surface coverage varies, with some cases showing a decrease in surface coverage at higher temperatures [402]. These detailed values provide insights into the effectiveness of non-UV radiated *A. phylicoides* extract as a corrosion inhibitor for different metals and acid environments at varying concentrations and temperatures.

Tables 6.45-6.48, illustrate a rise in surface coverage with an increase in the concentration of *A. phylicoides* plant extract. Table 6.48 particularly highlights that at 303K, the surface

© University of Venda

coverage increased from 0.6272 at 0ppm to 0.8270 at 1300ppm. The correlation between the concentration increase of a corrosion inhibitor and the rise in surface coverage is commonly linked to the adsorption behaviour of inhibitor molecules on the metal surface. This occurrence can be clarified by the mechanism where corrosion inhibitors function by adsorbing onto the metal surface, thereby forming a protective layer [403]. Adsorption is the process by which inhibitor molecules attach themselves to the metal surface [395]. The likelihood of inhibitor molecules adsorbing onto the metal surface is generally concentration-dependent. As the concentration of the inhibitor in the corrosive environment increases, more inhibitor molecules are available for adsorption [143]. With higher inhibitor concentrations, there are more inhibitor molecules in the solution, providing an increased number of adsorption sites on the metal surface. This abundance of inhibitor molecules allows for a more complete coverage of the metal surface. The formation of the protective layer is a dynamic process. At higher concentrations, inhibitor molecules can more effectively compete for and occupy available adsorption sites on the metal surface, leading to a denser and more protective layer. Higher inhibitor concentrations often result in enhanced inhibition efficiency [143]. The increased surface coverage corresponds to a more effective barrier against corrosive agents, reducing the metal's exposure to the environment [404]. It's important to note that there may be an optimal concentration range for a specific inhibitor beyond which further increases might not proportionally improve surface coverage. This is due to factors such as inhibitor solubility, saturation, and the nature of the adsorption process. While higher concentrations may enhance inhibition efficiency, economic considerations also play a role. The cost of the inhibitor and potential side effects at elevated concentrations may influence the practical application of corrosion inhibitors [405].

6.11.2 The Surface Coverage of Metal in the Presence of UV-Radiated *A. phylicoides*

Tables 6.49 – 6.52 provide details of the surface coverage of mild steel and zinc in the presence of UV radiated *A. phylicoides* under different conditions, specifically in sulphuric acid and hydrochloric acid environments. The surface coverage (θ) values represent the fraction of the metal surface covered by a protective film or corrosion product.

© University of Venda

Table 6.49: surface coverage on mild steel exposed to sulphuric acid (1.5M) in the presence of *A. phylicoides*

Concentration of *A. phylicoides* (ppm)	**Surface Coverage (θ)**			
	303K	**313K**	**323K**	**333K**
0.00	-	-	-	-
100	0.6092	0.5798	0.5413	0.4954
400	0.6917	0.6418	0.5713	0.5426
700	0.7442	0.6460	0.5919	0.5714
1000	0.8026	0.7015	0.6942	0.6851
1300	0.9554	0.9401	0.7942	0.7382

Table 6.50: Surface coverage on mild steel exposed to hydrochloric acid (1.5M) in the presence of *A. phylicoides*

Concentration of *A. phylicoides* (ppm)	**Surface Coverage (θ)**			
	303K	**313K**	**323K**	**333K**
0.00	-	-	-	-
100	0.6122	0.5788	0.5584	0.5405
400	0.6602	0.6440	0.6192	0.5943
700	0.7326	0.7030	0.6804	0.6600
1000	0.8045	0.7615	0.7279	0.6999
1300	0.9093	0.8719	0.8339	0.7921

Table 6.51: Surface coverage on zinc exposed in sulphuric acid (1.5M) in the presence of *A. phylicoides*

Concentration of *A. phylicoides* (ppm)	**Surface coverage (θ)**			
	303K	**313K**	**323K**	**333K**
0.00	-	-	-	-
100	0.6339	0.6227	0.6166	0.5733
400	0.7560	0.7285	0.6411	0.6019
700	0.8001	0.7662	0.7030	0.6704
1000	0.9131	0.8803	0.8428	0.8162
1300	0.9591	0.9226	0.9165	0.8663

© University of Venda

Table 6.52: Surface coverage on zinc exposed in hydrochloric acid (1.5M) in the presence of *A. phylicoides*

Concentration of *A. phylicoides* (ppm)	**Surface coverage (θ)**			
	303K	**313K**	**323K**	**333K**
0.00	-	-	-	-
100	0.5611	0.5548	0.5153	0.5103
400	0.6813	0.6600	0.6431	0.5902
700	0.7250	0.7137	0.7005	0.6682
1000	0.8297	0.7975	0.7353	0.7019
1300	0.9262	0.8434	0.8098	0.7712

In Table 6.49 and Table 6.50, which illustrate the surface coverage on mild steel in sulphuric acid and hydrochloric acid respectively, it's evident that as the concentration of *A. phylicoides* increases, there is a generally increasing trend in surface coverage across all temperatures (303K to 333K). This indicates that the presence of *A. phylicoides* tends to enhance the protective film on the mild steel surface, potentially mitigating corrosion. Notably, the effect is more pronounced at higher concentrations of *A. phylicoides* and at higher temperatures. However, at very high concentrations (1300 ppm), there seems to be a plateau effect where further increases in *A. phylicoides* concentration do not lead to significant improvements in surface coverage. Similar trends are observed in Table 6.51 and Table 6.52, which depict the surface coverage of zinc in sulphuric acid and hydrochloric acid respectively. Again, increasing concentrations of *A. phylicoides* generally lead to higher surface coverage, particularly evident at elevated temperatures. However, as with mild steel, there appears to be a saturation point at very high concentrations of *A. phylicoides*, indicating a limit to the protective capacity of the *A. phylicoides*. These results suggest that UV-radiated *A. phylicoides* may serve as a promising corrosion inhibitor for both mild steel and zinc in sulphuric and hydrochloric acid environments. However, optimal concentrations need to be carefully considered to maximize its effectiveness, and further studies may be warranted to elucidate the mechanisms underlying its protective effects.

Tables 6.49-6.52 exhibit a pattern like Tables 6.45-6.48. In Table 6.25, it is observed that as the concentration increases from 0ppm to 1300ppm at 303K, the surface coverage rises from 0.5611 to 0.9262. However, it's worth noting that at 0ppm, there is no *A. phylicoides* present,

© University of Venda

resulting in no surface coverage. This trend changes when the temperature increases from 303K to 333K, as the surface coverage decreases from 0.9262 to 0.7712 at 1300ppm. The relationship between inhibitor concentration and surface coverage is linked to the adsorption process. Higher concentrations offer more inhibitor molecules for adsorption, thereby increasing surface coverage and enhancing corrosion inhibition effectiveness [406]. This concentration-dependent behaviour is crucial in optimizing corrosion inhibition strategies. With the temperature increase from 303K to 333K, surface coverage decreases. The minimum surface coverage is achieved at 100ppm, correlating with a surface coverage of 0.5103 at 333K. Maximum surface coverage is attained at the lower temperature of 303K and a concentration of 1300ppm. It can be anticipated that to achieve surface coverage greater than 0.9262 at 303K, a concentration greater than 1300ppm must be utilized.

6.12 Inhibition Efficiency of Metals Offered by Non-UV Radiated and UV-Radiated *A. phylicoides*

The inhibition efficiency of a corrosion inhibitor is a measure of how effectively it reduces or prevents corrosion on a metal surface [129]. It is typically expressed as a percentage and represents the degree to which the inhibitor mitigates the corrosive process. The higher the inhibition efficiency, the more effective the corrosion inhibitor is at protecting the metal from corrosion. A 100% inhibition efficiency would mean that the corrosion is completely stopped in the presence of the inhibitor.

Inhibition efficiency is typically expressed as a percentage, providing a clear and easily interpretable metric. The percentage represents the reduction in corrosion rate achieved by the inhibitor. A higher inhibition efficiency percentage indicates a more effective corrosion inhibitor [141]. For example, an inhibitor with 80% inhibition efficiency is more effective at reducing corrosion than one with 50% inhibition efficiency under the same conditions. In an ideal scenario, a corrosion inhibitor with 100% inhibition efficiency would completely halt the corrosion process. However, achieving 100% inhibition is often challenging due to various practical factors and the complexity of corrosion mechanisms. Inhibition efficiency is often determined through experimental techniques, including weight loss measurements, electrochemical methods, and corrosion product analysis [407].

Inhibition efficiency is a critical parameter in the assessment of corrosion inhibitors, providing a quantitative measure of their effectiveness in protecting metal surfaces from

© University of Venda

corrosion. Achieving high inhibition efficiency is a key goal in corrosion control and materials protection strategies.

6.12.1 Inhibition Efficiency of Metals in the Presence of Non-UV Radiated *A. phylicoides* Extract

Tables 6.53-6.56 highlight the inhibition efficiency of mild steel and zinc specimens exposed to various concentrations of acid in the absence and presence of non-UV radiated *A. phylicoides* leaf extract.

Table 6.53: Inhibition Efficiency on mild steel exposed in sulphuric acid (1.5M) in the presence of *A. phylicoides* extract

Concentration of *A. phylicoides* (ppm)	**Inhibition Efficiency (%IE)**			
	303K	**313K**	**323K**	**333K**
0.00	-	-	-	-
100	84.25	79.45	70.41	72.53
400	84.56	81.48	72.10	73.55
700	87.92	85.68	72.59	74.67
1000	91.71	91.29	74.39	74.76
1300	94.04	93.77	75.38	75.75

Table 6.54: Inhibition Efficiency of mild steel exposed in hydrochloric acid (1.5M) in the presence of *A. phylicoides* extract

Concentration of *A. phylicoides* (ppm)	**Inhibition Efficiency (IE)**			
	303K	**313K**	**323K**	**333K**
0.00	-	-	-	-
100	75.53	72.18	70.34	76.16
400	78.22	72.26	73.94	78.13
700	89.55	80.81	77.04	78.19
1000	89.65	81.02	79.74	78.89
1300	92.34	89.57	83.00	79.48

© University of Venda

Table 6.55: Inhibition Efficiency of zinc exposed in sulphuric acid (1.5M) in the presence of *A. phylicoides* extract

Concentration of *A. phylicoides* (ppm)	**Inhibition Efficiency (IE)**			
	303K	**313K**	**323K**	**333K**
0.00	-	-	-	-
100	68.31	62.95	68.94	56.85
400	74.22	73.19	71.43	57.65
700	82.07	74.02	73.55	59.61
1000	84.09	77.11	76.79	59.82
1300	86.83	77.57	77.21	72.26

Table 6.56: Inhibition Efficiency on zinc exposed in hydrochloric acid (1.5M) in the presence of *A. phylicoides* extract

Concentration of *A. phylicoides* (ppm)	**Inhibition Efficiency (IE)**			
	303K	**313K**	**323K**	**333K**
0.00	-	-	-	-
100	62.72	65.12	55.29	52.03
400	63.43	66.98	65.19	64.23
700	63.73	70.44	68.26	66.24
1000	78.60	76.42	73.92	71.14
1300	82.70	76.77	76.69	73.36

In Table 6.53, which examines mild steel in sulphuric acid, there is a noticeable trend of increasing inhibition efficiency with higher concentrations of *A. phylicoides* extract. For instance, at 303K, inhibition efficiency rises from 84.25% at 100 ppm to 94.04% at 1300 ppm. Similarly, at 333K, the inhibition efficiency increases from 72.53% to 75.75% over the same concentration range. This suggests that *A. phylicoides* extract is increasingly effective at higher concentrations and temperatures in inhibiting the corrosion of mild steel in sulphuric acid. Table 6.54, which explores mild steel in hydrochloric acid, exhibits a similar trend, although it is less pronounced. Inhibition efficiency generally rises with increased *A. phylicoides* extract concentration and temperature. For instance, at 313K, inhibition efficiency climbs from 72.18% at 100 ppm to 89.57% at 1300 ppm. This indicates that *A. phylicoides* extract can inhibit the corrosion of mild steel in hydrochloric acid, with higher concentrations and temperatures enhancing its effectiveness. Tables 6.54 and 6.55 analyze zinc's inhibition efficiency in sulphuric acid and hydrochloric acid, respectively. In both

© University of Venda

cases, there's a trend of increasing inhibition efficiency with higher concentrations of *A. phylicoides* extract and temperatures. For instance, in Table 6.54 at 333K, inhibition efficiency rises from 56.85% at 100 ppm to 72.26% at 1300 ppm. Similarly, in Table 6.55 at 313K, inhibition efficiency increases from 52.03% at 100 ppm to 73.36% at 1300 ppm.

Tables 6.53-6.56 collectively demonstrate that *A. phylicoides* extract exhibits inhibition efficiency against corrosion for both mild steel and zinc in sulphuric acid and hydrochloric acid environments. The effectiveness of the inhibitor generally increases with higher concentrations of *A. phylicoides* extract and temperatures, indicating its potential application as a corrosion inhibitor. Tables 6.53-6.56 illustrate a direct relationship between the concentration of *A. phylicoides* extracts and inhibition efficiency. Specifically, Table 6.56 demonstrates that at 100ppm, there's a 62.72% inhibition efficiency at 303K, while concentrations of 400-700ppm correspond to inhibition efficiencies of 63.43% and 63.73% respectively. This pattern indicates that as concentration increases, inhibition efficiency also increases. Notably, at 1000ppm concentration, inhibition efficiency rises to 78.60%. Furthermore, the highest inhibition efficiency of 82.70% is achieved at a concentration of 1300ppm. This suggests that increasing the concentration beyond 1300ppm may bring inhibition efficiency closer to 100%.

Another important factor as indicated in Tables 6.53-6.56 is temperature since it seems to play a crucial role. When the temperature increases, the inhibition efficiency decreases. When the temperature increases, the inhibition efficiency often decreases due to several reasons: Higher temperatures provide molecules with more thermal energy, leading to increased kinetic motion. This can disrupt the interactions between the inhibitor molecules and the substrate, reducing the effectiveness of inhibition. Inhibitors typically work by binding to specific sites on enzymes or proteins. However, at higher temperatures, the bonds between the inhibitor and its target may weaken or break due to increased thermal motion, reducing the binding affinity and therefore the inhibition efficiency. *A. phylicoides* leave extract can undergo conformational changes at elevated temperatures, altering the shape and structure of the active site. This can affect the ability of inhibitors to bind effectively, thereby reducing inhibition efficiency. Higher temperatures can also enhance the reactivity of both the substrate and the inhibitor, leading to an increased rate of reaction. This can mitigate the inhibitory effects of the inhibitor, resulting in decreased inhibition efficiency. The relationship between temperature and inhibition efficiency is often complex and depends on the specific

© University of Venda

system being studied. However, in this study, higher temperatures tend to decrease inhibition efficiency.

6.12.2 Inhibition Efficiency of Metal Exposed in Acidic Media Using UV Radiated *A. phylicoides* Extracts

The study calculated the inhibition efficiency of *A. phylicoides* leaf extract when exposed to UV radiation and compared it with the inhibition efficiency achieved without UV exposure. Tables 7.57-7.60 display the inhibition efficiency of metals (zinc and mild steel) using *A. phylicoides* extract exposed to UV radiation at different temperatures.

Table 6.57: Inhibition Efficiency on mild steel exposed in sulphuric acid (1.5M) in the presence of *A. phylicoides*

Concentration of *A. phylicoides* (ppm)	**Inhibition efficiency (%)**			
	303K	**313K**	**323K**	**333K**
0.00	-	-	-	-
100	60.92	57.98	54.13	49.54
400	69.17	64.18	57.13	54.26
700	74.42	64.60	59.19	57.14
1000	80.26	70.15	69.42	68.51
1300	95.54	94.01	79.42	73.82

Table 6.58: Inhibition Efficiency on mild steel exposed in hydrochloric acid (1.5M) in the presence of *A. phylicoides*

Concentration of *A. phylicoides* (ppm)	**Inhibition efficiency (%)**			
	303K	**313K**	**323K**	**333K**
0.00	-	-	-	-
100	61.22	57.88	55.84	54.05
400	66.02	64.40	61.92	59.43
700	73.26	70.30	68.04	66.00
1000	80.45	76.15	72.79	69.99
1300	90.93	87.19	83.39	79.21

© University of Venda

Table 6.59: Inhibition Efficiency of zinc exposed in sulphuric acid (1.5M) in the presence of *A. phylicoides*

Concentration of *A. phylicoides* (ppm)	**Inhibition efficiency (%)**			
	303K	**313K**	**323K**	**333K**
0.00	-	-	-	-
100	63.39	62.27	61.66	57.33
400	75.60	72.85	64.11	60.19
700	80.01	76.62	70.30	67.04
1000	91.31	88.03	84.28	81.62
1300	95.91	92.26	91.65	86.63

Table 6.60: Inhibition Efficiency of zinc exposed in hydrochloric acid (1.5M) in the presence of *A. phylicoides*

Concentration of *A. phylicoides* (ppm)	**Inhibition efficiency (%)**			
	303K	**313K**	**323K**	**333K**
0.00	-	-	-	-
100	56.11	55.48	51.53	51.03
400	68.13	66.00	64.31	59.02
700	72.50	71.37	70.05	66.82
1000	82.97	79.75	73.53	70.19
1300	92.62	84.34	80.98	77.12

Tables 7.57-7.60 indicate that the inhibition efficiency of a metal is influenced by both the concentration of the corrosion inhibitor and the temperature. It is evident that as the temperature increases, the inhibition efficiency decreases. This trend is consistent with the findings in Tables 6.53-6.56. Conversely, as the temperature decreases, the inhibition efficiency increases. Concentration is a significant factor in this experiment, as higher concentrations result in higher inhibition efficiency. This behavior could be attributed to the greater availability of particles of *A. phylicoides* leaf extract at higher concentrations compared to lower concentrations, such as 100 ppm. The maximum inhibition efficiency at 1300 ppm of *A. phylicoides* was 92.62%. In contrast, at a concentration of 100 ppm, the inhibition efficiency was lower, at 56.11% at 303K. In Table 6.57, which examines mild steel in sulfuric acid, the inhibition efficiency generally increases with the concentration of *A. phylicoides* extract, regardless of UV exposure. Notably, at 1300 ppm and 303K, the

© University of Venda

inhibition efficiency significantly rises to 95.54% with UV exposure compared to 60.92% without UV exposure. This suggests that UV radiation enhances the effectiveness of *A. phylicoides* extract as a corrosion inhibitor for mild steel in sulphuric acid.

Table 6.58, investigating mild steel in hydrochloric acid, shows a similar trend. Inhibition efficiency rises with increasing *A. phylicoides* extract concentration, with UV exposure amplifying its effect. For example, at 1000 ppm and 303K, inhibition efficiency increases from 61.22% without UV exposure to 80.45% with UV exposure. This further emphasizes the positive impact of UV radiation on the corrosion inhibition properties of *A. phylicoides* extract. As shown in Table 6.59, zinc in sulphuric acid demonstrates a notable increase in inhibition efficiency with UV exposure across various concentrations and temperatures. At 1300 ppm and 303K, inhibition efficiency increases from 63.39% without UV exposure to 95.91% with UV exposure. This significant enhancement underscores the effectiveness of UV radiation in enhancing the corrosion inhibition capabilities of *A. phylicoides* extract for zinc in sulphuric acid. In Table 6.60, for zinc in hydrochloric acid, a similar trend is observed. UV exposure enhances the inhibition efficiency of *A. phylicoides* extract, especially at higher concentrations and temperatures. For instance, at 1000 ppm and 303K, inhibition efficiency rises from 0.8297% without UV exposure to 0.9262% with UV exposure. This highlights the role of UV radiation in improving the corrosion inhibition performance of *A. phylicoides* extract for zinc in hydrochloric acid. Tables 7.57-7.60 collectively demonstrate that UV radiation enhances the inhibition efficiency of *A. phylicoides* extract as a corrosion inhibitor for mild steel and zinc in sulphuric acid and hydrochloric acid environments. Higher concentrations and temperatures further augment this effect, indicating the potential of UV-treated *A. phylicoides* extract as an effective corrosion inhibitor in various industrial applications.

6.13 Adsorption Isotherm for Non-UV Radiated and UV Radiated *A. phylicoides* Extracts

The adsorption isotherm serves as a crucial technique for examining how inhibitor molecules interact with a metal surface [408]. Various adsorption isotherms exist, including Langmuir, Frumkin, and Temkin. In this study, the Langmuir adsorption isotherm emerged as the most suitable model. An adsorption isotherm for *A. phylicoides* extracts detail how the extract behaves when adsorbed onto a surface under varying conditions of concentration or pressure

© University of Venda

at a constant temperature. Essentially, it would illustrate the relationship between the amount of *A. phylicoides* extract adsorbed onto a surface and the concentration of the extract in the surrounding solution.

Typically, adsorption isotherms are plotted using different models like Langmuir equations, which help describe the behavior of the adsorbate (in this case, the *A. phylicoides* extract) on the adsorbent surface [409]. The plot provides valuable information on the adsorption behavior of *A. phylicoides* extract on metals under different conditions, offering insights into its potential application as a corrosion inhibitor and the factors influencing its adsorption onto the metal surface. Comparing the Langmuir adsorption isotherms of non-UV radiated, and UV-radiated *A. phylicoides* extract can provide valuable insights into how UV radiation affects the adsorption behavior of the extract. Understanding the Influence of UV Radiation: UV radiation can induce various chemical and structural changes in organic molecules [410]. Comparing the adsorption behavior of non-UV-radiated and UV-radiated *A. phylicoides* extract helps researchers elucidate how UV radiation affects the composition, structure, and surface activity of the extract. This understanding is crucial for optimizing the use of *A. phylicoides* extract as a corrosion inhibitor or in other applications. This necessitates the need to analyze Langmuir adsorption isotherm parameters as indicated in plots (figure 6.1-6.4) and Tables 6.61 -6.62. Figures 6.1–6.4 contain outliers, but these do not significantly affect the overall trend, as the best-fit line still adequately represents the data due to most points aligning with the expected pattern. These outliers may be due to surface heterogeneity, as the Langmuir isotherm assumes a uniform surface with identical adsorption sites, while metal surfaces often have imperfections that cause variations in adsorption at specific points. Additionally, impurities in the solution and human error might also contribute to these outliers.

© University of Venda

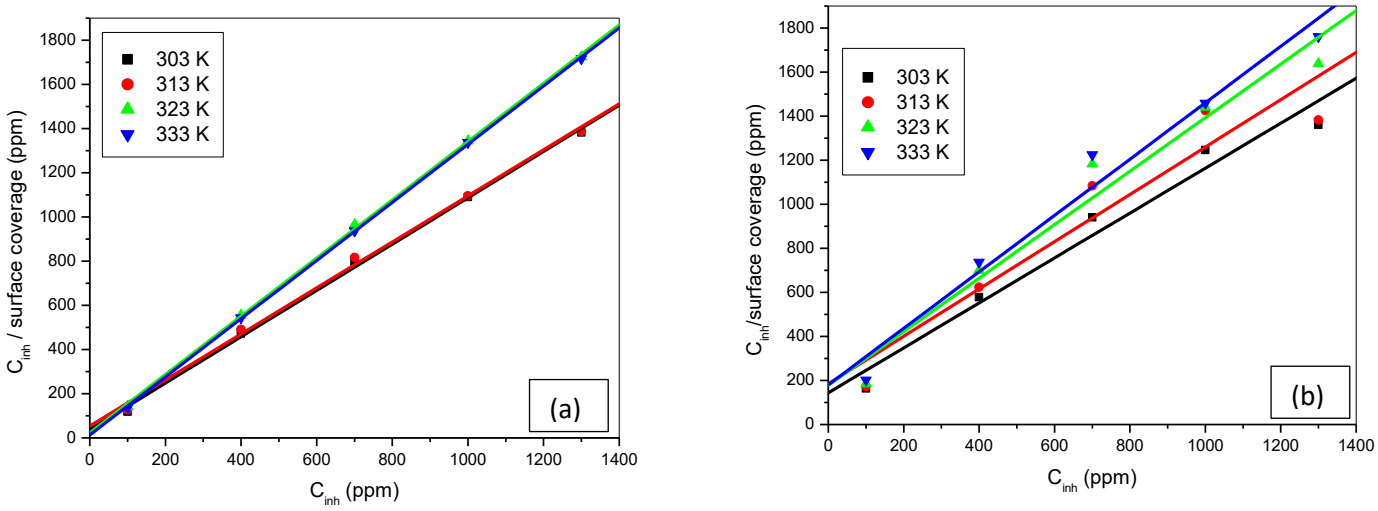


Figure 6.1: Langmuir adsorption isotherm for the adsorption of (a) non-UV radiated *A. phylicoides* extract, (b) UV radiated *A. phylicoides* extract on mild steel metal in 1.5 M HCl at 303 K, 313 K, 323 K, and 333 K.

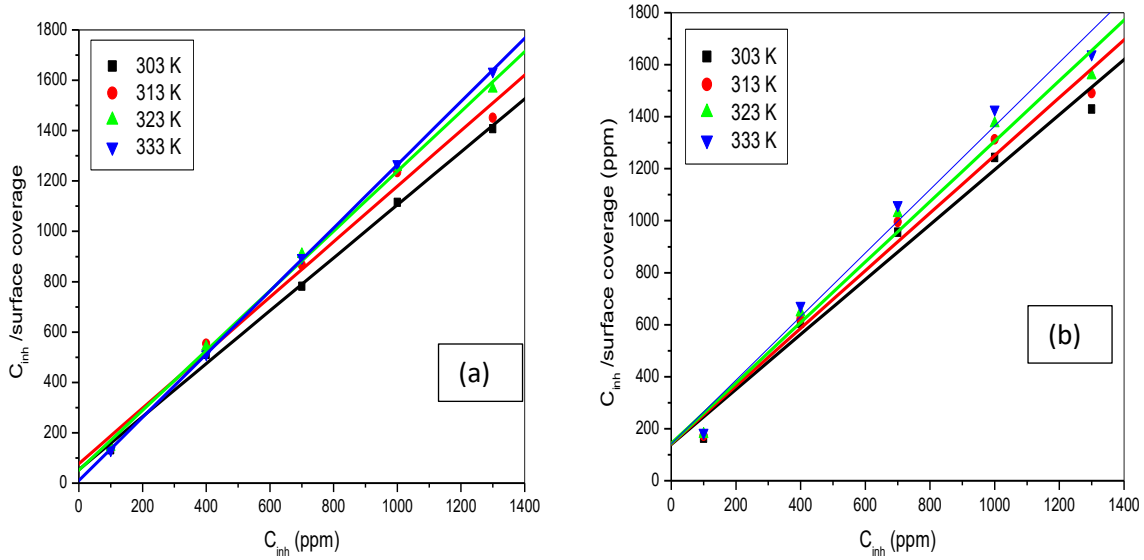


Figure 6.2: Langmuir adsorption isotherm for the adsorption of (a) non-UV radiated *A. phylicoides* extract, (b) UV radiated *A. phylicoides* extract on mild steel metal in 1.5 M H_2SO_4 at 303 K, 313 K, 323 K, and 333 K.

© University of Venda

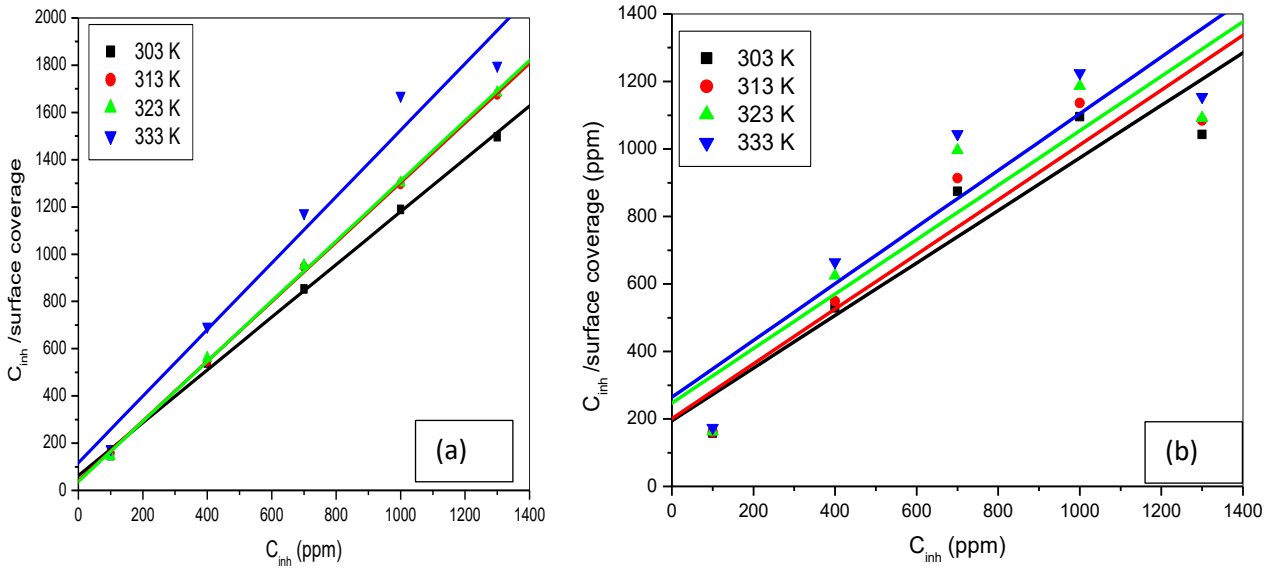


Figure 6.3: Langmuir adsorption isotherm for the adsorption of (a) non-UV radiated *A. phylicoides* extract, (b) UV radiated *A. phylicoides* extract on zinc metal in 1.5 M HCl at 303 K, 313 K, 323 K, and 333 K.

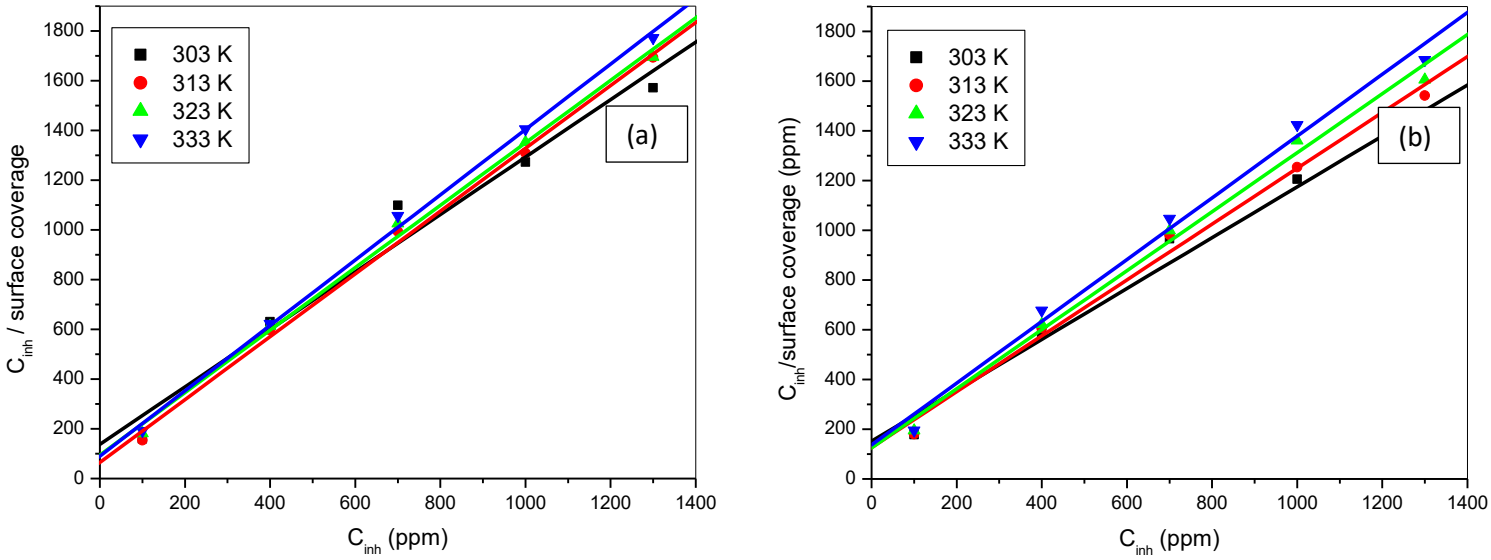


Figure 6.4: Langmuir adsorption isotherm for the adsorption of (a) non-UV radiated *A. phylicoides* extract, (b) UV radiated *A. phylicoides* extract on zinc metal in 1.5 M H_2SO_4 at 303 K, 313 K, 323 K, and 333 K.

The Langmuir adsorption isotherm is a commonly used model to describe the adsorption of molecules onto a solid surface [411]. It assumes that adsorption occurs through a monolayer coverage of adsorbate molecules on the surface [412]. This model provides insights into the

© University of Venda

behavior of adsorption systems and allows for the estimation of important parameters such as the adsorption equilibrium constant (K_{ads}) and the degree of surface coverage (θ). The Langmuir adsorption isotherm is governed by the equation [413].

$$\frac{C_{inh}}{\theta} = \frac{1}{k_{ads}} + C_{inh} \tag{6.1}$$

where C_{inh} is the concentration of the inhibitor, θ is the degree of surface coverage, and K_{ads} is the adsorption equilibrium constant, which is the intercept of the straight line. The value of the equilibrium constant is correlated to the Gibbs free energy.

$$(\Delta G^{o}_{ads} = -R\,T\,In(55.5\,K_{ads}) \tag{6.2}$$

where R is the gas constant; T is the absolute temperature.

In this study, K_{ads} is given in units of g/L, it needs to be converted to a dimensionless quantity by multiplying it by 1000 [414]. This adjustment ensures consistency in units and facilitates the calculation of the Gibbs free energy of adsorption (ΔG^{o}_{ads}).

The molar concentration of water, represented by 55.5 in Equation 60, reflects the concentration of water in pure liquid form, typically expressed in units of moles per liter (mol/L) or Molarity (M). Since we are converting K_{ads} to a dimensionless quantity, the concentration of water used for the conversion should also reflect this change. Therefore, the value of 55.5 in Equation 60 should be replaced by 1000 to maintain consistency with the units of K_{ads}. After making this modification, Equation 60 becomes Equation.

$$\Delta G^{o}_{ads} = -R\,T\,In(1000\,K_{ads}) \tag{6.3}$$

This modified equation ensures that the Gibbs free energy of adsorption is correctly calculated based on the adjusted adsorption equilibrium constant, facilitating the accurate interpretation of the thermodynamic properties of the adsorption process. The equation describes the relationship between the Gibbs free energy (ΔG^{o}_{ads}) of adsorption and the adsorption equilibrium constant (ΔG^{o}_{ads}) for a given inhibitor, such as *A. phylicoides* extract, on a solid surface. The negative sign indicates that the process is exergonic, meaning it releases energy. R represents the gas constant, while T is the absolute temperature in Kelvin. The natural logarithm (ln) of $1000 \cdot K_{ads}$ is taken to adjust the units of K_{ads} from g/L to a dimensionless quantity [415]. This adjustment ensures that the equation is consistent with the

© University of Venda

units used for (ΔG^{o}_{ads}) and facilitates accurate calculation of the Gibbs free energy of adsorption for *A. phylicoides* extract.

The equation provides a means to calculate the Gibbs free energy of adsorption for *A. phylicoides* extract based on the adsorption equilibrium constant, allowing for a deeper understanding of the thermodynamics of the adsorption process and its effectiveness as a corrosion inhibitor." The Langmuir adsorption isotherm and its associated equations are valuable tools for understanding and predicting the behavior of adsorption systems, including the adsorption of inhibitors like *A. phylicoides* extract onto metal surfaces for corrosion inhibition. They provide a theoretical framework for interpreting experimental data and designing effective corrosion protection strategies.

Table 6.61: Adsorption parameters from Langmuir Adsorption Isotherm plots for non-UV radiated *A. phylicoides* extract in 1.5 M H_2SO_4 and 1.5 M HCl.

	Metals	**Temp (K)**	**r^2**	**Slope**	**K_{ads} (L/mol)**	**$-\Delta G^{o}_{ads}$**
HCl	Mild steel	303	0,99910	1,04825	0.0261	-8.2173
		313	0,99843	1,0419	0.0186	-7.6069
		323	0,99978	1,31821	0.0430	-10.101
		333	0,99993	1,31679	0.0779	-12.059
	Zinc	303	0,99906	1,11728	0.0159	-6.9692
		313	0,99979	1,26148	0.0239	-8.2598
		323	0,99957	1,2732	0.0268	-8.8313
		333	0,98479	1,40805	0.0085	-5.9253
H_2SO_4	Mild steel	303	0,99879	1,05165	0.0187	-7.3778
		313	0,99527	1,10213	0.0129	-11.322
		323	0,99892	1,1871	0.0194	-7.9635
		333	0,99996	1,25476	0.0998	-12.745
	Zinc	303	0,98462	1,15556	0.0073	-5.0080
		313	0,99837	1,26366	0.0154	-7.1160
		323	0,99805	1,25592	0.0106	-6.3401
		333	0,99878	1,31423	0.0111	-6.6642

© University of Venda

Table 6.61 presents adsorption parameters derived from Langmuir Adsorption Isotherm plots for non-UV radiated *A. phylicoides* extract in two distinct acidic solutions: 1.5 M H_2SO_4 and 1.5 M HCl. It includes data for two different metals, mild steel, and zinc, investigated across varying temperatures from 303 K to 333 K. The coefficient of determination (r^2) serves as a measure of the goodness of fit of the Langmuir model to the experimental data. Higher values of r^2 indicate stronger agreement between the experimental and theoretical data, suggesting the model's reliability in describing the adsorption process [416]. Across the table, the r^2 values range from approximately 0.984 to 0.999, indicating high levels of fit for the Langmuir model in most cases.

The slope parameter reflects the steepness of the Langmuir adsorption isotherm plot, providing insights into the adsorption capacity of the metal surface [417]. Generally, higher slope values indicate greater adsorption capacity. In this context, the slope values range from around 1.04 to 1.41, suggesting varying degrees of adsorption capacity depending on the metal, temperature, and acidic medium. The adsorption equilibrium constant (K_{ads}) represents the affinity of the adsorbate (*A. phylicoides* extract) for the adsorbent (metal surface) [418]. Higher K_{ads} values indicate stronger adsorption interactions between the extract and the metal surface [419]. Values of K_{ads} in the table range from approximately 0.007 to 0.100 L/mol. These values suggest differing affinities of the *A. phylicoides* extract for mild steel and zinc surfaces under different temperatures and acidic conditions. Comparing the data between HCl and H_2SO_4 mediums reveals variations in adsorption parameters, indicating the influence of the acidic environment on the adsorption behaviour of the *A. phylicoides* extract. Additionally, comparing the adsorption parameters for mild steel and zinc provides insights into the different responses of these metals to the adsorption process. The table offers valuable insights into the adsorption behaviour of *A. phylicoides* extract on mild steel and zinc surfaces under various conditions, contributing to our understanding of its potential application as a corrosion inhibitor and the factors influencing its adsorption properties.

Table 6.61 presents adsorption parameters from Langmuir Adsorption Isotherm plots for non-UV radiated *A. phylicoides* extract in 1.5 M H_2SO_4 and 1.5 M HCl solutions, with a focus on the Gibbs free energy (ΔG^{o}_{ads}) values. These values are essential for understanding the thermodynamic favourability of the adsorption process, shedding light on the interaction between the inhibitor and metal surfaces, particularly in corrosive environments [420].

© University of Venda

In the HCl solution, both mild steel and zinc display negative (ΔG^{o}_{ads}) values across various temperatures, indicating that the adsorption process is thermodynamically favourable. The (ΔG^{o}_{ads}) values range from approximately -5.9253 kJ/mol to -12.059 kJ/mol for zinc and from approximately -7.6069 kJ/mol to -12.059 kJ/mol for mild steel. These negative values suggest that the adsorption occurs spontaneously, driven by favourable interactions between the inhibitor molecules and the metal surfaces, regardless of temperature [421].

Similarly, in the H_2SO_4 solution, both mild steel and zinc also exhibit negative (ΔG^{o}_{ads}) values, indicating favourable adsorption. The (ΔG^{o}_{ads}) values range from approximately -5.0080 kJ/mol to -12.745 kJ/mol for zinc and from approximately -7.3778 kJ/mol to -12.745 kJ/mol for mild steel across different temperatures. Again, these negative values confirm the thermodynamic favourability of the adsorption process, suggesting that it occurs spontaneously in H_2SO_4 environments [421].

The negative (ΔG^{o}_{ads}) values in both HCl and H_2SO_4 solutions highlight the effectiveness of non-UV radiated *A. phylicoides* extract as a corrosion inhibitor for both mild steel and zinc surfaces. The consistency of these negative values across different temperatures and metal types underscores the reliability and potential utility of the adsorption process for corrosion inhibition in acidic environments. This information is valuable for designing corrosion protection strategies and optimizing the use of *A. phylicoides* extract as a corrosion inhibitor in various industrial applications.

Table 6.62: Adsorption parameters from Langmuir Adsorption Isotherm plots for UV radiated *A. phylicoides* extract in 1.5 M H_2SO_4 and 1.5 M HCl.

	Metals	**Temp (K)**	**r^2**	**Slope**	**K_{ads} (L/mol)**	**ΔG^{o}_{ads} (KJ/mol)**
HCl	Mild steel	303	0,9829	1,02025	0.006960	-4.8879
		313	0,95380	1,07433	0.005391	-4.3844
		323	0,97990	1,21487	0.005600	-4.6266
		333	0,98593	1,28027	0.005532	-4.7360
	Zinc	303	0,93854	0,77862	0.005131	-4.1198
		313	0,93786	0,81117	0.004980	-4.1780
		323	0,90866	0,80682	0.004047	-3.7544

© University of Venda

		333	0,91316	0,84015	0.003782	-3.6831
H_2SO_4	Mild steel	303	0,98846	1,05659	0.007150	-4.9557
		313	0,98841	1,10951	0.007037	-5.0778
		323	0,98916	1,16251	0.006965	-5.2124
		333	0,99111	1,22270	0.007050	-5.4075
	Zinc	303	0,98801	1,02296	0.006585	-4.7484
		313	0,99517	1,12338	0.007929	-5.3884
		323	0,99566	1,18685	0.007978	-5.5771
		333	0,99488	1,24214	0.007308	-5.5069

Table 6.62 provides adsorption parameters derived from Langmuir Adsorption Isotherm plots for UV radiated *A. phylicoides* extract in two different acidic solutions: 1.5 M H_2SO_4 and 1.5 M HCl. It presents data for two different metals, mild steel, and zinc, studied across various temperatures ranging from 303 K to 333 K. The coefficient of determination (r^2) serves as an indicator of the goodness of fit of the Langmuir model to the experimental data [422]. Lower values of r^2 suggest weaker agreement between the experimental and theoretical data, potentially indicating less reliable fits for the Langmuir model. In this table, r^2 values range from approximately 0.908 to 0.986, indicating varying levels of fit across different conditions.

The slope parameter reflects the steepness of the Langmuir adsorption isotherm plot and provides insights into the adsorption capacity of the metal surface. Lower slope values suggest reduced adsorption capacity [423]. In this context, the slope values range from approximately 0.779 to 1.281, indicating varying degrees of adsorption capacity depending on the metal, temperature, and acidic medium.

The adsorption equilibrium constant (K_{ads}) represents the affinity of the adsorbate (UV-radiated *A. phylicoides* extract) for the adsorbent (metal surface). Higher K_{ads} values indicate stronger adsorption interactions between the extract and the metal surface. Values of K_{ads} in HCl range from approximately 0.0038 to 0.0069 L/mol, suggesting differing affinities of the UV-radiated *A. phylicoides* extract for mild steel and zinc surfaces under different temperatures and HCl conditions. Comparing the data between HCl and H_2SO_4 mediums reveals variations in adsorption parameters, indicating the influence of the acidic environment on the adsorption behavior of the UV-radiated *A. phylicoides* extract. Additionally, comparing

© University of Venda

the adsorption parameters for mild steel and zinc provides insights into the different responses of these metals to the adsorption process under UV radiation.

The coefficient of determination (r^2) measures the goodness of fit of the Langmuir model to the experimental data. For sulphuric acid, r^2 values range from approximately 0.988 to 0.995, indicating a high level of agreement between the experimental and theoretical data. This suggests that the Langmuir model effectively describes the adsorption behavior of UV-radiated *A. phylicoides* extract on both mild steel and zinc surfaces in both acidic solutions.

The slope parameter reflects the steepness of the Langmuir adsorption isotherm plot, which provides insights into the adsorption capacity of the metal surface. Across the table, slope values vary between approximately 1.02 to 1.24, indicating different degrees of adsorption capacity depending on the metal type, temperature, and acidic medium. Generally, higher slope values suggest greater adsorption capacity [423]. The adsorption equilibrium constant (K_{ads}) represents the affinity of the extract for the metal surface. Higher K_{ads} values indicate stronger adsorption interactions [424]. In this table, K_{ads} values range from approximately 0.0066 to 0.0079 L/mol, suggesting a relatively strong affinity of the UV-radiated *A. phylicoides* extract for the metal surfaces in both acidic solutions.

Comparing the adsorption parameters between mild steel and zinc, in H_2SO_4 and HCl solutions, reveals variations in adsorption behavior. For instance, zinc generally exhibits lower adsorption capacities compared to mild steel, and the adsorption parameters differ between the two acidic solutions. These differences highlight the importance of considering factors such as metal type and acidic environment when evaluating the effectiveness of the extract as a corrosion inhibitor. The table provides valuable insights into the adsorption behaviour of UV-radiated *A. phylicoides* extract on mild steel and zinc surfaces under various conditions, contributing to our understanding of its potential application as a corrosion inhibitor in acidic environments.

Table 6.62 provides essential insights into the adsorption behaviour of UV-radiated *A. phylicoides* extract in 1.5 M H_2SO_4 and 1.5 M HCl solutions, focusing on the Gibbs free energy (ΔG^o_{ads}) values. These values offer a glimpse into the thermodynamic spontaneity of the adsorption process, crucial for understanding the effectiveness of the extract as a corrosion inhibitor. Throughout the table, negative (ΔG^o_{ads}) values are observed, indicating that the adsorption process is thermodynamically favourable, irrespective of the solution's acidity or the metal type under consideration [420].

© University of Venda

In the HCl solution, both mild steel and zinc exhibit consistently negative (ΔG^{o}_{ads}) values across different temperatures, ranging from approximately -3.6831 kJ/mol to -4.8879 kJ/mol for zinc and from approximately -4.3844 kJ/mol to -5.4075 kJ/mol for mild steel. This suggests that the adsorption of the UV-radiated *A. phylicoides* extract onto these metal surfaces is spontaneous under the conditions tested, indicating a strong affinity between the inhibitor molecules and the metal surfaces in HCl.

Similarly, in the H_2SO_4 solution, both mild steel and zinc also display negative (ΔG^{o}_{ads}) values, ranging from approximately -4.7484 kJ/mol to -5.5771 kJ/mol for zinc and from approximately -4.9557 kJ/mol to -5.4075 kJ/mol for mild steel. These findings reinforce the thermodynamic favourability of the adsorption process, highlighting the efficacy of the UV-radiated *A. phylicoides* extract as a corrosion inhibitor in H_2SO_4 environments. The consistent negative (ΔG^{o}_{ads}) values across different temperatures and metal types underscore the reliability and effectiveness of the adsorption process for corrosion inhibition in both HCl and H_2SO_4 acidic environments. The thermodynamic spontaneity of the adsorption process suggests that it occurs spontaneously and is driven by favorable interactions between the inhibitor molecules and the metal surfaces, further supporting the potential utility of UV-radiated *A. phylicoides* extract as a corrosion inhibitor in industrial applications.

6.14 Temperature Effect for *A. phylicoides* Extracts

The temperature effect on *A. phylicoides* extracts for corrosion studies is crucial to understand as it can significantly influence the effectiveness of the extract as a corrosion inhibitor. Generally, an increase in temperature can accelerate corrosion processes due to increased molecular activity and reaction rates [425]. However, the effect of temperature on corrosion inhibition by *A. phylicoides* extracts may vary depending on several factors, including the chemical composition of the extract, the type of metal being protected, and the corrosive environment.

When conducting corrosion studies using *A. phylicoides* extracts as inhibitors, it's essential to investigate the temperature dependence of inhibition efficiency. This involves studying how the inhibition performance changes with temperature variations. Analyzing the inhibition efficiency at different temperatures helps researchers assess the thermal stability of the inhibitor and its ability to provide effective protection over a range of operating conditions.

© University of Venda

Arrhenius plots are commonly used to study the temperature dependence of corrosion processes and inhibition [426]. These plots relate the rate constant or corrosion rate to the reciprocal of temperature, typically expressed as $1/T$. The Arrhenius equation, which describes the relationship between the rate constant (k), temperature (T), activation energy (E_a), and pre-exponential factor (A), can be represented as:

$$k=A\cdot e(^{-EaRT}) \quad (6.4)$$

where:

- k is the rate constant.
- A is the pre-exponential factor.
- E_a is the activation energy.
- R is the gas constant.
- T is the absolute temperature.

Arrhenius plots shown in Figures 6.5-6.8, typically yield straight lines, with the slope representing $-E_a/R$ and the intercept representing $ln(A)$ [427]. The activation energy (E_a) is a measure of the energy barrier that reactant molecules must overcome for a chemical reaction to occur. Higher activation energies indicate slower reaction rates, while lower activation energies suggest faster reactions.

In the context of corrosion inhibition by *A. phylicoides* extracts, studying Arrhenius plots can provide insights into the thermodynamic and kinetic parameters governing the inhibition process. The activation energy (E_a) reflects the energy required for the inhibitor molecules to adsorb onto the metal surface and form a protective layer [260]. A lower activation energy suggests that the inhibitor can more readily adsorb onto the surface and inhibit corrosion [428]. Additionally, the entropy and enthalpy of adsorption can also be determined from the slope and intercept of Arrhenius plots, providing further information on the adsorption mechanism and the stability of the inhibitor-metal complex.

Analysing Arrhenius plots for mild steel and zinc corrosion in H_2SO_4 and HCl solutions using non-UV radiated and UV-radiated *A. phylicoides* plant extracts as inhibitors, researchers can gain insights into how temperature influences the inhibition process and the underlying thermodynamic and kinetic parameters. This understanding is crucial for optimizing the use

© University of Venda

of *A. phylicoides* extracts as corrosion inhibitors and designing effective corrosion protection strategies under various environmental conditions.

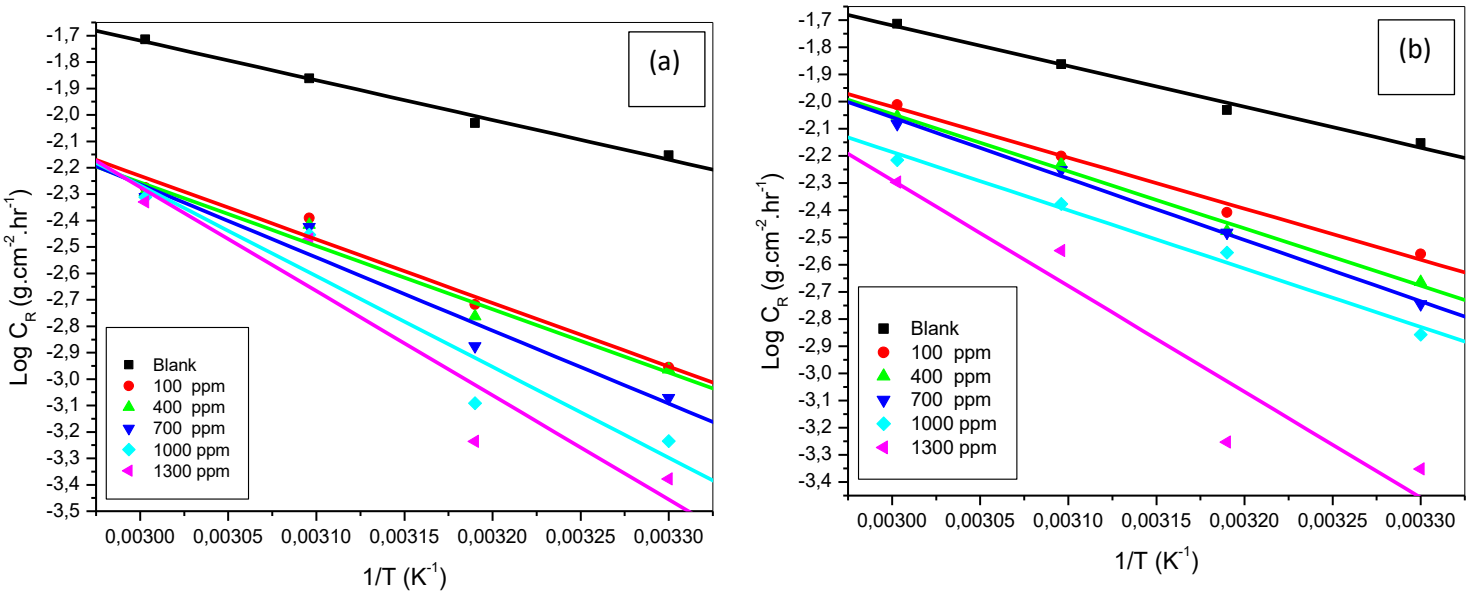


Figure 6.5: Arrhenius plots for mild steel metal corrosion in 1.5 M H_2SO_4 solution using (a) non-UV radiated *A. phylicoides,* (b) UV-radiated *A. phylicoides plant extract* as the inhibitor.

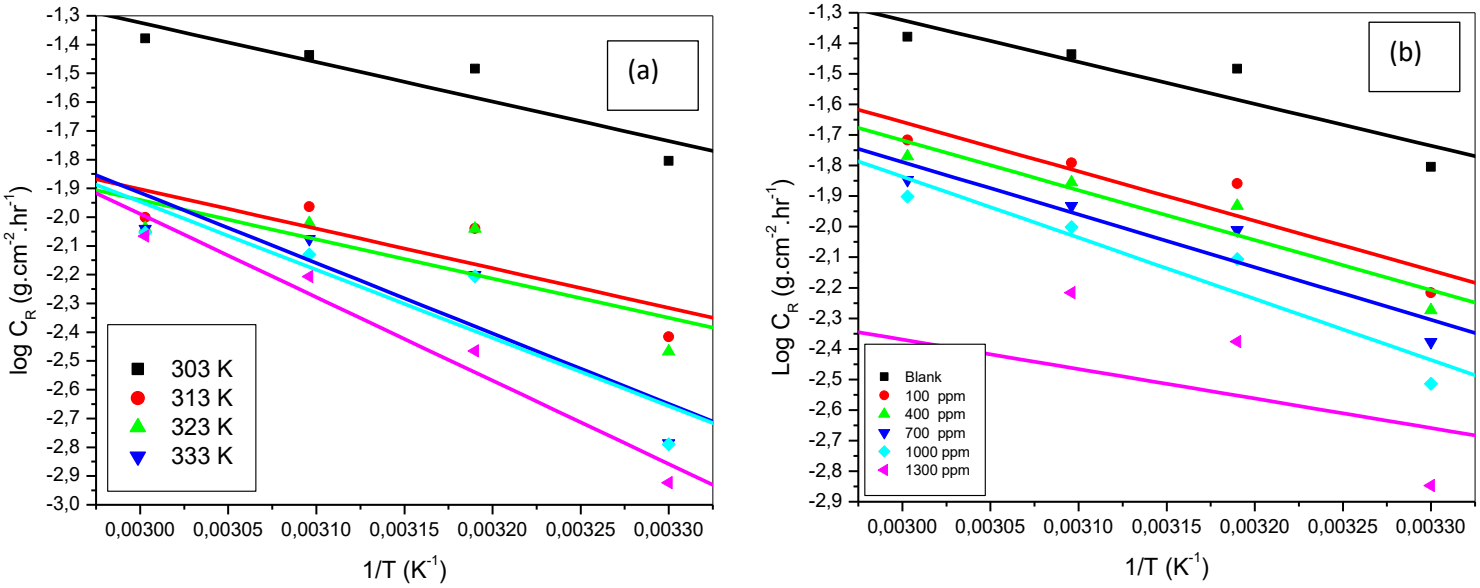


Figure 6.6: Arrhenius plots for mild steel metal corrosion in 1.5 M HCl solution (a) non-UV radiated *A. phylicoides* extract (b) UV-radiated *A. phylicoides plant extract* as the inhibitor.

© University of Venda

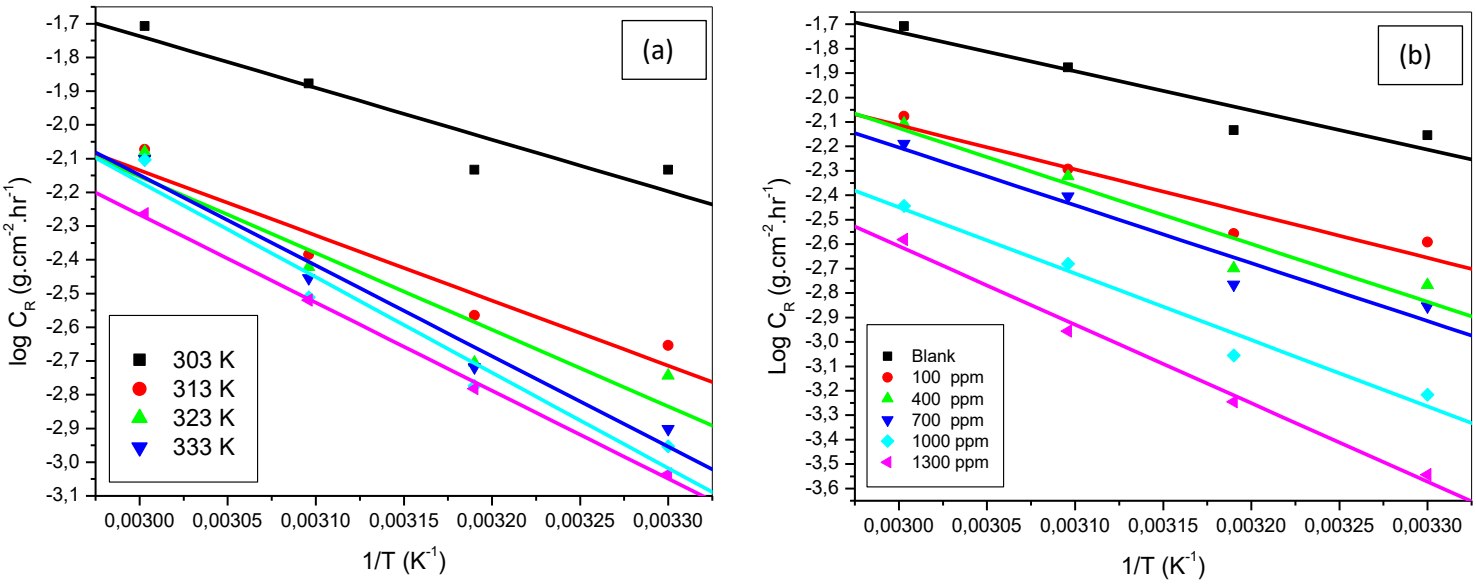


Figure 6.7: Arrhenius plots for zinc metal corrosion in 1.5 M H_2SO_4 solution (a) non-UV radiated (b) UV-radiated *A. phylicoides* plant extract as the inhibitor.

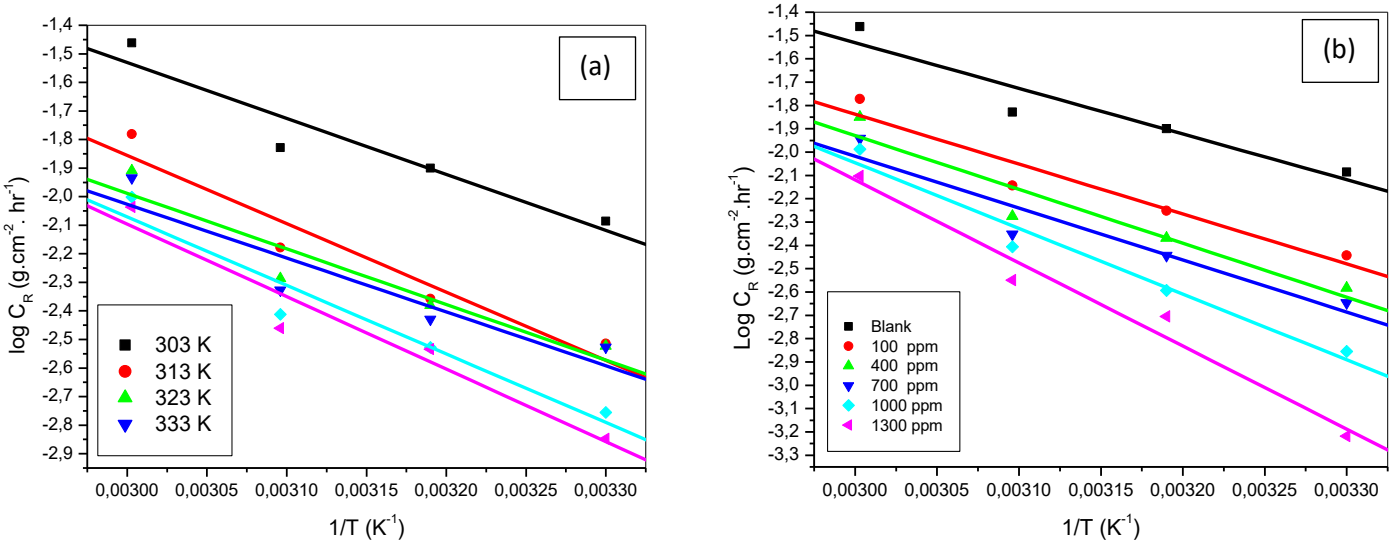


Figure 6.8: Arrhenius plots for zinc metal corrosion in 1.5 M HCl solution non-UV radiated and UV-radiated *A. phylicoides* plant extract as the inhibitor.

Additional insights into how temperature impacts inhibition efficiency were acquired by examining activation parameters like the enthalpy of activation (ΔH*) and entropy of activation (ΔS*). The correlation between corrosion rate, temperature, and these parameters is elucidated through a transition-state equation of a specific format.

© University of Venda

$$\log\left(\frac{C_R}{T}\right) = \left[\log\left(\frac{R}{Nh}\right) + \left(\frac{\Delta S*}{2.303R}\right)\right] + \left(\frac{-\Delta H*}{2.303R}\right)\left(\frac{1}{T}\right) \quad (6.5)$$

A plot of Log (C_R/T) on the y-axis against 1/T on the x-axis yield straight line with a slope equal to - ΔH/2.303R. The intercept is equal to log(R/Nh) + ΔS/2.303R where h is plank's constant, N is avogadro's constant, ΔS and ΔH is the entropy and enthalpy change, respectively [429]. These plots are shown in Figures 6.9-6.12.

To understand how temperature impacts inhibition efficiency, researchers examined activation parameters such as the enthalpy of activation (ΔH*) and entropy of activation (ΔS*). These parameters give insights into the energy barriers that must be overcome for the reaction to occur. This analysis helps in understanding how temperature affects corrosion rates and how inhibitors mitigate these effects by altering activation parameters.

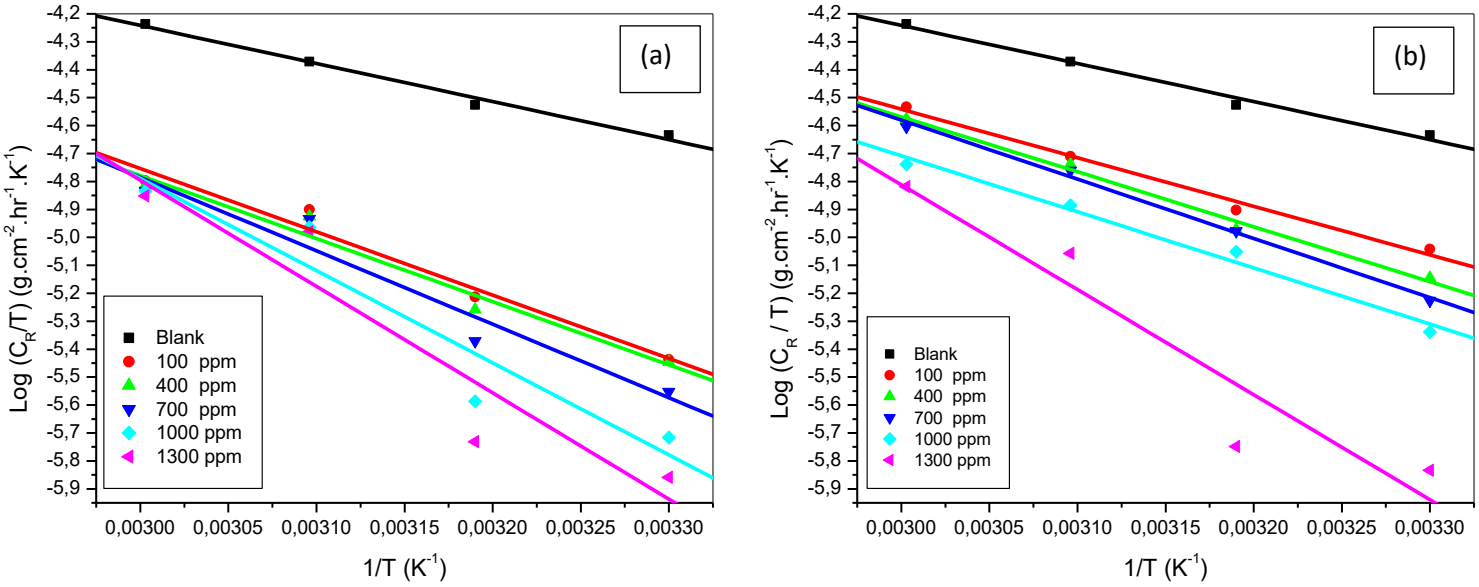


Figure 6.9: Transition state plots for mild steel metal corrosion in 1.5 M HCl solution in the absence and presence of different concentrations of *A. phylicoides* plant extract as the inhibitor.

© University of Venda

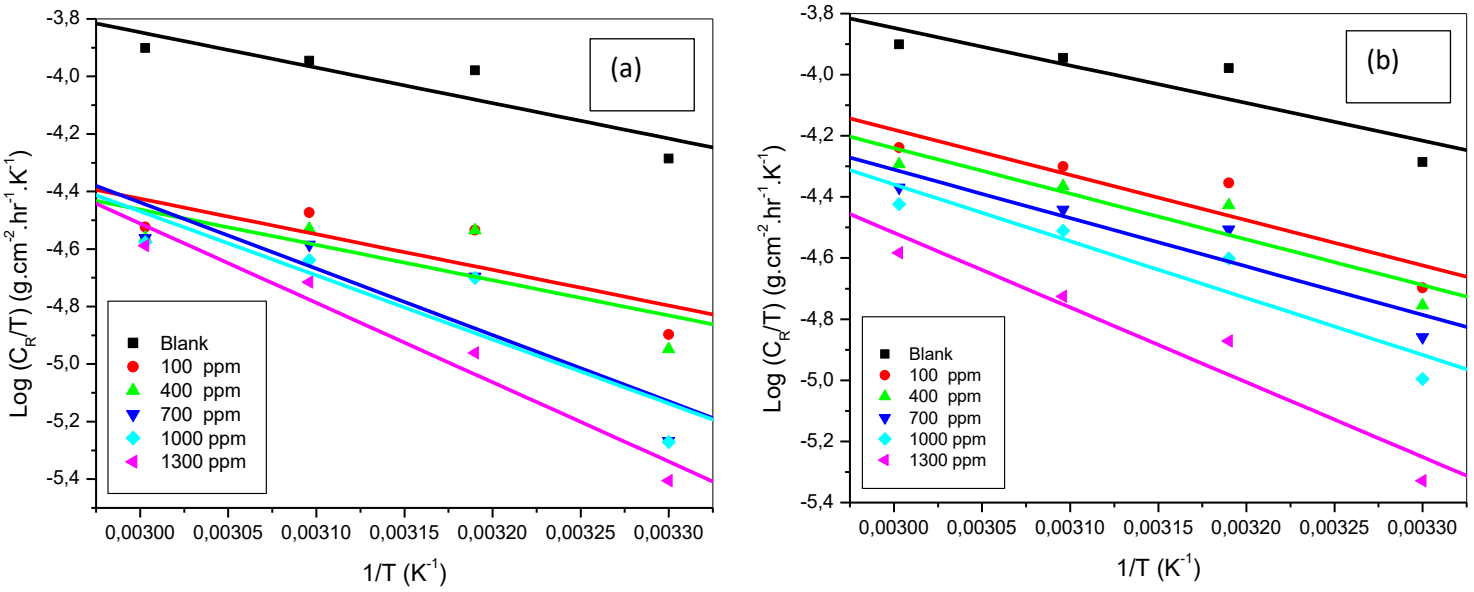


Figure 6.10: Transition state plots for mild steel metal corrosion in 1.5 M H_2SO_4 solution in the absence and presence of different concentrations of *A. phylicoides* plant extract as the inhibitor.

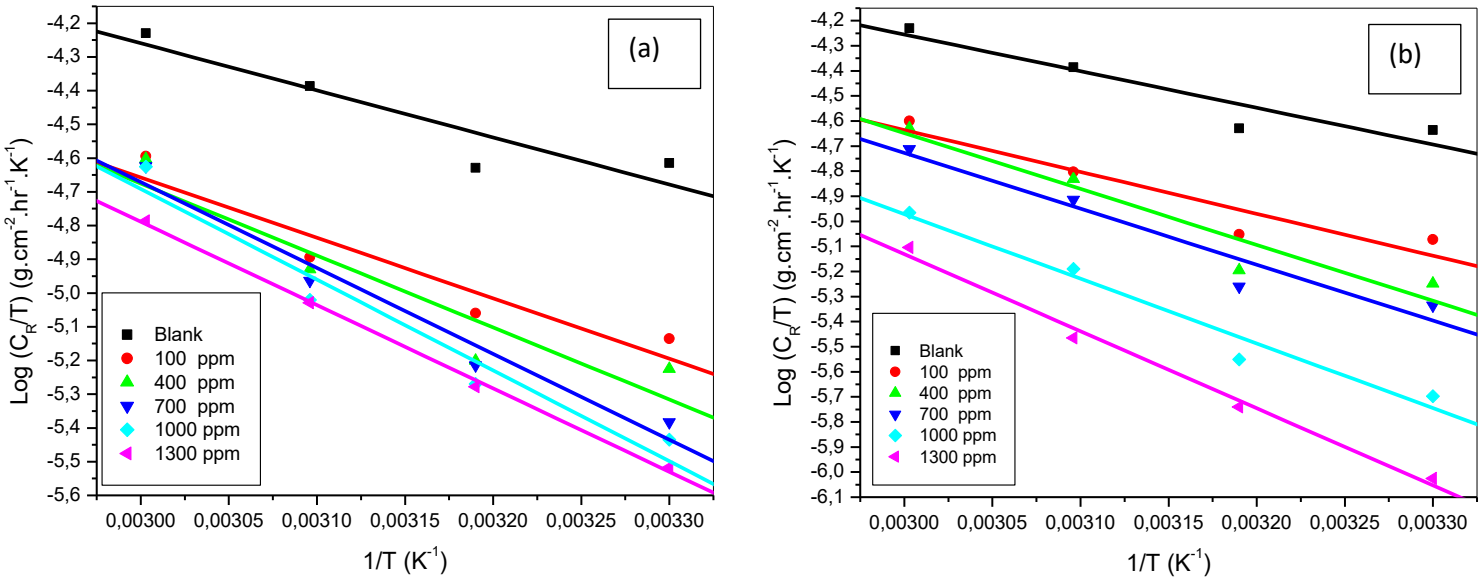


Figure 6.11: Transition state plots for zinc metal corrosion in 1.5 M HCl solution in the absence and presence of different concentrations of *A. phylicoides* plant extract as the inhibitor.

© University of Venda

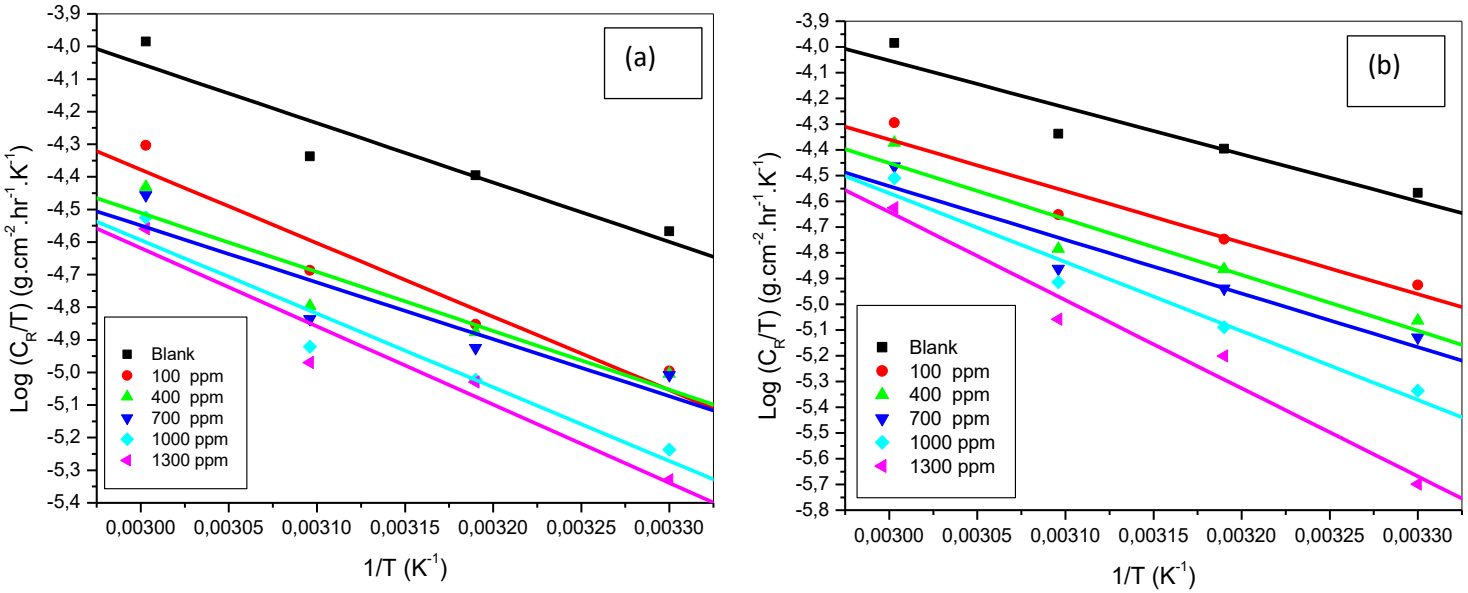


Figure 6.12: Transition state plots for zinc metal corrosion in 1.5 M H_2SO_4 solution in the absence and presence of different concentrations of *A. phylicoides* plant extract as the inhibitor.

Table 6.63: Arrhenius and transition parameters for the adsorption of different concentrations of non-UV radiated *A. phylicoides* in 1.5 M HCl on mild steel and zinc metal.

Acidic medium	**Metals**	**Concentration of inhibitors (ppm)**	**E_a (kJ.mol^{-1})**	**ΔH^* (kJ.mol^{-1})**	**$-\Delta S^*$ (J.mol^{-1}. K^{-1})**
HCl	Mild steel	00	28.75968	26.10664	200.47597
		100	46.07911	43.42547	158.31947
		400	45.91067	43.25696	159.30924
		700	52.97583	50.32201	138.24631
		1000	65.79146	63.13779	99.876577
		1300	75.52895	72.87560	70.77481
	Zinc	00	29.391735	26.73781	198.92859
		100	36.985385	34.33243	183.76046
		400	43.534895	40.88105	164.46377
		700	51.418058	48.76457	140.73099
		1000	54.207412	51.55344	132.74998
		1300	49.988097	47.33405	147.27243

© University of Venda

H_2SO_4	Mild steel	00	26.25110	23.59721	200.44475
		100	26.36081	23.70711	211.19308
		400	26.15930	23.50566	212.52369
		700	46.85603	44.20252	149.94592
		1000	45.32121	42.66744	155.15042
		1300	55.50391	52.85023	125.41274
	Zinc	00	37.52381	34.86996	170.58395
		100	45.83032	43.17724	151.88066
		400	37.28664	34.63286	180.05661
		700	36.08253	33.42940	184.40346
		1000	45.92597	43.27185	155.72755
		1300	48.64173	45.98786	148.05349

In Table 6.63, several noteworthy values and numbers provide crucial insights into the adsorption behavior of non-UV radiated *A. phylicoides* extract on mild steel and zinc surfaces in 1.5 M HCl and H_2SO_4 acidic solutions. One key parameter is the activation energy (E_a), which represents the energy barrier for the adsorption process. Notably, activation energies vary significantly across different concentrations and metal types. For instance, higher activation energies, such as the approximately 75 kJ/mol observed for mild steel in HCl at 1300 ppm concentration, suggest that higher concentrations require more energy for adsorption to occur. In contrast, lower activation energies, such as the approximately 37 kJ/mol observed for zinc in H_2SO_4 at 400 ppm concentration, indicate that adsorption is more facile at lower concentrations.

Another significant parameter is the enthalpy of adsorption (ΔH^*), which reflects the heat absorbed or released during adsorption. The enthalpy values show notable trends, particularly with concentration variations. For mild steel in HCl, enthalpy generally increases with increasing concentration, reaching approximately 73 kJ/mol at 1300 ppm concentration, indicating an exothermic adsorption process. In contrast, for zinc in H_2SO_4, enthalpy variations are less pronounced, suggesting a more consistent adsorption process across different concentrations.

Additionally, the negative entropy of adsorption ($-\Delta S^*$) provides insights into the change in disorder during adsorption [430]. Higher absolute values of $-\Delta S^*$ indicate greater disorder,

© University of Venda

with notable differences observed between acidic solutions and metal types. For example, for mild steel in HCl, the highest absolute value of $-\Delta S^*$ is observed at 0 ppm concentration, indicating a significant decrease in disorder upon adsorption. Conversely, for zinc in H_2SO_4, the lowest absolute value of $-\Delta S^*$ is observed at 700 ppm concentration, suggesting a lesser decrease in disorder compared to other concentrations.

Comparing values between acidic solutions and metals reveals significant variations, highlighting the influence of solution composition and metal type on the adsorption process. These insights contribute to a deeper understanding of the adsorption kinetics and thermodynamics of *A. phylicoides* extract on mild steel and zinc surfaces in acidic environments, informing optimization strategies for corrosion protection applications.

Table 6.64: Arrhenius and transition parameters for the adsorption of different concentrations of UV-radiated *A. phylicoides* in 1.5 M HCl on mild steel and zinc metal.

Acidic medium	**Metals**	**Concentration of inhibitors (ppm)**	**E_a (kJ.mol^{-1})**	**ΔH^* (kJ.mol^{-1})**	**$-\Delta S^*$ (J.mol^{-1}. K^{-1})**
HCl	Mild steel	00	28.760	26.11	200.479
		100	35.936	33.28	184.694
		400	40.296	37.64	172.141
		700	43.215	40.57	163.590
		1000	41.102	38.45	172.386
		1300	74.624	71.97	073.804
	Zinc	00	30.68	28.02	194.988
		100	34.64	31.99	190.381
		400	45.38	42.73	158.404
		700	45.35	42.70	160.000
		1000	52.02	49.39	144.600
		1300	61.54	58.89	119.168
		00	26.251	23.60	200.446
		100	30.969	28.32	192.682
		400	31.281	28.63	192.889

© University of Venda

H_2SO_4	Mild steel	700	32.981	30.33	189.148
		1000	38.279	35.63	174.173
		1300	18.476	46.86	143.504
	Zinc	00	37.52	34.87	170.59
		100	40.99	38.34	166.05
		400	44.25	41.60	158.03
		700	42.61	39.95	164.67
		1000	53.95	51.29	131.18
		1300	68.23	65.58	089.73

Table 6.64 presents Arrhenius and transition parameters detailing the adsorption of different concentrations of UV-radiated *A. phylicoides* extract in 1.5 M HCl and H_2SO_4 acidic solutions on mild steel and zinc metal surfaces. These parameters elucidate the intricate kinetics and thermodynamics governing the adsorption process, crucial for understanding the effectiveness of the extract as a corrosion inhibitor. The activation energy (E_a), representing the energy barrier for adsorption, exhibits notable variations across concentrations and metal types. Higher activation energies, like those observed for mild steel in HCl at 1300 ppm concentration (approximately 74.624 kJ/mol), suggest a slower adsorption process necessitating more energy. Conversely, zinc in H_2SO_4 at 1300 ppm concentration exhibits a similar trend with an E_a of approximately 68.23 kJ/mol. The enthalpy of adsorption (ΔH^*), reflecting the heat absorbed or released during adsorption, shows intriguing trends. For instance, ΔH^* values for mild steel in HCl generally increase with concentration, indicating an exothermic adsorption process. Conversely, zinc in H_2SO_4 displays less variation in $\Delta H*$, suggesting a more consistent adsorption process. The negative entropy of adsorption ($-\Delta S^*$), signifying the change in disorder during adsorption, varies across concentrations and metal types. For mild steel in HCl, the highest absolute $-\Delta S^*$ value, observed at 1300 ppm concentration, indicates a significant decrease in disorder upon adsorption. Conversely, zinc in H_2SO_4 displays the lowest absolute $-\Delta S^*$ value at 1300 ppm concentration, suggesting a lesser decrease in disorder. Comparing values between acidic solutions and metals reveals substantial differences, such as higher activation energies for mild steel compared to zinc, indicating a higher energy barrier for adsorption on mild steel surfaces. Additionally, variations in enthalpies of adsorption underscore differences in the heat released or absorbed

© University of Venda

during the adsorption process, further highlighting the complex interplay of factors influencing corrosion inhibition by UV-radiated *A. phylicoides* extract.

© University of Venda

University of Venda
Creating Future Leaders

CHAPTER SEVEN

RESULTS AND DISCUSSION

Electrochemical studies

(ES)

© University of Venda

7.1 Open Circuit Voltage (OCV)

Open Circuit Voltage (OCV) is a fundamental parameter in electrochemical studies [431]. It refers to the voltage between two electrodes when there's no current flowing between them. In corrosion studies, OCV can provide insights into the corrosion potential of a system. If the OCV is more negative, it indicates a higher tendency for corrosion to occur [432].

Measuring the OCV for 30 minutes in a corrosion study can provide valuable insights into the behavior of the system over time. This extended monitoring period allows for several key aspects to be addressed. Firstly, it enables the assessment of stability within the corrosion system [433]. Observing the OCV over an extended period helps researchers to determine if the corrosion process has reached equilibrium. A stable OCV indicates that the system has settled into a steady state, offering important information about its corrosion potential [434]. Furthermore, studying the OCV over time allows for the analysis of corrosion kinetics. Corrosion processes often involve multiple kinetic steps, and monitoring the OCV can provide insights into the rate of corrosion or the formation of corrosion products. In the context of studying the effectiveness of *A. phylicoides* extract as a corrosion inhibitor, monitoring the OCV for an extended period can reveal how it influences corrosion behavior over time. A decrease in OCV or a shift towards less negative values may indicate successful inhibition of corrosion processes. Moreover, studying the OCV over 30 minutes allows researchers to consider environmental factors that may impact corrosion. Variables such as temperature, humidity, and exposure to UV radiation can influence corrosion behavior, and observing the OCV over time helps understand how these factors affect the system. Lastly, if researchers are comparing the effects of UV radiation on corrosion inhibition by *A. phylicoides* extract, measuring the OCV for both UV-radiated and non-UV-radiated samples over the same period facilitates direct comparisons between different conditions, aiding in the evaluation of the extract's effectiveness as a corrosion inhibitor. Open circuit voltage UV-radiated and non-UV-radiated *A. phylicoides* on mild steel in H_2SO_4 and HCl solutions are shown in Figures 7.1-7.4.

© University of Venda

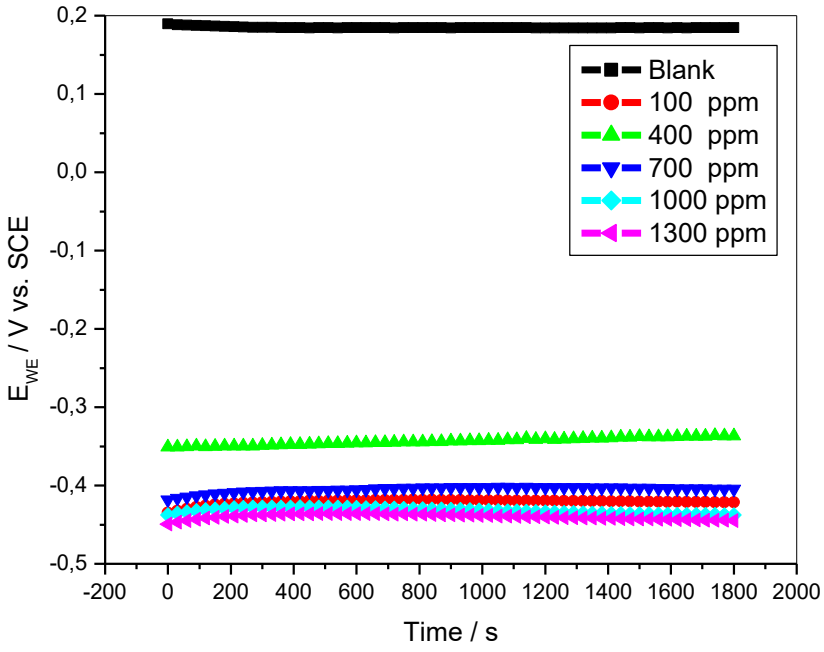


Figure 7.1: Open circuit voltage for mild steel 1.5 M H_2SO_4 solution and UV-radiated *A. phylicoides*

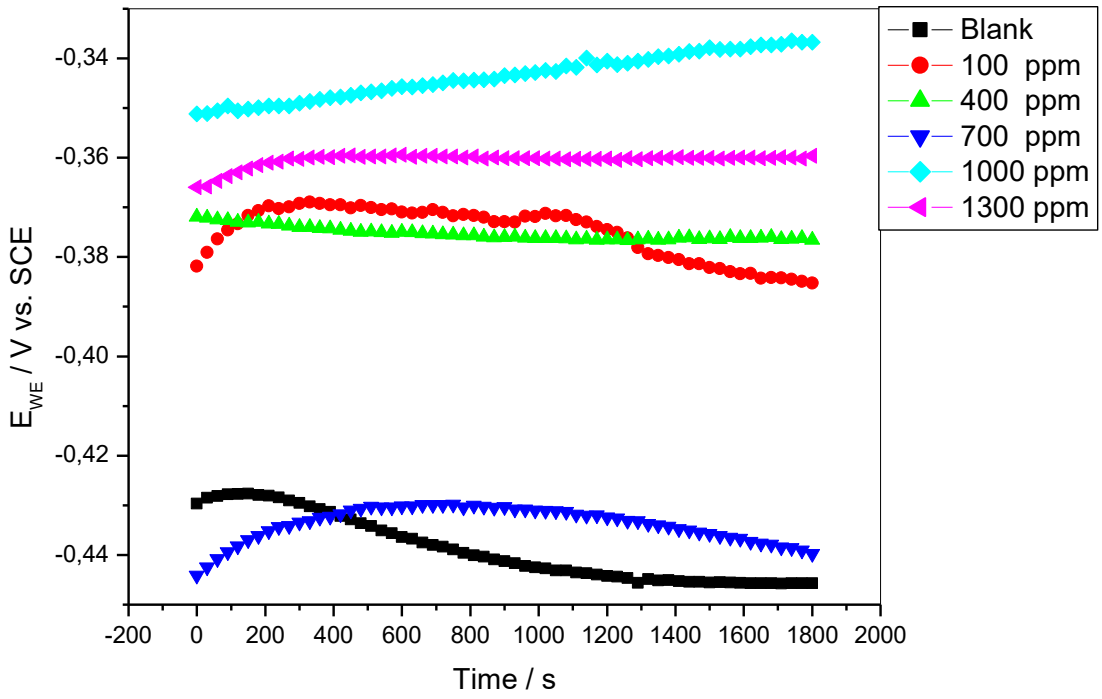


Figure 7.2: Open circuit voltage for mild steel 1.5 M H_2SO_4 solution and non-UV *radiated A. phylicoides*

© University of Venda

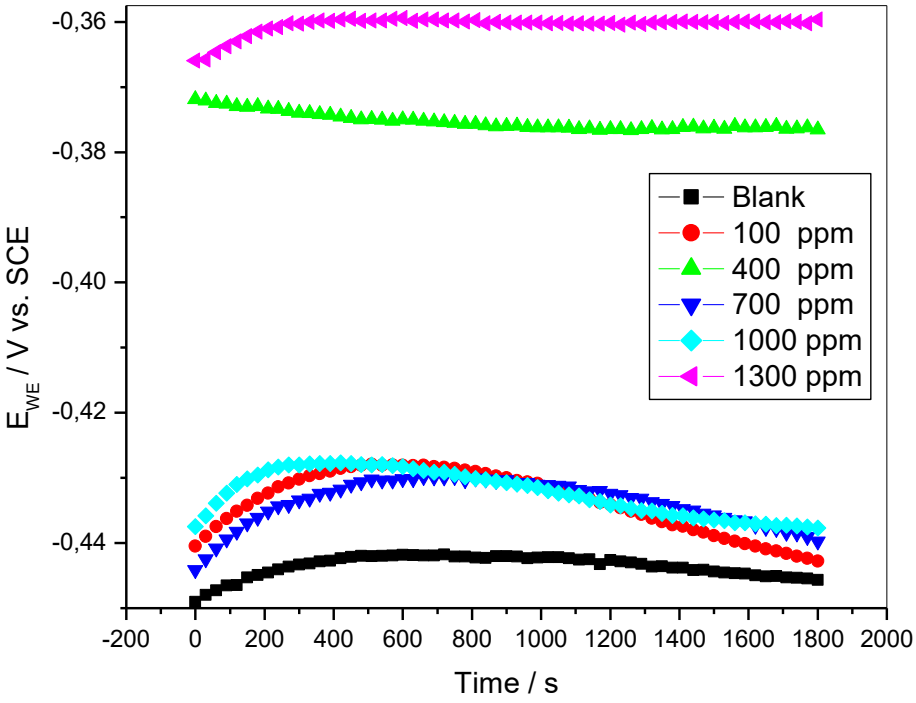


Figure 7.3: Open circuit voltage for mild steel 1.5 M HCl solution and non-UV radiated *A. phylicoides*.

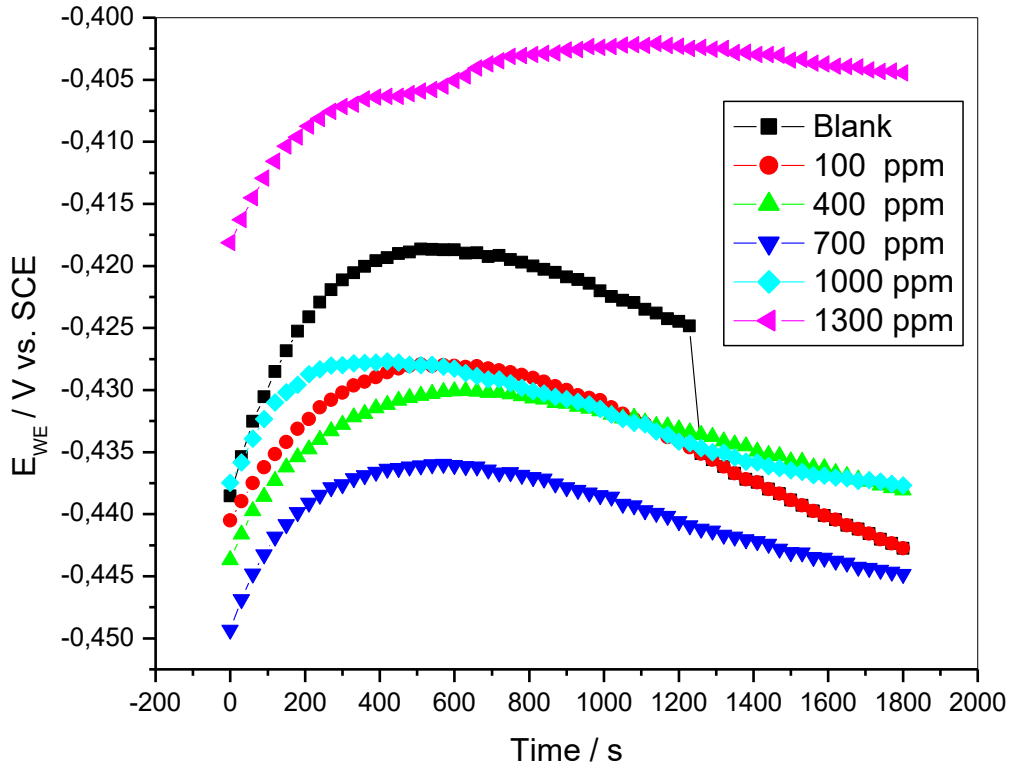


Figure 7.4: Open circuit voltage for mild steel 1.5 M HCl solution and UV radiated *A. phylicoides*.

© University of Venda

The research investigates how *A. phylicoides* extract influences the potential time pattern of mild steel in stagnant solutions of 1.5 M H_2SO_4 and HCl over a period of 30 minutes. Figure 7.1 illustrates the changes in OCV of the working electrode with and without various concentrations of the extract inhibitor. The shift of OCV potentials towards the cathodic side in inhibited solutions compared to the blank test indicates the extract inhibitor's notable ability to hinder the dissolution reaction of cathodic mild steel. This shift implies that the inhibitor could effectively impede corrosion by altering the metal surface's electrochemical behavior. Moreover, the stabilization of the OCV curve of the mild steel electrode after soaking in sulfuric and hydrochloric acid solutions for 1800 seconds suggests that the electrode surface reached equilibrium before further electrochemical processes were conducted. This stability suggests that the system attained a balanced state, providing a reliable foundation for subsequent analysis. The rise in potential in the blank solution is attributed to the formation and thickening of the oxide layer on the metal surface, a common occurrence in corrosive environments that contributes to passivation and reduces corrosion rates. Additionally, the specific surface adsorption effect may influence the potential of the blank solution, further impacting mild steel corrosion behavior. The results underscore the potential of *A. phylicoides* extract as an effective inhibitor in mitigating mild steel corrosion in acidic settings, offering insights into its possible applications in corrosion management strategies. Figures 7.2 and 7.3 depict the OCV-time behavior of mild steel in 1.5 M H_2SO_4 and HCl solutions with and without *A. phylicoides* extract. The OCV-time profile of the mild steel electrode in the corrosive medium was monitored for 1800 seconds, sufficient for the corrosion system to reach equilibrium. In both Figures 7.2 and 7.3, the time profile of the blank metal exhibits a more negative potential compared to the inhibited metal profile, which shifted towards a less negative potential. This observation suggests that anodic protection may be the favoured process. Furthermore, the shift towards a positive potential indicates the adsorption of the investigated inhibitor molecules on the active corrosion centres on the metal surface. Figure 7.4 shows no consistent trend in the OCV variation over time for electrodes with or without varying concentrations of the inhibitor, indicating that the extract acts as a mixed type of inhibitor. In the absence of the inhibitor, the OCV potential moves in a more negative direction, indicating the desorption of corrosion products from the metal surface.

Open circuit voltage UV-radiated and non-UV-radiated *A. phylicoides* on zinc in H_2SO_4 and HCl solutions are shown in Figures 7.5-7.8.

© University of Venda

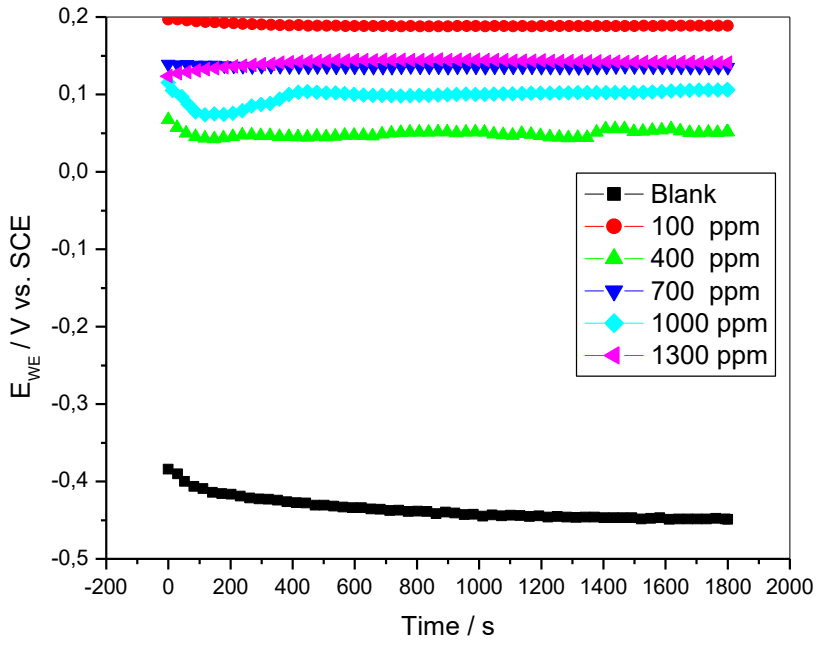


Figure 7.5: Open circuit voltage for zinc 1.5 M H_2SO_4 solution and non-UV radiated *A. phylicoides*.

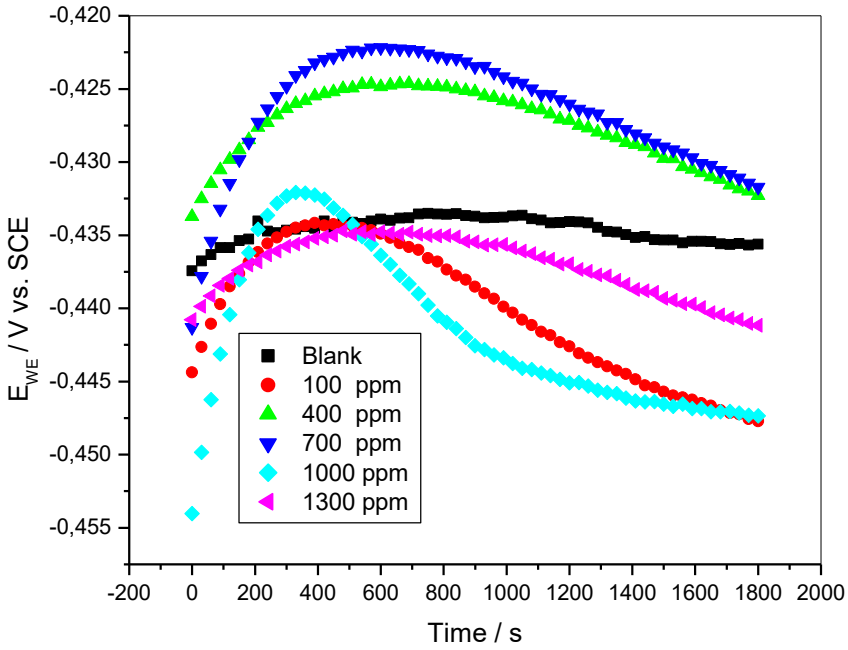


Figure 7.6: Open circuit voltage for zinc 1.5 M H_2SO_4 solution and UV radiated *A. phylicoides*.

© University of Venda

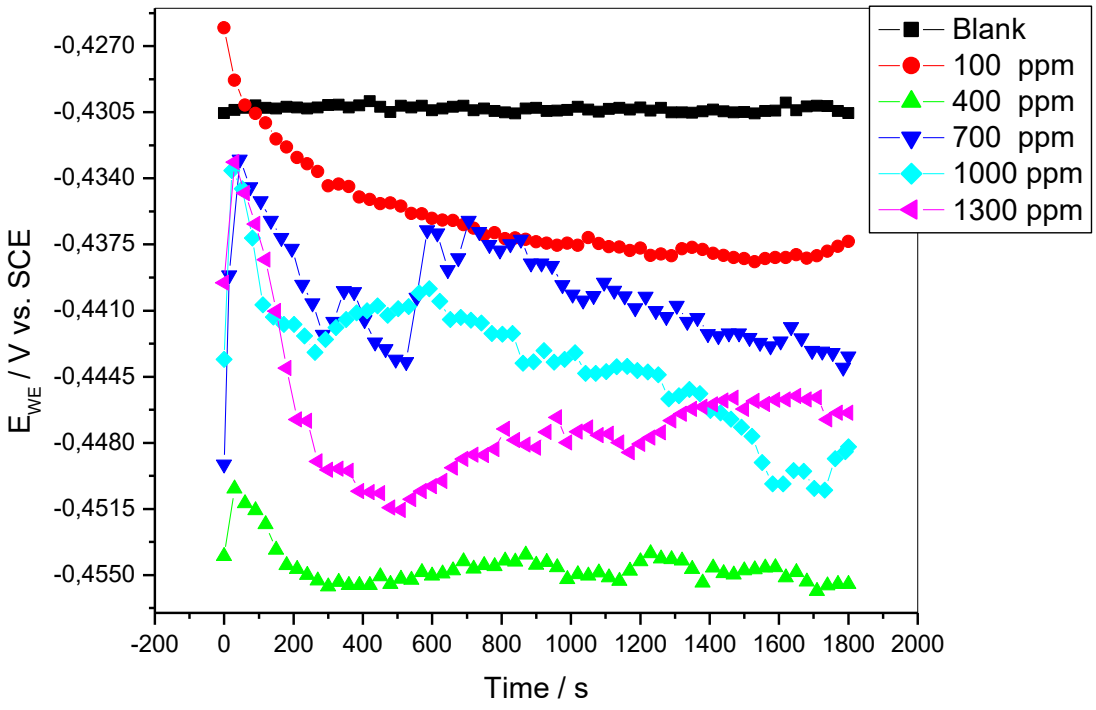


Figure 7.7: Open circuit voltage for zinc 1.5 M HCl solution and non-UV radiated *A. phylicoides*

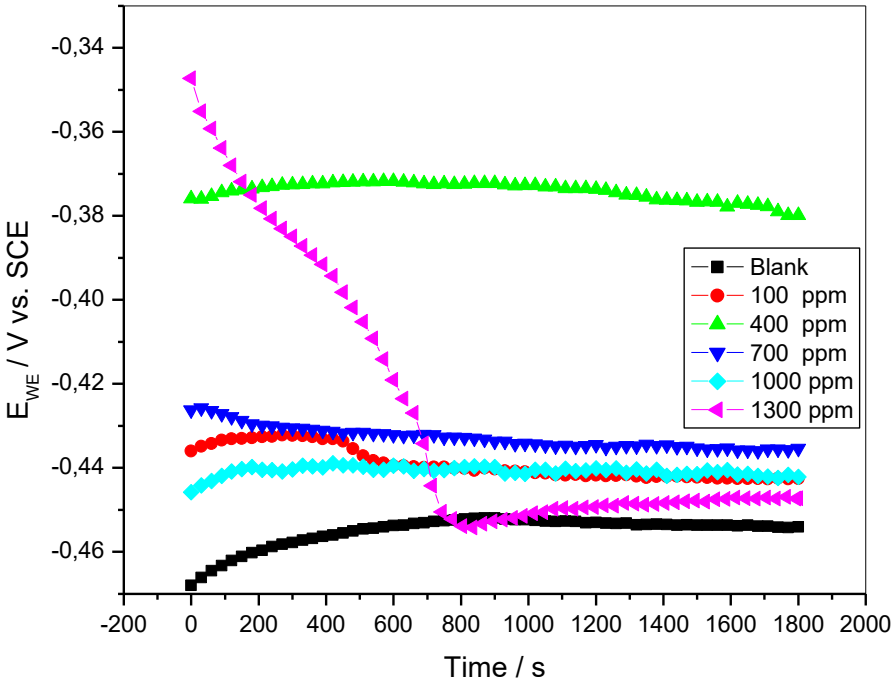


Figure 7.8: Open circuit voltage for zinc 1.5 M HCl solution and UV radiated *A. phylicoides*

© University of Venda

Figures 7.5 to 7.8 illustrate the OCV-time behavior of the zinc working electrode in the corrosive medium, monitored over 1800 seconds, a duration sufficient for the corrosion system to achieve equilibrium. Observing Figures 7.5 and 7.8, it is apparent that the time profile of the blank metal exhibits a more negative potential compared to the inhibited metal profile, which shifts towards a less negative potential. This shift implies that anodic protection might be the preferred process. In Figure 7.6, no consistent trend is evident in the OCV variation over time for electrodes with or without varying concentrations of the inhibitor. This suggests that the extract functions as a mixed type of inhibitor, indicating its potential for versatile corrosion inhibition mechanisms. These findings provide valuable insights into the behavior of zinc in corrosive environments and the inhibitory effects of the *A. phylicoides* extract, contributing to the understanding of corrosion mitigation strategies.

7. 2 Potentiodynamic Polarization (PDP)

Potentiodynamic polarization is an electrochemical technique used to study the corrosion behavior of metals in a solution [435]. It involves sweeping the potential (voltage) of a working electrode at a constant rate while monitoring the resulting current. This method provides information about the electrochemical processes occurring on the metal surface and helps in understanding the corrosion kinetics, corrosion potential, and polarization resistance. Analyzing the potentiodynamic polarization curves helps researchers gain insights into the corrosion behavior of metals, identify the type of corrosion mechanism, and evaluate the effectiveness of corrosion inhibitors. This information is valuable in the design and selection of materials for corrosion-resistant applications.

Corrosion of MS and Zn comprises a simultaneous anodic dissolution of mild steel and the cathodic reduction of hydrogen ions (Marques *et al*., 2016). Potentiodynamic polarization measurements were carried out to fully understand this process. To facilitate this objective, the current potential curves for MS and Zn in hydrochloric and sulphuric acid solutions were obtained in the absence and presence of various concentrations of *A. phylicoides* plant extract used as corrosion inhibitors at 30 °C, as shown in Figures 7.9 – 7.12

© University of Venda

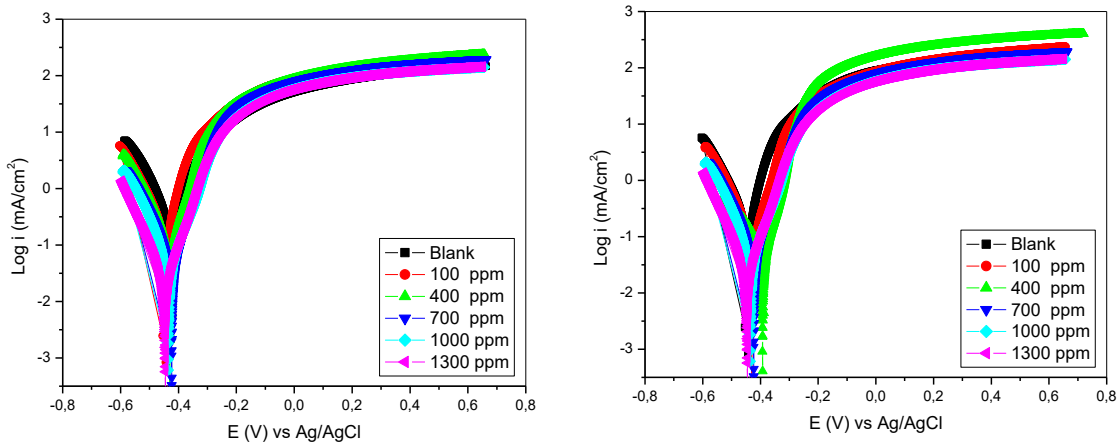


Figure 7.9: Tafel plots for MS in 1.5 M H_2SO_4 before and after UV exposure in the absence and presence of different concentrations of *A. phylicoides* extract

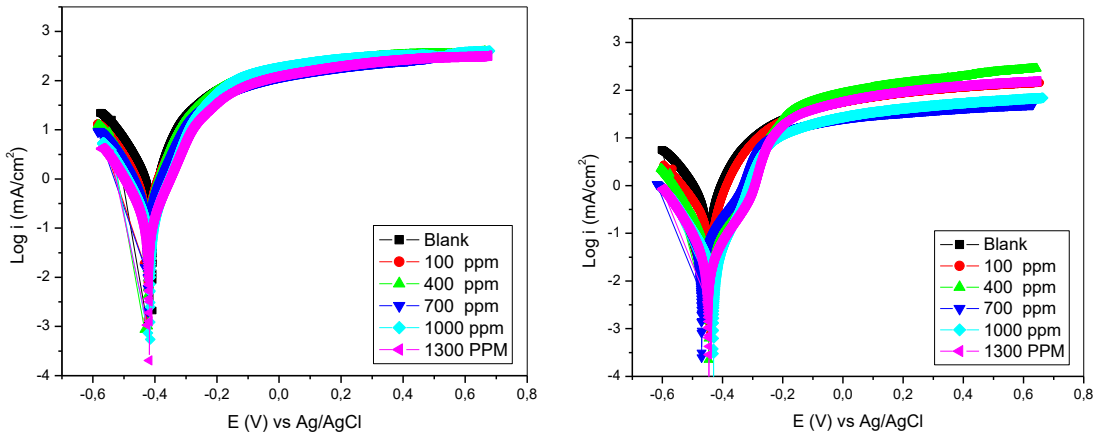


Figure 7.10: Tafel plots for MS in 1.5 M HCl before and after UV exposure in the absence and presence of different concentrations of *A. phylicoides* extract

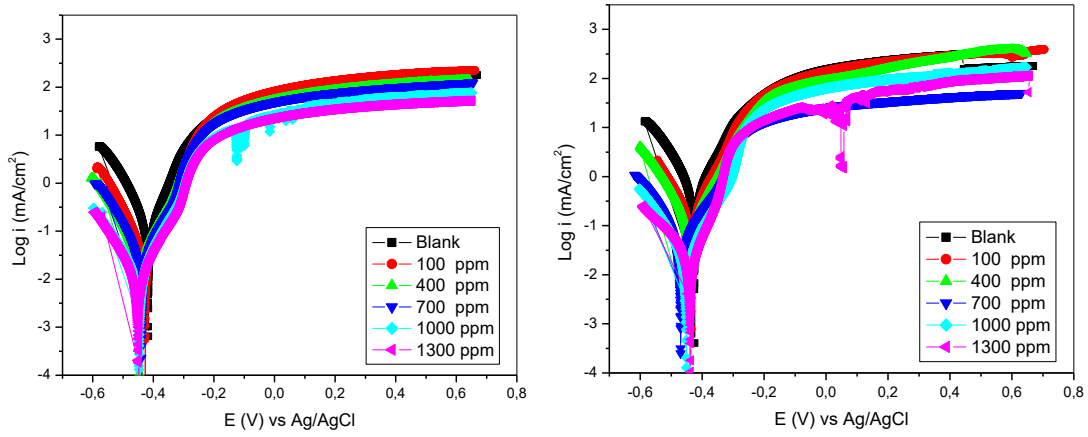


Figure 7.11: Tafel plots for Zn in 1.5 M H_2SO_4 before and after UV exposure in the absence and presence of different concentrations of *A. phylicoides* extract

© University of Venda

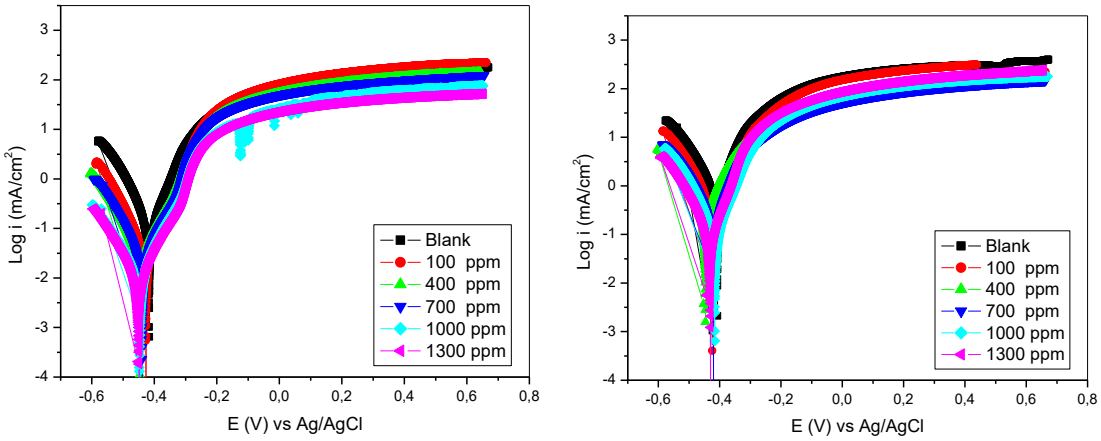


Figure 7.12: Tafel plots for Zn in 1.5 M HCl before and after UV exposure in the absence and presence of different concentrations of *A. phylicoides* extract.

The figures depict the anodic and cathodic half-reactions involved in the corrosion of mild steel and zinc in sulfuric and hydrochloric acid. It is noted that the introduction of all five concentrations of inhibitor affects both half-reactions. Extrapolating the linear Tafel segments from these curves gives significant potentiodynamic parameters such as corrosion current density (i_{corr}), corrosion potential (E_{corr}), anodic Tafel slope (ba), and cathodic Tafel slope (bc) were derived. These parameters are documented in Table 7.1. Subsequently, the potentiodynamic polarization inhibition efficiency (%IE_{PDP}) was calculated. In corrosion studies that involve the use of UV-radiated and non-UV-radiated *A. phylicoides* extract as inhibitors, Tafel plots serve as crucial analytical tools. These plots offer detailed quantitative insights into corrosion rates and various electrochemical parameters, including corrosion potential (E_{corr}), anodic and cathodic Tafel slopes (b_a and b_c), and corrosion current density (i_{corr}). By analyzing these parameters, researchers gain a deeper understanding of how effectively the inhibitors reduce corrosion rates on the metal surface. Furthermore, Tafel polarization plots facilitate a direct comparison of the inhibition efficiency between UV-radiated and non-UV-radiated *A. phylicoides* extracts. A similar trend was observed by Al-Otaibi *et al.* (2014), who studied the corrosion inhibition performance of various plant extracts on mild steel in acidic media. Plotting polarization curves for inhibited and uninhibited systems assists researchers in observing any shifts in the Tafel lines or alterations in their slopes. These changes signify the impact of the inhibitors on the kinetics of corrosion, helping researchers evaluate which form of *A. phylicoides* extract provides superior corrosion protection. Moreover, Tafel polarization plots aid in identifying the underlying corrosion mechanisms inhibited by UV-radiated and non-UV-radiated *A. phylicoides* extracts. A similar

© University of Venda

approach was employed by Shi *et al*. (2010), who utilized Tafel extrapolation to measure the corrosion rate of magnesium alloys. Variations in Tafel slopes or shifts in corrosion potential can reveal changes in the dominant corrosion processes, such as anodic dissolution or cathodic reduction. Understanding these mechanisms is crucial for developing effective corrosion inhibition strategies and optimizing the performance of the inhibitors. Additionally, Tafel plots assist researchers in optimizing the concentration of *A. phylicoides* extract as an inhibitor. Examining the effect of different inhibitor concentrations on corrosion rates and Tafel parameters assists researchers in determining the most efficient concentration for corrosion protection. This optimization process ensures the inhibitors are utilized effectively, maximizing their potential to mitigate corrosion damage on the metal surface. Tafel plots help confirm the mechanisms through which UV radiation enhances the effectiveness of *A. phylicoides* extract as a corrosion inhibitor. By comparing Tafel parameters for inhibited systems with and without UV radiation, researchers can elucidate the role of UV radiation in promoting inhibitor adsorption or altering the corrosion behavior of the metal surface. This confirmation of protection mechanisms is essential for designing corrosion protection strategies that harness the full potential of UV-radiated *A. phylicoides* extract as an inhibitor.

Table 7.1 The potentiodynamic polarization parameters of non-UV radiated *A. phylicoides* extracts and UV radiated *A. phylicoides* extracts for mild steel metal in sulphuric acid

Inhibitor conc. (ppm)	**-E_{corr}(mV) with Ag/AgCl**	**i_{corr} (μA.cm^2)**	**b_a (mV)**	**b_c (mV)**	**C_R (mm/year) X10^{-6}**	**R_p ($\Omega\cdot cm^2$)**	**%IE $_{PDP}$**
MS in H_2SO_4 *Using A. phylicoides* before UV radiation							
0.00	420,424	415,596	118,2	151,3	9.644	69.33	-
100	440,700	158,896	58,7	97,4	3.687	100.09	61,77
400	430,025	151,651	79,8	106,8	3.519	130.77	63,51
700	426,036	104,906	84,9	116,3	2.434	203.13	74,76
1000	439,435	87,195	92,8	102,9	2.023	242.99	79,02
1300	453,014	33,334	80,2	88,7	0.774	548.64	91,98
MS in H_2SO_4 *Using A. phylicoides* after UV radiation							
0.00	453,809	401,804	91,5	126,4	9.324	57.36	-
100	422,948	127,810	67,5	105,0	2.966	139.59	68,19
400	369,262	92,003	22,0	234,6	2.135	94.93	77,10
700	411,447	83,022	73,9	119,2	1.927	238.59	79,34
1000	438,738	77,462	90,1	99,5	1.798	265.05	80,72
1300	481,393	71,796	108,0	90,5	1.666	297.80	82,13
MS in HCl *Using A. phylicoides* before UV radiation							
0.00	403,340	815,660	66,2	107,5	18.928	21.81	-

© University of Venda

100	431,743	306,622	78,4	62,7	7.115	49.34	62,41
400	425,562	298,011	80,1	88,6	6.916	61.29	63,46
700	428,456	275,947	80,2	79,4	6.404	62.78	66,17
1000	429,474	207,560	86,6	90,6	4.817	92.63	74,55
1300	430,228	187,096	92,2	96,6	4.342	109.48	77,06
MS in HCl *Using A. phylicoides* after UV radiation							
0.00	452,308	958,063	156,0	192,4	22.233	39.04	-
100	450,850	230,291	102,2	131,1	5.344	108.28	75,97
400	451,406	116,960	105,7	116,0	2.714	205.32	87,79
700	490,088	103,565	122,5	118,4	2.403	252.43	89,19
1000	467,629	057,363	106,9	102,8	1.331	396.69	94,01
1300	444,492	25,903	93,8	90,5	0.601	772.12	97,30

Table 7.1 presents potentiodynamic polarization parameters for non-UV-radiated *A. phylicoides* extracts and UV-radiated *A. phylicoides* extracts used as inhibitors for mild steel in sulphuric acid. It outlines inhibitor concentrations measured in parts per million (ppm) alongside their corresponding corrosion potentials ($-E_{corr}$) with respect to the Ag/AgCl reference electrode. Generally, a more negative $-E_{corr}$ value indicates a higher tendency for the metal to corrode [436]. For non-UV radiated *A. phylicoides* extract $-E_{corr}$ values range from approximately 420 mV to 453 mV, with fluctuations observed across different inhibitor concentrations. Notably, the lowest $-E_{corr}$ value of 420 mV is recorded in the absence of the inhibitor (0.00 ppm), suggesting heightened corrosion susceptibility without inhibition. Conversely, the highest $-E_{corr}$ value of 453 mV is noted at the highest inhibitor concentration of 1300 ppm, indicating the least corrosion tendency with increased inhibitor presence. There appears to be a trend of decreasing corrosion potential with rising inhibitor concentration up to a certain threshold (around 1000 ppm), implying enhanced corrosion inhibition. However, a slight increase in $-E_{corr}$ at 1300 ppm suggests the possibility of an optimal inhibitor concentration beyond which further increments may not yield added corrosion protection or could even lead to adverse effects. The corrosion current density values range from approximately 33.3 $\mu A.cm^{-2}$ to 415.6 $\mu A.cm^{-2}$, indicating varying rates of corrosion inhibition across different inhibitor concentrations. Notably, there is a discernible trend of decreasing i_{corr} values with increasing non-UV radiated *A. phylicoides* extract concentration, suggesting improved corrosion inhibition as the concentration of the *A. phylicoides* extract rises. The highest i_{corr} value of 415.6 $\mu A.cm^{-2}$ is observed at 0.00 ppm, indicating a relatively high rate of corrosion in the absence of the inhibitor. Conversely, the lowest i_{corr} value of 33.3 $\mu A.cm^{-2}$ is recorded at the highest inhibitor concentration of 1300 ppm, suggesting the most effective inhibition of corrosion at this concentration. The provided table offers insights into the

© University of Venda

corrosion inhibition potential of *A. phylicoides* extract for mild steel in sulfuric acid, with varying inhibitor concentrations. It includes parameters such as anodic polarization resistance (b_a), cathodic polarization resistance (b_c), and inhibition efficiency (IE%). An increase in polarization resistance generally indicates a decrease in the corrosion rate. The data reveals that both anodic and cathodic polarization resistances increase with rising inhibitor concentration, suggesting a reduction in the rates of anodic and cathodic corrosion. Furthermore, the inhibition efficiency (IE%) shows a consistent upward trend with increasing inhibitor concentration, reaching its peak of 91.98% at the highest concentration of 1300 ppm. This indicates significant corrosion inhibition at higher concentrations of *A. phylicoides* extract. The findings support the conclusion that *A. phylicoides* extract demonstrates corrosion inhibition potential for mild steel in sulphuric acid, with higher concentrations proving more effective in mitigating corrosion. These results imply that *A. phylicoides* extract could serve as a promising corrosion inhibitor, particularly at elevated concentrations, warranting further investigation into its potential applications in corrosion control strategies.

For UV radiated *A. phylicoides* extracts utilized as inhibitors for mild steel metal in sulphuric acid. The $-E_{corr}$ values listed range from approximately 369 mV to 481 mV, showcasing variability across different inhibitor concentrations. The data indicates the potential of *A. phylicoides* extract as a corrosion inhibitor for mild steel in sulphuric acid, highlighting the importance of determining an optimal concentration for effective corrosion mitigation. An increase in polarization resistance typically correlates with a reduction in the corrosion rate. The data shows that both anodic and cathodic polarization resistances generally increase with higher inhibitor concentrations, indicating a decrease in the rates of anodic and cathodic corrosion [437]. Furthermore, inhibition efficiency (IE%) demonstrates an overall upward trend with increasing inhibitor concentration, reaching its peak of 82.13% at the highest concentration of 1300 ppm. This suggests significant corrosion inhibition at elevated concentrations of *A. phylicoides* extract. The findings support the notion that UV-radiated *A. phylicoides* extract exhibits corrosion inhibition potential for mild steel in sulfuric acid. Higher concentrations of the inhibitor tend to be more effective in mitigating corrosion, as evidenced by increased polarization resistances and inhibition efficiencies. These results imply that *A. phylicoides* extract could serve as a promising corrosion inhibitor, particularly at higher concentrations, and warrant further investigation for its potential applications in corrosion control strategies.

© University of Venda

It was necessary to also test the same experiments using a different acid which is HCl in this case. A similar trend has been observed, thus including, increment in inhibition efficiency as corrosion of *A. phylicoides* extract increases, maximum inhibition efficiency obtained in the absence of UV radiated *A. phylicoides* extract was 77.06% while for UV radiated *A. phylicoides* extract is 97.30% confirming that UV radiated *A. phylicoides* extract is likely to offer better protection to mild steel. I_{corr} values increase as the concentration of *A. phylicoides* extract increases. Table 7.1 show an increase in resistance polarization

Table 7.2 The potentiodynamic polarization parameters of non-UV radiated *A. phylicoides* extracts and UV radiated *A. phylicoides* extracts for mild steel metal in hydrochloric acid

Inhibitor conc. (ppm)	**$-E_{corr}$(mV) with Ag/AgCl**	**i_{corr} (μA.cm^2)**	**b_a (mV)**	**b_c (mV)**	**C_R (mm/year) x 10^{-6}**	**R_p (Ω·cm²)**	**%IE PDP**
Zn in H_2SO_4 *Using A. phylicoides* before UV radiation							
0.00	421,426	681,072	138,7	164,3	20.393	47.950	-
100	424,504	161,570	096,6	140,2	4.838	153.705	76,28
400	464,715	104,794	111,4	124,2	3.138	243.333	84,61
700	456,278	066,432	099,4	110,6	1.989	342.177	90,25
1000	489,257	031,992	112,1	108,3	0.958	747.631	95,30
1300	466,362	018,518	92,9	111,6	0.555	1188.772	97,28
Zn in H_2SO_4 *Using A. phylicoides* after UV radiation							
0.00	431,902	770,773	119,0	115,2	23.096	32.976	-
100	442,212	157,145	86,2	88,5	4.708	120.660	79,61
400	436,278	116,349	86,5	102,5	3.485	175.074	84,90
700	473,382	94,374	110,5	133,5	2.826	278.168	87,76
1000	488,209	58,462	103,2	111,8	1.749	398.580	92,42
1300	442,501	25,581	70,5	152,4	0.765	818.187	96,68
Zn in HCl *Using A. phylicoides* before UV radiation							
0.00	451,726	642,447	158,8	124,5	19.237	47.167	-
100	440,636	093,026	093,3	100,2	2.786	225.512	85,52
400	461,002	68,140	99,3	106,0	2.040	326.716	89,39
700	457,672	60,584	98,3	104,6	1.814	363.205	90,57
1000	476,920	24,710	101,3	108,4	0.740	920.182	96,15
1300	463,841	14,272	87,8	100,2	0.427	1423.723	97,78
Zn in HCl *Using A. phylicoides* after UV radiation							
0.00	430,124	635,379	126,3	111,2	17.993	40.413	-
100	429,777	171,427	53,7	31,4	4.859	50.188	73,02
400	455,102	117,958	53,7	20,4	3.342	54.421	81,44
700	418,229	110,428	49,9	64,3	3.132	110.477	82,62
1000	416,826	66,886	56,8	56,5	1.896	183.881	89,47
1300	431,909	58,055	55,5	58,3	1.645	212.660	90,86

© University of Venda

Table 7.2 displays potentiodynamic polarization parameters for mild steel (MS) in hydrochloric acid, comparing non-UV radiated and UV radiated *A. phylicoides* extracts as inhibitors. It includes inhibitor type and concentration, corrosion potential ($-E_{corr}$) with Ag/AgCl reference electrode, anodic (b_a) and cathodic (b_c) Tafel slopes, corrosion current density (i_{corr}), and percentage inhibition efficiency (%IE PDP). Data is presented for different inhibitor concentrations and conditions (before and after UV radiation) for two types of inhibitors: Zn in H_2SO_4 and MS in HCl.

For each type of inhibitor (Zn in H_2SO_4 or HCl), the table is divided into two sections: one for using *A. phylicoides* before UV radiation and another for using *A. phylicoides* after UV radiation. Within each section, data is provided for different concentrations of the inhibitor. For example, in the case of MS in HCl using *A. phylicoides* before UV radiation, at a concentration of 0.00 ppm, the corrosion potential ($-E_{corr}$) is 451.726 mV, the anodic Tafel slope (b_a) is 642.447 mV, the cathodic Tafel slope (b_c) is 158.8 mV, the corrosion current density (i_{corr}) is 124.5 $\mu A/cm^2$, and the percentage inhibition efficiency ($\%IE_{PDP}$) is not applicable as it serves as the baseline. As the concentration of the inhibitor increases, the corrosion potential, Tafel slopes, and inhibition efficiency change accordingly. This table provides a detailed comparison of the corrosion inhibition properties of *A. phylicoides* extracts under different conditions and concentrations, offering valuable insights for corrosion protection strategies. For zinc exposed to hydrochloric acid, the maximum inhibition efficiency was 97.78% without UV radiation and 90.86% with UV-radiated *A. phylicoides* extract. Conversely, when sulfuric acid was used, the maximum inhibition efficiency was 97.28% without UV radiation and 96.68% with UV-radiated *A. phylicoides* extract. This suggests that non-UV radiated *A. phylicoides* may offer better inhibition efficiency overall. There wasn't a consistent trend observed in the corrosion potential ($-E_{corr}$) values, as they fluctuated. However, the corrosion current density (i_{corr}) values at 0.00 ppm were higher than when *A. phylicoides* extract was present. Furthermore, as the concentration of *A. phylicoides* extract increased, the i_{corr} values decreased, indicating increased protection offered by the inhibitor on zinc.

In the absence of the inhibitor, zinc exhibited significantly high corrosion rates, with values reaching up to 23.10 mm/year, confirming its active dissolution in the corrosive medium. Upon the introduction of *A. phylicoides* at varying concentrations, a marked reduction in corrosion rate was observed. At 100 ppm, the corrosion rate dropped sharply, and at the

© University of Venda

highest concentration of 1300 ppm, values as low as 0.43 to 0.76 mm/year were recorded. This progressive decrease in corrosion rate with increasing inhibitor concentration indicates that the plant extract effectively suppresses zinc corrosion, likely by forming a protective film on the metal surface that impedes electrochemical reactions.

The polarization resistance (Rp) data further supports the inhibitory performance of *A. phylicoides*. In blank solutions, Rp values were relatively low, ranging from approximately 32 to 50 Ω·cm², indicating minimal resistance to charge transfer. However, in the presence of the inhibitor, Rp increased significantly, with values exceeding 1400 Ω·cm² at 1300 ppm. This substantial increase in Rp confirms the development of a surface barrier that resists both anodic and cathodic processes.

7.3 Electrochemical Impedance Spectroscopy (EIS)

The session delves into the examination of how mild steel and zinc corrode in acidic solutions, as well as the influence of *A. phylicoides* plant extract on corrosion prevention, utilizing electrochemical impedance spectroscopy. The study evaluates the efficacy of the extract in inhibiting corrosion both before and after exposure to UV radiation. Electrochemical impedance spectroscopy proves advantageous in monitoring the corrosion progression of metals over time [438]. The Nyquist plots, depicting impedance spectra, demonstrate the corrosion behavior of mild steel and zinc in various acidic solutions containing different concentrations of both UV-treated and untreated *A. phylicoides* leaves extract inhibitors at 303K. The size of these plots increases with higher inhibitor concentrations, indicating a charge transfer mechanism impacting the corrosion of mild steel and zinc in acidic environments. The presence of a single Nyquist semi-circle, whether with or without UV-radiated *A. phylicoides* extract, suggests that the corrosion of the working electrode involves a charge transfer process. Similar shapes of the Nyquist semi-circle for both the blank and the inhibitor indicate a shared corrosion mechanism. Moreover, with increasing concentrations of examined UV-radiated *A. phylicoides*, the Nyquist semi-circle diameters become larger compared to the uninhibited solution (blank). This suggests that a protective coating has been effectively deposited on the metal surface, preventing aggressive attacks by Cl^- and SO_4^{-2} ions. Zinc metal in aggressive solutions exhibits notably increased resistance in the presence of various concentrations of UV-radiated *A. phylicoides*, with

© University of Venda

corrosion inhibition efficiency rising alongside the concentration of UV-radiated *A. phylicoides* extract.

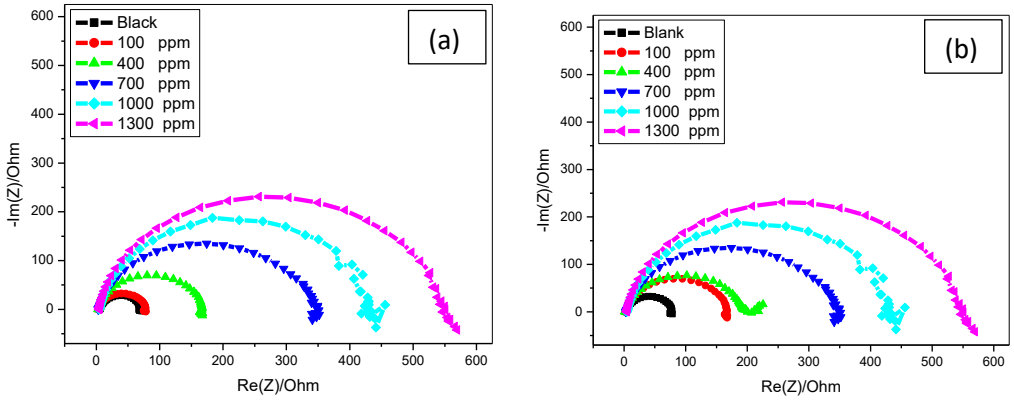


Figure 7.13: Nyquist plot for mild steel in sulphuric acid exposed in (a) non-UV radiation *A. phylicoides* extract and (b) UV radiation *A. phylicoides* extract

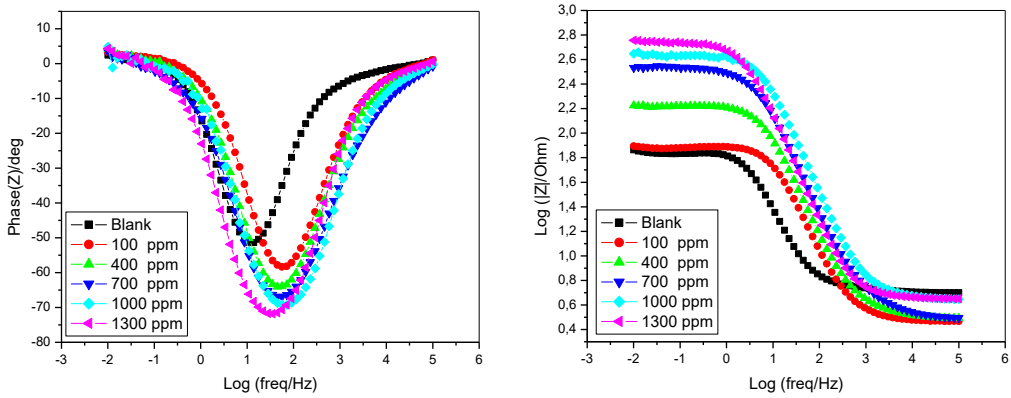


Figure 7.14: Bode plots of mild steel in 1.5 M H_2SO_4 in the absence and presence of different concentrations of non-UV radiated *A. phylicoides* extract inhibitor

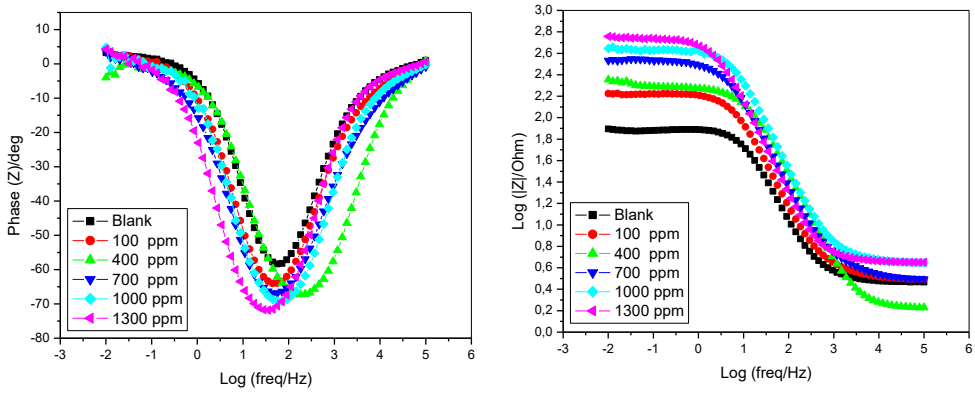


Figure 7.15: Bode plots of mild steel in 1.5 M H_2SO_4 in the absence and presence of different concentrations of UV radiated *A. phylicoides* extract inhibitor

© University of Venda

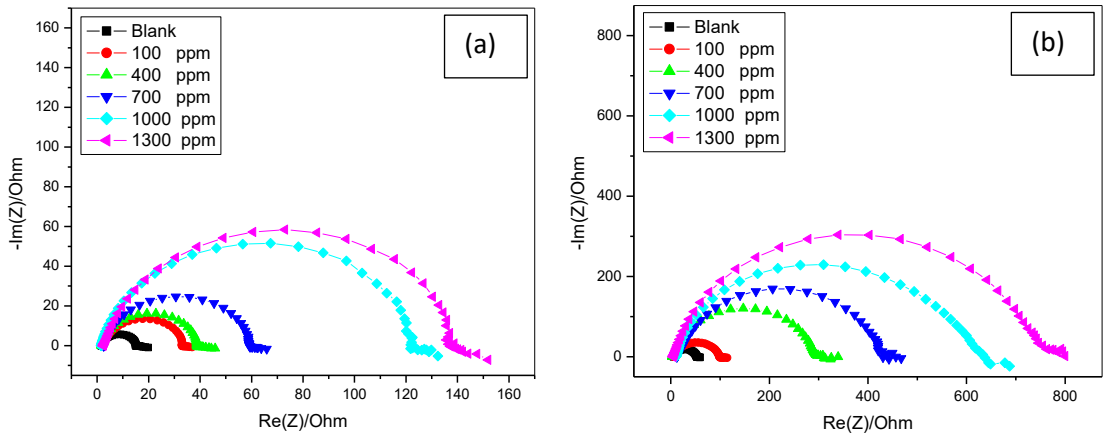


Figure 7.16: Nyquist plot for mild steel in hydrochloric acid exposed in (a) non-UV radiation *A. phylicoides* extract and (b) UV radiation *A. phylicoides* extract

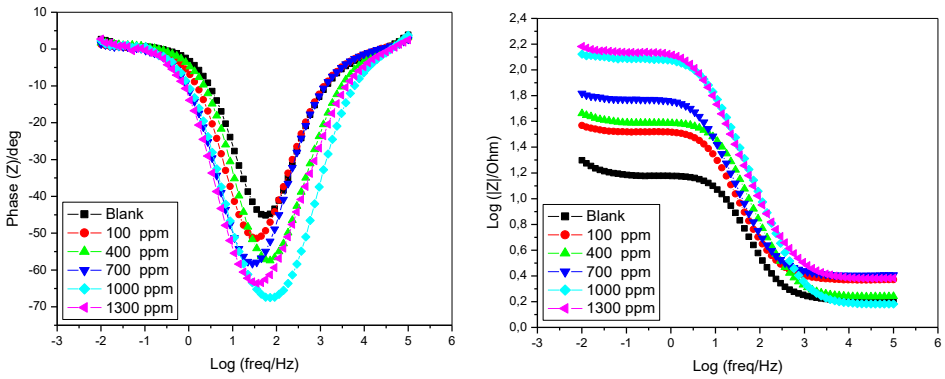


Figure 7.17: Bode plots of mild steel in 1.5 M HCl in the absence and presence of different concentrations of non-UV radiated *A. phylicoides* extract inhibitor

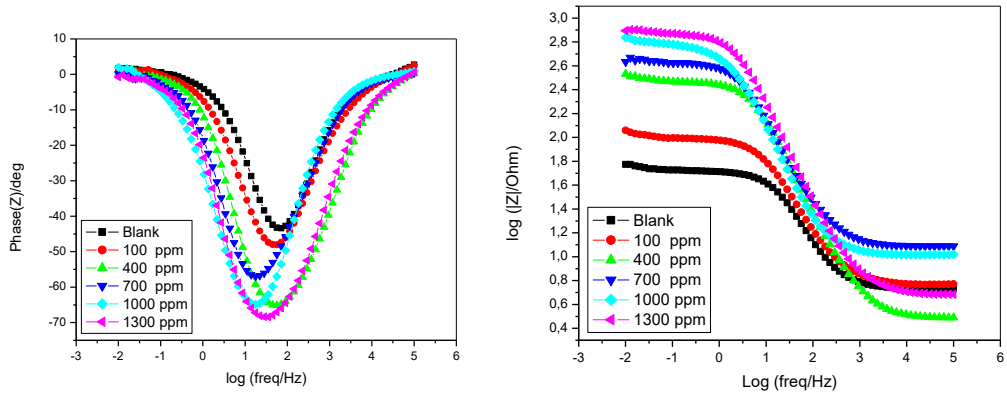


Figure 7.18: Bode plots of mild steel in 1.5 M HCl in the absence and presence of different concentrations of UV radiated *A. phylicoides* extract inhibitor

© University of Venda

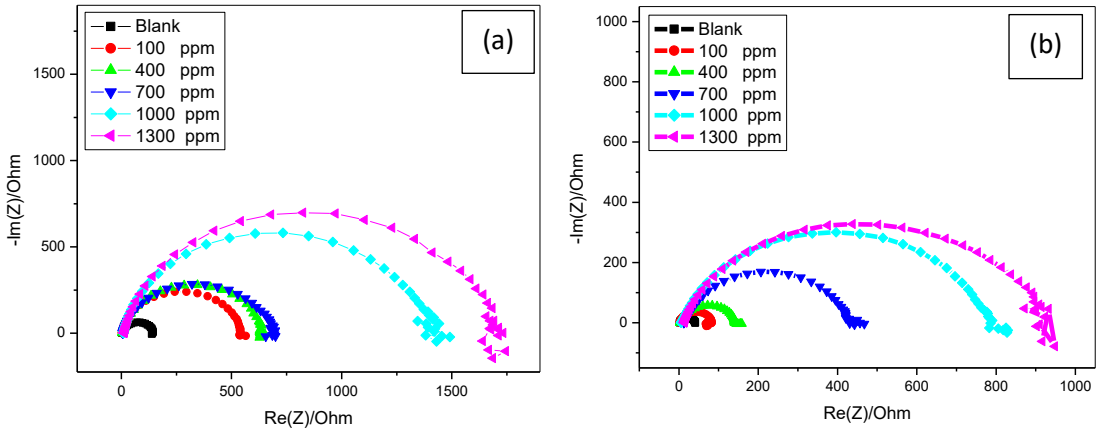


Figure 7.19: Nyquist plot for zinc in sulphuric acid exposed in (a) non-UV radiation *A. phylicoides* extract and (b) UV radiation *A. phylicoides* extract

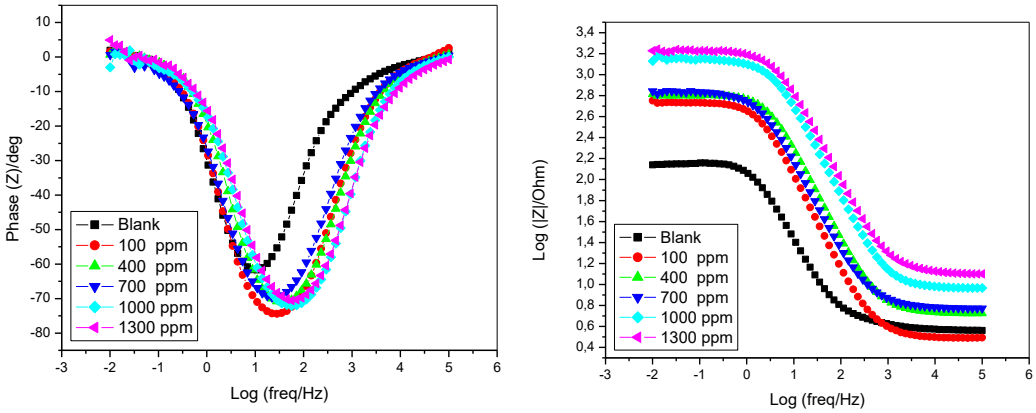


Figure 7.20: Bode plots of zinc in 1.5 M H_2SO_4 in the absence and presence of different concentrations of non-UV radiated *A. phylicoides* extract inhibitor

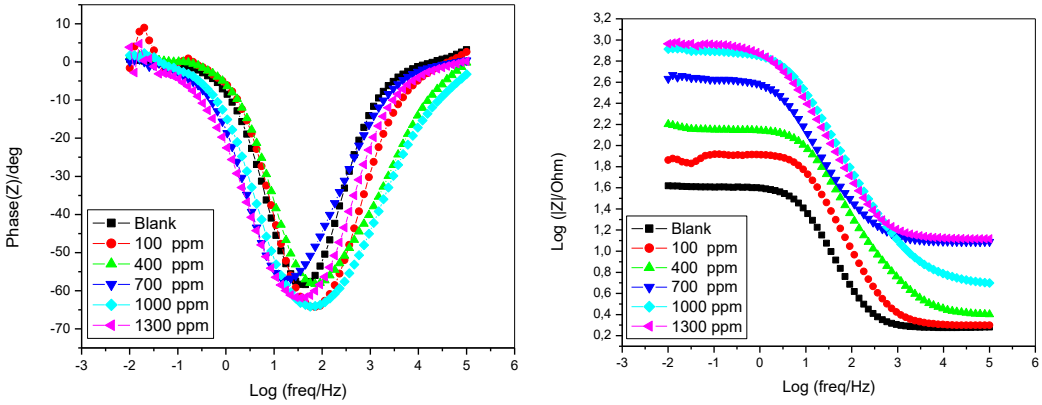


Figure 7.21: Bode plots of zinc in 1.5 M H_2SO_4 in the absence and presence of different concentrations of UV radiated *A. phylicoides* extract inhibitor

© University of Venda

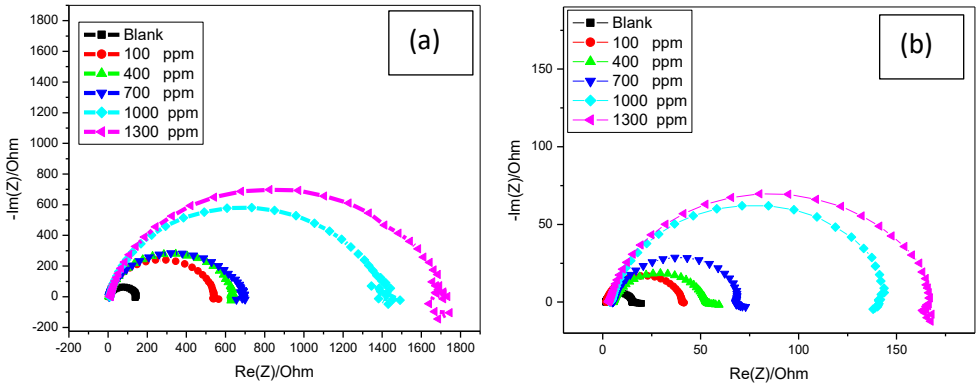


Figure 7.22: Nyquist plot for zinc in hydrochloric acid exposed in (a) non-UV radiation *A. phylicoides* extract and (b) UV radiation *A. phylicoides* extract

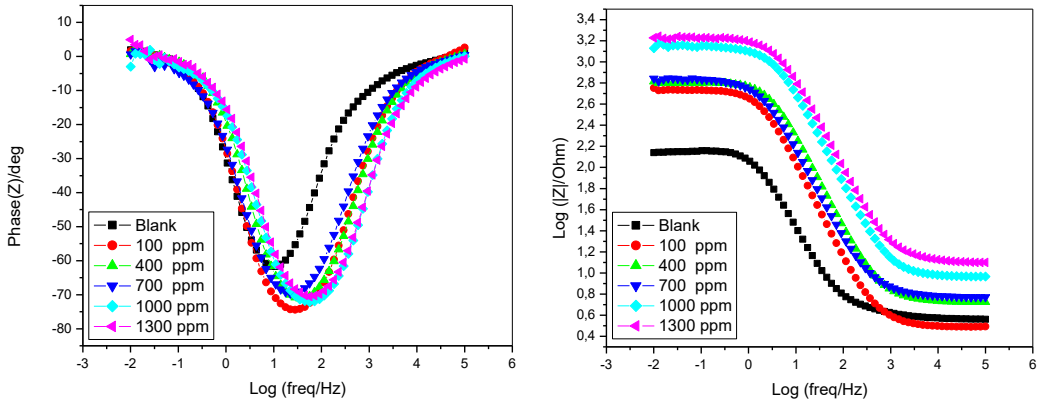


Figure 7.23: Bode plots of zinc in 1.5 M HCl in the absence and presence of different concentrations of non-UV radiated *A. phylicoides* extract inhibitor

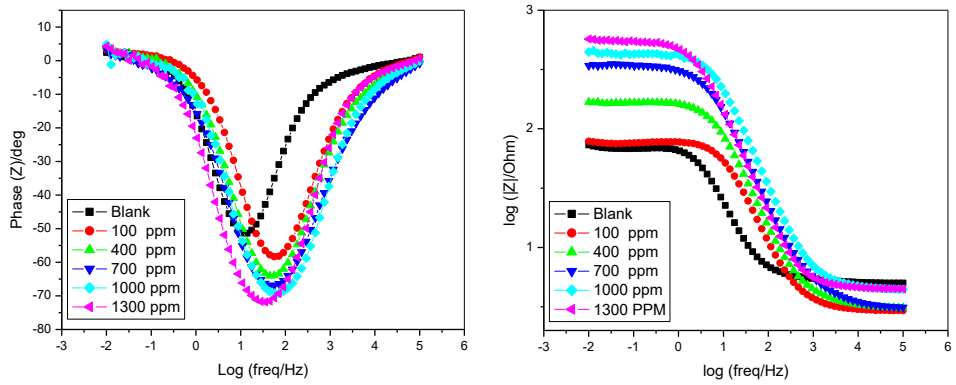


Figure 7.24: Bode plots of zinc in 1.5 M HCl in the absence and presence of different concentrations of UV-radiated *A. phylicoides* extract inhibitor

© University of Venda

Figures 7.13-7.24 display the Nyquist and Bode plots. The phase angle exhibited a single peak both with and without various concentrations of UV-radiated *A. phylicoides* extract, indicating the presence of a single time constant, mirroring the Nyquist plot. Increasing the inhibitor extract concentration resulted in higher impedance magnitude across all frequencies, suggesting UV-radiated *A. phylicoides* molecules' adsorption on the metal surface. The Bode plots showed a broadening trend at higher concentrations, indicating increased inhibitor molecule adsorption. The high-frequency section of the Bode and phase angle plots illustrates behaviour characteristics of an inhomogeneous surface layer, while the low-frequency region depicts charge transfer reactions. At 0 and 5 Hz, the phase angle and log impedance values were close to zero, indicating the resistive nature of zinc metal and the solution's resistance between the reference and zinc metal electrode. Figures 7.14 and 7.15 display Bode diagrams of zinc and mild steel with different inhibitor concentrations, showing that a wider frequency range with significant phase angles and increased impedance modulus at low frequencies were observed with higher *A. phylicoides* concentrations. Moreover, results from UV-radiated and non-UV-radiated *A. phylicoides* showed similar protective abilities on zinc and mild steel against corrosion in concentrations ranging from 100ppm to 1300ppm.

The corrosion reactions' impedance characteristics were elucidated using a straightforward electrical model consisting of solution resistance (R_s) indicated by R1, charge transfer resistance (R_{ct}) indicated by R2, and constant phase element (CPE) indicated by Q2 as illustrated in Figure 7.25.

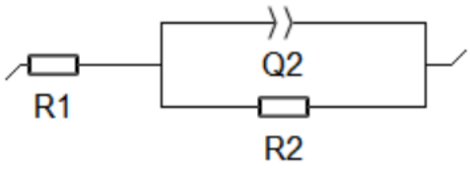


Figure 7.25: Equivalent circuit used to fit the impedance spectra obtained for MS and Zn corrosion in 1.50 M HCl, H_2SO_4 in the absence and presence of *A. phylicoides* extract

© University of Venda

Table 7.3: Electrochemical impedance spectroscopy (EIS) parameters such as the resistance of charge transfer (R_{ct}) and constant phase element (Q) using non-UV-radiated *A. phylicoides* in 1.5 M H_2SO_4 in mild steel metal

Inhibitor	**Metal**	**Concentration (ppm)**	**R1 (Ω)**	**Q2 (F.S(a-1) x10^{-3}**	**a2**	**R2 (Ω)**	**%IE**
A. phylicoides	Mild steel	00	5.2220	1.0460	0.8865	65.13	
		100	3.0080	0.3311	0.8792	74.89	13.03
		400	3.2560	0.2562	0.8686	165.5	60.65
		700	3.3140	0.1943	0.8402	345.9	81.17
		1000	4.5990	0.0099	0.8894	439.8	85.19
		1300	4.5710	0.1554	0.9053	545.2	88.05

Table 7.4: Electrochemical impedance spectroscopy (EIS) parameters such as the resistance of charge transfer (R_{ct}) and constant phase element (Q) using UV-radiated *A. phylicoides* in 1.5 M H_2SO_4 in mild steel metal

Inhibitor	**Metal**	**Concentration (ppm)**	**R1 (Ω)**	**Q2 (F.S(a-1) x10^{-3}**	**a2**	**R2 (Ω)**	**%IE**
A. phylicoides	Mild steel	00	5.2220	1.0460	0.8865	65.13	
		100	3.0146	0.0512	0.7890	171.3	61.98
		400	1.6770	0.1307	0.8581	196.9	66.92
		700	3.2110	0.2901	0.8701	351.3	81.46
		1000	4.5990	0.0099	0.8894	430.8	84.88
		1300	4.4510	0.1843	0.7021	555.7	88.28

Table 7.5: Electrochemical impedance spectroscopy (EIS) parameters such as the resistance of charge transfer (R_{ct}) and constant phase element (Q) using non-UV-radiated *A. phylicoides* in 1.5 M HCl in mild steel metal

Inhibitor	**Metal**	**Concentration (ppm)**	**R1 (Ω)**	**Q2 (F.S(a-1) x10^{-3}**	**a2**	**R2 (Ω)**	**%IE**
A. phylicoides	Mild steel	00	1.6160	1.3590	0.8641	14.16	-
		100	2.3570	0.9856	0.8758	31.69	55.32
		400	1.7430	0.5633	0.8816	38.38	63.11
		700	2.5610	0.7736	0.8905	58.11	75.63
		1000	1.5190	0.3237	0.8860	123.3	88.52
		1300	2.4350	0.4317	0.8563	139.9	89.88

© University of Venda

Table 7.6: Electrochemical impedance spectroscopy (EIS) parameters such as the resistance of charge transfer (R_{ct}) and constant phase element (Q) using UV-radiated *A. phylicoides* in 1.5 M HCl in mild steel metal

Inhibitor	**Metal**	**Concentration (ppm)**	**R1 (Ω)**	**Q2 (F.S(a-1) x10^{-3}**	**a2**	**R2 (Ω)**	**%IE**
A. phylicoides	Mild steel	00	1.6160	1.3590	0.8641	14.16	-
		100	5.8670	0.4161	0.7944	96.18	85.28
		400	3.1300	0.1923	0.8371	302.1	95.31
		700	12.35	0.2210	0.8181	430.6	96.71
		1000	10.43	0.2210	0.8632	607.4	97.67
		1300	4.969	0.1464	0.8450	766.5	98.15

Table 7.7: Electrochemical impedance spectroscopy (EIS) parameters such as the resistance of charge transfer (R_{ct}) and constant phase element (Q) using non-UV-radiated *A. phylicoides* in 1.5 M H_2SO_4 in zinc metal

Inhibitor	**Metal**	**Concentration (ppm)**	**R1 (Ω)**	**Q2 (F.S(a-1) x10^{-3}**	**a2**	**R2 (Ω)**	**%IE**
A. phylicoides	Zinc	00	1.8890	0.7551	0.9095	38.94	
		100	3.1520	0.1972	0.9152	544.2	92.84
		400	5.3890	0.1154	0.9001	637.4	93.89
		700	6.0610	0.1682	0.8794	686.2	94.33
		1000	9.3120	0.0044	0.8977	1397	97.21
		1300	12.88	0.0034	0.8847	1688	97.69

Table 7.8: Electrochemical impedance spectroscopy (EIS) parameters such as the resistance of charge transfer (R_{ct}) and constant phase element (Q) using UV-radiated *A. phylicoides* in 1.5 M H_2SO_4 in zinc metal

Inhibitor	**Metal**	**Concentration (ppm)**	**R1 (Ω)**	**Q2 (F.S(a-1) x10^{-3}**	**a2**	**R2 (Ω)**	**%IE**
A. phylicoides	Zinc	00	1.8890	0.7551	0.9095	38.94	
		100	2.0170	0.2801	0.9124	77.2	49.56
		400	2.5830	0.2750	0.7872	145.5	73.24
		700	12.35	0.2210	0.8181	430.6	90.96
		1000	5.2540	0.0099	0.7961	802.0	95.14
		1300	12.97	0.1134	0.8261	898.7	95.67

© University of Venda

Table 7.9: Electrochemical impedance spectroscopy (EIS) parameters such as the resistance of charge transfer (R_{ct}) and constant phase element (Q) using non-UV-radiated *A. phylicoides* in 1.5 M HCl in zinc metal

Inhibitor	**Metal**	**Concentration (ppm)**	**R1 (Ω)**	**Q2 (F.S(a-1) x10^{-3}**	**a2**	**R2 (Ω)**	**%IE**
A. phylicoides	Zinc	00	1.6200	1.2930	0.8721	13.79	
		100	3.1520	0.1972	0.9152	544.2	97.47
		400	5.3890	0.1154	0.9001	637.4	97.84
		700	6.0610	0.1682	0.8794	686.2	97.99
		1000	9.312	0.0044	0.8977	1397	99.01
		1300	12.888	0.0034	0.8847	1688	99.18

Table 7.10: Electrochemical impedance spectroscopy (EIS) parameters such as the resistance of charge transfer (R_{ct}) and constant phase element (Q) using UV-radiated *A. phylicoides* in 1.5 M HCl in zinc metal

Inhibitor	**Metal**	**Concentration (ppm)**	**R1 (Ω)**	**Q2 (F.S(a-1) x10^{-3}**	**a2**	**R2 (Ω)**	**%IE**
A. phylicoides	Zinc	00	1.6200	1.2930	0.8721	13.79	
		100	1.8890	0.7551	0.9095	38.94	64.59
		400	5.3700	0.4239	0.8295	48.61	71.63
		700	5.2220	1.0460	0.8865	65.13	78.83
		1000	3.8680	0.9759	0.8716	142.2	90.30
		1300	3.2560	0.2562	0.8686	165.5	91.67

Tables 7.3-7.10 present electrochemical impedance spectroscopy (EIS) parameters, including charge transfer resistance (R_{ct}) and constant phase element (Q), using both UV-radiated and non-UV-radiated *A. phylicoides* in an acidic environment for zinc and mild steel. Tables 7.3-7.10 depict varying levels of inhibition efficiency, which appear to rise with increasing concentrations of *A. phylicoides*. It is noteworthy that, in the case of zinc metal exposed to hydrochloric acid, non-UV-radiated *A. phylicoides* demonstrate higher inhibition efficiency compared to their UV-radiated counterpart. In an acidic environment, the inhibition efficiency of *A. phylicoides* plant extract exposed to UV radiation is lower for zinc metal compared to when non-UV radiated plant extract is utilized. This discrepancy can be attributed to various factors, including chemical degradation, structural alterations, and modified mechanisms resulting from UV exposure.

© University of Venda

UV radiation can cause the degradation or modification of active compounds found in plant extracts when utilized on zinc in an acidic medium [439]. This radiation has the potential to break chemical bonds or trigger photochemical reactions that alter the structure or characteristics of inhibitor molecules, diminishing their ability to effectively inhibit corrosion. For instance, the highest inhibition efficiency achieved at a concentration of 1300ppm was 99.18% for zinc exposed to hydrochloric acid when using non-UV radiated *A. phylicoides* extract. Conversely, when UV-radiated *A. phylicoides* is employed, the inhibition efficiency decreases to 91.67%. Tables 7.7-7.8 demonstrate that non-UV radiated *A. phylicoides* yield greater inhibition efficiency compared to radiated *A. phylicoides*. This trend suggests that non-UV radiated *A. phylicoides* perform better in both hydrochloric acid and sulfuric acid environments for zinc metal. The maximum inhibition efficiency recorded in Table 7.8 was 95.67% at 1300ppm; however, Table 7.7 exhibits an inhibition efficiency of 97.69% at the same concentration, affirming that non-UV radiated *A. phylicoides* is the superior inhibitor.

Table 7.3 illustrates an inhibition efficiency of 88.05% at 1300ppm for non-UV radiated *A. phylicoides* and 88.28% at 1300ppm for UV-radiated *A. phylicoides*, indicating a distinct response of mild steel compared to zinc metal. The inhibition efficiency values in Tables 7.3-7.4, particularly at 1300ppm, are closely aligned to the extent that one might infer no significant difference between them, given the narrow margin of 0.23% (88.28% - 88.05%). The overall trend observed from Tables 7.3-7.4 suggests that as the concentration of *A. phylicoides* increases from 100ppm to 1300ppm, the inhibition efficiency also increases.

Tables 7.5-7.6 demonstrate that UV-radiated *A. phylicoides* provide superior inhibition efficiency compared to non-UV-radiated *A. phylicoides* plant extract. This assertion is supported by the data in Table 7.5, which shows a minimum inhibition efficiency of 55.32% at the lowest concentration of 100 ppm for non-UV radiated *A. phylicoides*, whereas for UV-radiated *A. phylicoides*, the minimum inhibition efficiency at the same concentration of 100 ppm was 85.28%. This suggests that UV-radiated *A. phylicoides* plant extract offers better protection for mild steel in both hydrochloric acid and sulfuric acid environments. The positive aspect of this finding is that both UV-radiated and non-UV-radiated *A. phylicoides* can be considered effective corrosion inhibitors, and by increasing the concentration, it is evident that there is potential to maximize metal protection using *A. phylicoides* extract. The charge transfer resistance (R_{ct}) of the extract was observed to surpass that of the blank, and it showed an upward trend with rising concentrations of *A. phylicoides* extract. The introduction

© University of Venda

of UV-radiated *A. phylicoides* extracts notably augmented the R_{ct} values, consequently elevating the corrosion inhibition efficiency for zinc in both hydrochloric acid and sulfuric acid solutions. However, the opposite effect was observed for mild steel, as the presence of non-UV-radiated *A. phylicoides* enhanced the charge transfer resistance value instead of UV-radiated *A. phylicoides*.

The reduction in the constant phase element (CPE) values following the introduction of the *A. phylicoides* extract into the corrosive electrolyte implies an increase in surface smoothness due to *A. phylicoides* extract adsorption on the metal surface. This is corroborated by the rise in phase angles depicted in the Bode plots. The constant phase element exponent (n) values are used to characterize the corrosion process occurring on the metal surface, ranging from -1 to 1. A value of -1 represents inductance, 1 represents capacitance, and 0 represents resistance. Observing Table 8.8, for instance, at 1300ppm, the n value was approximately 0.8686, indicating a capacitive nature at the interface. The high n-value suggests that the extract formed a film on the surface of zinc and mild steel, enhancing its uniformity. While the CPE values do not exhibit a consistent trend, they generally decrease with increasing extract concentration, indicating extract adsorption on the metal surface, and hindering the formation of hostile corrosion cells.

© University of Venda

University of Venda
Creating Future Leaders

CHAPTER EIGHT

RESULTS AND DISCUSSION

Wettability study/ Contact angle

(WS)

© University of Venda

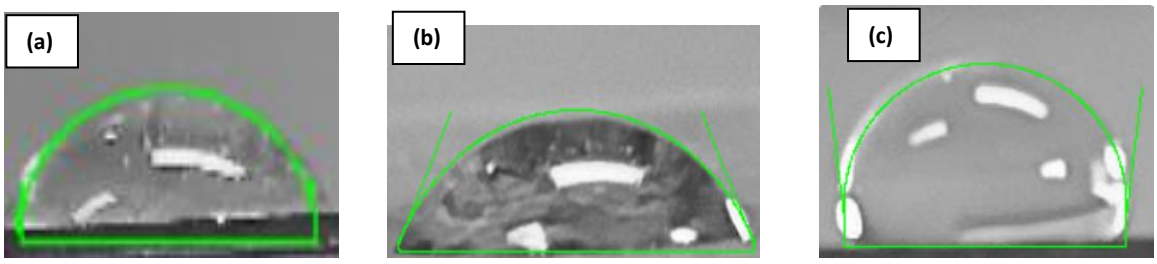
8.1. Contact angles (Wettability study)

In the study of corrosion inhibition, understanding the wettability of metal surfaces is paramount. A contact angle is a geometric parameter used to quantify the wetting behavior of a liquid droplet on a solid surface [440]. It measures the angle formed at the solid-liquid interface, with the solid surface serving as the baseline and the tangent to the droplet's surface at the contact point acting as the reference line. Contact angle measurements serve as a valuable tool in elucidating the interfacial behavior between a liquid corrosive environment and the metal substrate [441]. In this context, the focus is to conduct experiments on polished untreated metals substrate, metals substrate after 6 hours of immersion in 1.5 M HCl and 1.5 M H_2SO_4 with no inhibitor, and in the presence of 1300 ppm of radiated *A. phylicoides extract*. A 'blank' surface denotes the untreated or unmodified metal exposed in an acidic medium, while an 'inhibitor' refers to a substance applied to mitigate corrosion. Typically, the contact angle on a blank surface is smaller, reflecting its higher surface energy and greater affinity for the corrosive liquid. Conversely, on an inhibitor-treated surface, one expects to observe a larger contact angle, indicative of reduced wettability and improved corrosion resistance. This expectation arises from the altered surface chemistry brought about by the inhibitor, which serves to minimize the interaction between the corrosive environment and the metal substrate. Thus, by examining contact angles, researchers can gain valuable insights into the effectiveness of corrosion inhibitors and their impact on surface wettability.

The form of a droplet affects how well it adheres to and spreads on a metal surface, determining its wettability. Wettability decreases as the contact angle increases, and conversely [442]. Surfaces with contact angles of 90° or less are hydrophilic, meaning they strongly attract water, while those with angles of 90° or more are hydrophobic, showing less affinity for water [443]. Whether a surface is hydrophobic or hydrophilic influences the extent of corrosion on steel surfaces exposed to water. Inhibitors function as surfactants, attaching to the inner metal surface and creating a hydrophobic layer that shields the metal from water contact. Results indicate that the introduction of both non-radiated and UV-radiated *A. phylicoides* extracts increased the contact angle, sometimes transforming the metal surface into a lipophilic layer with contact angles surpassing or equaling 90°. Research suggests that surfaces demonstrating hydrophobic characteristics typically exhibit enhanced resistance to corrosion [444]. A more detailed examination of the wettability of mild steel and zinc metals in aggressive solution environments follows. Figures 8.1-8.8 show the surface

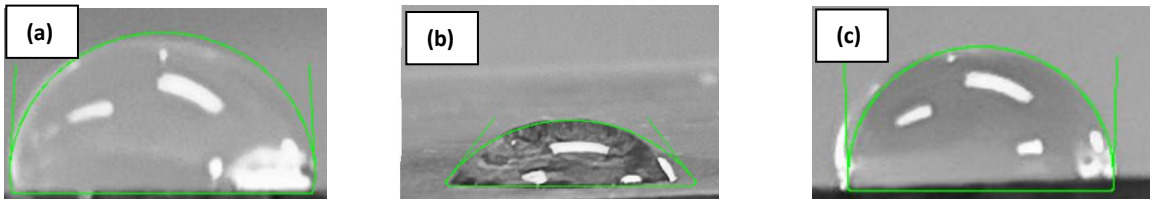
© University of Venda

wettability behaviors of zinc and mild steel in the absence and presence of *A. phylicoides* extract.



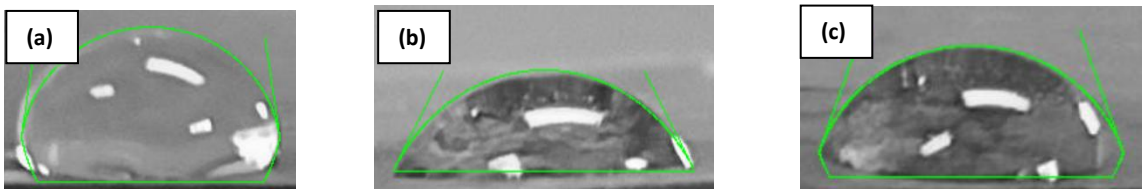
83.135° 62.589° 97.148°

Figure 8.1: Surface wettability behaviors of (a) polished untreated zinc metal substrate, (b) zinc metal substrate after 6 hours of immersion in 1.5 M HCl medium with no inhibitor, and (c) in the presence of 1300 ppm of non-radiated *A. phylicoides* extract



86.548° 52.248° 91.983°

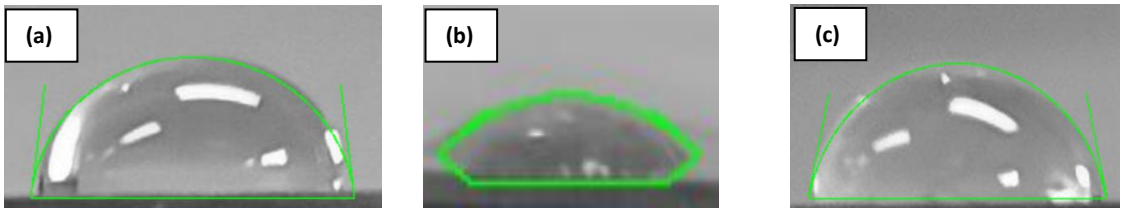
Figure 8.2: Surface wettability behaviors of (a) polished untreated zinc metal substrate, (b) zinc metal substrate after 6 hours of immersion in 1.5 M H_2SO_4 medium with no inhibitor, and (c) in the presence of 1300 ppm of non-radiated *A. phylicoides* extract



80.932° 59.008° 70.412°

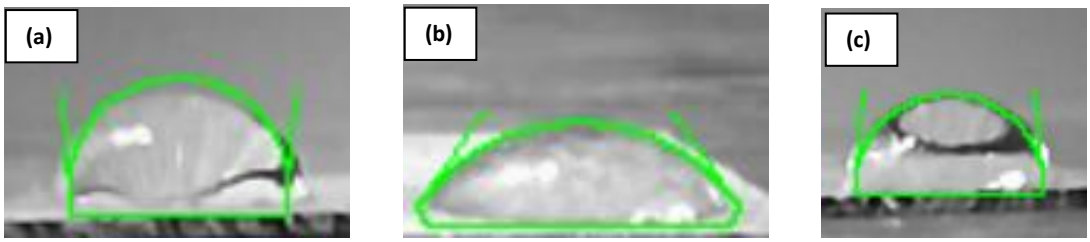
Figure 8.3: Surface wettability behaviors of (a) polished untreated zinc metal substrate, (b) zinc metal substrate after 6 hours of immersion in 1.5 M HCl medium with no inhibitor, and (c) in the presence of 1300 ppm of radiated *A. phylicoides* extract

© University of Venda



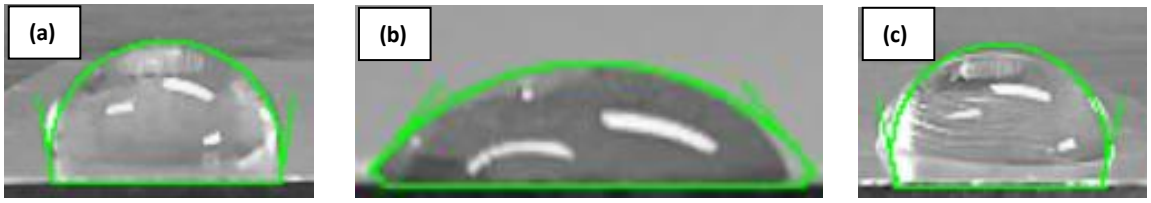
81.404º 30.862º 76.244º

Figure 8.4: Surface wettability behaviors of (a) polished untreated zinc metal substrate, (b) zinc metal substrate after 6 hours of immersion in 1.5 M H_2SO_4 medium with no inhibitor, and (c) in the presence of 1300 ppm of radiated *A. phylicoides* extract



96.501º 55.631º 84.884º

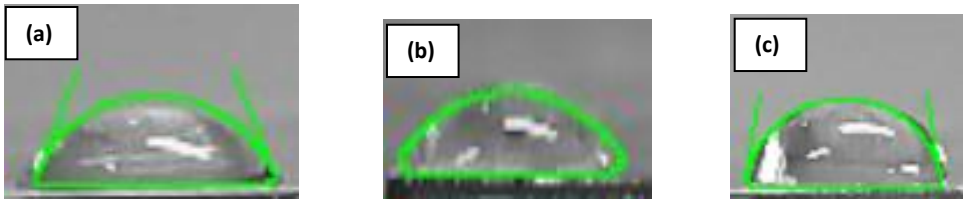
Figure 8.5: Surface wettability behaviors of (a) polished untreated mild steel metal substrate, (b) mild steel metal substrate after 6 hours of immersion in 1.5 M HCl medium with no inhibitor, and (c) in the presence of 1300 ppm of non-radiated *A. phylicoides* extract



99.317º 51.620º 105.714º

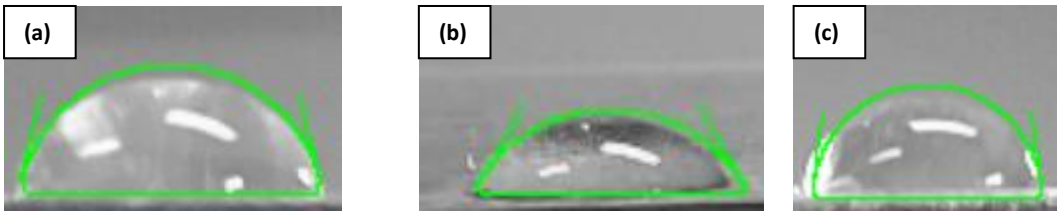
Figure 8.6: Surface wettability behaviors of (a) polished untreated mild steel metal substrate, (b) mild steel metal substrate after 6 hours of immersion in 1.5 M H_2SO_4 medium with no inhibitor, and (c) in the presence of 1300 ppm of non-radiated *A. phylicoides* extract

© University of Venda



68.553° 43.342° 79.223°

Figure 8.7: Surface wettability behaviors of (a) polished untreated mild steel metal substrate, (b) mild steel metal substrate after 6 hours of immersion in 1.5 M HCl medium with no inhibitor, and (c) in the presence of 1300 ppm of radiated *A. phylicoides* extract



75.302° 59.469° 82.505°

Figure 8.8: Surface wettability behaviors of (a) polished untreated mild steel metal substrate, (b) mild steel metal substrate after 6 hours of immersion in 1.5 M H_2SO_4 medium with no inhibitor, and (c) in the presence of 1300 ppm of radiated *A. phylicoides*.

Figures 8.1 and 8.3 (c) illustrate the contact angle outcomes for zinc metal treated with non-radiated and UV-radiated *A. phylicoides* extracts. The non-UV-radiated *A. phylicoides* extract produced a contact angle greater than 90°, specifically 97.148°, indicating a hydrophobic surface. In contrast, the UV-radiated extract resulted in a contact angle of 70.412°, signifying increased surface wettability. A similar investigation was conducted by Sajid and Kiran (2018), who examined the effects of corrosion and surface roughness on the wettability of ASTM A36 steel. (Sajid, H. U., & Kiran, R. (2018). This indicates that the non-radiated *A. phylicoides* extract serves as a more effective inhibitor for zinc metal in HCl acid compared to the UV-radiated counterpart. Similar trends were observed in Figures 8.2 and 8.4 (c) for zinc exposed to H_2SO_4, where the contact angle surpassed 90° with the non-UV radiated *A. phylicoides* extract at 91.983°, while it remained below 90° with the UV-radiated *A. phylicoides* extract at 76.244°. The non-UV-radiated *A. phylicoides* extract offers superior inhibition compared to its UV-radiated counterpart. Additionally, H_2SO_4 is less corrosive than HCl. Figures 8.6 and 8.8 depict the behavior of mild steel in H_2SO_4 with non-radiated and

© University of Venda

UV-radiated *A. phylicoides* extracts. The contact angles for water droplets on the mild steel surface were measured at 105.714° and 82.505°, respectively. This suggests that the non-UV-radiated *A. phylicoides* extract performs better as a corrosion inhibitor for mild steel in sulfuric acid compared to the UV-radiated *A. phylicoides* extract [443]. In both non-radiated and UV-radiated *A. phylicoides* extract environments in hydrochloric acid, as shown in Figures 8.5 and 8.7, the contact angles were less than 90°, indicating minimal alteration to the metal surface. The contact angles measured at 84.884° and 79.223° for non-radiated and UV-radiated *A. phylicoides* extracts, respectively, while untreated mild steel displayed angles of 55.631° and 43.342° for non-UV-radiated and UV-radiated *A. phylicoides* extracts, respectively. The increase in contact angle in the presence of the inhibitor provides straightforward evidence of the extract's effectiveness in fortifying the metal against corrosion attacks [444].

© University of Venda

University of Venda
Creating Future Leaders

CHAPTER NINE

RESULTS AND DISCUSSION

Scanning Electron Microscopy

(SEM)

© University of Venda

9.1 Scanning Electron Microscopy (SEM) and Energy Dispersive Spectroscopy (EDS)

In the study of metal corrosion influenced by UV radiation and acidic environments such as HCl and H_2SO_4, SEM and EDS play indispensable roles in providing detailed insights into the physical and chemical changes occurring at the metal surface. SEM provides high-resolution imaging of surface morphology and microstructure, revealing the formation of corrosion features such as pits, cracks, and changes in texture that can indicate varying degrees of corrosion damage [445]. This technique also helps in visualizing the morphology of corrosion products formed under different conditions, offering clues about the corrosion mechanisms at play. On the other hand, EDS complements SEM by providing elemental composition analysis of these corrosion products [446]. Mapping the distribution of elements across the metal surface has been observed from EDS, which also helps identify the specific chemical constituents of corrosion products, which is crucial for understanding how non-UV radiated and UV radiation *A. phylicoides extract* and different acids interact with the metal substrate. Together, SEM and EDS provide a comprehensive analytical approach that not only visualizes but also characterizes the complex interactions between *A. phylicoides* extract and acidic environments, contributing significantly to the study of metal corrosion under these unique conditions. The Phenom Pro X is a versatile SEM equipped with an integrated EDS system, designed for high-resolution imaging and elemental analysis of samples [447 - 453].

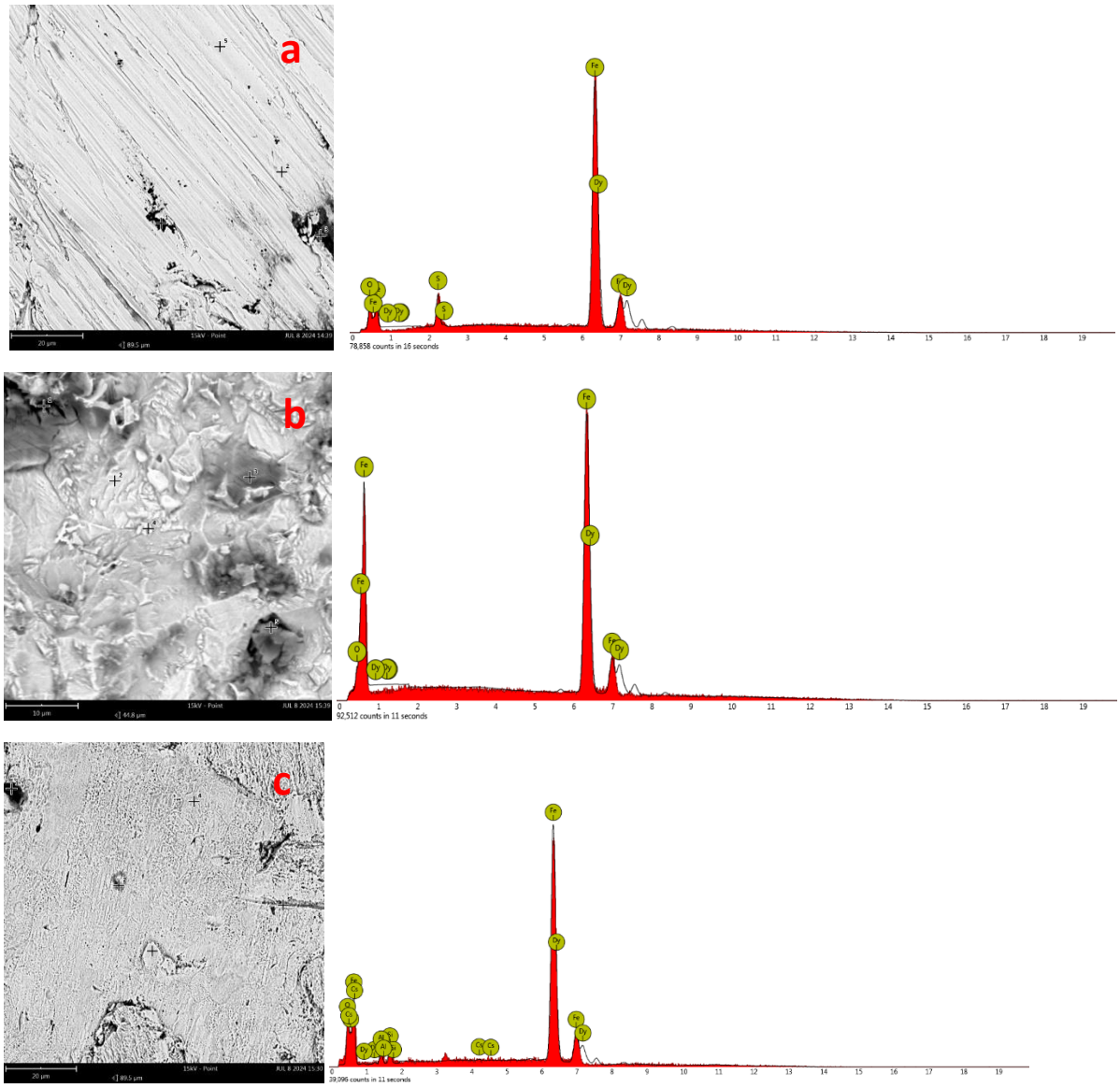
9.1.1 Scanning Electron Microscopy (SEM) images

SEM and EDS were conducted using polished mild steel and zinc metals [454]. The metals were initially analyzed in their polished state to establish a baseline for comparison. Polishing the metals ensures a smooth, uniform surface, free from contaminants and irregularities. This allows for accurate assessment of any changes or damage caused by exposure to sulphuric and hydrochloric acid. This initial analysis provides a clear reference point to evaluate the extent of corrosion and the effectiveness of protective treatments, such as the introduction of *A. phylicoides* extracts. To investigate potential protective effects, non-UV-radiated and UV-radiated *A. phylicoides* extracts were introduced in the presence of HCl and H_2SO_4 to determine if the extent of metal damage would be reduced. Using both HCl and H_2SO_4 instead of just one acid provides a comprehensive understanding of the corrosion behavior of metals in different acidic environments. HCl and H_2SO_4 have distinct chemical properties and interactions with metals, which can lead to varying corrosion mechanisms and rates. Testing

© University of Venda

both acids assists researchers evaluate the metals' resistance to a broader range of acidic conditions that may be encountered in practical applications.

Using UV-radiated and non-UV-radiated *A. phylicoides* extracts allows for a comparison of protective effects on metal surfaces. UV radiation can alter the chemical composition and properties of the *A. phylicoides* extract, potentially enhancing or diminishing its corrosion inhibition capabilities. Studying both forms of the extract assists researchers in determining whether UV radiation improves the extract's effectiveness and understanding the underlying mechanisms responsible for any observed differences in corrosion protection. This comparison helps to identify the most effective treatment for mitigating acid-induced corrosion [455]. The images obtained from SEM are as follows:



© University of Venda

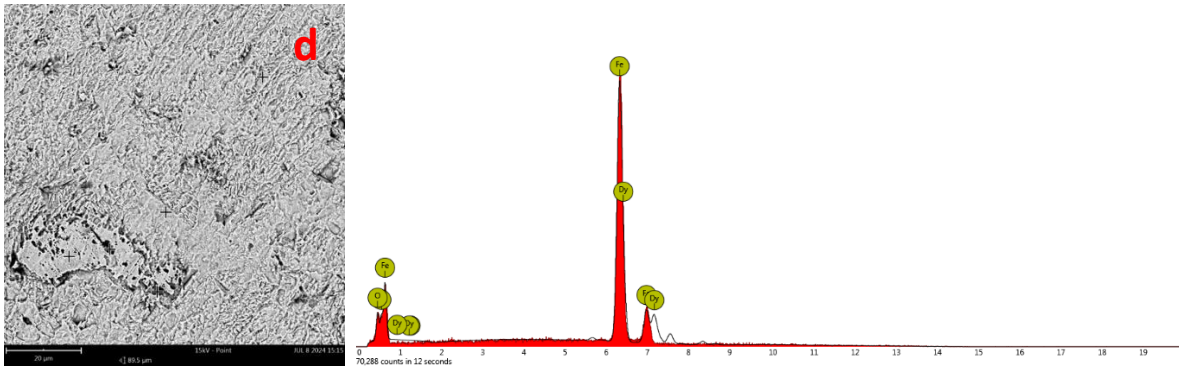


Figure 9.1: SEM images and EDS spectra of MS surface of (a) polished MS, (b) MS exposed in H_2SO_4, (c) MS exposed in H_2SO_4 in the presence of non-UV-radiated bush tea (d) MS exposed in H_2SO_4 in the presence of UV-radiated *A. phylicoides*

The surface morphology of the polished metal, as indicated in Figure 9.1a, is initially smooth due to the removal of surface irregularities and imperfections during the polishing process. When immersed in sulphuric acid, the acidic environment aggressively reacts with the metal, leading to corrosion. As shown in Figure 9.1b, sulphuric acid rapidly degrades the metal surface, forming pits, cracks, and other corrosion products that result in a rough and damaged appearance. A similar observation was reported by Zerbst *et al*. (2019), who discussed how defects such as cavities, dents, and corrosion pits contribute to the failure of metallic components. The introduction of a corrosion inhibitor protects the metal surface from the corrosive effects of sulphuric acid. Corrosion inhibitors are substances that, when added in small concentrations, significantly reduce the corrosion rate of metals. In the presence of an inhibitor, the metal surface remains smoother because the inhibitor effectively mitigates the aggressive action of the acid. When forming a protective barrier or film, the inhibitor preserves the integrity of the polished surface, preventing corrosion-induced roughness and damage. Consequently, the surface appears smoother and less degraded compared to the metal exposed to sulphuric acid without the inhibitor. Similar results were observed by Berce *et al*. (2024), who reported surface preservation in treated metals exposed to boiling-induced aging and fouling.

EDS analysis of the polished metal surface (Figure 9.1a) identified five key elements: iron (Fe), oxygen (O), silicon (Si), dysprosium (Dy), and strontium (Sr). The dominance of iron is expected, as the base metal is primarily composed of Fe, resulting in strong, intense peaks in the EDS spectra. This finding aligns with Azoulay *et al*. (2013), who observed similar elemental patterns in the analysis of ferrous corrosion products on iron artifacts. The presence

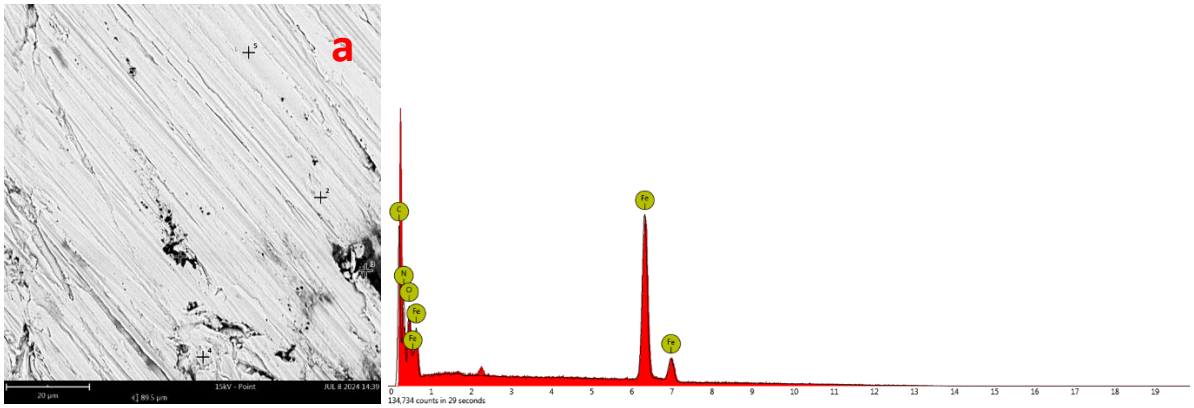
© University of Venda

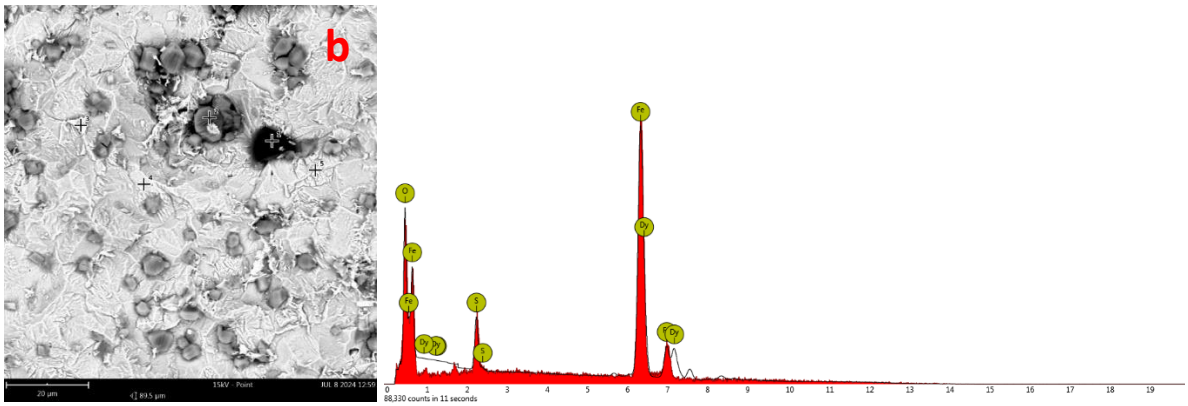
of oxygen likely indicates surface oxidation or iron oxide formation due to exposure to air. Silicon may be present as an impurity or from environmental contamination, commonly introduced during manufacturing or handling. The detection of Dy and Sr, though less common, could be attributed to specific alloying elements or surface treatments designed to enhance mechanical or magnetic properties. These elements provide insight into the alloy composition and surface conditions of the polished metal.

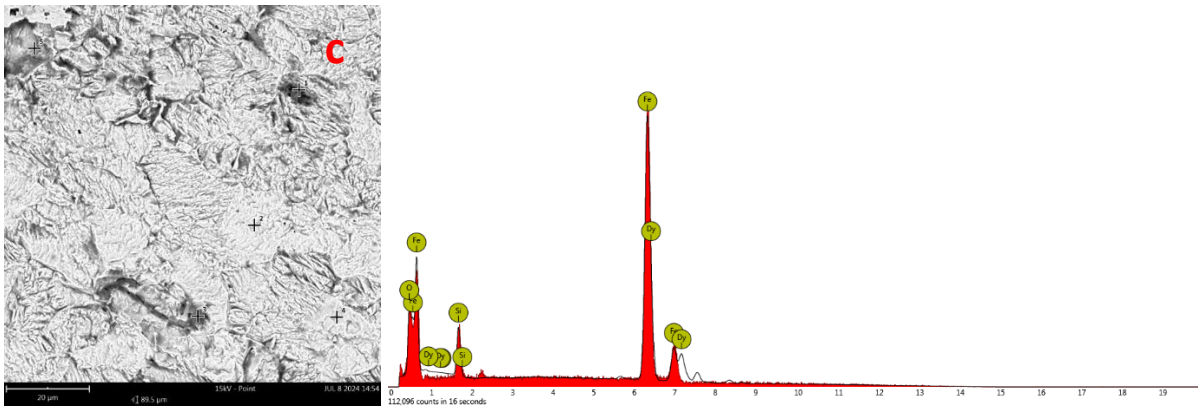
EDS analysis of the surface after exposure to sulphuric acid (Figure 9.1b) shows notable changes. Detected elements include Fe, O, sulfur (S), Dy, lead (Pb), and cobalt (Co). The reduced Fe percentage suggests significant deterioration of the mild steel surface due to corrosion. This is consistent with findings by Kruizenga and Gill (2014), who documented iron depletion in stainless steels exposed to aggressive media. The increase in oxygen suggests oxidation or the formation of corrosion products. The presence of sulfur indicates sulfuric acid adsorption on the surface. Dy, Pb, and Co may result from contamination, alloying elements, or impurities introduced during corrosion or sample preparation. The data confirm the corrosive effect of sulphuric acid, evidenced by decreased Fe content and the appearance of new elements on the surface [448].

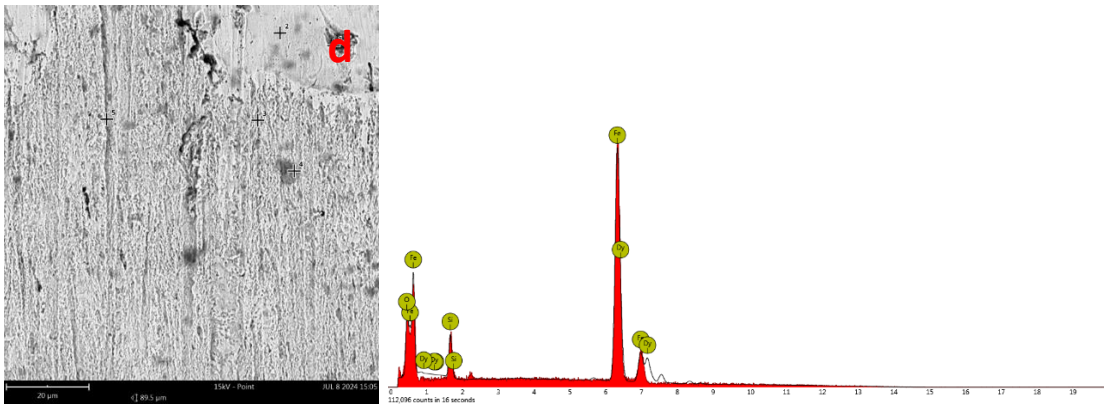
EDS analysis of mild steel samples treated with *A. phylicoides* extract as a corrosion inhibitor (Figures 9.1c and 9.1d) reveals distinct differences from untreated samples. The spectra primarily show Fe, O, and Dy. The high Fe content is comparable to the polished metal, indicating minimal corrosion. This suggests the *A. phylicoides* extract effectively inhibits corrosion by preserving the Fe content. Notably, the absence of significant sulfur peaks implies that the extract prevents sulfuric acid from attacking the surface. The formation of a protective film by the extract likely hinders acid penetration, maintaining surface smoothness. These findings confirm that *A. phylicoides* acts as a potent corrosion inhibitor, reducing the acid's impact and preserving the surface integrity of the metal.

© University of Venda









© University of Venda

Figure 9.2: SEM micrograph of MS surface of (a) polished MS, (b) MS exposed in HCl, (c) MS exposed in HCl in the presence of non-UV-radiated *A. phylicoides* (d) MS exposed in HCl in the presence of UV-radiated *A. phylicoides* extract.

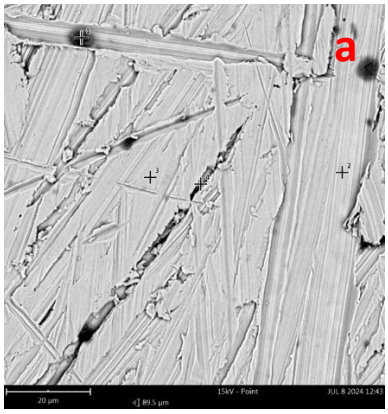
SEM micrograph in Figure 9.2a shows the surface morphology of polished mild steel before exposure to hydrochloric acid. The surface is smooth, indicating no signs of corrosion or damage. Figure 9.2b depicts the mild steel surface after exposure to hydrochloric acid, revealing significant roughness and major dark spots, likely due to the corrosive action of the acid attacking the metal. In Figure 9.2c, the mild steel exposed to hydrochloric acid in the presence of non-UV-radiated *A. phylicoides* extract shows minimized damage. Although some dark spots are still observed, they are significantly reduced, indicating that the bush tea extract provides a protective effect against acid corrosion. Similarly, Figure 9.2d shows mild steel exposed to hydrochloric acid in the presence of UV-radiated *A. phylicoides* extract, where the surface is smoother and has fewer dark spots compared to the sample exposed to acid alone. This suggests that the UV-radiated *A. phylicoides* extract is effective in protecting the metal surface from corrosion. Overall, Figures 9.2c and 9.2d demonstrate that both non-UV-radiated and UV-radiated *A. phylicoides* extracts act as corrosion inhibitors, reducing the extent of surface damage caused by hydrochloric acid. The metal surfaces in the presence of these inhibitors appear smoother and more closely resemble the polished mild steel surface shown in Figure 9.2a, indicating that the *A. phylicoides* extracts can restore the metal surface to a certain extent, mitigating the corrosive effects of the acid [448, 449].

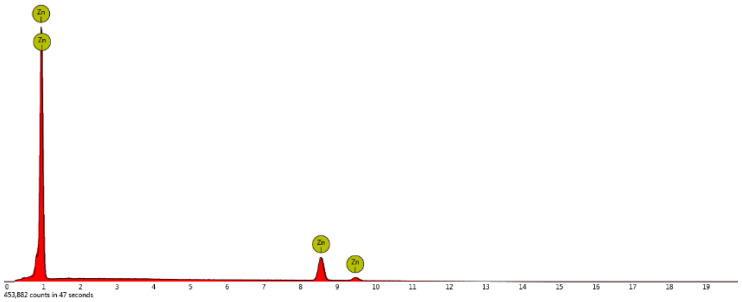
EDS Figure 9.2 (a) (EDS). Polishing the mild steel is an essential step because it removes surface imperfections and oxides, providing a clean and uniform surface. This ensures more accurate and consistent experimental results by reducing variability caused by surface contaminants. Repeating the experiment with HCl, even though results for sulphuric acid are already available, is crucial for comparative analysis. Different acids interact differently with metals, and studying these interactions with HCl can reveal specific effects and mechanisms that are not observable with sulphuric acid. This comprehensive understanding is important for various applications and material performance evaluations. The introduction of HCl to the polished mild steel surface has led to a reduction in the percentage of iron (Fe). This suggests that HCl causes significant dissolution or alteration of the iron. The EDS analysis has identified several elements on the steel surface, with iron (Fe), oxygen (O), and dysprosium (Dy) being the dominant ones. The presence of dysprosium, which is unusual, might indicate contamination or a particular experimental condition. Figure 9.2(b) provides detailed data on

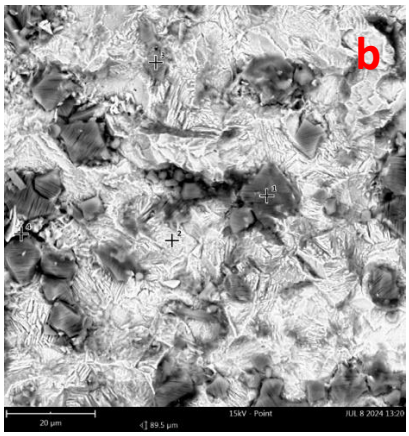
© University of Venda

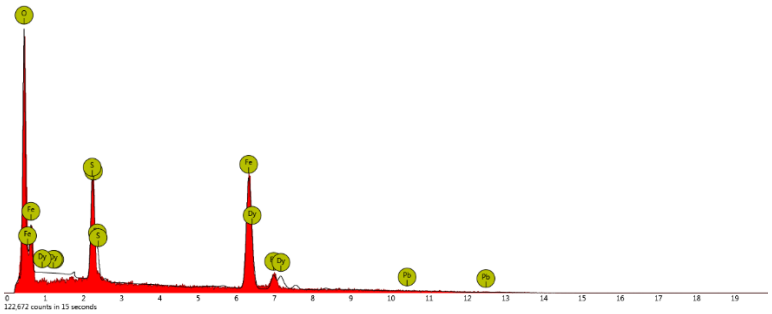
the percentages and distribution of these elements, offering a visual or tabular representation of the experimental findings. The presence of carbon and nitrogen when using HCl but not H_2SO_4 can be due to environmental contamination, the formation of complex compounds, specific chemical reactions facilitated by HCl, or inherent differences in the chemical properties of the two acids. These factors contribute to the variations observed in the EDS results. The higher percentage of iron (Fe) on mild steel in the presence of a corrosion inhibitor compared to its absence can be explained by the protective role of the inhibitor. Corrosion inhibitors form a protective film on the metal surface, preventing or significantly reducing the interaction between the corrosive environment and the metal [450]. This protective layer minimizes the dissolution of iron into the environment, thereby maintaining a higher percentage of iron on the surface. In the absence of a corrosion inhibitor, the metal surface is more susceptible to oxidation and corrosion, leading to the formation of corrosion products such as iron oxides (rust) or other compounds that can detach from the surface, reducing the detectable iron content. In contrast, the presence of an inhibitor reduces the rate of these processes, preserving the iron in its metallic form on the surface. Corrosion inhibitors often work by adsorbing onto the metal surface, forming a barrier that blocks corrosive agents. This adsorption can also prevent the leaching of iron from the surface into the surrounding environment. As a result, the EDS analysis detects a higher concentration of iron on the protected surface [457]. Additionally, corrosion inhibitors can prevent localized forms of corrosion, such as pitting, which can lead to significant material loss in specific areas. By preventing these localized attacks, the overall iron content on the surface remains higher in the presence of the corrosion inhibitor. Some inhibitors also facilitate the formation of a passive oxide layer that is stable and adherent. This passivation layer can further protect the iron underneath from corrosive attack, leading to higher retained iron content on the surface. The higher percentage of iron detected in the presence of a corrosion inhibitor is due to the inhibitor's ability to protect the metal surface from corrosive processes, maintain the integrity of the surface, and prevent the loss of iron into the environment. This protection results in a higher retention of iron on the steel surface, as evidenced by the EDS analysis.

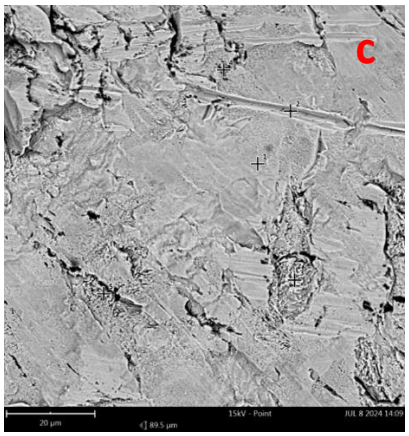
© University of Venda

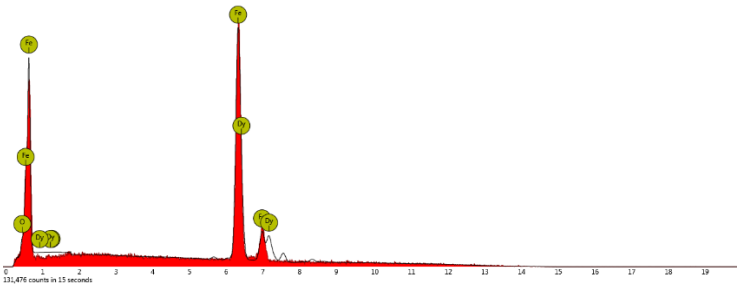




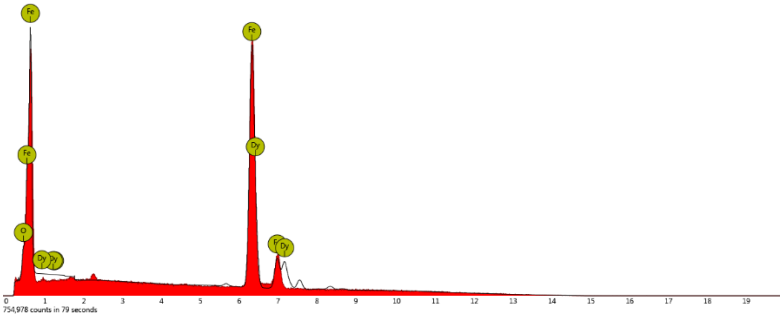












© University of Venda

Figure 9.3: SEM micrograph of Zn surface of (a) polished Zn, (b) Zn exposed in H_2SO_4, (c) Zn exposed in H_2SO_4 in the presence of non-UV-radiated bush tea (d) Zn exposed in H_2SO_4 in the presence of UV-radiated *A. phylicoides*

Figure 9.3 presents the EDS results and SEM micrographs of zinc surfaces subjected to various conditions in sulphuric acid. Surface roughness varies notably across samples due to the extent of corrosion and the influence of corrosion inhibitors.

The polished zinc surface appears smooth, as expected, due to the removal of surface irregularities during polishing. Upon exposure to sulphuric acid without any inhibitor, the zinc surface becomes significantly rougher. This is a result of direct acid-metal interaction, which leads to the formation of corrosion products and pitting. Similar findings have been reported by Torabianfard *et al*. (2025), who observed notable surface degradation in unprotected metal exposed to corrosive environments.

In contrast, when zinc is immersed in sulphuric acid containing non-UV-radiated *A. phylicoides* (bush tea) extract, the surface remains relatively smoother. This indicates that the extract functions as an effective corrosion inhibitor, likely by adsorbing onto the metal surface and forming a protective barrier that limits metal-acid contact. Likewise, exposure to UV-radiated *A. phylicoides* extract results in a similarly smooth surface. The UV treatment may enhance the inhibitor's effectiveness by activating or modifying phytochemical components that contribute to barrier formation. This results in superior protection against corrosion and a reduction in surface degradation [451].

The rough surface observed in the uninhibited sample highlights the aggressive nature of sulphuric acid toward zinc, while the smoother surfaces seen with both inhibitor types reflect the efficiency of the protective films in mitigating acid attack. These trends are consistent with observations by Zhang *et al*. (2024), who also reported reduced surface damage and corrosion rates in the presence of effective inhibitors.

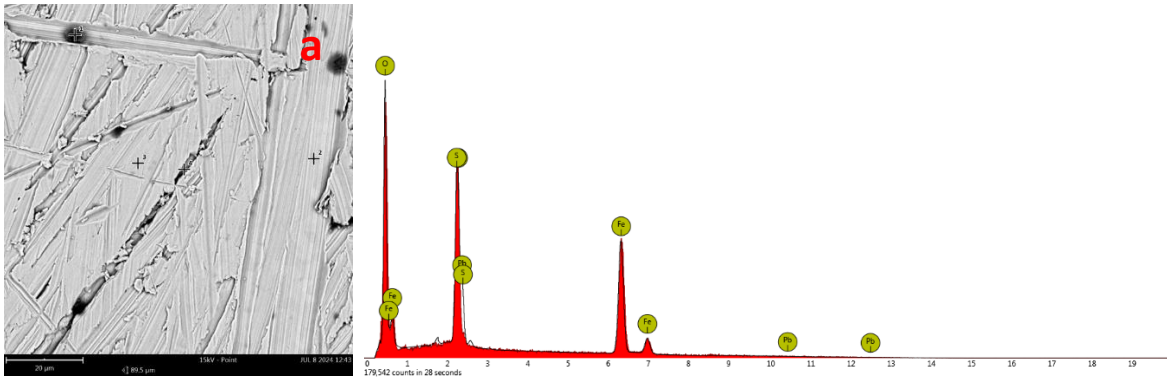
The EDS analysis reveals that most selected points on the zinc surface consist of 100% Zn, while one spot shows additional elements: oxygen (O), calcium (Ca), and silicon (Si). This deviation may be attributed to localized surface contamination, environmental exposure, or variations in microstructural reactivity. The oxygen content could indicate the formation of zinc oxide (ZnO), resulting from oxidation either from atmospheric exposure or dissolved oxygen in the acid. Calcium and silicon may originate from impurities in the acid, environmental dust, or residuals from polishing agents used during sample preparation.

© University of Venda

Such heterogeneity suggests the presence of localized reaction zones where unique interactions occurred, possibly due to uneven acid or inhibitor exposure or inherent variations in the zinc surface. These localized deposits may include compounds like calcium sulfate or silicon dioxide (SiO_2), altering the elemental profile at specific points.

A particularly important observation is the absence of sulfur in the EDS spectra following inhibitor application. In samples without inhibitors, sulfur is typically detected due to the formation of zinc sulfate, a product of zinc's reaction with sulphuric acid. However, when a corrosion inhibitor is present, this reaction is suppressed. The inhibitor forms a protective film that prevents sulfuric acid from interacting directly with the zinc, thereby inhibiting the formation of sulfur-containing corrosion products.

The disappearance of sulfur from the EDS results is a strong indicator of the inhibitor's effectiveness. It confirms that the protective layer formed on the metal surface successfully blocks the corrosive action of sulfuric acid, preserving the integrity of the zinc and reducing the formation of $ZnSO_4$ and similar species.



© University of Venda

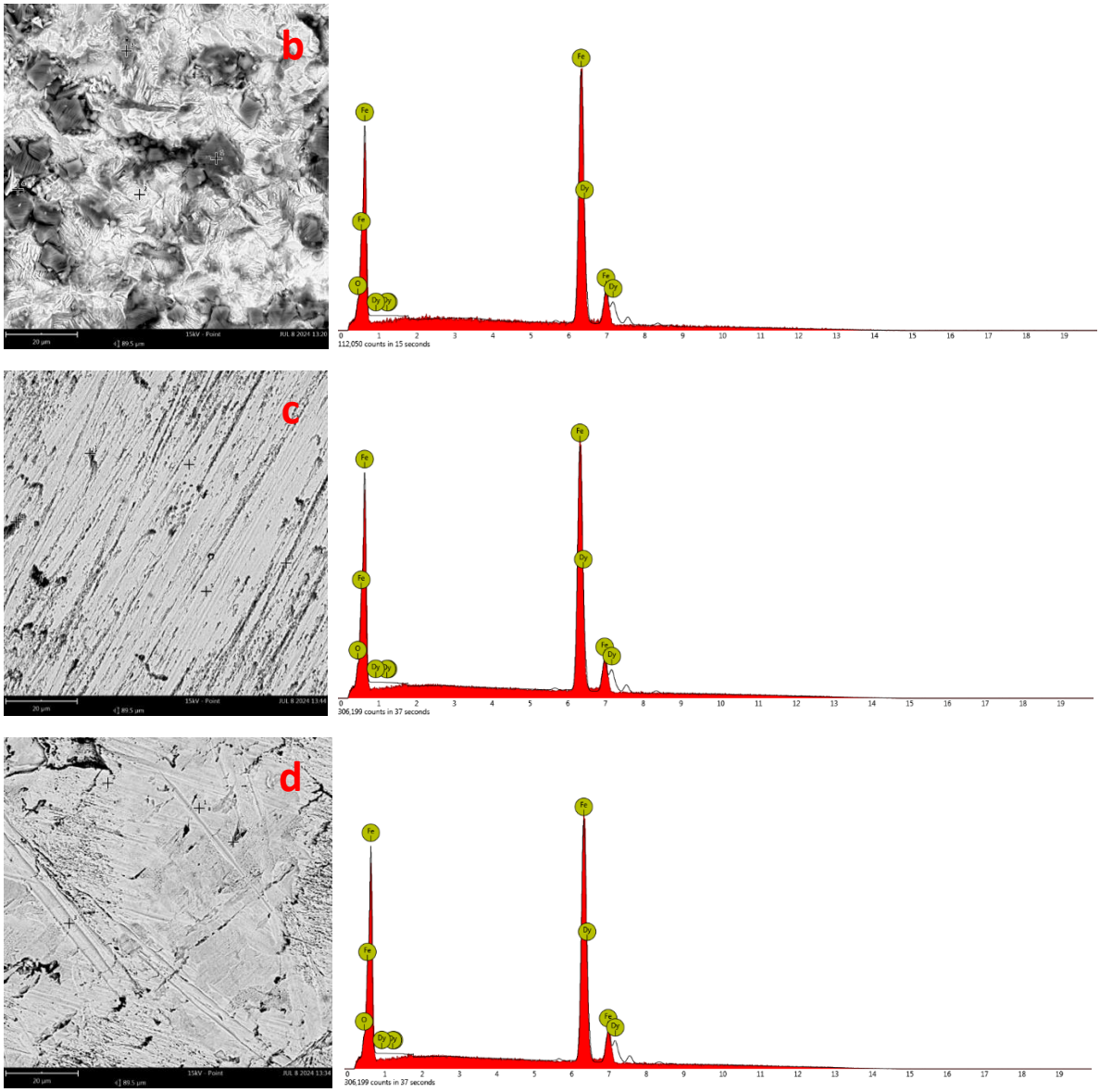


Figure 9.4: SEM micrograph of Zn surface of (a) polished Zn, (b) Zn exposed in HCl, (c) Zn exposed in HCl in the presence of non-UV-radiated bush tea (d) Zn exposed in HCl in the presence of UV-radiated *A. phylicoides* extract.

The results obtained with sulphuric acid are similar to those obtained with hydrochloric acid. In the absence of an inhibitor, the zinc metal surface becomes rough due to corrosion, while in the presence of an inhibitor, the surface remains smooth. Here's why this happens: When zinc is exposed to a corrosive acid like HCl or H_2SO_4 without an inhibitor, the acid reacts with the zinc, leading to significant corrosion. This reaction produces various corrosion products and pits on the surface, resulting in a rough texture. The corrosive acids cause the zinc to dissolve, forming compounds such as zinc chloride ($ZnCl_2$) or zinc sulfate ($ZnSO_4$), depending on the acid used. This dissolution and the formation of corrosion products increase the surface roughness. In contrast, when a corrosion inhibitor is introduced, such as bush tea

© University of Venda

(either non-UV-radiated or UV-radiated), it forms a protective layer on the zinc surface. This layer acts as a barrier, preventing the acid from coming into direct contact with the zinc. The inhibitor molecules absorb onto the metal surface, blocking the active sites and reducing the overall reaction rate between the acid and the zinc. The protective film created by the inhibitor minimizes the dissolution of zinc and the formation of corrosion products, thereby maintaining the surface integrity [450]. This results in a much smoother surface compared to the rough, corroded surface observed without the inhibitor. The presence of the inhibitor effectively mitigates the corrosive attack of the acid, preserving the polished nature of the zinc surface. Additionally, the smoothness observed with both non-UV-radiated and UV-radiated bush tea suggests that both forms of the inhibitor are effective in protecting the zinc surface. UV radiation might enhance the inhibitory properties by activating certain compounds within the *A. phylicoides*, leading to an even more robust protective barrier. In summary, the zinc surface becomes rough when exposed to HCl or H_2SO_4 without an inhibitor due to extensive corrosion and the formation of corrosion products. When a corrosion inhibitor is introduced, it forms a protective layer that prevents the acid from attacking the zinc, resulting in a smooth surface. This protective action of the inhibitor is crucial in preserving the integrity of the zinc metal in corrosive environments.

Figure 9.4 (a) shows the presence of oxygen on a zinc metal surface exposed to HCl and detected through EDS (Energy Dispersive Spectroscopy) can be attributed to several factors. Zinc metal can oxidize when exposed to air, forming zinc oxide (ZnO). The presence of HCl can accelerate this process by removing any protective layers of zinc hydroxide or carbonate [452]. Additionally, surface contamination or residues can also contribute to oxygen peaks in the EDS spectrum. In EDS analysis, the high-intensity peak of oxygen indicates a significant presence of oxygen atoms in the sample. This could be due to the formation of zinc oxide, residual water from reactions involving hydrogen, or surface contamination.

In the presence of *A. phylicoides* extracts, various spots on zinc metal showed dominant elements such as Dysprosium (Dy), Oxygen (O), and Iron (Fe). Interestingly, the presence of a corrosion inhibitor led to a reduction in the hydrogen peak. This suggests that the inhibitor is likely effective in mitigating corrosion processes that typically generate hydrogen gas, possibly by forming a protective barrier on the zinc surface or altering the chemical environment in a way that inhibits hydrogen evolution [453].

© University of Venda

University of Venda
Creating Future Leaders

CHAPTER TEN

RESULTS AND DISCUSSION

Computational studies

(CS)

© University of Venda

10 Computational Studies Results

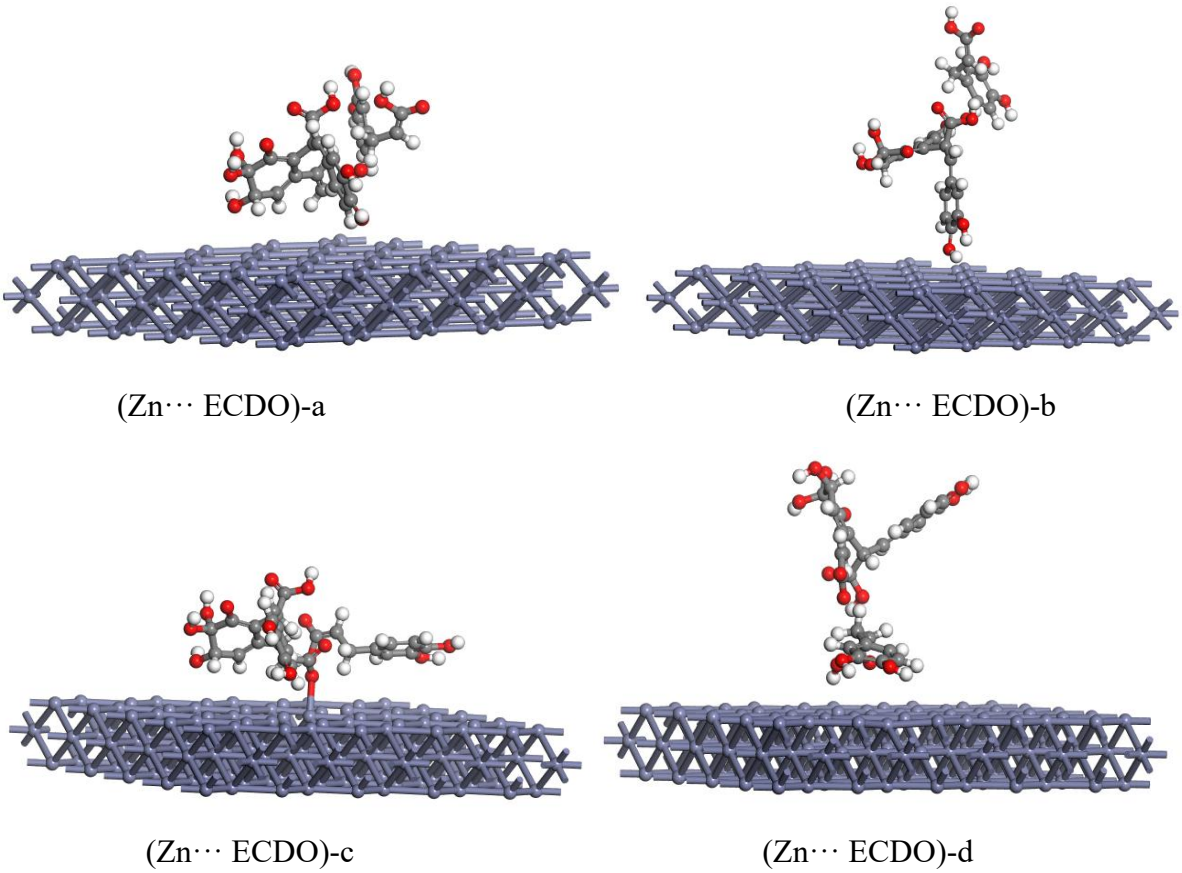
10.1 Introduction

This chapter presents the results of quantum chemical studies on the compounds for which the experimental results have been reported in the previous chapters. The results are organized in such a manner that the interaction between the compounds and the zinc surface is reported first, and the interactions between the inhibitors and the iron surface are presented last. The data that will be presented in this section includes the bond distance, relative energy, and interaction energies. Relative energy provides information on the preferred complex structures between the inhibitor and the metal surface while the bond distances and interaction energies provide the strength of interactions between the inhibitor and the metal surface.

10.2 Interaction of Zinc Metal Surface with the Inhibitor Molecules

The results for the interaction between E)-4-(3-(1-carboxy-2-(3,4-dihydroxyphenyl)ethoxy)-3-oxoprop-1-en-1-yl)-2-(3,4-dihydroxyphenyl)-6,7,7-trihydroxy-2,3,6,7-tetrahydrobenzofuran-3-carboxylic acid (ECDO) and the Zinc surface are shown in Figure 10.1. There were four ECDO···Zn interaction structures identified. The relative values as well as the interaction energy values suggest that the preferred structure is (Zn··· ECDO)-c. In this structure, the bond distance between the inhibitor and the metal surface is 2.339 Å, which indicates very strong interactions. Although all other structures demonstrate high binding energies, the relative energy values identify only (Zn··· ECDO)-c as the possible structure.

© University of Venda



(Zn··· ECDO)-a (Zn··· ECDO)-b

(Zn··· ECDO)-c (Zn··· ECDO)-d

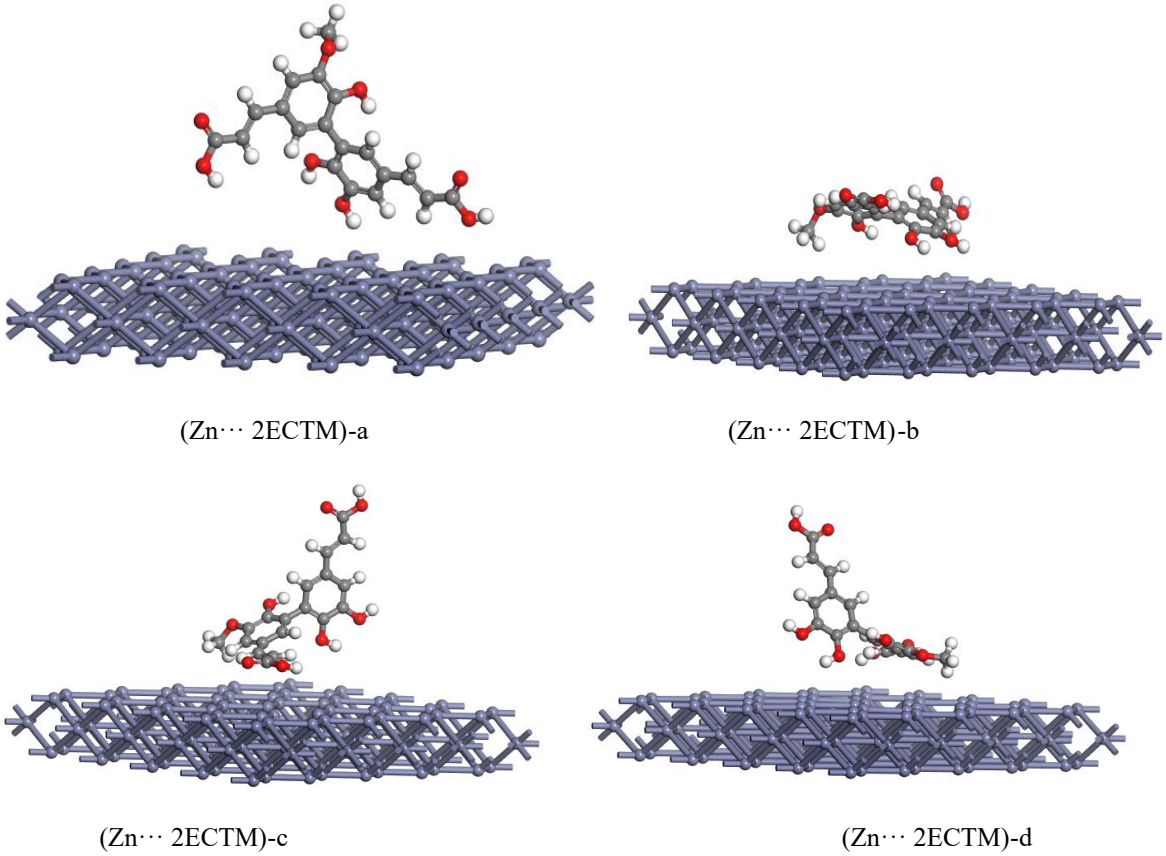
Figure 10.1: Different adsorption geometries of ECDO molecule on the Zn (111) surface in water solution.

Table 10.1: Relative Energies and interaction energies for the ECDO adsorption sites on zinc (111) surface.

Structure	Total energy (Ha)	Relative energy (kcal/mol)	ΔE_{inter} (kcal/mol)
(Zn··· ECDO)-a	-36184.046026	10.587	-491.703
(Zn··· ECDO)-b	-36184.041185	13.625	-488.665
(Zn··· ECDO)-c	-36184.062898	0.000	-502.290
(Zn··· ECDO)-d	-36184.046829	10.083	-492.207
(Zn··· 2ECTM)-a	-35423.283457	5,818	-264.932
(Zn··· 2ECTM)-b	-35423.290056	1,677	-269.073
(Zn··· 2ECTM)-c	-35423.287560	3,243	-267.506
(Zn··· 2ECTM)-d	-35423.292728	0.000	-270.749
(Zn···3BDA)-a	-36068,526467	22,161	-345.2963075
(Zn···3BDA)-b	-36068,537515	15,228	-352.2289275
(Zn···3BDA)-c	-36068,561782	0.000	-367.4564700
(Zn···3BDA)-d	-36068,559074	1,699	-365.7572000
(Zn···3DCT)-a	-36068.526472	0.000	-354.5092625

© University of Venda

The structures showing the interaction between (2E)-3-{5'-[(1E)-2-carboxyeth-1-en-1-yl]-2',3',6-trihydroxy-5-methoxy-[1,1'-biphenyl]-3-yl]prop-2-enoic acid (2ECTM) and the Zn surface are reported in Figure 10.2 while the energies are reported in Table 10.1. Nearly three of the structures obtained have relative energy below 4 kcal/mol so it is possible to consider that they are both significantly relevant. The interaction energy for the Zn···2ECTM is approximately 270 kcal/mol, indicating that it is lower than that found for (Zn··· ECDO). In other words, ECDO can be considered a better inhibitor than 2ECTM for the Zn surface.



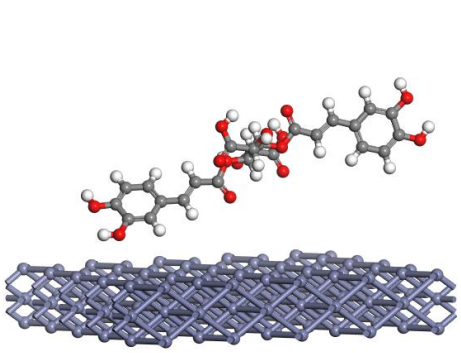
(Zn··· 2ECTM)-a (Zn··· 2ECTM)-b

(Zn··· 2ECTM)-c (Zn··· 2ECTM)-d

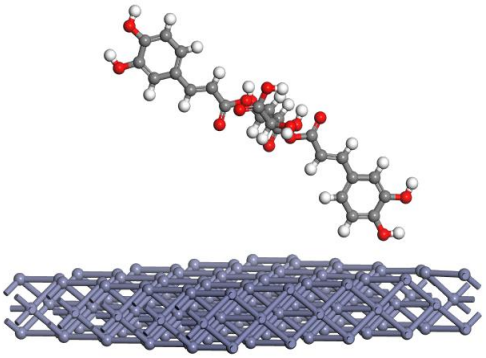
Figure 10.2: Different adsorption geometries of 2ECTM molecules on the Zn (111) surface in water solution.

The structures representing interactions between 3,4-bis(((E)-3-(3,4-dihydroxyphenyl)acryloyl)oxy)-2,5-dihydroxyhexanedioic acid (3BDA) and the Zn surface are reported in Figure 10.3 while the energies are reported in Table 10.1. Four structures were identified, of which only two, (Zn···3BDA)-c and (Zn···3BDA)-d, can be considered to exist because their energy difference is below 4 kcal/mol. The interaction energy for the Zn···3BDA is higher than that of Zn··· 2ECTM, but lower than that for Zn··· ECDO.

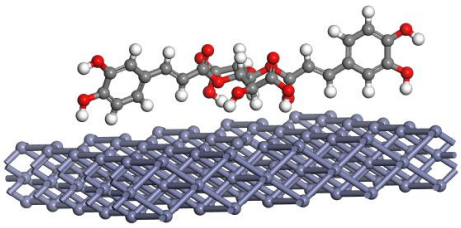
© University of Venda



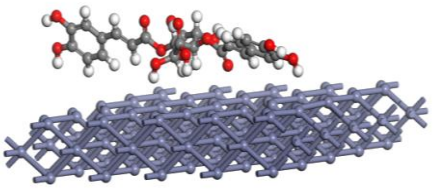
(Zn···3BDA)-a



(Zn···3BDA)-b



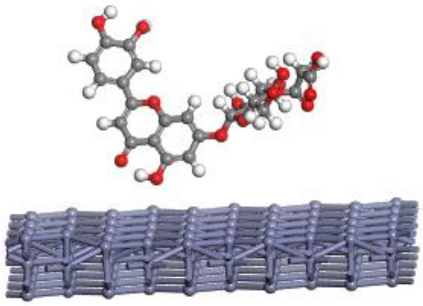
(Zn···3BDA)-c



(Zn···3BDA)-d

Figure 6.3: Different adsorption geometries of 3BDA molecule on the Zn (111) surface in water solution.

The optimize 3-((6-((2-(3,4-dihydroxyphenyl)-5-hydroxy-4-oxo-4H-chromen-7-yl)oxy)-3,4,5-trihydroxytetrahydro-2H-pyran-2-yl)methoxy)-3-oxopropanoic acid (3DCT) is shown in Figure 10.4. Only one stable structure was found. It has binding energy slightly lower than that for Zn···3BDA. The O atom is 3.203 **Å** to the surface.



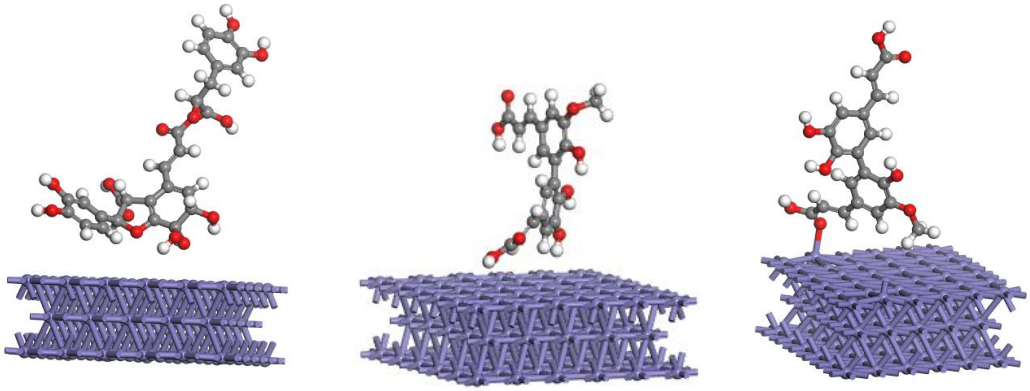
(Zn···3DCT)-a

Figure 10.4: Different adsorption geometries of 3DCT molecules on the Zn (111) surface in water solution.

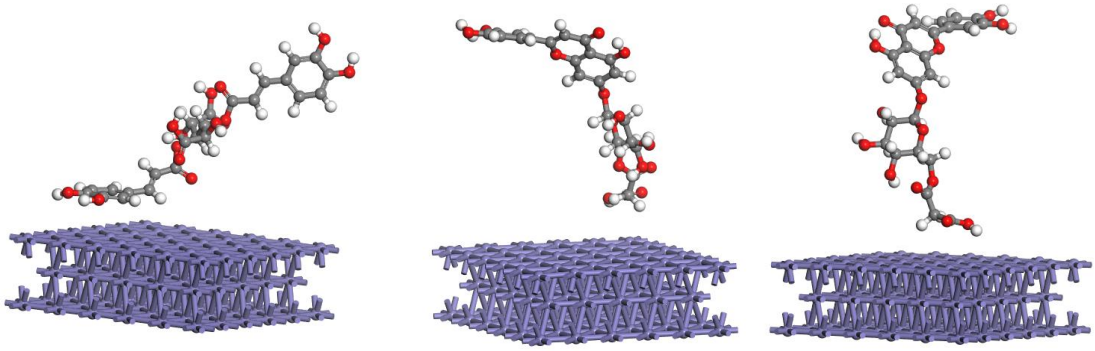
© University of Venda

10.3 Interaction of Mild Steel Surface with the Inhibitor Molecules

The Fe···inhibitor optimized structures are shown in Figure 10.5 while the interaction energies for the structures are reported in Table 10.2. The order increase in terms of the strength of interaction of the inhibitor with the metal surface is such that 2ECTM < 3BDA < 3BDA < ECDO. In other words, ECDO is the preferred inhibitor for interaction with the Fe surface. The high binding energies suggest that all compounds are able to protect the metal surface through chemical adsorption.



(Fe···ECDO) (Fe···2ECTM)-a (Fe···2ECTM)-b



(Fe···3BDA)-a (Fe···3DCT)-a (Fe···3DCT)-b

Figure 10.5: Adsorption geometry of inhibitor molecules on the Fe (111) surface in water solution.

© University of Venda

Table 10.2 Optimized energies for stable inhibitor molecules adsorption on Fe (111) surface.

Structure	FA + metal (Ha)	relative energy (kcal/mol)	ΔE_{inter} (kcal/mol)
(Fe···ECDO)	-12858.135045		-572.75188
(Fe···2ECTM)-a	-12097,358233	11,919	-337.0434275
(Fe···2ECTM)-b	-12097,377227	0.000	-348.9621625
(Fe···3BDA)	-12742.655675		-451.56406
(Fe···3DCT)-a	-12742,623929	8,907	-440.8520075
(Fe···3DCT)-b	-12742,638123	0,000	-449.7587425

© University of Venda

University of Venda
Creating Future Leaders

CHAPTER ELEVEN

CONCLUSIONS

© University of Venda

11 Conclusions and Recommendations

After completing various methods to investigate the corrosion inhibition of *A. phylicoides* extract on mild steel and zinc metals in acidic solutions of 1.5 M hydrochloric acid and sulphuric acid, the following conclusions and recommendations were drawn from the obtained results:

11.1 Conclusions

- Liquid Chromatography-Mass Spectrometry (LC-MS)

The LC-MS chromatogram highlighted distinctions between the non-UV radiated and UV-radiated *A. phylicoides* extracts, confirming the occurrence of geometric isomers which is important in this study since its focus on plants that can undergo geometrical isomerization. Additionally, it facilitated the identification of metabolites within the *A. phylicoides* extract.

- FTIR

Fourier Transform Infrared Spectroscopy (FTIR) has been employed to confirm the adsorption of non-UV radiated and UV radiated *A. phylicoides* extract onto the mild steel and zinc surface during the corrosion process. This adsorption formed a protective layer, which helps in preventing further corrosion of the mild steel and zinc. FTIR analysis provided valuable information about the chemical composition and molecular structure of the protective layer formed on the mild steel and zinc surface, thus supporting the conclusion that the extract effectively protects the metal from corrosion.

- Gravimetric analysis

The gravimetric analysis technique was employed to assess the weight loss of mild steel and zinc metal in 1.5 M hydrochloric acid and sulphuric acid at varying temperatures. This method was utilized to determine the corrosion rate and the percentage inhibition efficiency of both non-UV-radiated and UV-radiated *A. phylicoides* extracts. Under harsh conditions, observed at 333 K, the non-UV radiated *A. phylicoides* extract exhibited higher percentage inhibition efficiency for mild steel compared to the UV-radiated *A. phylicoides* extract. Conversely, the UV-radiated *A. phylicoides* extract demonstrated elevated inhibition efficiency at 303 K for zinc in both sulphuric and hydrochloric acid solutions, as well as for mild steel in sulphuric acid, except for mild steel in hydrochloric acid, where the non-UV radiated *A. phylicoides* extract displayed superior inhibition efficiency.

© University of Venda

- PDP

The inhibition efficiency percentage determined through Potentiodynamic Polarization (PDP) analysis revealed that the non-UV radiated *A. phylicoides* extract outperformed the UV-radiated *A. phylicoides* extract, except in the case of mild steel in hydrochloric acid. This underscores the superior corrosion inhibitory properties of the non-UV-radiated *A. phylicoides* extract compared to the UV-radiated *A. phylicoides* extract. Additionally, higher concentrations of *A. phylicoides* extract were associated with a decrease in corrosion current density, indicating a correlation between extract concentration and corrosion inhibition.

- EIS

The diameter of the semi-circle in the Nyquist plot for mild steel and the circle diameter for zinc metal increased with higher concentrations of both non-UV radiated and UV-radiated *A. phylicoides* extracts. This phenomenon contributed to the enhancement of corrosion inhibition efficiency. Notably, the non-UV radiated *A. phylicoides* extract exhibited greater percentage inhibition efficiency compared to the UV-radiated *A. phylicoides* for zinc metal, except in the case of mild steel in hydrochloric acid, as evidenced by Potentiodynamic Polarization (PDP) analysis.

- Contact angle

The conclusion drawn from the findings is that non-radiated *A. phylicoides* extract demonstrates superior inhibitive properties compared to UV-radiated *A. phylicoides* extract when it comes to protecting zinc and mild steel metals against corrosion in acidic environments. This conclusion is supported by the observation of higher contact angles, indicative of greater hydrophobicity and thus better corrosion resistance, with non-radiated extract treatments. Additionally, it is noted that sulphuric acid appears to be less aggressive than hydrochloric acid in terms of inducing corrosion. These results suggest that non-radiated *A. phylicoides* extract can be considered a promising corrosion inhibitor for metals exposed to acidic conditions, potentially offering practical applications in corrosion prevention strategies.

- Scanning Electron Microscopy (SEM) and Energy Dispersive X-ray Spectroscopy (EDS)

The SEM and EDS analyses demonstrated that both HCl and H_2SO_4 cause significant corrosion damage to mild steel and zinc. However, the introduction of *A. phylicoides* extracts,

© University of Venda

particularly the non-UV radiation *A. phylicoides*, effectively mitigated this damage. These findings suggest that non-UV radiated *A. phylicoides* extract could serve as a potent natural corrosion inhibitor for metals exposed to acidic environments, potentially extending the lifespan and durability of these materials in practical applications.

- Computational studies

The research delved into the adsorption and interaction energy between inhibitor molecules and the metal surface, revealing negative energies across the board, indicative of spontaneous interaction. With all energies surpassing -100 kcal/mol, it suggests a chemisorption phenomenon of the compounds onto the metal surface. The considerable energies observed imply a high level of inhibition efficiency. Typically, subjecting *A. phylicoides* extract to UV radiation diminishes its efficacy as a corrosion inhibitor due to alterations in its metabolites induced by UV exposure. Therefore, it is recommended to utilize *A. phylicoides* exclusively as a corrosion inhibitor for mild steel and zinc in HCl and H_2SO_4 solutions in its original, unexposed form, steering clear of UV radiation exposure.

11.2 Contribution and Recommendations

This study has made significant contributions to the field of green corrosion inhibition and geometric isomerization, including:

- Confirmation of UV-induced geometrical isomerization in *A. phylicoides* leaf extract using LC-MS, showing transformation of certain compounds from *trans* to *cis* configurations.
- Demonstration of corrosion inhibition potential of both non-UV-radiated and UV-radiated *A. phylicoides* extracts against mild steel and zinc in 1.5 M HCl and H_2SO_4 using weight loss, electrochemical, and surface analysis techniques.
- Establishment of temperature influence, revealing that *A. phylicoides* extracts are more effective at lower temperatures for mild steel and zinc in hydrochloric acid.

This study maintains the following recommendations:

- The use of *A. phylicoides* leaf extract is recommended as a viable green alternative to conventional organic and inorganic corrosion inhibitors, particularly for applications

© University of Venda

involving mild steel and zinc in acidic environments. Its eco-friendly nature makes it suitable for sustainable industrial use.

- Scaling up the application of *A. phylicoides* extract, including its formulation into commercial corrosion inhibitor products, should be explored.
- Long-term field studies and application trials in real-world industrial environments are necessary to validate the lab-scale results and assess performance under fluctuating conditions.
- Extending research to other metals, such as copper, aluminium, and stainless steel, may further broaden the extract's applicability.

© University of Venda

References

1. Wang, Q., *et al*., *Application of biomass corrosion inhibitors in metal corrosion control: a review.* Molecules, 2023. **28**(6): p. 2832.
2. Mbedzi, D.T., *et al*., *Ultraviolet (UV) light-induced geometrical isomerization of cinnamic acid containing molecules: A plausible, non-enzymatic approach to modify metabolite composition of plant extracts.* South African Journal of Botany, 2022. **150**: p. 845-850.
3. Rani, B.A. and B.B.J. Basu, *Green inhibitors for corrosion protection of metals and alloys: an overview.* International Journal of corrosion, 2012. **2012**(1): p. 380217.
4. Haldhar, R., *et al*., *Corrosion inhibitors: industrial applications and commercialization*, in *Sustainable corrosion inhibitors II: Synthesis, design, and practical applications*. 2021, ACS Publications. p. 219-235.
5. Koch, G.H., *et al*., *Cost of corrosion in the United States*, in *Handbook of environmental degradation of materials*. 2005, Elsevier. p. 3-24.
6. Liaaen-Jensen, S. and B.F. Lutnœes, *E/Z isomers and isomerization*, in *Carotenoids: Volume 4: Natural Functions*. 2008, Springer. p. 15-36.
7. Sui, Q., D. Borchardt, and D.L. Rabenstein, *Kinetics and equilibria of cis/trans isomerization of backbone amide bonds in peptoids.* Journal of the American Chemical Society, 2007. **129**(39): p. 12042-12048.
8. Novák, P., *Environmental deterioration of metals.* Environmental Deterioration of Materials; Escrig, F., Managing Ed.; WIT Press: Boston, 2007: p. 27-71.
9. Schweitzer, P.A., *Metallic materials: physical, mechanical, and corrosion properties*. Vol. 19. 2003: CRC press.
10. Birat, J.-P., *Society, materials, and the environment: The case of steel.* Metals, 2020. **10**(3): p. 331.
11. Obike, A., *et al*., *Review of the losses and devastation caused by corrosion in the Nigeria oil industry for over 30 years.* International Journal of corrosion and scale inhibition, 2020. **9**(1): p. 74-91.
12. Cramer, S., *et al*., *Corrosion prevention and remediation strategies for reinforced concrete coastal bridges.* Cement and Concrete Composites, 2002. **24**(1): p. 101-117.
13. Kadhim, M.G. and M.T. Ali, *A critical review on corrosion and its prevention in the oilfield equipment.* Journal of petroleum research and studies, 2017. **7**(2): p. 162-189.
14. Rathish, R., *et al*., *Corrosion issues in electronic equipments-an overview.* International Journal of Corrosion and Scale Inhibition, 2019. **8**(4): p. 799-815.
15. Koch, G., *Cost of corrosion.* Trends in oil and gas corrosion research and technologies, 2017: p. 3-30.
16. Harsimran, S., K. Santosh, and K. Rakesh, *Overview of corrosion and its control: A critical review.* Proc. Eng. Sci, 2021. **3**(1): p. 13-24.
17. Nazeer, A.A. and M. Madkour, *Potential use of smart coatings for corrosion protection of metals and alloys: A review.* Journal of Molecular Liquids, 2018. **253**: p. 11-22.
18. Cole, I.S. and D. Marney, *The science of pipe corrosion: A review of the literature on the corrosion of ferrous metals in soils.* Corrosion science, 2012. **56**: p. 5-16.
19. Shreir, L.L., *Corrosion: corrosion control*. 2013: Newnes.
20. Sherif, E.-S.M., *The role of corrosion inhibitors in protecting metallic structures against corrosion in harsh environments.* The role of colloidal systems in environmental protection, 2014: p. 509-526.
21. Natesan, M., G. Venkatachari, and N. Palaniswamy, *Kinetics of atmospheric corrosion of mild steel, zinc, galvanized iron and aluminium at 10 exposure stations in India.* Corrosion Science, 2006. **48**(11): p. 3584-3608.
22. Palanisamy, G., *Corrosion inhibitors.* Corrosion inhibitors, 2019. **2019**: p. 1-24.
23. Yadla, S.V., *et al*., *A review on corrosion of metals and protection.* International Journal of Engineering Science & Advanced Technology, 2012. **2**(3): p. 637-644.
24. Lewandowski, Z. and H. Beyenal, *Mechanisms of microbially influenced corrosion*. 2008, Springer.

© University of Venda

25. Sato, N., *Basics of corrosion chemistry.* Green Corrosion Chemistry and Engineering, 2012. **1**.
26. El-Meligi, A., *Corrosion preventive strategies as a crucial need for decreasing environmental pollution and saving economics.* Recent Patents on Corrosion Science, 2010. **2**(1).
27. Prasad, A.R., A. Kunyankandy, and A. Joseph, *Corrosion inhibition in oil and gas industry: Economic considerations.* Corrosion inhibitors in the oil and gas industry, 2020: p. 135-150.
28. Bowles, S.L., *et al*., *Intestinal transport and absorption of bioactive phenolic compounds from a chemically characterized aqueous extract of Athrixia phylicoides.* Journal of ethnopharmacology, 2017. **200**: p. 45-50.
29. Rampedi, I. and J. Olivier, *The use and potential commercial development of Athrixia phylicoides.* Acta Academica, 2005. **37**(3): p. 165-183.
30. Zakeri, A., E. Bahmani, and A.S.R. Aghdam, *Plant extracts as sustainable and green corrosion inhibitors for protection of ferrous metals in corrosive media: A mini review.* Corrosion Communications, 2022. **5**: p. 25-38.
31. Salleh, S.Z., *et al*., *Plant extracts as green corrosion inhibitor for ferrous metal alloys: A review.* Journal of Cleaner Production, 2021. **304**: p. 127030.
32. Obanijesu, E.O., *et al*., *Corrosion education as a tool for the survival of natural gas industry.* Nafta, 2010. **61**(12): p. 555-563.
33. Badawi, A. and I. Fahim, *A critical review on green corrosion inhibitors based on plant extracts: Advances and potential presence in the market.* Int. J. Corros. Scale Inhib, 2021. **10**(4): p. 1385-1406.
34. Bhaskaran, R., *et al*., *A review of differing approaches used to estimate the cost of corrosion (and their relevance in the development of modern corrosion prevention and control strategies).* Anti-Corrosion Methods and Materials, 2005. **52**(1): p. 29-41.
35. Signé, L. and C. Johnson, *Africa's mining potential: Trends, opportunities, challenges and strategies.* Policy paper, 2021(21/10).
36. Lahiri, A.K., *Applied metallurgy and corrosion control.* Indian Institute of Metals (ed.) Applied Metallurgy and Corrosion Control, 2017. **38**.
37. Azapagic, A., *Developing a framework for sustainable development indicators for the mining and minerals industry.* Journal of cleaner production, 2004. **12**(6): p. 639-662.
38. Reuter, M.A., *et al*., *Challenges of the circular economy: a material, metallurgical, and product design perspective.* Annual Review of Materials Research, 2019. **49**(1): p. 253-274.
39. Cutler, C.P., *Use of metals in our society.* Metal Allergy: From Dermatitis to Implant and Device Failure, 2018: p. 3-16.
40. Sin, J.R., *Investigation of the corrosion and tribocorrosion behaviour of metallic biomaterials*. 2015, Luleå tekniska universitet.
41. Zehra, S., M. Mobin, and R. Aslam, *Corrosion prevention and protection methods*, in *Eco-Friendly Corrosion Inhibitors*. 2022, Elsevier. p. 13-26.
42. Yang, L.J., *Risk Analysis and Mitigation Strategies for Preventing Corrosion during Industrial Power Failure.*
43. Bockris, J.O.M. and A.K. Reddy, *Electrochemistry in materials science.* Modern electrochemistry 2B: Electrodics in chemistry, engineering, biology, and environmental science, 2000: p. 1637-1788.
44. Kamachimudali, U., T. Sridhar, and B. Raj, *Corrosion of bio implants.* Sadhana, 2003. **28**: p. 601-637.
45. Zuleta, E.C., *et al*., *The oxidative stability of biodiesel and its impact on the deterioration of metallic and polymeric materials: a review.* Journal of the Brazilian Chemical Society, 2012. **23**: p. 2159-2175.
46. Asri, R., *et al*., *Corrosion and surface modification on biocompatible metals: A review.* Materials Science and Engineering: C, 2017. **77**: p. 1261-1274.
47. Chatterjee, C. and A. Lefcovitch, *The Gulf of Mexico oil disaster: some legal issues.* Amicus Curiae, 2010. **84**: p. 17.
48. Burlando, M., *et al*., *Investigation of the weather conditions during the collapse of the Morandi Bridge in Genoa on 14 August 2018.* Natural Hazards and Earth System Sciences Discussions, 2019. **2019**: p. 1-42.

© University of Venda

49. Hailwood, M., *Release of hazardous vapours at LG Polymers chemical plant in Visakhapatnam, Andhra Pradesh, India.* Loss Prevention Bulletin, 2020(274).
50. Alawode, A.J. and I. Ogunleye, *Maintenance, Security, and Environmental Implications of Pipeline Damage and Ruptures in the Niger Delta Region.* Maintenance, Security, and Environmental Implications of Pipeline Damage and Ruptures in the Niger Delta Region., 2011. **12**(1): p. 1-9.
51. Manik, J.A., J. Yardley, and B. Dhaka, *Building collapse in Bangladesh leaves scores dead.* The New York Times, 2013. **24**: p. A1.
52. Chellan, N., *et al*., *A toxicological assessment of Athrixia phylicoides aqueous extract following sub-chronic ingestion in a rat model.* Human & experimental toxicology, 2008. **27**(11): p. 819-825.
53. Revie, R.W., *Corrosion and corrosion control: an introduction to corrosion science and engineering*. 2008: John Wiley & Sons.
54. Sharma, S.K., *et al*., *Green corrosion inhibitors: an overview of recent research green corrosion inhibitors: an overview of recent research.* Journal of Corrosion Science and Engineering, 2008. **11**: p. 1-14.
55. Kaningini, A.G., *et al*., *Effect of optimized precursor concentration, temperature, and doping on optical properties of ZnO nanoparticles synthesized via a green route using bush tea (Athrixia phylicoides DC.) leaf extracts.* ACS omega, 2022. **7**(36): p. 31658-31666.
56. Mitsika, E., *Study of the corrosion behavior of S560 and S700 steels.* 2021.
57. Tamura, H., *The role of rusts in corrosion and corrosion protection of iron and steel.* Corrosion Science, 2008. **50**(7): p. 1872-1883.
58. Cicek, V., *Cathodic protection: Industrial solutions for protecting against corrosion*. 2013: John Wiley & Sons.
59. Czaban, M., *Aircraft corrosion–review of corrosion processes and its effects in selected cases.* Fatigue of Aircraft Structures, 2018. **2018**(10): p. 5-20.
60. Crolet, J., *Mechanisms of uniform corrosion under corrosion deposits.* Journal of materials science, 1993. **28**: p. 2589-2606.
61. Szklarska-Smialowska, Z., *Pitting corrosion of aluminum.* Corrosion science, 1999. **41**(9): p. 1743-1767.
62. Betts, A. and L. Boulton, *Crevice corrosion: review of mechanisms, modelling, and mitigation.* British corrosion journal, 1993. **28**(4): p. 279-296.
63. Zhang, X., *Galvanic corrosion.* Uhlig's Corrosion Handbook, 2011. **51**: p. 123.
64. Andresen, P.L., *Emerging issues and fundamental processes in environmental cracking in hot water.* Corrosion, 2008. **64**(5): p. 439-464.
65. Galvele, J. and S. de De Micheli, *Mechanism of intergranular corrosion of Al-Cu alloys.* Corrosion Science, 1970. **10**(11): p. 795-807.
66. McDowell, J., *et al*., *Fretting corrosion.* Anti-Corrosion methods and materials, 1954. **1**(7): p. 247-252.
67. Wan, Y., *et al*., *Corrosion behavior of copper at elevated temperature.* International Journal of Electrochemical Science, 2012. **7**(9): p. 7902-7914.
68. Borrelli, P., *et al*., *Soil erosion modelling: A global review and statistical analysis.* Science of the total environment, 2021. **780**: p. 146494.
69. Wang, Z., *et al*., *Predicting aqueous stability of solid with computed Pourbaix diagram using SCAN functional.* npj Computational Materials, 2020. **6**(1): p. 160.
70. Frankel, G., *Fundamentals of corrosion kinetics.* Active protective coatings: new-generation coatings for metals, 2016: p. 17-32.
71. Martinez, S. and M. Metikoš-Huković, *A nonlinear kinetic model introduced for the corrosion inhibitive properties of some organic inhibitors.* Journal of Applied Electrochemistry, 2003. **33**: p. 1137-1142.
72. Li, F.M., *et al*., *Corrosion chemistry of electrocatalysts.* Advanced Materials, 2022. **34**(52): p. 2200840.
73. Shreir, L.L., *Corrosion: metal/environment reactions*. 2013: Newnes.

© University of Venda

74. Guo, S., *et al*., *A critical review of corrosion development and rust removal techniques on the structural/environmental performance of corroded steel bridges.* Journal of cleaner production, 2019. **233**: p. 126-146.
75. Danielewski, M., *Kinetics of gaseous corrosion processes*, in *Corrosion: Fundamentals, Testing, and Protection*. 2003, ASM International. p. 97-105.
76. Heard, D.E., *Rapid acceleration of hydrogen atom abstraction reactions of OH at very low temperatures through weakly bound complexes and tunneling.* Accounts of chemical research, 2018. **51**(11): p. 2620-2627.
77. Cheng, X., *et al*., *Investigation of oxide film formation on 316L stainless steel in high-temperature aqueous environments.* Electrochimica Acta, 2011. **56**(17): p. 5860-5865.
78. Young, D.J., *High temperature oxidation and corrosion of metals*. Vol. 1. 2008: Elsevier.
79. Song, J., *et al*., *Corrosion protection of electrically conductive surfaces.* Metals, 2012. **2**(4): p. 450-477.
80. Yang, H. and N. Wu, *Ionic conductivity and ion transport mechanisms of solid-state lithium-ion battery electrolytes: A review.* Energy Science & Engineering, 2022. **10**(5): p. 1643-1671.
81. Cardoso, M., S. Amaral, and E. Martini, *Temperature effect in the corrosion resistance of Ni–Fe–Cr alloy in chloride medium.* Corrosion Science, 2008. **50**(9): p. 2429-2436.
82. Cooper, D.R., *et al*., *Component level strategies for exploiting the lifespan of steel in products.* Resources, Conservation and Recycling, 2014. **84**: p. 24-34.
83. North, N.A. and I.D. MacLeod, *Corrosion of metals*, in *Conservation of marine archaeological objects*. 1987, Elsevier. p. 68-98.
84. Rodríguez, J.J.S., F.J.S. Hernandez, and J.E.G. González, *The effect of environmental and meteorological variables on atmospheric corrosion of carbon steel, copper, zinc and aluminium in a limited geographic zone with different types of environment.* Corrosion Science, 2003. **45**(4): p. 799-815.
85. Kumar, V., *et al*., *Atmospheric corrosion of materials and their effects on mechanical properties: A brief review.* Materials Today: Proceedings, 2021. **44**: p. 4677-4681.
86. Abbas, M. and M. Shafiee, *An overview of maintenance management strategies for corroded steel structures in extreme marine environments.* Marine Structures, 2020. **71**: p. 102718.
87. Taleb Berrouane, M., *Dynamic corrosion risk assessment in the oil and gas production and processing facility*. 2020, Memorial University of Newfoundland.
88. Adumene, S., *Dynamic corrosion risk-based integrity assessment of marine and offshore systems*. 2021, Memorial University of Newfoundland.
89. Kibler, M., P. Cassidy, and J. Ong, *Analysis of coating blister failures and associated coating and substrate risks.* Journal of Protective Coatings & Linings, 2020. **37**(4): p. 20-25.
90. Murray, R.W., *Nanoelectrochemistry: metal nanoparticles, nanoelectrodes, and nanopores.* Chemical reviews, 2008. **108**(7): p. 2688-2720.
91. Örnek, C., C. Leygraf, and J. Pan, *On the Volta potential measured by SKPFM–fundamental and practical aspects with relevance to corrosion science.* Corrosion Engineering, Science and Technology, 2019. **54**(3): p. 185-198.
92. Hou, B., *et al*., *The cost of corrosion in China.* npj Materials Degradation, 2017. **1**(1): p. 4.
93. Roberge, P.R., *Corrosion inspection and monitoring*. 2007: John Wiley & Sons.
94. Balamurugan, A., *et al*., *Corrosion aspects of metallic implants—An overview.* Materials and corrosion, 2008. **59**(11): p. 855-869.
95. Milošev, I., *et al*., *Metals for joint replacement*, in *Joint replacement technology*. 2021, Elsevier. p. 65-122.
96. Konttinen, Y., *et al*., *Metals for joint replacement*, in *Joint replacement technology*. 2014, Elsevier. p. 81-151.
97. Fessler, R.R., *Pipeline corrosion.* Report, US Department of Transportation Pipeline and Hazardous Materials Safety Administration, Baker, Evanston, IL, 2008.
98. Singh, B. and J.N. Britton. *Offshore Risk Based Corrosion Integrity Management-A New Methodology*. in *NACE CORROSION*. 2001. NACE.
99. Montemor, M.F., *Functional and smart coatings for corrosion protection: A review of recent advances.* Surface and Coatings Technology, 2014. **258**: p. 17-37.

© University of Venda

100. Popoola, L.T., *et al*., *Corrosion problems during oil and gas production and its mitigation.* International Journal of Industrial Chemistry, 2013. **4**: p. 1-15.
101. Vidal, F., R. Vicente, and J.M. Silva, *Review of environmental and air pollution impacts on built heritage: 10 questions on corrosion and soiling effects for urban intervention.* Journal of Cultural Heritage, 2019. **37**: p. 273-295.
102. Aljibori, H., A. Alamiery, and A. Kadhum, *Advances in corrosion protection coatings: A comprehensive review.* Int. J. Corros. Scale Inhib, 2023. **12**(4): p. 1476-1520.
103. Baglioni, M., *et al*., *Advanced materials in cultural heritage conservation.* Molecules, 2021. **26**(13): p. 3967.
104. Abubakar, A.S., *et al*., *Integrating Life Cycle Cost Analysis into Pipeline Asset Integrity Management: A Comprehensive Approach in Decision Support Systems.* Journal of Hunan University Natural Sciences, 2024. **51**(1).
105. Kandil, M.E. *Maintaining the Integrity of Mature Facilities, a Typical Vogue to Ensure an Outstanding HSE*. in *International Petroleum Technology Conference*. 2005. IPTC.
106. Bastidas-Arteaga, E. and M.G. Stewart, *Economic assessment of climate adaptation strategies for existing reinforced concrete structures subjected to chloride-induced corrosion.* Structure and Infrastructure Engineering, 2016. **12**(4): p. 432-449.
107. Singh, R., *Corrosion control for offshore structures: cathodic protection and high-efficiency Coating*. 2014: Gulf Professional Publishing.
108. Chowwanonthapunya, T., S. Piriyawat, and W. Suphamitmongkol, *An Economic Consideration Guideline for the Selection of Corrosion-Control Strategies.* Srinakharinwirot Engineering Journal, 2016. **11**(2).
109. Musa, A.Y., *et al*., *Electrochemical and quantum chemical calculations on 4, 4-dimethyloxazolidine-2-thione as inhibitor for mild steel corrosion in hydrochloric acid.* Journal of Molecular Structure, 2010. **969**(1-3): p. 233-237.
110. Huang, I.-W., *et al*., *Dependence on temperature, pH, and Cl− in the uniform corrosion of aluminum alloys 2024-T3, 6061-T6, and 7075-T6.* Electrochimica Acta, 2016. **199**: p. 242-253.
111. Hyman, A.E., *Inspection, repair and rehabilitation of concrete structures due to corrosion.* International Journal of Materials and Product Technology, 2005. **23**(3-4): p. 309-337.
112. Alabtah, F.G., E. Mahdi, and F.F. Eliyan, *The use of fiber reinforced polymeric composites in pipelines: A review.* Composite Structures, 2021. **276**: p. 114595.
113. Laureys, A., *et al*., *Use of existing steel pipeline infrastructure for gaseous hydrogen storage and transport: A review of factors affecting hydrogen induced degradation.* Journal of Natural Gas Science and Engineering, 2022. **101**: p. 104534.
114. Zhang, X.G., *Corrosion of zinc and zinc alloys*, in *Corrosion: Materials*. 2005, ASM International. p. 402-417.
115. Odnevall Wallinder, I. and C. Leygraf, *A critical review on corrosion and runoff from zinc and zinc-based alloys in atmospheric environments.* Corrosion, 2017. **73**(9): p. 1060-1077.
116. Al Jabri, H., *et al*., *Zinc oxide nanoparticles and their biosynthesis: overview.* Life, 2022. **12**(4): p. 594.
117. Haas, K.H., *Application of Metal Oxide Nanoparticles and their Economic Impact.* Metal Oxide Nanoparticles: Formation, Functional Properties, and Interfaces, 2021. **1**: p. 29-65.
118. Pelino, M., *Recycling of zinc-hydrometallurgy wastes in glass and glass ceramic materials.* Waste management, 2000. **20**(7): p. 561-568.
119. Wehner, L.A., *Investigating High-Capacity Materials for Application in Flexible Lithium-Sulfur and Zinc-Ion Batteries*. 2023, ETH Zurich.
120. Kaya, M., S. Hussaini, and S. Kursunoglu, *Critical review on secondary zinc resources and their recycling technologies.* Hydrometallurgy, 2020. **195**: p. 105362.
121. Price, S.J. and R.B. Figueira, *Corrosion protection systems and fatigue corrosion in offshore wind structures: current status and future perspectives.* Coatings, 2017. **7**(2): p. 25.
122. Reboul, M. and B. Baroux, *Metallurgical aspects of corrosion resistance of aluminium alloys.* Materials and Corrosion, 2011. **62**(3): p. 215-233.
123. Brown, R.E. and H.L. Willis, *The economics of aging infrastructure.* IEEE Power and Energy Magazine, 2006. **4**(3): p. 36-43.

© University of Venda

124. Firouzdor, V., *et al*., *Corrosion of a stainless steel and nickel-based alloys in high temperature supercritical carbon dioxide environment.* Corrosion Science, 2013. **69**: p. 281-291.
125. Pilone, D., *Ferritic stainless steels for high temperature applications in oxidizing environments.* Recent Patents on Materials Science, 2009. **2**(1): p. 27-31.
126. Sequeira, C.A., *et al*., *On the performance of commercially available corrosion-resistant nickel alloys: a review.* Corrosion Reviews, 2016. **34**(4): p. 187-200.
127. İpek, M., *et al*., *An expert system based material selection approach to manufacturing.* Materials & Design, 2013. **47**: p. 331-340.
128. Ferraris, F., *et al*. *Measuring system for enhanced cathodic corrosion protection*. in *2012 IEEE International Instrumentation and Measurement Technology Conference Proceedings*. 2012. IEEE.
129. Kadhim, A., *et al*., *Corrosion inhibitors. A review.* International Journal of Corrosion and Scale Inhibition, 2021. **10**(1): p. 54-67.
130. Farh, H.M.H., M.E.A.B. Seghier, and T. Zayed, *A comprehensive review of corrosion protection and control techniques for metallic pipelines.* Engineering Failure Analysis, 2023. **143**: p. 106885.
131. Nixon, W.A. and J. Xiong, *Investigation of materials for the reduction and prevention of corrosion on highway maintenance equipment*. 2009, IIHR Hydroscience and Engineering, University of Iowa.
132. Balyanov, A., *et al*., *Corrosion resistance of ultra fine-grained Ti.* Scripta Materialia, 2004. **51**(3): p. 225-229.
133. Panchal, J., *et al*., *Comprehensive review and critical data analysis on corrosion and emphasizing on green eco-friendly corrosion inhibitors for oil and gas industries.* Journal of Bio-and Tribo-Corrosion, 2021. **7**(3): p. 107.
134. Page, C., V. Ngala, and M. Page, *Corrosion inhibitors in concrete repair systems.* Magazine of Concrete Research, 2000. **52**(1): p. 25-37.
135. Bender, R., *et al*., *Corrosion challenges towards a sustainable society.* Materials and corrosion, 2022. **73**(11): p. 1730-1751.
136. Habib, S., R. Shakoor, and R. Kahraman, *A focused review on smart carriers tailored for corrosion protection: Developments, applications, and challenges.* Progress in Organic Coatings, 2021. **154**: p. 106218.
137. Verma, C., *et al*., *Recent developments in sustainable corrosion inhibitors: design, performance and industrial scale applications.* Materials Advances, 2021. **2**(12): p. 3806-3850.
138. Jia, R., *et al*., *Microbiologically influenced corrosion and current mitigation strategies: a state of the art review.* International biodeterioration & biodegradation, 2019. **137**: p. 42-58.
139. Ma, I.W., *et al*., *A concise review on corrosion inhibitors: types, mechanisms and electrochemical evaluation studies.* Journal of Coatings Technology and Research, 2022: p. 1-28.
140. Ahmed, M.A., S. Amin, and A.A. Mohamed, *Current and emerging trends of inorganic, organic and eco-friendly corrosion inhibitors.* RSC advances, 2024. **14**(43): p. 31877-31920.
141. Shwetha, K., B. Praveen, and B.K. Devendra, *A review on corrosion inhibitors: types, mechanisms, electrochemical analysis, corrosion rate and efficiency of corrosion inhibitors on mild steel in an acidic environment.* Results in Surfaces and Interfaces, 2024: p. 100258.
142. Abdel-Karim, A.M. and A.M. El-Shamy, *A review on green corrosion inhibitors for protection of archeological metal artifacts.* Journal of Bio-and Tribo-Corrosion, 2022. **8**(2): p. 35.
143. Aslam, R., *et al*., *A comprehensive review of corrosion inhibitors employed to mitigate stainless steel corrosion in different environments.* Journal of Molecular Liquids, 2022. **364**: p. 119992.
144. Wei, H., *et al*., *Green inhibitors for steel corrosion in acidic environment: state of art.* Materials Today Sustainability, 2020. **10**: p. 100044.
145. Pasche, S., *et al*., *Effects of ionic strength and surface charge on protein adsorption at PEGylated surfaces.* The Journal of Physical Chemistry B, 2005. **109**(37): p. 17545-17552.

© University of Venda

146. Wirtanen, T., *et al*., *Cathodic corrosion of metal electrodes—how to prevent it in electroorganic synthesis.* Chemical Reviews, 2021. **121**(17): p. 10241-10270.
147. Rivetti, M.L.S., *et al*., *Corrosion inhibitors for reinforced concrete.* Corrosion inhibitors, principles and recent applications, 2018: p. 35-58.
148. Schmuki, P., *From Bacon to barriers: a review on the passivity of metals and alloys.* Journal of Solid State Electrochemistry, 2002. **6**: p. 145-164.
149. Lerotholi, L., *et al*., *Bush tea (Athrixia phylicoides): A review of the traditional uses, bioactivity and phytochemistry.* South African Journal of Botany, 2017. **110**: p. 4-17.
150. Siko, M.N., *The use of the Athrixia phylicoides plant in Tshwane: an anthropological study*. 2016, University of South Africa.
151. Mabona, U., *Antimicrobial activity of southern African medicinal plants with dermatological relevance*. 2014.
152. Tshikhudo, P., K. Ntushelo, and F. Mudau, *Users' perception of traditional knowledge and the use of wild bush tea (Athrixia phylicoides) in selected areas of the Vhembe District, Limpopo Province, South Africa.* Indilinga African Journal of Indigenous Knowledge Systems, 2016. **15**(3): p. 360-375.
153. Lye, K.A., *et al*., *Botanical-medicinal dictionary for East Africa.* Makerere Herbarium Handbook, 2008(2).
154. Welcome, A. and B.-E. Van Wyk, *An inventory and analysis of the food plants of southern Africa.* South African Journal of Botany, 2019. **122**: p. 136-179.
155. Tenorio, A.T., *et al*., *Processing concepts for the use of green leaves as raw materials for the food industry.* Journal of cleaner production, 2017. **164**: p. 736-748.
156. Barletta, M., *et al*., *Scratch, wear and corrosion resistant organic inorganic hybrid materials for metals protection and barrier.* Materials & Design, 2015. **69**: p. 130-140.
157. Song, W., *et al*., *Poly (vinyl alcohol) for multi-functionalized corrosion protection of metals: a review.* Journal of Cleaner Production, 2023. **394**: p. 136390.
158. Agrawal, A. and K.K. Sahu, *An overview of the recovery of acid from spent acidic solutions from steel and electroplating industries.* Journal of hazardous materials, 2009. **171**(1-3): p. 61-75.
159. Le Veen, H.H. and L. Hallinger, *The role of pepsin, peptic inhibitory substances, and hydrochloric acid in normal subjects and in the production of peptic ulcers.* The Journal of Clinical Investigation, 1947. **26**(4): p. 761-772.
160. Casas, J., F. Alvarez, and L. Cifuentes, *Aqueous speciation of sulfuric acid–cupric sulfate solutions.* Chemical engineering science, 2000. **55**(24): p. 6223-6234.
161. Emam, E.A., *Clay adsorption perspective on petroleum refining industry.* Industrial Engineering, 2018. **2**(1): p. 19-25.
162. Bajpai, P., *Pulp and paper industry: Chemicals*. 2015: Elsevier.
163. Stupnišek-Lisac, E., S. Podbršček, and T. Sorić, *Non-toxic organic zinc corrosion inhibitors in hydrochloric acid.* Journal of Applied Electrochemistry, 1994. **24**(8): p. 779-784.
164. Rudnik, E., G. Włoch, and L. Szatan, *Comparative studies on acid leaching of zinc waste materials.* Metallurgical Research & Technology, 2018. **115**(1): p. 110.
165. Owoeye, F.T., *et al*., *Investigation of corrosion performance of aluminum and zinc alloys in three acidic media.* Engineering Reports, 2020. **2**(1): p. e12103.
166. Bråtveit, M., *et al*., *Exposure to sulfuric acid in zinc production.* Annals of occupational hygiene, 2004. **48**(2): p. 159-170.
167. Rudnik, E., *Recovery of zinc from zinc ash by leaching in sulphuric acid and electrowinning.* Hydrometallurgy, 2019. **188**: p. 256-263.
168. Mizuta, S., *et al*., *Hydrogen production from hydrogen sulfide by the iron-chlorine hybrid process.* Industrial & engineering chemistry research, 1991. **30**(7): p. 1601-1608.
169. de la Fuente, D., *et al*., *Long-term atmospheric corrosion of mild steel.* Corrosion Science, 2011. **53**(2): p. 604-617.
170. Groysman, A., *Corrosion monitoring.* Corrosion Reviews, 2009. **27**(4-5): p. 205-343.
171. Andrade, C. and C. Alonso, *Corrosion rate monitoring in the laboratory and on-site.* Construction and building materials, 1996. **10**(5): p. 315-328.

© University of Venda

172. De Jong, O. and D. Treagust, *The teaching and learning of electrochemistry*, in *Chemical education: Towards research-based practice*. 2002, Springer. p. 317-337.
173. Saveant, J.M., *Catalysis of chemical reactions by electrodes.* Accounts of Chemical Research, 1980. **13**(9): p. 323-329.
174. Trasatti, S., *Electrochemistry and environment: the role of electrocatalysis.* International journal of hydrogen energy, 1995. **20**(10): p. 835-844.
175. Xia, D.-H., *et al*., *Electrochemical measurements used for assessment of corrosion and protection of metallic materials in the field: A critical review.* Journal of Materials Science & Technology, 2022. **112**: p. 151-183.
176. Leng, W., *et al*., *Investigation of the kinetics of a TiO2 photoelectrocatalytic reaction involving charge transfer and recombination through surface states by electrochemical impedance spectroscopy.* The Journal of Physical Chemistry B, 2005. **109**(31): p. 15008-15023.
177. Ribeiro, D. and J. Abrantes, *Application of electrochemical impedance spectroscopy (EIS) to monitor the corrosion of reinforced concrete: A new approach.* Construction and Building Materials, 2016. **111**: p. 98-104.
178. Lewyn, L.L., *et al*., *Analog circuit design in nanoscale CMOS technologies.* Proceedings of the IEEE, 2009. **97**(10): p. 1687-1714.
179. Van Haeverbeke, M., M. Stock, and B. De Baets, *Equivalent electrical circuits and their use across electrochemical impedance spectroscopy application domains.* Ieee Access, 2022. **10**: p. 51363-51379.
180. Kaiser, C.J., *The capacitor handbook*. 2012: Springer Science & Business Media.
181. Burgmayer, P. and R.W. Murray, *Ion gate electrodes. Polypyrrole as a switchable ion conductor membrane.* The Journal of Physical Chemistry, 1984. **88**(12): p. 2515-2521.
182. Merriam, J., *Induced polarization and surface electrochemistry.* Geophysics, 2007. **72**(4): p. F157-F166.
183. Cheng, Y., *et al*., *A study of the corrosion of aluminum alloy 2024-T3 under thin electrolyte layers.* Corrosion Science, 2004. **46**(7): p. 1649-1667.
184. Ramírez Barat, B. and E. Cano, *In situ electrochemical impedance spectroscopy measurements and their interpretation for the diagnostic of metallic cultural heritage: a review.* ChemElectroChem, 2018. **5**(19): p. 2698-2716.
185. Macdonald, J.R., *Impedance spectroscopy.* Annals of biomedical engineering, 1992. **20**: p. 289-305.
186. Iribarren, J.I., *et al*., *Corrosion rate evaluation by gravimetric and electrochemical techniques applied to the metallic reinforcing structures of a historic building.* Journal of Cultural Heritage, 2017. **27**: p. 153-163.
187. Zehra, S., M. Mobin, and R. Aslam, *Corrosion inhibitors: An introduction*, in *Environmentally Sustainable Corrosion Inhibitors*. 2022, Elsevier. p. 47-67.
188. Firouzi, A., M. Abdolhosseini, and R. Ayazian, *Service life prediction of corrosion-affected reinforced concrete columns based on time-dependent reliability analysis.* Engineering Failure Analysis, 2020. **117**: p. 104944.
189. Baboian, R., *Corrosion tests and standards: application and interpretation*. Vol. 20. 2005: ASTM international.
190. Arteaga, C.C., *Corrosion evaluation of AISI-309 exposed to 50 mol% Na2SO4–50 mol% V2O5 at high temperature applying electrochemical techniques and the weight loss method.* International Journal of Electrochemical Science, 2012. **7**(12): p. 12283-12300.
191. Wood, R.J., *Tribo-corrosion of coatings: a review.* Journal of Physics D: Applied Physics, 2007. **40**(18): p. 5502.
192. White, J. and S. Akhter, *Adsorbate-adsorbate interactions during coadsorption on metals.* Critical Reviews in Solid State and Material Sciences, 1988. **14**(2): p. 131-173.
193. Bacsik, Z., J. Mink, and G. Keresztury, *FTIR spectroscopy of the atmosphere. I. Principles and methods.* Applied spectroscopy reviews, 2004. **39**(3): p. 295-363.
194. Fernández-Carrasco, L., *et al*., *Infrared spectroscopy in the analysis of building and construction materials.* Infrared spectroscopy–Materials science, engineering and technology, 2012. **510**.

© University of Venda

195. Coury, C. and A.M. Dillner, *A method to quantify organic functional groups and inorganic compounds in ambient aerosols using attenuated total reflectance FTIR spectroscopy and multivariate chemometric techniques.* Atmospheric Environment, 2008. **42**(23): p. 5923-5932.
196. Paluszkiewicz, C., *et al*., *FT-IR study of montmorillonite–chitosan nanocomposite materials.* Spectrochimica Acta Part A: Molecular and Biomolecular Spectroscopy, 2011. **79**(4): p. 784-788.
197. Mayerhöfer, T.G., A.V. Pipa, and J. Popp, *Beer's law-why integrated absorbance depends linearly on concentration.* ChemPhysChem, 2019. **20**(21): p. 2748-2753.
198. Inkson, B.J., *Scanning electron microscopy (SEM) and transmission electron microscopy (TEM) for materials characterization*, in *Materials characterization using nondestructive evaluation (NDE) methods*. 2016, Elsevier. p. 17-43.
199. Zhou, W., *et al*., *Fundamentals of scanning electron microscopy (SEM).* Scanning microscopy for nanotechnology: techniques and applications, 2007: p. 1-40.
200. Kosasih, F., *Low Dose Analytical Electron Microscopy of Hybrid Perovskite Photovoltaic Devices*. 2022.
201. Ruette, F., C. Gonzalez, and M. Sanchez, *Atomic orbital participation on a chemical bond through a binding energy partitioning scheme.* Journal of Molecular Structure: THEOCHEM, 2001. **549**(1-2): p. 9-22.
202. Scimeca, M., *et al*., *Energy Dispersive X-ray (EDX) microanalysis: A powerful tool in biomedical research and diagnosis.* European journal of histochemistry: EJH, 2018. **62**(1).
203. Cotton, F.A., *My life in the golden age of chemistry: more fun than fun*. 2014: Elsevier.
204. Seed, L., *The significance of organisms in corrosion.* Corrosion Reviews, 1990. **9**(1-2): p. 1-102.
205. Al-Amiery, A., W.N.R.W. Isahak, and W.K. Al-Azzawi, *Sustainable corrosion Inhibitors: A key step towards environmentally responsible corrosion control.* Ain Shams Engineering Journal, 2024: p. 102672.
206. Feiler, C., *et al*., *In silico screening of modulators of magnesium dissolution.* Corrosion science, 2020. **163**: p. 108245.
207. Obi-Egbedi, N., I. Obot, and M.I. El-Khaiary, *Quantum chemical investigation and statistical analysis of the relationship between corrosion inhibition efficiency and molecular structure of xanthene and its derivatives on mild steel in sulphuric acid.* Journal of Molecular Structure, 2011. **1002**(1-3): p. 86-96.
208. Shahini, M., *et al*., *Superior inhibition action of the Mish Gush (MG) leaves extract toward mild steel corrosion in HCl solution: Theoretical and electrochemical studies.* Journal of Molecular Liquids, 2021. **332**: p. 115876.
209. Haque, J., *et al*., *Corrosion inhibition of mild steel in 1M HCl using environmentally benign Thevetia peruviana flower extracts.* Sustainable Chemistry and Pharmacy, 2021. **19**: p. 100354.
210. Sedik, A., *et al*., *Dardagan Fruit extract as eco-friendly corrosion inhibitor for mild steel in 1 M HCl: Electrochemical and surface morphological studies.* Journal of the Taiwan Institute of Chemical Engineers, 2020. **107**: p. 189-200.
211. Ezeugo, J., O. Onukwuli, and M. Omotioma, *Optimization of corrosion inhibition of Picralima nitida leaves extract as green corrosion inhibitor for zinc in 1.0 M HCl.* World News of Natural Sciences, 2017(15): p. 139-161.
212. Fouda, A., O. Mohamed, and H. Elabbasy, *Ferula hermonis plant extract as safe corrosion inhibitor for zinc in hydrochloric acid solution.* Journal of Bio-and Tribo-Corrosion, 2021. **7**(4): p. 135.
213. Ferkous, H., *et al*., *A comparative study of novel synthesized sulfamide compounds: Electrochemical, morphological, XPS, and theoretical investigations on copper corrosion inhibition in 1.0 M HCl.* Journal of Molecular Liquids, 2024. **394**: p. 123781.
214. Yıldız, R., *et al*., *Corrosion behavior of mild steel in 1 M HCl with Cyclotrichium niveum as a green inhibitor.* Materials Chemistry and Physics, 2024. **312**: p. 128654.
215. Yeo, J., *Antioxidant capacity and phenolic profiles of lentils as affected by processing*. 2018, Memorial University of Newfoundland.

© University of Venda

216. Fernández-Solis, C.D., *et al*., *Fundamentals of electrochemistry, corrosion and corrosion protection.* Soft Matter at Aqueous Interfaces, 2016: p. 29-70.
217. Brycki, B.E., *et al*., *Organic corrosion inhibitors.* Corrosion inhibitors, principles and recent applications, 2018. **3**: p. 33.
218. Chaubey, N., *et al*., *Frontiers and advances in green and sustainable inhibitors for corrosion applications: A critical review.* Journal of Molecular Liquids, 2021. **321**: p. 114385.
219. Battie, C. and M. Verschoore, *Cutaneous solar ultraviolet exposure and clinical aspects of photodamage.* Indian Journal of Dermatology, Venereology and Leprology, 2012. **78**: p. 9.
220. Sharma, R. and N. Singh, *Introduction to UV-B Radiation*, in *UV-B Radiation and Crop Growth*. 2023, Springer. p. 1-11.
221. Blatchley III, E.R., *et al*., *Far UV-C radiation: An emerging tool for pandemic control.* Critical Reviews in Environmental Science and Technology, 2023. **53**(6): p. 733-753.
222. Khaldi, C., *et al*., *Corrosion effect on the electrochemical properties of LaNi3. 55Mn0. 4Al0. 3Co0. 75 and LaNi3. 55Mn0. 4Al0. 3Fe0. 75 negative electrodes used in Ni–MH batteries.* Materials Science and Engineering: B, 2010. **175**(1): p. 22-28.
223. Khan, A., *et al*., *Frontiers and challenges in electrochemical corrosion monitoring; surface and downhole applications.* Sensors, 2020. **20**(22): p. 6583.
224. Encinas-Sánchez, V., *et al*., *Electrochemical impedance spectroscopy (EIS): An efficient technique for monitoring corrosion processes in molten salt environments in CSP applications.* Solar energy materials and solar cells, 2019. **191**: p. 157-163.
225. Urquidi-Macdonald, M. and D. Macdonald, *Modeling mechanisms in biocorrosion.* Understanding Biocorrosion, 2014: p. 243-277.
226. Jee, Y., *et al*., *High performance Bi-layered electrolytes via atomic layer deposition for solid oxide fuel cells.* Journal of Power Sources, 2014. **253**: p. 114-122.
227. Inzelt, G., *Electrode potentials*, in *Handbook of reference electrodes*. 2013, Springer. p. 1-24.
228. Goldman, D.E., *Potential, impedance, and rectification in membranes.* The Journal of general physiology, 1943. **27**(1): p. 37-60.
229. Oh, S.-E. and B.E. Logan, *Proton exchange membrane and electrode surface areas as factors that affect power generation in microbial fuel cells.* Applied microbiology and biotechnology, 2006. **70**: p. 162-169.
230. Rathnayaka, R., *et al*., *"EduPotStat": Construction and testing of a low cost potentiostat.* 2020.
231. Jin, M., *et al*., *Electrochemical characterization of solid Ag/AgCl reference electrode with different electrolytes for corrosion monitoring of steel in concrete.* Electrochemistry, 2016. **84**(6): p. 383-389.
232. Mansfeld, F., *Tafel slopes and corrosion rates from polarization resistance measurements.* Corrosion, 1973. **29**(10): p. 397-402.
233. Srinivasan, S., *Electrode/electrolyte interfaces: Structure and kinetics of charge transfer*, in *Fuel Cells: From fundamentals to applications*. 2006, Springer. p. 27-92.
234. Verma, D.K., *Density functional theory (DFT) as a powerful tool for designing corrosion inhibitors in aqueous phase.* Advanced engineering testing, 2018. **87**.
235. Shi, Z., M. Liu, and A. Atrens, *Measurement of the corrosion rate of magnesium alloys using Tafel extrapolation.* Corrosion science, 2010. **52**(2): p. 579-588.
236. Ibrahimi, B.E., J.V. Nardeli, and L. Guo, *An overview of corrosion.* Sustainable corrosion inhibitors I: fundamentals, methodologies, and industrial applications, 2021: p. 1-19.
237. Maurya, R., *et al*., *Relationship between the electron-transfer coefficients of the oxygen reduction reaction estimated from the Gibbs free energy of activation and the Butler–Volmer equation.* Physical Chemistry Chemical Physics, 2023. **25**(1): p. 700-707.
238. Fahim, A., *et al*., *A critical examination of corrosion rate measurement techniques applied to reinforcing steel in concrete.* Materials and Corrosion, 2018. **69**(12): p. 1784-1799.
239. Komary, M., *et al*., *Low-cost technologies used in corrosion monitoring.* Sensors, 2023. **23**(3): p. 1309.
240. Trentin, A., *et al*., *Electrochemical characterization of polymeric coatings for corrosion protection: A review of advances and perspectives.* Polymers, 2022. **14**(12): p. 2306.

© University of Venda

241. Randviir, E.P. and C.E. Banks, *Electrochemical impedance spectroscopy: an overview of bioanalytical applications.* Analytical methods, 2013. **5**(5): p. 1098-1115.
242. Cohen, I., *et al*., *Long term stability of capacitive de-ionization processes for water desalination: The challenge of positive electrodes corrosion.* Electrochimica Acta, 2013. **106**: p. 91-100.
243. Kohn, E.C. and L.A. Liotta, *Molecular insights into cancer invasion: strategies for prevention and intervention.* Cancer research, 1995. **55**(9): p. 1856-1862.
244. Baer, R., *et al*., *Ab initio study of the alternating current impedance of a molecular junction.* The Journal of chemical physics, 2004. **120**(7): p. 3387-3396.
245. Kötz, R. and M. Carlen, *Principles and applications of electrochemical capacitors.* Electrochimica acta, 2000. **45**(15-16): p. 2483-2498.
246. Angst, U.M., *Challenges and opportunities in corrosion of steel in concrete.* Materials and Structures, 2018. **51**(1): p. 4.
247. Landolfo, R., L. Cascini, and F. Portioli, *Modeling of metal structure corrosion damage: A state of the art report.* Sustainability, 2010. **2**(7): p. 2163-2175.
248. Shipilov, S., *What corrosion costs Canada: or, can we afford to ignore corrosion.* Materials Development and Performance of Sulphur Capture Plants, CIM, Montreal, Quebec, 2009: p. 55-76.
249. Goldstein, J.I., *et al*., *Scanning electron microscopy and X-ray microanalysis*. 2017: springer.
250. Egerton, R., P. Li, and M. Malac, *Radiation damage in the TEM and SEM.* Micron, 2004. **35**(6): p. 399-409.
251. Dutta, A., *Fourier transform infrared spectroscopy.* Spectroscopic methods for nanomaterials characterization, 2017: p. 73-93.
252. Hammiche, A., *et al*., *Photothermal FT-IR spectroscopy: A step towards FT-IR microscopy at a resolution better than the diffraction limit.* Applied spectroscopy, 1999. **53**(7): p. 810-815.
253. Segneanu, A.E., *et al*., *Organic compounds FT-IR spectroscopy*. Vol. 145. 2012: InTech Romania.
254. Wang, Z.-H., *et al*., *Generation of equal-intensity coherent optical beams by binary geometrical phase on metasurface.* Applied Physics Letters, 2016. **108**(26).
255. Wing, R.R. and J.O. Hill, *Successful weight loss maintenance.* Annual review of nutrition, 2001. **21**(1): p. 323-341.
256. Plota, A. and A. Masek, *Lifetime prediction methods for degradable polymeric materials—A short review.* Materials, 2020. **13**(20): p. 4507.
257. Gillespie, R.J. and E.A. Robinson, *Electron domains and the VSEPR model of molecular geometry.* Angewandte Chemie International Edition in English, 1996. **35**(5): p. 495-514.
258. Saraswati, T.E., *et al*. *Understanding valence-shell electron-pair repulsion (VSEPR) theory using origami molecular models*. in *Journal of Physics: Conference Series*. 2017. IOP Publishing.
259. Cruz-Cabeza, A.J. and J. Bernstein, *Conformational polymorphism.* Chemical reviews, 2014. **114**(4): p. 2170-2191.
260. Ebenso, E.E., *et al*., *Molecular modelling of compounds used for corrosion inhibition studies: a review.* Physical Chemistry Chemical Physics, 2021. **23**(36): p. 19987-20027.
261. Hehre, W.J., *A guide to molecular mechanics and quantum chemical calculations*. Vol. 2. 2003: Wavefunction Irvine, CA.
262. De Regt, H.W., *Erwin Schrödinger*, in *Ernst Mach's Vienna 1895–1930: Or Phenomenalism as Philosophy of Science*. 2001, Springer. p. 85-104.
263. Erbil, H., *A Simple Solution of the Time-Independent Schrodinger Equation in One Dimension.* arXiv preprint quant-ph/0305158, 2003.
264. Picón, A., *Time-dependent Schrödinger equation for molecular core-hole dynamics.* Physical Review A, 2017. **95**(2): p. 023401.
265. Claverie, P. and S. Diner, *The concept of molecular structure in quantum theory: interpretation problems.* Israel Journal of Chemistry, 1980. **19**(1-4): p. 54-81.
266. Rau, A.R.P., *Two electrons in a Coulomb potential. Double-continuum wave functions and threshold law for electron-atom ionization.* Physical Review A, 1971. **4**(1): p. 207.

© University of Venda

267. Cederbaum, L.S., *Born–Oppenheimer approximation and beyond for time-dependent electronic processes.* The Journal of chemical physics, 2008. **128**(12).
268. Abedi, A., N.T. Maitra, and E. Gross, *Correlated electron-nuclear dynamics: Exact factorization of the molecular wavefunction.* The Journal of chemical physics, 2012. **137**(22).
269. Deumens, E., *et al*., *Time-dependent theoretical treatments of the dynamics of electrons and nuclei in molecular systems.* Reviews of Modern Physics, 1994. **66**(3): p. 917.
270. Hertel, I.V., *et al*., *Multi-electron Atoms.* Atoms, Molecules and Optical Physics 1: Atoms and Spectroscopy, 2015: p. 495-547.
271. Altunbulak, M. and A. Klyachko, *The Pauli principle revisited.* Communications in Mathematical Physics, 2008. **282**: p. 287-322.
272. Lu, T., *A comprehensive electron wavefunction analysis toolbox for chemists, Multiwfn.* The Journal of Chemical Physics, 2024. **161**(8).
273. Koohrokhi, T., S. Kartal, and A. Mohammadi, *Anti-PT transformations and complex non-Hermitian PT-symmetric superpartners.* Annals of Physics, 2023. **459**: p. 169490.
274. Kobus, J. and S. Lehtola, *Review of the finite difference Hartree-Fock method for atoms and diatomic molecules, and its implementation in the x2dhf program.* arXiv preprint arXiv:2408.03679, 2024.
275. Weser, O., *et al*., *Stochastic generalized active space self-consistent field: Theory and application.* Journal of chemical theory and computation, 2021. **18**(1): p. 251-272.
276. Lehtola, S., F. Blockhuys, and C. Van Alsenoy, *An overview of self-consistent field calculations within finite basis sets.* Molecules, 2020. **25**(5): p. 1218.
277. Kowol, F., *Analytically exact solution of the Schrödinger equation.* system. **2**: p. 0.
278. Onishi, T., *Molecular Orbital Calculation*, in *Ferroelectric Perovskites for High-Speed Memory: A Mechanism Revealed by Quantum Bonding Motion*. 2022, Springer. p. 125-141.
279. Gu[1], F.L., J. Yu, and W. Yang, *Chemical Concepts from Molecular Orbital Theory Feng Long Gu[1], Jincheng Yu[2], and Weitao Yang2 1 South China Normal University, School of Environment, Ministry of Education, Key Laboratory of Theoretical Chemistry of Environment, Guangzhou 510006, People's Republic of China 2 Duke University, Department of Chemistry, Box 90346, Durham, NC 27708-0346, USA.* Exploring Chemical Concepts Through Theory and Computation, 2024: p. 1.
280. Paschoal, D.F.d.S., *et al*., *Basis sets for heavy atoms*, in *Basis Sets in Computational Chemistry*. 2021, Springer. p. 183-214.
281. Bo, Z., *The Intrinsic Nature of Chemical Bond Based on Proton and Electron as Electric Monopole Pairs.* Available at SSRN 4030602.
282. Majumdar, D., *et al*., *Slater-Type Orbitals*, in *Basis Sets in Computational Chemistry*. 2021, Springer. p. 17-40.
283. Lehtola, S., *Polarized Gaussian basis sets from one-electron ions.* The Journal of Chemical Physics, 2020. **152**(13).
284. Speake, B., *Electronic Structure Methods for Large Molecular Systems and Materials in Strong Magnetic Fields*. 2023, University of Nottingham.
285. Pauls, M., D. Schnieders, and R. Dronskowski, *Embedded localized molecular-orbital representations for periodic wave functions.* The Journal of Physical Chemistry A, 2023. **127**(31): p. 6541-6551.
286. Forster, A. and L. Visscher, *GW100: A slater-type orbital perspective.* Journal of chemical theory and computation, 2021. **17**(8): p. 5080-5097.
287. García Pérez, C., *Basis sets in computational chemistry: analysis of the second period diatomic fluorides*. 2020.
288. Oleynichenko, A.V., *et al*., *LIBGRPP: A library for the evaluation of molecular integrals of the generalized relativistic pseudopotential operator over Gaussian functions.* Symmetry, 2023. **15**(1): p. 197.
289. Zhou, Y., *Quantum Chemistry in Solid-State Simulations: Gaussian Basis Sets Development and ab-initio Green's Function Based Realistic System Applications*. 2022.
290. Zhu, J.-Y., *et al*., *From bonds to interactions: Comprehensive molecular characterization via polarizable bond-dipole approach.* Physical Chemistry Chemical Physics, 2023. **25**(43): p. 29867-29880.

© University of Venda

291. Anderson, J.S., A. de Jesús Mortera-Carbonell, and C.F. Matta, *Nonnuclear maxima in the molecular electron density*, in *Advances in Quantum Chemical Topology Beyond QTAIM*. 2023, Elsevier. p. 375-388.
292. Bauschlicher Jr, C.W., *The reliability of the small-core lanthanide effective core potentials.* Theoretical Chemistry Accounts, 2022. **141**(3): p. 11.
293. Chi, Y.-C. and C. Huang, *High-quality local pseudopotentials for metals.* Journal of Chemical Theory and Computation, 2024. **20**(8): p. 3231-3241.
294. Nandy, A., *et al*., *Computational discovery of transition-metal complexes: from high-throughput screening to machine learning.* Chemical reviews, 2021. **121**(16): p. 9927-10000.
295. Schultze, J., *Tackling multi-reference systems with quantum monte carlo methods*. 2023, Dissertation, RWTH Aachen University, 2023.
296. Hoffmann, M., *et al*., *Magnetic and Electronic Properties of Complex Oxides from First-Principles.* physica status solidi (b), 2020. **257**(7): p. 1900671.
297. McArdle, S., *et al*., *Quantum computational chemistry.* Reviews of Modern Physics, 2020. **92**(1): p. 015003.
298. Khomskii, D.I. and S.V. Streltsov, *Orbital effects in solids: Basics, recent progress, and opportunities.* Chemical Reviews, 2020. **121**(5): p. 2992-3030.
299. Luo, T., *et al*., *Rational design of active sites in alumina-based catalysts to optimize antibonding-orbital occupancy for tetrafluoromethane decomposition.* Environmental Science: Nano, 2023. **10**(12): p. 3307-3316.
300. Hamlin, T.A., *et al*., *Energy decomposition analysis in the context of quantitative molecular orbital theory*. 2021, De Gruyter: Berlin. p. 199-212.
301. Apriliyanto, Y.B. and N. Nurrosyid, *Comparative Analysis of Electronic Structures Calculations: A Simple Test Case Set for Kohn-Sham Density Functional Theory and Hartree-Fock Methods.* Indonesian Journal of Chemical Studies, 2023. **2**(2): p. 54-60.
302. Lehtola, S., *Straightforward and accurate automatic auxiliary basis set generation for molecular calculations with atomic orbital basis sets.* Journal of Chemical Theory and Computation, 2021. **17**(11): p. 6886-6900.
303. Steinhauser, M.O., *Computational Methods on Electronic/Atomistic Scale*, in *Computational Multiscale Modeling of Fluids and Solids: Theory and Applications*. 2022, Springer. p. 229-275.
304. Coşkun, M. and M. Ertürk, *Double hyperbolic cosine basis sets for LCAO calculations.* Molecular Physics, 2022. **120**(17): p. e2109527.
305. Wojtkiewicz, J. and P.H. Chankowski, *Ground state energies of the hubbard models and the hartree–fock approximation.* Reports on Mathematical Physics, 2023. **92**(2): p. 227-241.
306. Jensen, S.R., *et al*., *Kinetic energy-free Hartree–Fock equations: an integral formulation.* Journal of Mathematical Chemistry, 2023. **61**(2): p. 343-361.
307. Kraus, P., *Basis set extrapolations for density functional theory.* Journal of Chemical Theory and Computation, 2020. **16**(9): p. 5712-5722.
308. Prasad, V.K., A. Otero-de-la-Roza, and G.A. DiLabio, *Fast and accurate quantum mechanical modeling of large molecular systems using small basis set Hartree–Fock methods corrected with atom-centered potentials.* Journal of Chemical Theory and Computation, 2022. **18**(4): p. 2208-2232.
309. Herbert, J.M., *Density-functional theory for electronic excited states*, in *Theoretical and computational photochemistry*. 2023, Elsevier. p. 69-118.
310. Liu, W., *et al*., *Gadolinium changes the local electron densities of nickel 3d orbitals for efficient electrocatalytic CO2 reduction.* Angewandte Chemie International Edition, 2022. **61**(18): p. e202201166.
311. Sabet, M.M., *et al*., *Minimal length implications on the Hartree–Fock theory.* Physica Scripta, 2021. **96**(12): p. 125016.
312. Li, L., *et al*., *Kohn-Sham equations as regularizer: Building prior knowledge into machine-learned physics.* Physical review letters, 2021. **126**(3): p. 036401.
313. Cuierrier, E., P.-O. Roy, and M. Ernzerhof, *The factorization ansatz for non-local approximations to the exchange–correlation hole.* The Journal of Chemical Physics, 2022. **156**(18).

© University of Venda

314. Suresh, C.H., G.S. Remya, and P.K. Anjalikrishna, *Molecular electrostatic potential analysis: A powerful tool to interpret and predict chemical reactivity.* Wiley Interdisciplinary Reviews: Computational Molecular Science, 2022. **12**(5): p. e1601.
315. Chaudhary, M.K., *et al.*, *Computational evaluation on molecular stability, reactivity, and drug potential of frovatriptan from DFT and molecular docking approach.* Computational and Theoretical Chemistry, 2020. **1191**: p. 113031.
316. Ruedenberg, K., *Atoms and interatomic bonding synergism inherent in molecular electronic wave functions.* The Journal of Chemical Physics, 2022. **157**(2).
317. Domingo, L.R. and N. Acharjee, *Molecular electron density theory: a new theoretical outlook on organic chemistry.* Frontiers in Computational Chemistry, 2020: p. 174-227.
318. López, R. and R. Gómez, *Band-gap energy estimation from diffuse reflectance measurements on sol–gel and commercial TiO 2: a comparative study.* Journal of sol-gel science and technology, 2012. **61**: p. 1-7.
319. Radhi, A.H., *et al.*, *HOMO-LUMO energies and geometrical structures effecton corrosion inhibition for organic compounds predict by DFT and PM3 methods.* NeuroQuantology, 2020. **18**(1): p. 37.
320. Miar, M., *et al.*, *Theoretical investigations on the HOMO–LUMO gap and global reactivity descriptor studies, natural bond orbital, and nucleus-independent chemical shifts analyses of 3-phenylbenzo [d] thiazole-2 (3 H)-imine and its para-substituted derivatives: Solvent and substituent effects.* Journal of Chemical Research, 2021. **45**(1-2): p. 147-158.
321. Islam, N. and D.C. Ghosh, *On the electrophilic character of molecules through its relation with electronegativity and chemical hardness.* International Journal of Molecular Sciences, 2012. **13**(2): p. 2160-2175.
322. Sánchez-Márquez, J., *et al.*, *Introducing "UCA-FUKUI" software: reactivity-index calculations.* Journal of molecular modeling, 2014. **20**: p. 1-13.
323. Pérez, P., *et al.*, *The electrophilicity index in organic chemistry*, in *Theoretical and computational chemistry*. 2007, Elsevier. p. 139-201.
324. Islam, N. and C.C. Ghosh, *The Time Evolution of the Electronegativity Part-2: Applications*, in *Modern Trends in Chemistry and Chemical Engineering*. 2011, Apple Academic Press. p. 40-63.
325. Torrent-Sucarrat, M., *et al.*, *On the applicability of local softness and hardness.* Physical Chemistry Chemical Physics, 2010. **12**(5): p. 1072-1080.
326. Huang, Y., *et al.*, *Evaluating frontier orbital energy and HOMO/LUMO gap with descriptors from density functional reactivity theory.* Journal of molecular modeling, 2017. **23**: p. 1-12.
327. Sun, Z., *et al.*, *Low band gap polycyclic hydrocarbons: from closed-shell near infrared dyes and semiconductors to open-shell radicals.* Chemical Society Reviews, 2012. **41**(23): p. 7857-7889.
328. Nayak, P.K. and N. Periasamy, *Calculation of electron affinity, ionization potential, transport gap, optical band gap and exciton binding energy of organic solids using 'solvation' model and DFT.* Organic Electronics, 2009. **10**(7): p. 1396-1400.
329. Lindahl, A., *et al.*, *The electron affinity of tungsten.* The European Physical Journal D, 2010. **60**(2): p. 219-222.
330. Choudhary, V., *et al.*, *DFT calculations on molecular structures, HOMO–LUMO study, reactivity descriptors and spectral analyses of newly synthesized diorganotin (IV) 2-chloridophenylacetohydroxamate complexes.* Journal of computational chemistry, 2019. **40**(27): p. 2354-2363.
331. Shankar, R., K. Senthilkumar, and P. Kolandaivel, *Calculation of ionization potential and chemical hardness: a comparative study of different methods.* International Journal of Quantum Chemistry, 2009. **109**(4): p. 764-771.
332. Bacal, M. and M. Wada, *Negative hydrogen ion production mechanisms.* Applied physics reviews, 2015. **2**(2).
333. D'Andrade, B.W., *et al.*, *Relationship between the ionization and oxidation potentials of molecular organic semiconductors.* Organic Electronics, 2005. **6**(1): p. 11-20.
334. Oganov, A.R. and C.W. Glass, *Crystal structure prediction using ab initio evolutionary techniques: Principles and applications.* The Journal of chemical physics, 2006. **124**(24).

© University of Venda

335. Lu, Y., X. Shu, and X. Liao, *Size effect for achieving high mechanical performance body-centered cubic metals and alloys.* Sci. China Mater, 2018. **61**: p. 1495-1516.
336. Wu, Z., *et al*., *Temperature dependence of the mechanical properties of equiatomic solid solution alloys with face-centered cubic crystal structures.* Acta Materialia, 2014. **81**: p. 428-441.
337. Gao, M.C., *et al*., *High-entropy alloys in hexagonal close-packed structure.* Metallurgical and Materials Transactions A, 2016. **47**: p. 3322-3332.
338. Callister Jr, W.D. and D.G. Rethwisch, *Fundamentals of materials science and engineering: an integrated approach*. 2020: John Wiley & Sons.
339. French, A.D. and M. Santiago Cintrón, *Cellulose polymorphy, crystallite size, and the Segal Crystallinity Index.* Cellulose, 2013. **20**: p. 583-588.
340. Marcos, C., *Periodicity, Crystalline Lattices, Symbols, and Notations*, in *Crystallography: Introduction to the Study of Minerals*. 2022, Springer. p. 13-47.
341. Zhang, J.-M., *et al*., *General compliance transformation relation and applications for anisotropic cubic metals.* Materials Letters, 2008. **62**(8-9): p. 1328-1332.
342. Makola, M. M., Dubery, I. A., Koorsen, G., Steenkamp, P. A., Kabanda, M. M., Du Preez, L. L., & Madala, N. E. (2016). The Effect of Geometrical Isomerism of 3, 5-Dicaffeoylquinic Acid on Its Binding Affinity to HIV-Integrase Enzyme: A Molecular Docking Study. *Evidence-Based Complementary and Alternative Medicine*, *2016*(1), 4138263.
343. Hopfgartner, G., C. Husser, and M. Zell, *High-throughput quantification of drugs and their metabolites in biosamples by LC-MS/MS and CE-MS/MS: possibilities and limitations.* Therapeutic drug monitoring, 2002. **24**(1): p. 134-143.
344. Zwiener, C. and F.H. Frimmel, *LC-MS analysis in the aquatic environment and in water treatment technology–a critical review: Part II: Applications for emerging contaminants and related pollutants, microorganisms and humic acids.* Analytical and bioanalytical chemistry, 2004. **378**: p. 862-874.
345. Lu, X., *et al*., *LC–MS-based metabonomics analysis.* Journal of Chromatography B, 2008. **866**(1-2): p. 64-76.
346. Nägele, E., *et al*., *2D-LC/MS techniques for the identification of proteins in highly complex mixtures.* Expert review of proteomics, 2004. **1**(1): p. 37-46.
347. Kalili, K.M. and A. de Villiers, *Recent developments in the HPLC separation of phenolic compounds.* Journal of separation science, 2011. **34**(8): p. 854-876.
348. Ramphinwa, M.L., *et al*., *Effect of UV-induced geometrical isomerization of hydroxyl-cinnamic acid-containing molecules of bush tea (Athrixia phylicoides DC.) using UHPLC-QTOF-MS.* Scientia Horticulturae, 2022. **301**: p. 111124.
349. Ebada, S.S., *et al*., *Methods for isolation, purification and structural elucidation of bioactive secondary metabolites from marine invertebrates.* Nature protocols, 2008. **3**(12): p. 1820-1831.
350. Ahmed ES, J. and G.M. Ganesh, *A comprehensive overview on corrosion in RCC and its prevention using various green corrosion inhibitors.* Buildings, 2022. **12**(10): p. 1682.
351. Sithuba, T., Kabanda, M. M., Madala, N. E., & Murulana, L. C. (2024). Exploration of UV-induced geometrical isomer-enriched Helichrysum kraussii extract as a corrosion inhibitor for Al (111) surface in 1.0 M hydrochloric acid: An experimental and theoretical study. *Results in Surfaces and Interfaces*, *16*, 100268.
352. Ludwig, M., K. Dührkop, and S. Böcker, *Bayesian networks for mass spectrometric metabolite identification via molecular fingerprints.* Bioinformatics, 2018. **34**(13): p. i333-i340.
353. Wintle, B.A., *et al*., *The use of Bayesian model averaging to better represent uncertainty in ecological models.* Conservation biology, 2003. **17**(6): p. 1579-1590.
354. Ludwig, M., *et al*., *ZODIAC: Database-independent molecular formula annotation using Gibbs sampling reveals unknown small molecules.* biorxiv, 2019: p. 842740.
355. Ludwig, M., *et al*., *De novo molecular formula annotation and structure elucidation using SIRIUS 4.* Computational methods and data analysis for metabolomics, 2020: p. 185-207.

© University of Venda

356. Eriksson, L., *et al*., *Methods for reliability and uncertainty assessment and for applicability evaluations of classification-and regression-based QSARs.* Environmental health perspectives, 2003. **111**(10): p. 1361-1375.
357. Mombeshora, M., G.F. Chi, and S. Mukanganyama, *Research Article Antibiofilm Activity of Extract and a Compound Isolated from Triumfetta welwitschii against Pseudomonas aeruginosa.* 2021.
358. Ezeamaku, U., *et al*., *Corrosion inhibition of aluminum using guava leaf extract as an inhibitor.* Moroccan Journal of Chemistry, 2023. **11**(3): p. 11-3 (2023) 763-779.
359. Veilleux, C.C., *et al*., *Color vision and niche partitioning in a diverse neotropical primate community in lowland Amazonian Ecuador.* Ecology and Evolution, 2021. **11**(10): p. 5742-5758.
360. Kim, G., *et al*., *Highly sunlight reflective and infrared semi-transparent nanomesh textiles.* ACS nano, 2021. **15**(10): p. 15962-15971.
361. Kaur, S. and A. Sharma, *Performance estimation of SISO and MIMO Ro-FSO link under atmospheric turbulence.* Optical and Quantum Electronics, 2024. **56**(1): p. 48.
362. Espinoza, A., *et al*., *Glucofuranose as Corrosion Inhibitor in Api 5l X70 Steel Immersed in Saline Medium by Different Hydrodynamic Conditions and Theoretical Study.* Guillermo E. and Galván-Martínez, Ricardo and Orozco-Cruz, Ricardo and Leon, Juan Pablo and Miralrio, A. and Castro, M. and Martínez Jiménez, Anatolio, Glucofuranose as Corrosion Inhibitor in Api 5l X70 Steel Immersed in Saline Medium by Different Hydrodynamic Conditions and Theoretical Study.
363. Arokiasamy, P., *et al*., *Metakaolin/sludge based geopolymer adsorbent on high removal efficiency of Cu2+.* Case Studies in Construction Materials, 2022. **17**: p. e01428.
364. Wang, D., Y. Tian, and L. Jiang, *Abnormal Properties of Low-Dimensional Confined Water.* Small, 2021. **17**(31): p. 2100788.
365. Gao, X., *et al*., *Behaviors and influencing factors of the heavy metals adsorption onto microplastics: A review.* Journal of Cleaner Production, 2021. **319**: p. 128777.
366. Merdas, S.M. and M.Y. Hayal, *Heterocyclic compounds containing N atoms as corrosion inhibitors: a review.* Journal of Bioscience and Applied Research, 2021. **7**(2): p. 93-103.
367. Celik, S., S. Akyuz, and A.E. Ozel, *The Importance of Polymers in Medicine and Their FTIR and Raman Spectroscopic Investigations*, in *Development, Properties, and Industrial Applications of 3D Printed Polymer Composites*. 2023, IGI Global. p. 170-187.
368. Bellamy, C., *Administering central-local relations, 1871-1919: the local government board in its fiscal and cultural context*. 1988: Manchester University Press.
369. Pisareva, A., *et al*., *The structure and properties of phenol-2, 4-disulfonic acid dihydrate.* Russian Journal of Physical Chemistry A, Focus on Chemistry, 2008. **82**: p. 355-363.
370. Zellner, M.B. and J.G. Chen, *Surface science and electrochemical studies of WC and W2C PVD films as potential electrocatalysts.* Catalysis Today, 2005. **99**(3-4): p. 299-307.
371. Dubova, H.Y., *Advances in research on food aroma recovery.* 2017.
372. Charron, A., *et al*., *Quantitative interpretation of divergence between PM10 and PM2. 5 mass measurement by TEOM and gravimetric (Partisol) instruments.* Atmospheric Environment, 2004. **38**(3): p. 415-423.
373. Thompson, M., *et al*., *Harmonized guidelines for the use of recovery information in analytical measurement.* Pure and applied chemistry, 1999. **71**(2): p. 337-348.
374. Punpruk, S., M. Thammachart, and Y. Gunaltun. *Field testing of volatile corrosion inhibitors and evaluation of batch treatment efficiency by cooled probe*. in *NACE CORROSION*. 2010. NACE.
375. Amin, M.A., *et al*., *A study of the inhibition of iron corrosion in HCl solutions by some amino acids.* Corrosion science, 2010. **52**(5): p. 1684-1695.
376. Xu, Y., *et al*., *Study on corrosion behavior and mechanism of AISI 4135 steel in marine environments based on field exposure experiment.* Science of the Total Environment, 2022. **830**: p. 154864.
377. Lundström, J.N., *et al*., *Methods for building an inexpensive computer-controlled olfactometer for temporally-precise experiments.* International Journal of Psychophysiology, 2010. **78**(2): p. 179-189.

© University of Venda

378. Watson, J.G., *et al*., *Filter processing and gravimetric analysis for suspended particulate matter samples.* Aerosol Science and Engineering, 2017. **1**: p. 93-105.
379. Timmen, L., *et al*., *Absolute gravimetry with the Hannover meters JILAg-3 and FG5-220, and their deployment in a Danish-German cooperation.* ZfV-Zeitschrift für Geodäsie, Geoinformation und Landmanagement, 2008(zfv 3/2008).
380. Laurent, B.A., B.M. Bennett, and R.M. Harrington. *Development of test methods and factors for evaluation of oilfield corrosion inhibitors at high temperature*. in *NACE CORROSION*. 2017. NACE.
381. Aziz, I.A.A., *et al*., *Weight loss, thermodynamics, SEM, and electrochemical studies on N-2-methylbenzylidene-4-antipyrineamine as an inhibitor for mild steel corrosion in hydrochloric acid.* Lubricants, 2022. **10**(2): p. 23.
382. Husaini, M., B. Usman, and M.B. Ibrahim, *Evaluation of corrosion behaviour of aluminum in different environment.* Bayero Journal of Pure and Applied Sciences, 2018. **11**(1): p. 88-92.
383. Kocaefe, D., *et al*., *Thermogravimetric study of high temperature treatment of aspen: effect of treatment parameters on weight loss and mechanical properties.* Journal of Materials Science, 2007. **42**: p. 854-866.
384. Quadri, T.W., *et al*., *Fundamentals of corrosion chemistry*, in *Environmentally Sustainable Corrosion Inhibitors*. 2022, Elsevier. p. 25-45.
385. Meletis, E., *et al*., *Electrolytic plasma processing for cleaning and metal-coating of steel surfaces.* Surface and coatings technology, 2002. **150**(2-3): p. 246-256.
386. Wilson, M.R., *et al*., *Nanoparticle interactions with zinc and iron: Implications for toxicology and inflammation.* Toxicology and applied pharmacology, 2007. **225**(1): p. 80-89.
387. McCafferty, E. and N. Hackerman, *Kinetics of iron corrosion in concentrated acidic chloride solutions.* Journal of the Electrochemical Society, 1972. **119**(8): p. 999.
388. Singh, A.K. and M. Quraishi, *Investigation of adsorption of isoniazid derivatives at mild steel/hydrochloric acid interface: Electrochemical and weight loss methods.* Materials Chemistry and Physics, 2010. **123**(2-3): p. 666-677.
389. Stringer, J., *High-temperature corrosion of superalloys.* Materials Science and Technology, 1987. **3**(7): p. 482-493.
390. Sun, J., *et al*., *Review on microwave–metal discharges and their applications in energy and industrial processes.* Applied Energy, 2016. **175**: p. 141-157.
391. Goidanich, S., L. Lazzari, and M. Ormellese, *AC corrosion. Part 2: Parameters influencing corrosion rate.* Corrosion Science, 2010. **52**(3): p. 916-922.
392. Zuo, R., *Biofilms: strategies for metal corrosion inhibition employing microorganisms.* Applied microbiology and biotechnology, 2007. **76**(6): p. 1245-1253.
393. Migahed, M., *et al*., *Synthesis of some novel non ionic surfactants based on tolyltriazole and evaluation their performance as corrosion inhibitors for carbon steel.* Egyptian Journal of Petroleum, 2013. **22**(1): p. 149-160.
394. Touir, R., *et al*., *Sodium gluconate as corrosion and scale inhibitor of ordinary steel in simulated cooling water.* Corrosion Science, 2008. **50**(6): p. 1530-1537.
395. Kokalj, A., *et al*., *What determines the inhibition effectiveness of ATA, BTAH, and BTAOH corrosion inhibitors on copper?* Journal of the American Chemical Society, 2010. **132**(46): p. 16657-16668.
396. Budijono, S.J., *et al*., *Block copolymer surface coverage on nanoparticles.* Colloids and Surfaces A: Physicochemical and Engineering Aspects, 2010. **360**(1-3): p. 105-110.
397. Taylor, C., *Corrosion informatics: an integrated approach to modelling corrosion.* Corrosion Engineering, Science and Technology, 2015. **50**(7): p. 490-508.
398. Zaki, A., *et al*., *Non-destructive evaluation for corrosion monitoring in concrete: A review and capability of acoustic emission technique.* Sensors, 2015. **15**(8): p. 19069-19101.
399. Dong, Y. and D.M. Frangopol, *Risk-informed life-cycle optimum inspection and maintenance of ship structures considering corrosion and fatigue.* Ocean Engineering, 2015. **101**: p. 161-171.
400. Abd El Haleem, S., S. Abd El Wanees, and A. Bahgat, *Environmental factors affecting the corrosion behaviour of reinforcing steel. VI. Benzotriazole and its derivatives as corrosion inhibitors of steel.* Corrosion Science, 2014. **87**: p. 321-333.

© University of Venda

401. Singh, P., *et al*., *Electrochemical, theoretical, and surface morphological studies of corrosion inhibition effect of green naphthyridine derivatives on mild steel in hydrochloric acid.* The Journal of Physical Chemistry C, 2016. **120**(6): p. 3408-3419.
402. Maayta, A. and N. Al-Rawashdeh, *Inhibition of acidic corrosion of pure aluminum by some organic compounds.* Corrosion science, 2004. **46**(5): p. 1129-1140.
403. Hughes, A.E., *et al*., *Designing green, self-healing coatings for metal protection.* NPG Asia Materials, 2010. **2**(4): p. 143-151.
404. Lazorenko, G., A. Kasprzhitskii, and T. Nazdracheva, *Anti-corrosion coatings for protection of steel railway structures exposed to atmospheric environments: A review.* Construction and Building Materials, 2021. **288**: p. 123115.
405. Sastri, V.S., *Green corrosion inhibitors: theory and practice*. 2012: John Wiley & Sons.
406. Boughoues, Y., *et al*., *Adsorption and corrosion inhibition performance of some environmental friendly organic inhibitors for mild steel in HCl solution via experimental and theoretical study.* Colloids and Surfaces A: Physicochemical and Engineering Aspects, 2020. **593**: p. 124610.
407. El Azzouzi, M., *et al*., *Some hydrazine derivatives as corrosion inhibitors for mild steel in 1.0 M HCl: weight loss, electrochemichal, SEM and theoretical studies.* Journal of Molecular Liquids, 2016. **221**: p. 633-641.
408. Ituen, E., O. Akaranta, and A. James, *Evaluation of performance of corrosion inhibitors using adsorption isotherm models: an overview.* Chem. Sci. Int. J, 2017. **18**(1): p. 1-34.
409. Syafiuddin, A., *et al*., *Application of the kinetic and isotherm models for better understanding of the behaviors of silver nanoparticles adsorption onto different adsorbents.* Journal of environmental management, 2018. **218**: p. 59-70.
410. Rastogi, R.P., *et al*., *Molecular mechanisms of ultraviolet radiation-induced DNA damage and repair.* Journal of nucleic acids, 2010. **2010**(1): p. 592980.
411. Al-Ghouti, M.A. and D.A. Da'ana, *Guidelines for the use and interpretation of adsorption isotherm models: A review.* Journal of hazardous materials, 2020. **393**: p. 122383.
412. Liu, S., *Cooperative adsorption on solid surfaces.* Journal of colloid and interface science, 2015. **450**: p. 224-238.
413. Sohn, S. and D. Kim, *Modification of Langmuir isotherm in solution systems—definition and utilization of concentration dependent factor.* Chemosphere, 2005. **58**(1): p. 115-123.
414. Sung, W., *Some observations on surface partitioning of Cd, Cu, and Zn in estuaries.* Environmental science & technology, 1995. **29**(5): p. 1303-1312.
415. Maiti, A., *et al*., *Adsorption of arsenite using natural laterite as adsorbent.* Separation and Purification Technology, 2007. **55**(3): p. 350-359.
416. Stephens, C.I.A., *The Paradoxical Effect of National Diversity and Inclusion Management on Organizational Commitment*. 2023: Liberty University.
417. Saha, P., *et al*., *Insight into adsorption equilibrium, kinetics and thermodynamics of Malachite Green onto clayey soil of Indian origin.* Chemical Engineering Journal, 2010. **165**(3): p. 874-882.
418. Wu, C.-H., *et al*., *Modeling competitive adsorption of molybdate, sulfate, selenate, and selenite using a Freundlich-type multi-component isotherm.* Chemosphere, 2002. **47**(3): p. 283-292.
419. Park, J.-H., *et al*., *Competitive adsorption of heavy metals onto sesame straw biochar in aqueous solutions.* Chemosphere, 2016. **142**: p. 77-83.
420. Flórez, E., C. Jimenez-Orozco, and N. Acelas, *Unravelling the influence of surface functional groups and surface charge on heavy metal adsorption onto carbonaceous materials: An in-depth DFT study.* Materials Today Communications, 2024. **39**: p. 108647.
421. Salvestrini, S., L. Ambrosone, and F.-D. Kopinke, *Some mistakes and misinterpretations in the analysis of thermodynamic adsorption data.* Journal of Molecular Liquids, 2022. **352**: p. 118762.
422. Sithuba, T., *et al*., *Exploration of UV-induced geometrical isomer-enriched Helichrysum kraussii extract as a corrosion inhibitor for Al (111) surface in 1.0 M hydrochloric acid: An experimental and theoretical study.* Results in Surfaces and Interfaces, 2024. **16**: p. 100268.

© University of Venda

423. Xia, G. and W.P. Ball, *Adsorption-partitioning uptake of nine low-polarity organic chemicals on a natural sorbent.* Environmental science & technology, 1999. **33**(2): p. 262-269.
424. Chen, G., *et al*., *Revealing the mechanisms of mercury adsorption on metal-doped kaolinite (001) surfaces by first principles.* Journal of Hazardous Materials, 2022. **431**: p. 128586.
425. Desimone, M., G. Gordillo, and S.N. Simison, *The effect of temperature and concentration on the corrosion inhibition mechanism of an amphiphilic amido-amine in CO2 saturated solution.* Corrosion Science, 2011. **53**(12): p. 4033-4043.
426. Amin, M.A., *et al*., *Monitoring corrosion and corrosion control of iron in HCl by non-ionic surfactants of the TRITON-X series–Part II. Temperature effect, activation energies and thermodynamics of adsorption.* Corrosion science, 2011. **53**(2): p. 540-548.
427. Wolfe, J. and D. Bagnall, *Arrhenius plots—curves or straight lines?* Annals of Botany, 1980. **45**(4): p. 485-488.
428. Khadom, A., *et al*., *Electrochemical, activations and adsorption studies for the corrosion inhibition of low carbon steel in acidic media.* Portugaliae Electrochimica Acta, 2009. **27**(6): p. 699-712.
429. Alaneme, K., *et al*., *Corrosion inhibition and adsorption characteristics of rice husk extracts on mild steel immersed in 1M H2SO4 and HCl solutions.* International Journal of Electrochemical Science, 2015. **10**(4): p. 3553-3567.
430. Azhagiya Singam, E., *et al*., *Thermodynamics of adsorption on graphenic surfaces from aqueous solution.* Journal of chemical theory and computation, 2018. **15**(2): p. 1302-1316.
431. Zhang, R., *et al*., *A study on the open circuit voltage and state of charge characterization of high capacity lithium-ion battery under different temperature.* Energies, 2018. **11**(9): p. 2408.
432. Demir, K.Ç., *The investigation of the corrosion behavior of CZTS thin films prepared via electrodeposition.* Materials Science in Semiconductor Processing, 2021. **123**: p. 105553.
433. Zhang, S. and T. Jow, *Aluminum corrosion in electrolyte of Li-ion battery.* Journal of Power Sources, 2002. **109**(2): p. 458-464.
434. Petzl, M. and M.A. Danzer, *Advancements in OCV measurement and analysis for lithium-ion batteries.* IEEE Transactions on energy conversion, 2013. **28**(3): p. 675-681.
435. Sabzi, M., *et al*., *Study of the effect of temperature on corrosion behavior of galvanized steel in seawater environment by using potentiodynamic polarization and EIS methods.* Materials Research Express, 2019. **6**(7): p. 076508.
436. Binninger, T., *et al*., *Thermodynamic explanation of the universal correlation between oxygen evolution activity and corrosion of oxide catalysts.* Scientific reports, 2015. **5**(1): p. 12167.
437. Khaled, K., *Studies of the corrosion inhibition of copper in sodium chloride solutions using chemical and electrochemical measurements.* Materials Chemistry and Physics, 2011. **125**(3): p. 427-433.
438. Feliu Jr, S., *Electrochemical impedance spectroscopy for the measurement of the corrosion rate of magnesium alloys: Brief review and challenges.* Metals, 2020. **10**(6): p. 775.
439. Basnet, P., *et al*., *A review on bio-synthesized zinc oxide nanoparticles using plant extracts as reductants and stabilizing agents.* Journal of Photochemistry and Photobiology B: Biology, 2018. **183**: p. 201-221.
440. Bayer, I.S. and C.M. Megaridis, *Contact angle dynamics in droplets impacting on flat surfaces with different wetting characteristics.* Journal of Fluid Mechanics, 2006. **558**: p. 415-449.
441. Behera, S.K., *et al*., *Effect of microstructure on contact angle and corrosion of ductile iron: Iron–graphite composite.* Langmuir, 2019. **35**(49): p. 16120-16129.
442. Gu, H., *et al*., *Investigation on contact angle measurement methods and wettability transition of porous surfaces.* Surface and Coatings Technology, 2016. **292**: p. 72-77.
443. Crick, C.R. and I.P. Parkin, *Preparation and characterisation of super-hydrophobic surfaces.* Chemistry–A European Journal, 2010. **16**(12): p. 3568-3588.
444. Wang, J., *et al*., *Fabrication of hydrophobic surface with hierarchical structure on Mg alloy and its corrosion resistance.* Electrochimica Acta, 2010. **55**(22): p. 6897-6906.
445. Niverty, S., *et al*., *Multiscale investigation of corrosion damage initiation and propagation in AA7075-T651 alloy using correlative microscopy.* Corrosion Science, 2021. **185**: p. 109429.

© University of Venda

446. Volovitch, P., *et al*., *Understanding corrosion via corrosion product characterization: II. Role of alloying elements in improving the corrosion resistance of Zn–Al–Mg coatings on steel.* Corrosion Science, 2011. **53**(8): p. 2437-2445.
447. Ouakki, M., *et al*., *Insights into corrosion inhibition mechanism of mild steel in 1 M HCl solution by quinoxaline derivatives: electrochemical, SEM/EDAX, UV-visible, FT-IR and theoretical approaches.* Colloids and Surfaces A: Physicochemical and Engineering Aspects, 2021. **611**: p. 125810.
448. Kapłonek, W. and K. Nadolny, *Review of the advanced microscopy techniques used for diagnostics of grinding wheels with ceramic bond.* Journal of Machine Engineering, 2012. **12**(4): p. 81--98.
449. Norris, J.L. and R.M. Caprioli, *Analysis of tissue specimens by matrix-assisted laser desorption/ionization imaging mass spectrometry in biological and clinical research.* Chemical reviews, 2013. **113**(4): p. 2309-2342.
450. Reed, S.J.B., *Electron microprobe analysis and scanning electron microscopy in geology*. 2005: Cambridge university press.
451. Saghiri, M.A., *et al*., *Back-scattered and secondary electron images of scanning electron microscopy in dentistry: a new method for surface analysis.* Acta Odontologica Scandinavica, 2012. **70**(6): p. 603-609.
452. van Der Ent, A., *et al*., *X-ray elemental mapping techniques for elucidating the ecophysiology of hyperaccumulator plants.* New Phytologist, 2018. **218**(2): p. 432-452.
453. De Maeztu, M.A., J.I. Alava, and C. Gay-Escoda, *Ion implantation: surface treatment for improving the bone integration of titanium and Ti6Al4V dental implants.* Clinical oral implants research, 2003. **14**(1): p. 57-62.
454. Fayomi, O. and A. Popoola, *An investigation of the properties of Zn coated mild steel.* International Journal of Electrochemical Science, 2012. **7**(7): p. 6555-6570.
455. Duan, W., *et al*., *Enhancing acid corrosion resistance in alkaline-activated materials with water treatment residue and blast-furnace slag.* Construction and Building Materials, 2024. **447**: p. 138105.
456. Ali, A., N. Zhang, and R.M. Santos, *Mineral characterization using scanning electron microscopy (SEM): a review of the fundamentals, advancements, and research directions.* Applied Sciences, 2023. **13**(23): p. 12600.
457. Phillips, D.H., *et al*., *Performance evaluation of a zerovalent iron reactive barrier: mineralogical characteristics.* Environmental Science & Technology, 2000. **34**(19): p. 4169-4176.

© University of Venda